SOVIET ASTRONOMY

AJ

JULY - AUG

VOLUME 1, NUMBER 4 ~~APRIL~~ 1957

A MODEL OF THE INNER CORONA BASED ON RADIO DATA

B. N. Panovkin

Recent measurements of the distribution of radio brightness across the solar disc on decimeter wavelengths show that the maximum brightness does not coincide with the solar limb, as predicted theoretically, but is shifted and lies inside the optical disc. This displacement increases with increasing wavelength. This fact cannot be explained by a simple isothermic model of the solar corona.

A new model of the solar corona with a temperature gradient is proposed and this model agrees with the observational data.

The possibility of the existence of a new nonthermal component is discussed.

The problem of the thermal emission from the sun in the radio-frequency region has been repeatedly investigated by a number of research workers in the Soviet Union and abroad. According to V.L.Ginzburg, [1], I.S. Shklovskii [2], and D. Martyn [3] the thermal emission from the sun is mainly governed by the electron temperature of the upper chromosphere and the corona.

Many of the features of solar radio waves, derived from the data obtained at different wavelengths, were adequately explained by means of a simple model of the upper layers of the solar atmosphere in which the electron-density distribution is taken from the data of van de Hulst [4] or Baumbach [5] and the electron temperatures of the chromosphere and the corona are assumed to be equal to $3\text{-}5 \cdot 10^{5\circ}$K and $10^{6\circ}$K, respectively.

This type of theoretical investigation was carried out by D. Martyn [3]. However, there are errors in some of D. Martyn's calculations. A more elaborate and detailed analysis was carried out by I.S. Shklovskii and S.B. Pikel'ner [6]. These investigations showed that the solar radio radiation has several distinguishing features. The most characteristic of these are the following:

1. The effective temperature of the radiation increases with increasing wavelength.
2. There is considerable emission from regions outside the optical disc on centimeter and meter wavelengths.
3. There is an increase in brightness at the limb of the sun at centimeter and decimeter wavelengths.

4. The region emitting in decimeter and meter wavelengths has an elliptical shape at the time of the minimum of solar activity.

A detailed calculation of the distribution of radio emission across the solar disc for various values of the corona temperature was carried out by S. Smerd [7]. The first attempts to determine the distribution of radio brightness were made by means of eclipse observations [8-13]. A detailed study of the features of the distribution could not be made because of the nature of the eclipse observations. But on the whole, the data of these observations were in good agreement with theory. The interferometer method [15, 16] was found to be the most effective method for studying the radio-brightness distribution.

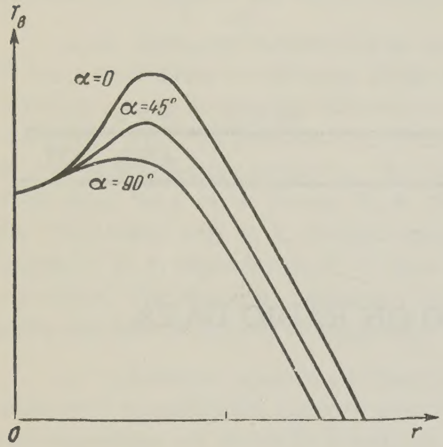

Fig. 1. λ = 50 cm; M.A. Ovsiankin and B.N. Panovkin 1955-1956.

The results of the early interferometer observations, however, did not agree with the theoretical data. Observations by Machin [17] on a wavelength of λ = 3.7 m gave too large an extension beyond the optical disc of the regions of radio emission. The data of Stanier [18] did not show limb brightening on a wavelength of λ = 50 cm. However, the more careful investigations of O'Brien [19] yielded results for the meter wavelengths which were in satisfactory agreement with the theory. Moreover, the investigation of the solar radio-brightness distribution at decimeter wavelengths carried out by V.V. Vitkevich [13] and Christiansen and Hindman [20] established the presence of a marked limb brightening.

The variation of the radio-emission intensity with wavelength is well established from the combined measurements of the flux density of the radiation from the quiet sun on various wavelengths.

Interferometric measurements recently carried out have yielded a number of extremely interesting and important results which cannot be explained with the help of the model described above. These observations were carried out by Firor [21] on a wavelength of 1.45 m, O'Brien and Tandberg-Haussen [22], Swarup and Parthasarathy [23] on λ = 60 cm, M.A. Ovsiankin and B.N. Panovkin [24] on λ = 50 cm, M.A. Ovsiankin, B.N. Panovkin and A.P. Shutov on λ = 24 cm. These data are presented in Figure 1 and Table 1.

TABLE 1

Observers	Year of observation	λ, cm	Position of brightness maximum in terms of $R_\odot$	The ratio $\frac{T_B \text{ max}}{T_B \text{ center}}$	Remarks
Christiansen and Warburton [25]	1953-1954	21	0.96	1.6	A two-dimensional isophot distribution was obtained
V.V. Vitkevich [15]	1952	24	1.0	2.0	Histogram method
M.A. Ovsiankin, B.N. Panovkin and A.P. Shutov	1956	24	1.0	2.2	One-dimensional distribution derived on the assumption of circular symmetry
M.A. Ovsiankin and B.N. Panovkin	1955-1956	50	0.65	1.6	Two-dimensional distribution
Swarup and Parthasarathy [23]	1954-1955	60	0.80	1.5	One-dimensional distribution
O'Brien and Tandberg-Haussen [22]	1954	60	0.60	1.5	Two-dimensional distribution
O'Brien [19]	1952	140	–	1.0	Two-dimensional distribution
Firror [21]	1953-1955	145	0.60	1.1	Two one-dimensional distributions for an equatorial and a polar region

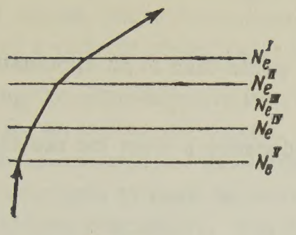

Fig. 2.

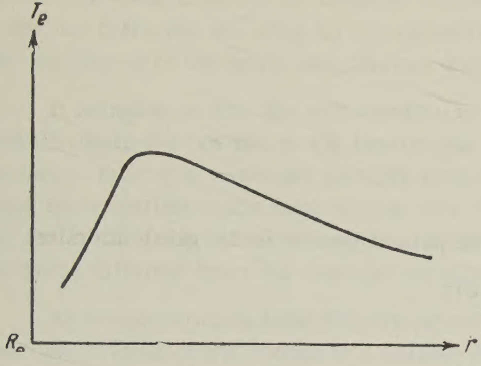

Fig. 3.

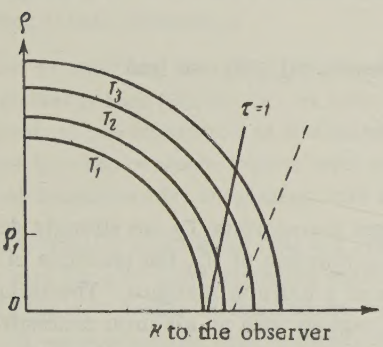

Fig. 4.

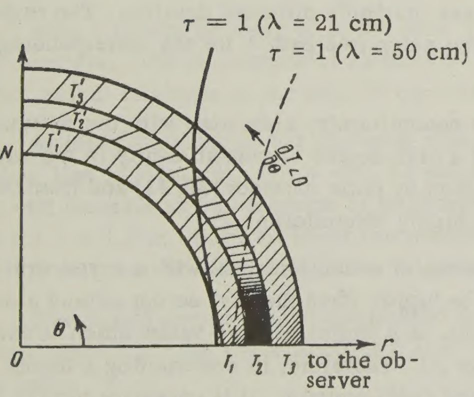
τ = 1 (λ = 21 cm)
τ = 1 (λ = 50 cm)
T_3'
T_2'
T_1'
N
$\frac{\partial T}{\partial \theta} < 0$
θ
0
T_1 T_2 T_3 to the observer
r

Fig. 5.

It can be clearly seen that the maximum of the radio-brightness distribution is not at the edge of the optical disc, as predicted by the theory, but occurs at some distance from the edge, nearer to the center of the sun.

The slight disagreement between the data of the various authors can be explained by the fact that the various observations were not carried out in the same way. In some observations the results were in the form of one-dimensional distributions, i.e., the distributions projected on an axis passing in a definite direction through the center of the sun. Other observations yielded two-dimensional distributions which, obviously, are more valuable and reliable. Moreover, it must be noted that the various observations were obtained at different times, so that, probably, there are variations due to the dependence of the shape of the distribution on the solar-activity cycle.

On the whole, it can be noted that the intensity maximum on wavelengths of the order of 21-24 cm is almost at the optical edge of the sun, possibly with a small displacement towards the center of the disc. On wavelengths of the order of 50-60 cm the intensity maximum does not fall at the optical edge. Finally, at wavelengths of 1.4-1.5 m the increase of brightness, if it exists at all, is small and the shape of the distribution approaches that of a flat-topped distribution with darkening at the edge of the optical disc.

It must also be noted that, because of the finite resolving power of the interferometers, smoothed-out distributions are obtained and the ratio of the maximum intensity to the intensity at the center of the disc is underestimated.

The observations presented in [22, 24 and 25], in which complete isophot maps of the brightness distribution were obtained, show that the distribution for the polar regions is markedly different from that for the equatorial regions. On wavelengths of the order of 21 cm limb darkening is observed in the polar regions, while limb brightening is only observed in a region within 50-60° from the equator. On wavelengths of the order of 50-60 cm there is limb brightening in the polar regions also, but not as markedly as in the equatorial regions. On wavelengths of the order of 1.4-1.5 m and longer, the shape of the distributions for the polar and equatorial regions is approximately the same.

Thus, the "radio-model" of the upper layers of the solar atmosphere must explain, at least qualitatively, all of the above features of the radio-brightness distribution, of which the most important is the fact that the brightness maximum does not fall on the edge of the optical disc. It is strange that this important fact has not been considered by the specialists engaged in the investigation of the radio emission from the sun, and, up to the present, no papers have appeared dealing with the interpretation of this phenomenon.

It is obvious that from the simple model of the corona, which has been used up to the present time, it inescapably follows that the increase of brightness in the whole range of decimeter wavelengths must occur at the optical edge of the solar disc.

Let us consider the possible modifications of the simple model which would lead to an explanation of the observed facts.

The brightness temperature $T_B(\rho)$ for a given direction which is at a distance ρ from the radial ray is given by the integral relation (for example, see [26])

$$T_B(\rho) = \int\limits_0^{\tau_\rho} T(\tau) e^{-\tau} d\tau. \tag{A}$$

The optical thickness τ is determined from

$$\tau = \int \varkappa ds,$$

where κ is the absorption coefficient and s is the arc length along the path of the ray in the given direction.

If ρ is measured in solar radii $R_\odot$ ($R_\odot = 6.9 \cdot 10^{10}$ cm), then [27]

$$\tau = 2.321 \int \frac{\nu(s)(1 - n^2(s))}{n(s)} ds.$$

Here ν is the effective number of electron-ion collisions, and n is the coefficient of refraction for the given wavelength.

Taking into account the dependence of ν and n on the electron density N_e [28], we find

$$\tau \propto \int \frac{N_e^2}{n} ds.$$

Thus τ and, consequently, the corresponding value of the brightness temperature T_B are strongly dependent on the degree of nonuniformity of the solar atmosphere. Since τ is a function of N_e^2, the presence of nonuniformity will lead to an increased value of τ as compared to the case of a uniform medium. The influence of the factor 1/n is not large, since for the time being we will consider regions with an electron concentration $N_e \ll N_{e,\text{crit}}$. In general, refraction of rays passing through a nonuniform region will increase the path length s, and, consequently, the value of τ (Figure 2).

It is known [28, 29] that the solar corona has a well-developed rayed structure. The rays of coronal matter extend approximately in a radial direction. The individual rays have markedly different densities. The regions of nonuniformity have large dimensions which are comparable to the mean free path $\overline{\lambda}$ for the corresponding layers (for the corona $\overline{\lambda}$ is of the order of 10^8-10^9 cm).

Moreover, it is possible that there are regions of small-scale nonuniformity associated with the existence of longitudinal plasma waves in the solar corona. The presence of a high degree of nonuniformity in the outer layers of the corona, the so-called "supercorona," has been established by radio methods [30, 31] and from this fact we can conclude that the deeper layers of the corona are also highly nonuniform.

Simple geometrical considerations indicate that, in the presence of nonuniformities with a rayed structure which occur in the solar corona, the degree of nonuniformity will be higher when the rays do not extend along a radial direction. Obviously the degree of nonuniformity increases, as ρ increases, to a value which is determined by the degree of nonuniformity of the outer corona (for large ρ). Therefore, in constructing a model of the solar corona, which would lead to an explanation of the observed radio emission, it is necessary to take into account both the general nonuniformity of the corona, as well as the variation of the degree of nonuniformity with change of the position distance ρ.

Unfortunately, at the present time no reliable determinations are available of the degree of nonuniformity of the solar corona, while the radioastronomical methods for determining the degree of nonuniformity are based on the use of a definite model (with the exception of the data on the "supercorona," mentioned above).

Taking the nonuniformity into account, we will find that there will be some changes in the distributions calculated for an isothermal corona. The distribution for a given wavelength λ will correspond to the distribution for a somewhat smaller wavelength in the nonuniform model. The transition from limb brightening on decimeter wavelengths to limb darkening on meter wavelengths will also occur at shorter wavelengths than in the case of a uniform atmosphere. The distributions for the other wavelengths will also be correspondingly "shifted."

The increase of the degree of nonuniformity with increasing ρ will lead to a slower rise of the brightness towards the solar limb for the range of wavelengths in which there is an increase of the brightness. However, it is obvious that even allowing for the nonuniformity of the corona, the simple isothermal model cannot explain the occurrence of the brightness maxima away from the edge of the solar disc in the decimeter range.

It seems to us that the only possibility for explaining satisfactorily the characteristic features of the radio emission from the sun lies in the investigation of the solar-corona model with the inclusion of a temperature gradient. From the combined astrophysical data (for example, see Allen's review [32]) it is possible to determine the variation of the temperature with distance from the solar surface. It is obvious that we are considering the variation of the average temperature since there are local regions in the corona where the temperature is markedly different from the average temperature.

As we go outwards from the comparatively cold chromosphere, the temperature already rises sharply in the inner regions of the corona to a certain maximum value and then monotonically decreases in the outer layers of the corona. O'Brien and Bell [33] have shown that it is possible to explain the large extension, outside the solar disc, of the radio emission on meter wavelengths on the assumption that the kinetic temperature of the corona varies as $T = 2 \cdot 10^6 R^{-3}$ °K for $R > 1.2 R_\odot$. Figure 3 shows a possible variation of the temperature with increasing radial distance ρ.

Let us consider, first of all qualitatively, the problem of deriving a model for the "radiocorona." Consider an equatorial region (Figure 4). At some distance $\underline{r}$ there exists a zone with an increased temperature T_2 which corresponds to the maximum of the curve $T(r)$ shown in Figure 3. On either side of the high-temperature region there are low-temperature regions with temperatures T_1 and T_3. We assume that the corona is not uniform, the degree of nonuniformity increasing with increasing distance ρ.

It is usually considered that the effective emission level is one for which the optical depth $\tau \approx 1$. Let us assume that for $\rho = 0$ the effective emission level is the layer with the temperature T_1. The brightness temperature T_B for $\rho = 0$ will be determined by the emission from the level T_1 and the absorption in the overlying layers. If we now choose appropriately the variation of the degree of nonuniformity with ρ and take into account the geometrical increase of the path-length segments in the zones T_1, T_2 and T_3 with increasing ρ, then for a certain distance ρ_1 the layer T_2 will become the effective level with $\tau \sim 1$ and, since $T_2 > T_1$, the brightness temperature T_B will correspondingly increase.

With a further increase of ρ, the zone T_3 will become the effective level and the brightness temperature will decrease. The occurrence of an increase of the brightness is therefore not associated with the sudden change of the optical thickness at the edge of the solar disc.

At lower frequencies the thickness τ increases and the effective levels $\tau \approx 1$ will lie at a greater height (dashed line in Figure 4). For $\rho = 0$, T_2 will become the effective level, the temperature at the center of the disc will increase and an increase of brightness will not be observed, which corresponds to the observed distribution for $\lambda \geq 1.5$ m. For still lower frequencies, the outer cold zone T_3 will become the effective emission layer and this will lead to a decrease of the brightness temperature at the center.

The model discussed is characterized by a higher optical thickness than the isothermal model considered earlier, since from the above account it is clear that already at $\lambda = 50$ cm the optical thickness must be greater than unity.

The required form of the distribution for the polar regions can be obtained, if we make use of the fact that in the polar region the electron temperature is lower than that in the equatorial region (Figure 5). If the temperature decreases with increasing latitude θ, then with a suitable choice of the gradient $dT_e/d\theta$ we can obtain a decrease of the brightness temperature towards the poles at a wavelength of the order of 21 cm. At lower frequencies the optical thickness is greater and the height of the effective level can increase faster with increasing latitude than the fall of the temperature; this will lead to an increase of the brightness (but less markedly than in the equatorial region).

Finally, on meter wavelengths for which $\tau \gg 1$, the distribution of brightness will, on the whole, be similar to that for the equatorial regions (limb darkening).

Thus, from a qualitative discussion of the approximate nonisothermal model it follows that, in principle, the nonisothermal model can be used to explain the characteristic features of the radio-brightness distribution in the range of decimeter and meter wavelengths.

The derivation of the model which would give a quantitative description of the radio-brightness distribution is associated with great difficulties which arise because of the scarcity of information available on the degree of nonuniformity of the corona. The following approach appears to be the best. A model of the nonisothermal corona is constructed on the basis of some reasonable assumptions about the degree of nonuniformity of the various layers of the solar atmosphere, the temperature gradient, and the electron-density distribution. The parameters are chosen in a way which ensures that the model provides the best agreement with the observational data. Proceeding from observational data and other theoretical considerations, we then make this first-approximation model more accurate.

In constructing this first-approximation model, we have assumed that the electron density in the corona is distributed according to the data of van de Hulst [4], that the degree of nonuniformity of the corona increases towards the edge of the optical disc, and that it increases with distance from the solar surface.

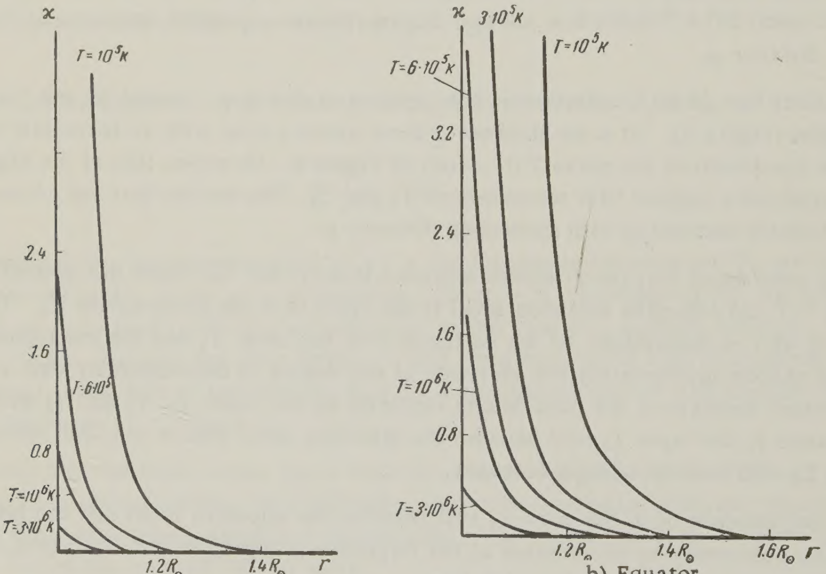

a) Pole

b) Equator

Fig. 6.

The expression given by V.L. Ginsburg [27] was found to be the most suitable for calculating the value of the absorption coefficient:

$$\varkappa = \frac{\nu_{\text{eff}}}{c} \frac{1-n^2}{n} R_\odot$$

Here, the solar radius $R_\odot$ is taken as the unit of distance. ν_{eff} is the effective number of electron-ion collisions. For the solar corona ν_{eff} is given by the expression

$$\nu_{\text{eff}} = 5.5 \frac{N_e}{T_e^{3/2}} \ln \left(\gamma_2 \cdot 10^4 \frac{T_e^{3/2}}{N^{1/3}} \right);$$

substituting numerical values, we have

$$\varkappa = 12 \cdot 76 \frac{N_e}{T_e^{3/2}} \frac{1 - n^2}{n} \ln \left(\gamma_2 \cdot 10^4 \frac{T_e^{3/2}}{N^{1/3}} \right).$$

The coefficient of refraction is determined from the well-known relation

$$n^2 = 1 - \frac{4\pi e^2 N_c}{m\omega^2}.$$

The values of the absorption coefficient were calculated for various temperatures between 10^5 and $3 \cdot 10^6$ °K. The dependence of the coefficient of refraction $\underline{n}$ on the temperature T could be neglected to the accuracy of the computations, since the correction did not exceed 5% even for $T = 3 \cdot 10^6$ °K. The dependence of the coefficient of refraction on the temperature is given in [34]:

$$n^2 = 1 - \frac{4\,\pi e^2 N_e}{m\omega^2} [1 + \beta^2 + \beta^4 + \ldots],$$

where

$$\beta = \frac{1}{c} \sqrt{\frac{3kT_e}{m}}.$$

The correction terms do not exceed 10^{-2} even for $T = 3 \cdot 10^6$ °K.

As an example, Figure 6 shows the calculated curves of the absorption coefficient κ for $\lambda = 50$ cm.

Astrophysical data [32] indicate only the general trend of the variation of electron temperature T_e with distance from the solar surface. The results of O'Brien and Bell indicate that there is a fall of temperature in the inner layers which does not affect the radio emission in the range of decimeter wavelengths. There are no reliable data on the degree of nonuniformity of the corona. In this situation there is no need to construct a model by means of an exact solution of the integral relation (A). Therefore, a simpler approximate method was used.

The corona was divided into a number of zones at different heights above the solar surface. In each zone the electron temperature T_e and the absorption coefficient κ were assumed constant and equal to their mean value for the given zone. The degree of nonuniformity χ was also assumed constant for a fixed value of ρ. Having assigned a value to T_2 and χ, we can easily calculate the value of the optical thickness. The optical thickness for the i-th zone is

$$\tau_i(\rho) = \overline{\varkappa}^i \chi^i(\rho)\, \Delta s^i(\rho);$$

$\Delta s(\rho)$ is the extension of the given zone along the line of sight:

$$\Delta s^i(\rho) = \sqrt{r_{i+1}^2 - \rho^2} - \sqrt{r_i^2 - \rho^2}.$$

The brightness temperature $T_B(\rho)$ is obviously given by

$$T_B(\rho) = \sum_{i=0}^{n} T_i \left(1 - e^{-\tau_i(\rho)}\right) e^{-\sum\limits_{k=0}^{i} \tau_k(\rho)}.$$

The calculations were carried out for the equatorial and polar regions separately. It appears that the solution is not unique. Several models can be constructed which, on the whole, satisfy the requirements of the problem.

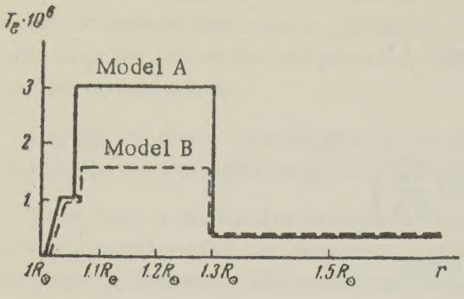

Fig. 7.

In what follows we give examples of simple models with temperature gradients which provide an explanation of the observations.

Model A. It was assumed that the temperature distribution is that shown in Figure 7. The functions $\chi(\rho)$ and $\chi(r)$ were taken as shown in Figure 8. On these assumptions, using the method described above, we calculated the radio-brightness distribution. This model is in good quantitative agreement with the observational data. The values of the central temperatures for the range of decimeter wavelengths were found to be somewhat overestimated. From Figure 9 it can be seen that the year of observation should be taken into account, since the shape of the distribution is strongly dependent on the period of solar activity. This effect is confirmed by observations.

In model B a more reasonable value is taken for the central-zone temperature ($1.5 \cdot 10^6$°K) which is less than that in model A. Model B gives better quantitative agreement with observation in the rangeof decimeter wavelengths. However, the value of the central temperature for the "critical" wavelength $\chi \approx 1.5$ m is found to be underestimated (by ~25%) (Figure 10).

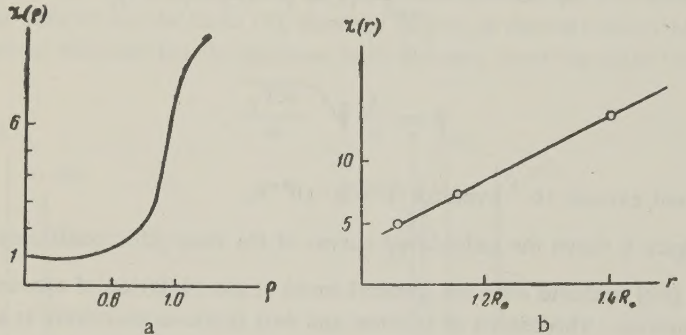

a b

Fig. 8.

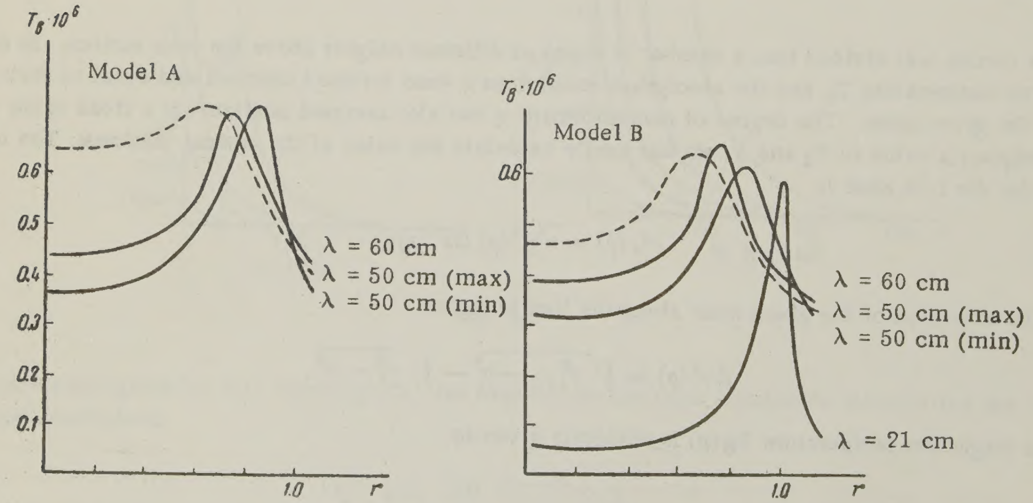

Fig. 9.

Thus, even very approximate models with a temperature gradient provide a good explanation of the remarkable fact that on decimeter wavelengths the brightening does not occur at the optical edge of the solar disc.

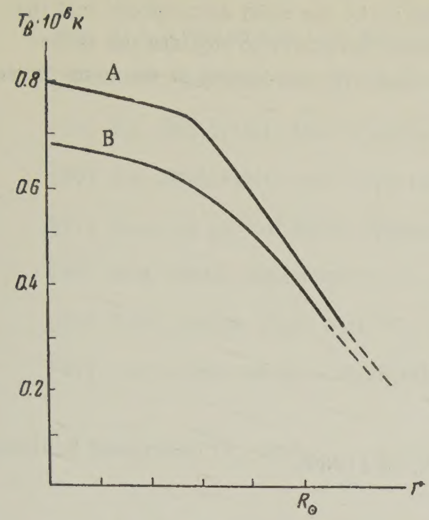

Fig. 10.

On longer wavelengths the radio-brightness distribution across the solar disc is to a large extent determined by the refraction of the radio radiation. It is necessary to take refraction into account for wavelengths $\lambda > 1.5$ m. For these wavelengths, the optical thickness τ is large and the outer layers of the corona play an important part. It is therefore necessary to take into account the temperature gradient $\partial T/\partial r$ in these layers, i.e., to construct a different model from the ones presented above which, on the whole, describe the distribution of parameters in the inner corona. Such a model with a monotonic fall of the temperature in the outer layers was constructed in the paper of O'Brien and Bell [33] mentioned above.

The investigation of the models shows that the corona must be considered to be optically thicker than it was assumed earlier. There is an upper limit to the possible values of the optical thickness of the corona determined by several factors.

The ultraviolet emission from the solar corona, as well as the optical thickness, is proportional to $\chi(\rho)\int N_e^2 ds$ [35]. Will an increased degree of nonuniformity χ lead to an excess of ultraviolet radiation?

According to Ia.L. Al'pert [37], the number of photons emitted by the sun with an energy greater than the ionization potential of the atoms and molecules giving ions in an ionospheric layer, and which fall per second on a unit surface of the earth's atmosphere is

$$s_0 = 10^{10} - 4 \cdot 10^{10} \text{ cm}^{-2} \text{ sec}^{-1}.$$

Assuming that the ionization potential of the atoms and molecules responsible for the formation of ions in the ionosphere is of the order of 10 ev, we find that the required flux of ultraviolet radiation is

$$s \approx 16 \cdot 10^{-2} - 64 \cdot 10^{-2} \text{ erg cm}^{-2} \text{ sec}^{-1}.$$

At the same time, according to I.S. Shklovskii's estimates [35], at the surface of the earth the flux of hard radiation from the corona is

$$s \approx 3.7 \cdot 10^{-2} \text{ erg cm}^{-2} \text{ sec}^{-1}.$$

Thus, an increase of the ultraviolet-radiation flux by a factor of ~5-10 (which follows from the average degree of nonuniformity assumed for the inner coronal layers in models A and B) will not upset the balance.

Another factor which governs the upper limit to the optical thickness in the various models is the increase of the absorption of the nonthermal radiation, originating in the deep layers of the corona, in the range of meter wavelengths.

In this connection we may note that the problem of the intensity of the nonthermal radiation escaping from the inner layers of the solar corona is closely associated with the problem of the mechanism by which the radiation is produced and, in particular, with the problem of the transformation of the longitudinal plasma waves into transverse radio waves. Generally speaking, a small amount of energy is required for the excitation of the observed radiation-flux densities. Mechanisms for an efficient escape of radio radiation from an excited plasma have been proposed in several papers which have recently appeared [38-40]. All of these mechanisms and, particularly, the one proposed by the author for the transformation of longitudinal into transverse waves at local nonuniformities of the corona, which are present because of the same longitudinal plasma waves (the transformation of a longitudinal wave by a longitudinal wave), lead to a radio-wave energy outflow which is considerably greater (in the case of some mechanisms by several orders of magnitude) than that necessary to explain the observed phenomena.

Summarizing what has been said, it must be noted that the whole of the observational data unavoidably leads to the conclusion that there is a temperature gradient in the upper layers of the solar atmosphere and that the corona is highly nonuniform. The model of the inner layers of the corona necessary to explain the radio-brightness distribution in the range of meter wavelengths is in good agreement with the model of the outer layers [34] and with modern astrophysical data.

LITERATURE CITED

[1] V.L. Ginzburg Doklady Akad. Nauk SSSR 52, 491 (1946).

[2] I.S. Shklovskii, Astron. J. (USSR) 23, 333 (1946).

[3] D. Martyn, Nature 158, 632 (1946).

[4] H.C. van de Hulst, Bull. Astron. Inst. Neth. 410, 135 (1950).

[5] S. Baumbach, Astronomische Nachrichten 263, 121 (1937).

[6] I.S. Shklovskii and S.B. Pikel'ner, Izv. Krymsk. astrofiz. obs. 6, 29 (1950).

[7] S.F. Smerd, Australian J. Sci. Research A3, 34 (1950).

[8] A.E. Covington, Nature 159, 405 (1947).

[9] J.H. Piddington and I.V. Hindman, Australian J. Sci. Research A2, 524 (1949).

[10] M. Laffineur, Compt. rend. 228, 1636 (1946); 234, 1528 (1952).

[11] J.F. Denisse, Compt. rend. 233, 917 (1951); 234, 1597 (1952).

[12] W.H. Christiansen, D.E. Jabsle and B.Y. Mills, Australian J. Sci. Research A2, 506 (1949).

[13] V.V. Vitkevich, Proc. of the Fifth All-Union Conference on Cosmogony [in Russian] (Izd. AN SSSR, Moscow).

[14] J.C. Minett and N.R. Labrum, Australian J. Sci. Research A3, 60 (1950).

[15] V.V. Vitkevich, Astron. J. (USSR) 29, 450 (1952).

[16] L.L. McCready, J.L. Pawsey and R. Payne-Scott, Proc. Roy. Soc. 190A, 357 (1947).

[17] K.E. Machin, Nature 167, 889 (1951).

[18] H.M. Stanier, Nature 165, 354 (1950).

[19] P.A. O'Brien, Monthly Notices, Roy. Astron. Soc. 113, 597 (1953).

[20] W.N. Christiansen and J.V. Hindman, Nature 167, 635 (1951).

[21] J. Firor, Astrophys. J. 123, 320 (1955).

[22] P.A. O'Brien and E. Tandberg-Haussen, Observatory 75, 884 (1955).

[23] G. Swarup and R. Parthasarathy, Observatory 75, 884 (1955).

[24] M.A. Ovsiankin and B.N. Panovkin, Radiotekh. i Elektron. 1, 6 (1956).

[25] W.H. Christiansen and J.A. Warburton, Australian J. Phys. 8, 473 (1955).

[26] Theoretical Astrophysics, Ambartsumian (editor) [in Russian] (GITTL, 1952).

[27] V.L. Ginsburg, The Theory of Radio-Wave Propagation in the Ionosphere [in Russian] (GITTL, 1949).

[28] H.C. van de Hulst, Bull. Astron. Inst. Neth. 410, 150 (1950).

[29] G.M. Nikol'skii, Astron. J. (USSR) 33, 588 (1956).

[30] V.V. Vitkevich, Doklady Akad. Nauk SSSR 77, 583 (1951).

[31] K.E. Machin and F.G. Smith, Nature 170, 319 (1952).

[32] C.W. Allen, Repts. on Progr. in Phys. 17, 135 (1954).

[33] P.A. O'Brien and C.J. Bell, Nature 173, 219 (1954).

[34] M.E. Gertsenshtein, J. Exptl.-Theoret. Phys. (USSR) 22, 303 (1952).

[35] I.S. Shklovskii, Solar Corona [in Russian] (GITTL, 1951).

[36] I.S. Shklovskii, Astron. J. (USSR) 23, 203 (1946).

[37] Ia.L. Al'pert, J. Exptl.-Theoret. Phys. (USSR) 18, 995 (1948).

[38] G.B. Field, Astronomy J. 12, 160 (1955).

[39] R.W. Larenz, Naturwiss. 42, 253 (1953).

[40] V.V. Zhelezniakov, Radiotekh. i Elektron. 1, 840 (1956).

Received December 14, 1956

PHOTOMETRY OF THE IMAGES OF SOME PLANETARY NEBULAE

Iu. K. Gulak

Results of absolute photometric measurements of the planetary nebulae NGC 6720, 7009 and 7662 in nebular lines are reported. The distribution of brightness in the images are shown in Figures 1, 2 and 3 in the form of isophots. The brightness is expressed in visual magnitudes per square second. The total brightness of the nebulae in nebular lines is compared with their total brightness.

The physical processes in planetary nebulae have been well explained. This was facilitated by the idealization of the spatial form of the nebulae which are often represented as uniform, spherical, and sometimes hollow clouds. At the same time the results of the theory of radiation equilibrium, the dynamics of planetary nebulae and other problems depend on the distribution of matter in the body of the nebula which may, in fact, vary considerably [1]. It is therefore of major importance to carry out detailed studies of the images of some typical planetary nebulae.

One of the main methods of studying planetary nebulae is the absolute photometry of monochromatic images which gives the distribution of brightness over the nebular surface. Apart from the work of L. Berman [2] who reported monochromatic isophots for two nebulae, the subject has received very little attention. A number of valuable studies by B. A. Vorontsov-Vel'iaminov [1], and also the work of E. Brodskaia [3], were devoted to a study of the distribution of brightness in the images of nebulae but were concerned with the integral distribution only.

In the present paper a short account is given of some work carried out in 1952-1953 on the photographic determination of the absolute values of brightness, and the distribution of brightness, in the images of planetary nebulae in nebular lines.

The nebulae NGC 6720, 7009 and 7662 were chosen for this purpose. The photographs were taken at the main focus of the 40-cm refractor of the Abastuman Astrophysical Observatory on Ilford Zenith plates, using a green filter prepared from an aniline dye ("Acid Green AZO"). The effective wavelength of this combination, as obtained in preliminary experiments, was found to be 4690 A, and the range of sensitivity was 4380-5100 A.

Our receiver (filter, plate) reacted almost exclusively to the radiation in the nebular lines, and only to a much lesser degree to H_β radiation, due to the relatively low intensity of the latter and the other lines in the region of the spectral sensitivity of the receiver. *

We could not take into account the H_β radiation in the various nebular regions separately, since we had no data on the distribution of brightness in H_β-images of the objects under investigation. However, it is well known that the emission in nebular and hydrogen lines of planetary nebulae is almost the same and can be represented by similar isophots [1], i. e., the intensity ratio $N_1 : N_2 : N_\beta$ may, in the first approximation, be taken as constant for the whole nebula. Thus, using this natural assumption and knowing the above ratio for the nebula as a whole [5] and the spectral characteristics of the receiver, it is easy to take into account H_β radiation.

---

* The continuous nebular emission has also very little effect on measurements in the nebular lines since their total intensity in the region 4,000-5,000 A turns out to be only of the order of the intensity of the H_δ line [4]).

The corrections for the nebulae NGC 7009 and 7662 turned out to be equal to $0^m.19$ and $0^m.12$. No corresponding data exist for the NGC 6720, but judging by the remarks of Curtis, and reproductions of "slitless" spectrograms [6], the H_β emission from this nebula is much weaker compared with its emission in the nebular lines than is the case in the former nebulae.

In order to standardize the negatives the method of extrafocal photography was used. It can be shown that the basic formula for this method may be written in the form

$$M_0 = m_s + 2.5\log\frac{\pi(d'')^2}{4} - 2.5\log\frac{b_0}{b_s} - 2.5\log R,$$

where M_0 is the brightness of the object in stellar magnitudes per square second m_s the visual magnitude of the standard star in one of the generally accepted photometric systems, d" the diameter of the extrafocal disc in seconds, b_0/b_s the ratio of apparent brightnesses of the object and the standard in the photometric system employed, and 2.5 log R is a term which reduces the ratio b_0/b_s to the photometric system in which the standard star is expressed. Depending on the given conditions, R may vary within wide limits. In the standardization of negatives the quantity R is determined using the expression

$$R = \frac{V_0}{P_0 K_0 T_0 S_0} \frac{\int\limits_0^\infty I_\lambda P_\lambda K_\lambda T_\lambda S_\lambda d\lambda}{\int\limits_0^\infty I_\lambda V_\lambda d\lambda},$$

where I_λ is the distribution of energy in the spectrum of the standard star, P, K, T, and S are the spectral coefficients of atmospheric transmission, the optics of the instrument, the filter, and the sensitivity of the receiver used in the comparison of the standard and the object, V_λ and V_0 the spectral sensitivity of the receiver through which the brightness m_s of the standard star is determined.

The visual magnitudes of the standard stars for NGC 7009 and 7662 were taken from the PD catalogue and were reduced to the Harvard system using the formulas given in [7]. The star BD 30° 2921 was used for NGC 6720. The visual magnitude of this star, reduced by G. A. Tikhov [8] from BD to the Harvard system, is $9^m.80$. The color index for this star obtained using a linear spectrograph is $+ 0^m.39$, i. e., its photographic magnitude is $10^m.19$. Using the data in the BSD catalogue, for which the photographic magnitudes were determined independently, the magnitude of this star was estimated to be $10^m.15$. The good agreement between the photographic magnitudes indicates that the assumed value of m_{vis} for this star is sufficiently accurate.

The energy distribution in the spectra of standard stars was derived from average color temperatures which are characteristic of objects of corresponding spectral classes [9]. The spectral classification was taken from the BSD catalogue.

The transmission coefficients of the atmosphere P_λ, P_0 and of the optics of the instrument K_λ, K_0 were taken as constant and equal in pairs in view of the narrow sensitivity band of the detector. The spectral transparency of the filter was investigated using a UM-2 monochromator.

In order to determine the spectral sensitivity of the Ilford Zenith plates, we used sensitigrams obtained on the GOI spectrosensitometer and kindly supplied by T. A. Kochlashvili of the Abastuman Observatory.

In the calculation of the correction term R the spectral sensitivity curve of the eye for "daytime vision" was taken into account.

A summary of the observed data is given in Table 1 in which the respective columns give the number of the nebula, the date of observation, the stellar time of the midpoint of the exposure, the duration of the exposure, the BD number of the standard star, the time of the midpoint of the exposure in the case of the standard, and the visual magnitude of the star.* In addition about 40 trial photographs were taken.

In 6-8 hours after the observations, the scale of the tube photometer was photographed on the plates used in the photography of the nebula and the standard, and with the same light filter and exposure. A special screen prepared from a mixture of gypsum and magnesium was illuminated by scattered daylight. Immediately after the scale was photographed the set of plates (nebula, standard, scale) was developed in the same dish. Thus, no cumulative effect was allowed to take place.

---

*The standard was photographed with the same exposure as the corresponding nebula.

TABLE 1

NGC	Dates(1952)	S_0	ΔS	BD	S_s	m_{vis}
6720	15—16/VI	$17^h54^m53^s$	1^h50^m	30°2921	$15^h49^m40^s$	$9.^m80$
7009	15—16/VII	21 33 08	0 10	86°79	20 40 13	6. 80
7662	19—20/VII	22 25 30	0 9	45°4321	22 50 30	5. 12

Photometric field errors were excluded by the fact that photographs were taken in the center of the field of view of the telescope in each case.

Nightly photoelectric and daily actinometric observations, which have been carried out at the Abastuman Observatory over a number of years, have shown that the coefficient of transparency of the atmosphere is subject to small seasonal changes but remains constant from night to night within a season [10, 11, 12].* According to the data reported by N. L. Magalashvili [13] for the period May 7 to July 29, 1945, the coefficient of transparency lies within the range 0.71-0.73 (photographic) and 0.85-0.86 (photovisual).

Detailed and careful studies of the total and spectral transparency of the atmosphere at the Abastuman Observatory [14] have shown that there is a remarkable agreement between the coefficients of transparency obtained at the Abastuman Observatory and those obtained at the Mount Wilson Observatory and used in the present work. Since, simultaneously with our observations, the electrophotometry of stars, in which the photographic and photovisual transparency of the atmosphere was determined, was carried out, the admissibility of the assumed values of P_λ was checked in each separate case.

The interstellar absorption was taken into account in accordance with [15], bearing in mind the results of [16] and, in particular, in the case of NGC 7662 the absorption per kpc was taken equal to the average of the values obtained by E. K. Kharadze for areas 42 and 43. The distances to the nebulae were taken from the catalogue of planetary nebulae [1].

All the photometric measurements were carried out on a MF-2 microphotometer. Characteristic curves were constructed for each set of plates separately. The mean brightness of the background was taken as unity and the brightness of the various details was expressed relative to it [16].

For all the nebulae measurements were carried out along 24 radial directions, at equal angles to each other. The rotation of the negative was carried out by means of a special attachment and the position angle could be determined to within ± 0°.1. The readings of the microphotometer were taken at every 2".1 in the case of NGC 6720, and 1".5 in the case of the remaining nebulae. The diaphragm of the microphotometer was in the form of a square with sides 1".43 long.

The brightness was measured at 700, 330 and 430 points on the images of the objects under consideration respectively. The values of brightness of the regions investigated lie within the ranges $17^m.47$-$20^m.60$, $14^m.02$-$17^m.42$ and $14^m.95$-$17^m.65$. The results were plotted in the form of isophots. When plotting each of these isophots the gradient of brightness between neighboring measurements was assumed to be constant.

Isophots obtained in nebular lines for the nebulae NGC 6720, 7009 and 7662 are shown in Figures 1-3.

NGC 6720. The size of the photometered image was 3.60 × 3.20 mm which on the scale of the negative corresponds to 108" × 96".

To begin with, one notes the similarity between the isophots for this nebula obtained in integral light [1] and the inner regions of the picture shown here. The distribution of brightness is symmetric relative to the major and minor axes of the image. The main bright ring is bounded by almost regular concentric ellipses (the curves $18^m.18$ and $20^m.18$). The brightness maxima lie at equal distances from the center. On either side of the major axis there are areas of increased brightness whose isophots have the form of a sickle.

The relatively low brightness along the major axis is characteristic of the majority of ring nebulae, including the present nebula. It is clearly noticeable that the greater the maximum brightness in a given direction the faster is its fall-off on the outer boundary of the nebula.

---

* The electrophotometric observations were carried out on clear nights.

In addition to the main ring, darkish formations are found in the peripheral regions of the nebula. This suggests a diffusing ring which, possibly, at one time enveloped the bright regions of the nebula.

NGC 7009. The size of the photometered image was 1.00 × 1.30 mm which corresponds to 30" × 39".

A comparison of the isophots obtained using the H_δ line [2] and the isophots given in the present paper confirms the well known result that the spatial distribution of radiating OIII atoms is identical with the distribution of hydrogen atoms. A certain similarity is also observed in the He^+ case. There is very little in common with isophots obtained using the lines 3727-3729 A which is probably due to a difference in the conditions of excitation of oxygen giving rise to the nebular lines and the violet doublet.

In the outer regions of the nebular image, a uniform increase in brightness towards the center is observed. In the peripheral areas of the bright part of the nebula projections resembling ends of ellipses may be observed along its minor axis. This suggests that one deals here with interpenetrating ellipsoidal shells whose major axes are mutually perpendicular. The characteristic bend in the inner isophots rapidly disappears and is not observed in the central regions. It is possible that one of the layers is so weak that its contribution to the brightness is not measureable in the bright regions of the nebula.

The peripheral formations resemble a diffusing ring which at one time enveloped the part of the nebula which is now bright.

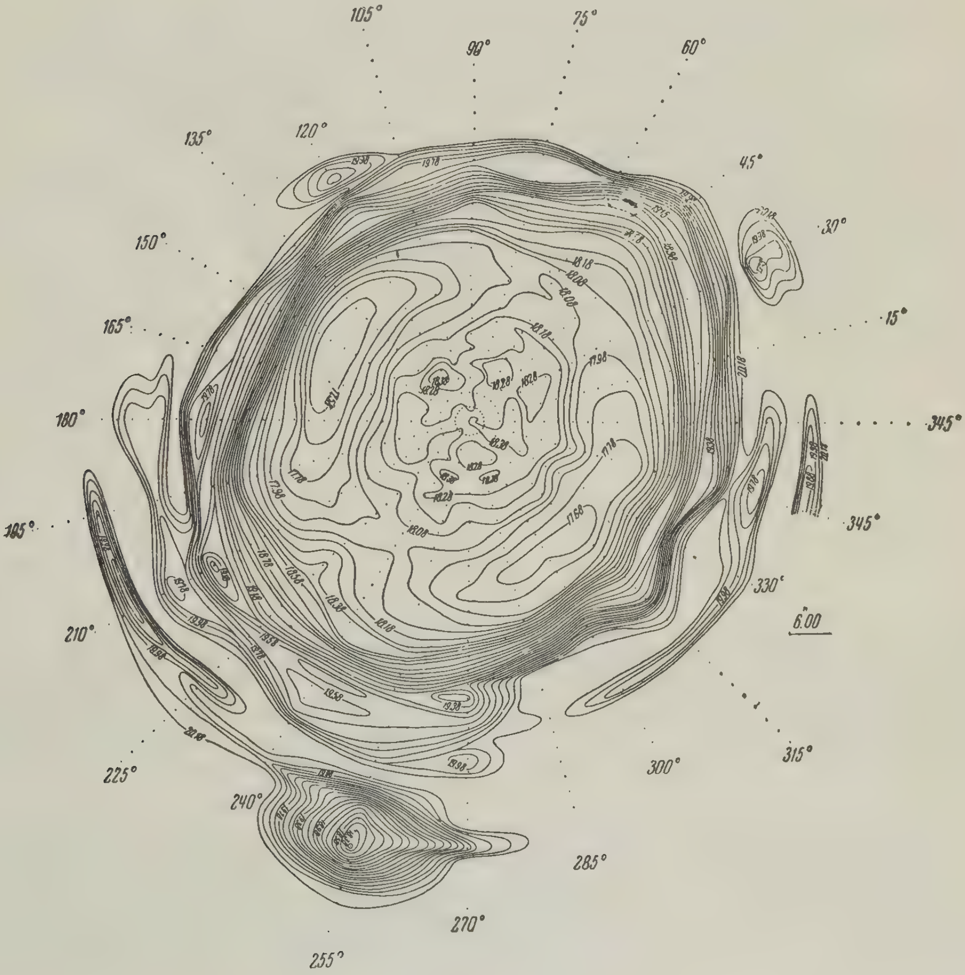

Fig. 1.

NGC 7662 was classified as IIIa + IV in [1], according to its external appearances, i. e., a ring-like formation is superimposed upon a circular disc with a complex and nonuniform distribution of brightness. These structural characteristics are clearly seen on the isophot plot shown here. However, the increase in brightness towards the center along the different radii of the disc is almost uniform and curves of equal brightness have almost circular form. In the classification of B. A. Vorontsov-Vel'iaminov this area of the nebula is closer to type IIa.

The inner bright region of the nebula is in the form of an open elliptical ring. The maximum brightness is observed in the middle of the ring, along the whole of its length.

The size of the nebula, determined from the dimensions of the outer disc, is, according to the catalogue, 28" x 32". We have succeeded in detecting the presence of radiating matter over a much greater region. The dimensions of the photometered image were 1.75 x 1.75 mm which corresponds to 52".5 x 52".5.

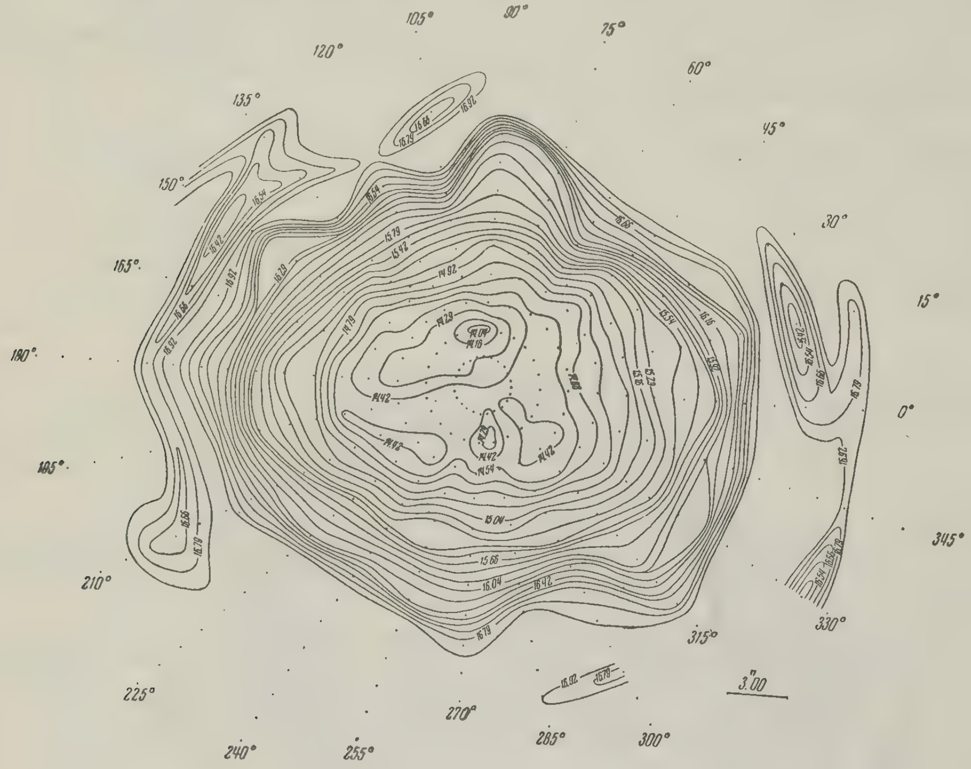

Fig. 2.

In addition to the well-known structural shapes, the nebula NGC 7662 has also some external formations. The position of these formations is extremely interesting. The separate and not very dark but well defined regions are disposed in such a way that if one draws a continuous smooth curve through their brightness maxima one obtains a spiral. Beginning at the disc of the nebula (p = 320°) its arm extends over 480°. At the point opposite to the beginning of the spiral one observes a region of increased brightness.

It is interesting that in the nebulae NGC 6720 and 7009 the total emission at the different position angles is constant to within 3 and 8% respectively, which has already been pointed out in [1] in the case of NGC 6720 (5%). B. A. Vorontsov-Vel'iaminov sees in this a confirmation of Zanstra's postulate which states that the nebula completely absorbs ultraviolet radiation from the nucleus. We are more inclined to consider that the above fact indicates that the spatial distribution of the emitting matter is symmetric in the above nebulae.

As was stated above, the majority of the isophots for the above nebulae are in the form of almost regular concentric ellipses of different eccentricity. The problem of how closely one can approximate the observed curves of equal brightness by ellipses, and how the parameters of these ellipses vary as one passes from the periphery towards the center of the image, is of well known interest. In this connection we used the method described by P. N. Kholopov [17].

Tables 2, 3 and 4 give the parameters of the ellipses which approximate to the curves of equal brightness in the images of the nebulae NGC 6720, 7009, and 7662, respectively. The first column gives the brightness corresponding to the isophot, and the subsequent columns give the major axis a of the ellipse, the ratio of the semiaxes η, and the position angle φ of the major semiaxis of the ellipse in an arbitrary system of coordinates common to all the nebulae.

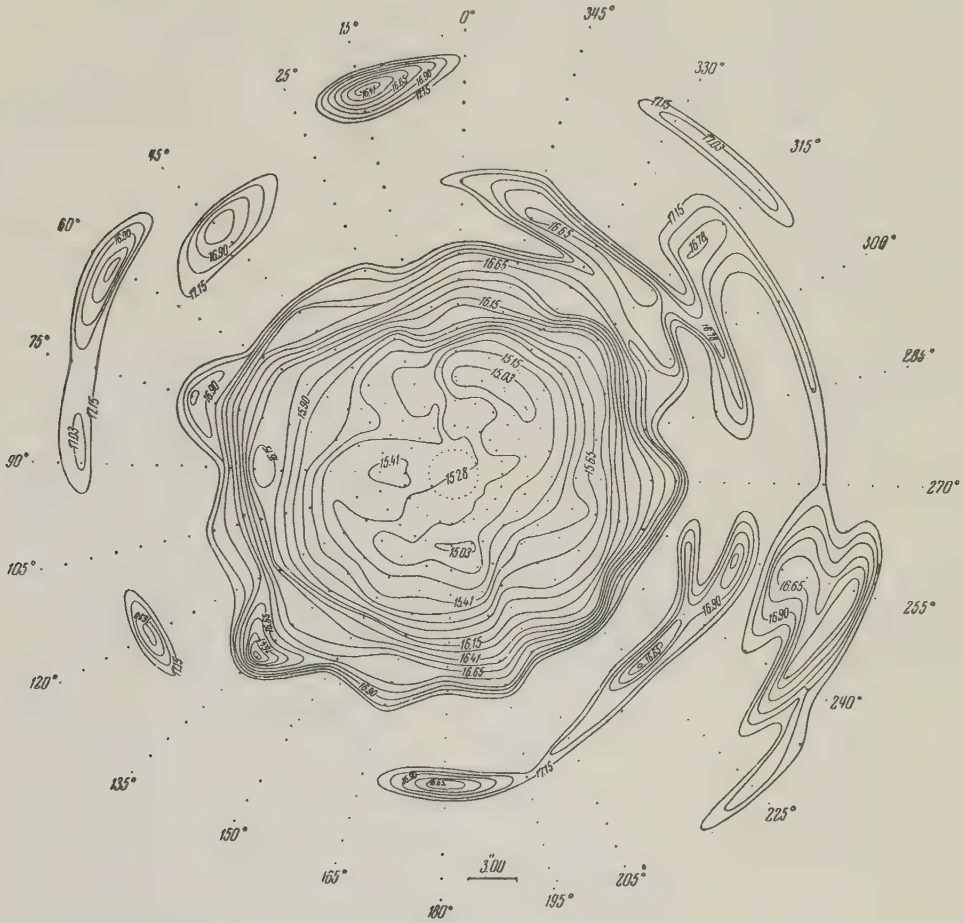

Fig. 3.

First of all, it must be stated that the curves of equal brightness for all the nebulae can be sufficiently well approximated by ellipses for which the ratio of the semiaxes lies between 0.63 and 0.93. Within the limits of error, the orientation of the major axes of the ellipses in the first two nebulae is the same; in the case of NGC 7662 no conclusion can be drawn because of appreciable errors in the calculations, and because its outer shell may, in the first approximation, be considered as spherical.* The bright ring in NGC 6720 is in reality bounded by concentric ellipses having an eccentricity of 0.63.

One notes the fact that the isophots for NGC 7009 can be quite well represented by concentric ellipses with almost equal eccentricities. However, it is easy to see that beginning with the isophots $15^m.16$, and as one goes towards the outer part, there is a continuous, although small, decrease in the eccentricity. The opposite and better defined picture is observed in NGC 6720, while the general character of changes in the eccentricity in the inner parts of both these nebulae is the same. The nebula NGC 7662 is characterized by a continuous decrease in the eccentricity.

---

* The inner isophots were not studied because of their rather peculiar form.

TABLE 2

M	$a\pm\Delta a$	$\eta\pm\Delta\eta$	$\varphi\pm\Delta\varphi$
18^m18	14″7 ± 1″0	0.78 ± 0.07	60°41′ ± 10°42′
18.08	17.4 ± 1.2	0.74 ± 0.07	53 29 ± 8 56
18.08	28.2 ± 0.9	0.91 ± 0.04	48 28 ± 15 20
18.38	31.2 ± 0.7	0.93 ± 0.03	51 54 ± 14 40
18.68	34.8 ± 1.0	0.85 ± 0.04	53 44 ± 7 13
18.98	37.2 ± 1.2	0.83 ± 0.04	53 39 ± 7 10
19.28	39.3 ± 1.5	0.82 ± 0.04	52 16 ± 7 10
19.58	41.7 ± 1.7	0.81 ± 0.04	49 04 ± 7 23
19.88	45.0 ± 2.2	0.78 ± 0.05	52 22 ± 7 20
20.18	47.1 ± 2.5	0.78 ± 0.06	54 29 ± 7 38

TABLE 3

M	$a\pm\Delta a$	$\eta\pm\Delta\eta$	$\varphi\pm\Delta\varphi$
14^m54	6″0 ± 0.″5	0.80 ± 0.10	163°49′ ± 15°12′
14.79	7.8 ± 0.5	0.75 ± 0.06	178 27 ± 4 48
14.92	8.2 ± 0.4	0.80 ± 0.05	181 01 ± 4 48
15.16	9.6 ± 0.5	0.78 ± 0.05	180 45 ± 4 48
15.42	10.8 ± 0.5	0.78 ± 0.05	178 45 ± 4 12
15.66	11.6 ± 0.5	0.79 ± 0.05	178 06 ± 4 12
15.92	12.2 ± 0.5	0.83 ± 0.05	173 14 ± 5 24
16.16	12.9 ± 0.6	0.84 ± 0.06	172 38 ± 10 36
16.42	13.6 ± 0.6	0.84 ± 0.05	172 17 ± 10 00
16.66	14.2 ± 0.6	0.84 ± 0.05	176 24 ± 10 00
16.92	15.0 ± 0.6	0.85 ± 0.05	174 10 ± 10 00

TABLE 4

M	$a\pm\Delta a$	$\eta\pm\Delta\eta$	$\varphi\pm\Delta\varphi$
15^m41	9″3 ± 1.″0	0.64 ± 0.09	144°16′ ± 7°48′
15.53	9.8 ± 0.9	0.69 ± 0.08	143 18 ± 7 54
15.65	10.0 ± 0.5	0.79 ± 0.05	137 20 ± 5 40
15.78	10.4 ± 0.3	0.86 ± 0.04	126 19 ± 8 48
16.03	11.1 ± 0.3	0.90 ± 0.03	119 14 ± 10 48
16.28	12.0 ± 0.3	0.92 ± 0.03	105 27 ± 12 12
16.53	12.9 ± 0.4	0.91 ± 0.04	112 39 ± 12 24
16.78	13.6 ± 0.3	0.93 ± 0.03	136 35 ± 15 06
17.03	14.4 ± 0.4	0.93 ± 0.04	136 07 ± 13 48
17.15	15.0 ± 0.4	0.90 ± 0.04	135 15 ± 11 36

As was already pointed out,the structure of the images of NGC 6720 and 7009 is very similar, which is probably due to a similarity in the spatial distribution of the radiating matter. The regular form of the curves of equal brightness and the identical orientation of their major axes, as well as the presence of symmetry in the distribution of brightness in the images of the above nebulae, suggest that the spatial form of layers of equal emission is a figure of revolution.

We cannot compare our results of absolute photometry of images of nebulae with the data of other authors since no such data exist. The estimates of the absolute brightness of NGC 6720 quoted in [3] give some idea of the brightness in integral light. However, one cannot agree with the author of [3] that the measured brightness is expressed in the units of the photographic system. In fact,by using the usual formula for the standardization of extrafocal photographs of stars [18], E. Brodskaia operates with photometric quantities which cannot be directly compared, namely, the photographic magnitude of the standard star and the ratio of brightness of the object and the standard star in the photometric system corresponding to the spectral sensitivity of the radiation detector employed.

We have calculated the total visual stellar magnitudes of the above nebulae in nebular lines. In the first column of Table 5 we give the number of the nebula, in the second the visual magnitude according to the data of F. Hopman [19], and in the third the brightness of the nebula in nebular lines in visual magnitudes according to our determination.*

TABLE 5

NGC	m_{vis}	m_{neb}
6720	$8^{m}78$	$8.^{m}99$
7009	—	8. 12
7662	8.41	8. 58

Remembering that in visual photometry of planetary nebulae only an insignificant percentage of radiation in the lines H_{α}, H_{β} and others is introduced into the total brightness, the agreement between the data given in Table 5 is good. It must be noted that had we used the well-known formula for the standardization of extrafocal photographs of stars given in [18], the quantity m_{neb} would have turned out smaller than m_{vis}.

The author is deeply indebted to A. F. Bogorodskii for suggesting this problem and his supervision of the present work, and to Prof. E. K. Kharadze for giving him the opportunity of carrying out the observations at the Abastuman Astrophysical Observatory.

Sumsk State Pedagogical Institute

Received August 17, 1956

LITERATURE CITED

[1] B. A. Vorontsov-Vel'iaminov, Gas Nebulae and New Stars [in Russian] (Izd. AN SSSR, 1948).

[2] L. Berman, Lick Observatory Bull. 15, 86 (1930).

[3] E. S. Brodskaia, Astron. J. (USSR) 20, 58 (1943).

[4] T. Page, Astrophys. J. 96, 78 (1942).

[5] L. Aller, Astrophys. J. 93, 236 (1941).

[6] H. Curtis, Lick Observatory Bull. 13 (1918).

[7] P. P. Parenago, Uspekhi Astr. Nauk 4 (Izd. AN SSSR, 1948).

[8] G. A. Tikhov, Trudy GAO** 66, Ser. II (1951).

[9] E. R. Mustel', Uspekhi Astr. Nauk 3 (Izd. AN SSSR, 1947).

[10] V. B. Nikonov, Soobshch. AN Gruz. SSR 3, No. 16, 509 (1942).

[11] T. G. Megrelishvili, Biull. Abast. obs. 9, 105 (1948).

[12] Sh. M. Chkhaidze, Biull. Abast. obs., II, 163 (1950).

[13] N. L. Magalashvili, Biull. Abast. obs. 10, 45 (1949).

[14] N. B. Kalandadze, Biull. Abast. obs. 10, 107 (1949).

[15] P. P. Parenago, Astron. J. (USSR) 22, 129 (1945).

---

*The values of m_{neb} are free of interstellar absorption ($0^{m}.23$, $0^{m}.12$ and $0^{m}.15$) and in the case of NGC 7009 and 7662 they are also free of the effect of the H_{β} emission.

It must be pointed out that our magnitudes are not the usual visual ones since in the calculation of R we only took into account the visibility curve V_{λ} without taking into account the transmission of the standard apparatus. However, as the comparison given below indicates, this difference is apparently not very great.

**Main Astronomical Observatory (in Pulkovo).

[16] E. K. Kalandadze, Biull. Abast. obs. 12 (1952).

[17] P. N. Kholopov, Astron.J. (USSR) 29, 671 (1952).

[18] N. N. Sytinskaia, Absolute Photometry of Extended Celestial Objects [in Russian] (A. A. Zhdanov Leningrad State University Press, 1948).

[19] F. Hopman, Astronomische Nachrichten 214, 425 (1921).

ON THE KINEMATIC PECULIARITIES OF B STARS

A. Ia. Filin

The problem of the kinematic peculiarities of B stars is investigated in this paper. The kinematic parameters of the B stars are determined from the radial and spatial velocities. The influence of the following three factors on the kinematic constants is investigated: 1) motion along a spiral arm, 2) admixture of stars of the spherical component, 3) error in the value of the mean absolute magnitude of B stars; it is shown that none of them can explain the peculiarities of B-star motions. It is established that the B0-B1 stars do not have any kinematic peculiarities. It is shown that for the B stars in the vicinity of the sun the normal form of the Kamm function is disrupted. It is concluded that there is a connection between the peculiarities of the B-star motions and the Local System.

INTRODUCTION

At the present time, there is no agreement on the causes of the kinematic peculiarities of B stars. At the same time, in view of the modern ideas on the problem of the origin of stars, the problem of the B stars is very important.

In the majority of cases the early B stars belong to the young galactic objects which to some extent still show the influence of the initial conditions prevailing when they were formed. These initial conditions are undoubtedly related to the observed peculiarities of B stars. The study of the individual kinematic peculiarities without relating them to other phenomena, for example, the physical characteristics and the spatial distribution, is incorrect. That a fifty-years' study of B stars has not led to a satisfactory explanation of the kinetmatic peculiarities of their motion up to the present, is a direct consequence of the methodologically incorrect way of setting the problem. To a large extent, the result of the incorrect approach and, because of this, the one-sided trend of the investigations is that up to now no detailed investigations of the spectra of a large number of B stars have been made, thus limiting the possibility of making various comparisons.

The only feature directly connected with the process of B-star formation which can be considered to be reliably established is the presence of the Local System. Even if the direct demonstration of the existence of the Local System introduces the well-known difficulties and can sometimes lead to contradictory results, the comparative study of spirals carried out by B.A. Vorontsov-Vel'iaminov [1] shows that the spiral arms of the Sc-type galaxies are mainly determined by concentrations of hot giants, of the type of the Local System, i.e., the hot giants in the spiral arms mainly exist in concentrations of various sizes.

Therefore, the Local System is a reliably established observation and the surmise that there is some connection between the peculiarities of the B-star motion and the presence of the Local System is completely natural and logical. The possibility of such a connection has already been considered in [2] and some of the peculiarities were satisfactorily explained by the rotation of the Local System [3, 4]. However, this work has not been developed further, and the question of explaining the other peculiarities remains open.

The problem of the connection between the kinematic peculiarities of B stars and the Local System is of considerable interest, particularly since it has not been investigated in detail up to the present time. The aim of the present paper, which is the first part of a work on the kinematic peculiarities of B stars, is to fill this gap in the study of B-star motions. In addition, other possibilities are also considered, but they either do not explain the observed peculiarities at all or only partially explain some of them.

1. Brief History of the Problem

The problem of the study of B-star motions can be said to have originated in 1904 when Adams and Frost [5] discovered the K-effect. In 1910 Kapteyn and Frost [6] confirmed its existence. After this, a large number of investigations of B-star motions were carried out and about ten explanations of the K-effect were proposed. All of these hypotheses are listed below.

1. The motion of B stars in elliptical orbits with high eccentricities [7, 8].
2. The motion of the Scorpius-Centaurus stream [9].
3. The regional nonstationary nature of the Local System [10].
4. The slow decrease of stellar masses [11].
5. The presence of convective currents in the atmospheres of B stars [12].
6. The experimental errors in the standard wavelength [13].
7. The acceleration of the motion of B-star groups as the result of mutual attraction [14].
8. The instability of circular orbits on the periphery of the Galaxy [15].

There is no need here to criticize separately each of these hypotheses, because they have been criticized in the paper of Torondzhadze [16]. Let us only point out that the above hypotheses suffer from a common defect, namely, in explaining the K-effect we have to assume the presence of other peculiarities which also need explaining. In addition, the numerous determinations of the K-effect vary considerably and, in particular, some of the values obtained can be completely explained by the Einstein effect; this happens, for example, in the case of Ali [17], who moreover did not find a decrease of K with distance as is customarily accepted. Pismis and Prieto [18] also found that for stars nearer than 750 ps the K-effect is small, while for more distant stars it is negative. Because of these results, it is questionable whether there is a large positive K-effect since it is hard to say what its value is and what has to be explained.

All of the above hypotheses have been proposed specifically to explain the K-effect. However, the existence of the K-effect follows from the theory of a nonstationary Galaxy. It is just the K-effect which describes the magnitude of the deviation of a stellar orbit from a circular orbit. In particular, the negative value of K for the long-period cepheids indicates that they move, on the average, in contracting orbits [28]. B stars, just as the long-period cepheids, belong to the young objects of the Galaxy. Therefore, it can be expected that both of these groups will also be similar kinematically. In the following we will see that the K-effect for B stars is also found to be negative. However, this does not mean that an exhaustive explanation of the K-effect has been found, since other kinematic peculiarities exist and the causes producing them can affect the magnitude of K.

After the discovery of galactic rotation some other peculiarities of the B-star motions were discovered, but for some reason or other the explanation of the K-effect was taken to be the main problem. This exclusive attention to the K-effect is not justified at all. In the presence of the other peculiarities, a successful explanation of the K-effect would not have solved the problem of the B stars. Using this approach, we would find it necessary to introduce a separate cause to explain each peculiarity. It is quite likely that further peculiarities will be discovered as the accuracy of the observations is increased and more varied methods are used; then all of the different causes will lead to contradictions. Even these purely formal considerations are enough to convince oneself that the problem has not been correctly set.

All of the peculiarities are undoubtedly associated and have a common cause. In individual cases other factors can also play a part, but the dominant cause must be the same. The search for this single cause, this basic feature, is the main problem in the study of B stars. Only with this approach to the problem of B-star motion can we hope to obtain satisfactory results. From this point of view, the above hypotheses used in attempting to explain the K-effect are only of historical interest.

The paper of Torondzhadze [16] is the only one in which the problem of the kinematic peculiarities of B stars is presented quite correctly; the peculiarities are considered to be the result of initial conditions associated with star formation. Starting from the assumption that the origin of B stars surrounding the sun is connected with the expansion of stellar associations, the author explains almost all of the observed peculiarities of B-star motion. However, since the hypothesis of the expansion of associations is not sufficiently substantiated (there are indications of this in the literature [19, 20]), the consequences of this hypothesis are also insufficiently substantiated, among them being the explanation of the kinematic peculiarities of B stars.

2. Observational Material

The results of the present work were mainly obtained using radial velocities. 1270 B stars with known radial velocities were used. The main data on these stars (radial velocities, spectra, distances) were taken from a card catalogue of the GAISh Department of Stellar Astronomy. As a rule, the spectra were determined from several sources and in most cases there were at least two determinations. When the distance of individual stars was calculated, the absolute magnitude was taken equal to the mean absolute magnitude of the appropriate subclass [21]. Absorption was taken into account by the method of P.P. Parenago [22]. The error of the individual distances determined in this way is 25%. The radial velocities were corrected for the Einstein red shift. The following corrections were taken (km/sec):

Spectrum	B0	B1	B2	B3	B4	B5
Correction	−2.0	−1.7	−1.4	−1.1	−1.0	−0.9

Stars of the Scorpius-Centaurus stream were excluded.

Improved values of the proper motions were taken from P.I. Bakulin's list [23] and for the investigations we selected 336 stars for which the error in the tangential velocity does not exceed 8 km/sec. In the following only these 336 stars were used in the calculations involving proper motions.

3. Kinematic Parameters of B Stars

Both the radial and spatial velocities were used to determine the kinematic constants. In the case of radial velocities, the conditional equations of the following type were solved by the method of least squares:

$$-X\cos l\cos b - Y\sin l\cos b - Z\sin b + P\sin 2l\cos^2 b -$$
$$- Q\cos 2l\cos^2 b + K\bar{r}\cos^2 b - V_r = 0,$$

where

$$P = A\bar{r}\cos 2l_0,\quad Q = A\bar{r}\sin 2l_0.$$

Standard symbols are used: X, Y, Z are the components of the sun's velocity along the axes of the usual galactic rectangular system of coordinates (the X axis is directed to the point $l = 0$, $b = 0$, the Y axis to the point $l = 90$, $b = 0$ and the Z axis to the point $b = 90°$), l and b are the spherical galactic coordinates of the star, A is the galactic-rotation constant, K is the K-effect constant, $\bar{r}$ is the mean distance of the stars considered from the sun, l_0 is the longitude of the rotation center and V_r is the observed radial velocity. $A\bar{r}$ and l_0 are given by the equations

$$A\bar{r} = \sqrt{P^2 + Q^2},\ \tan 2l_0 = \frac{Q}{P}.$$

The 1270 stars were divided into 36 groups (18 for the northern and 18 for the southern hemisphere), each group belonging to a longitude interval of 20°. The results of the solution are given in the second column of Table 1. The solar-velocity components given in the third column were determined from the spatial velocities

$$X = -\bar{V}_X,\ Y = -\bar{V}_Y,\ Z = -\bar{V}_Z.$$

When we calculated V_X, V_Y and V_Z, the proper motions corrected for the error in the precession constant were transformed into $\mu_l \cos b$ and μ_b with the help of Ohlsson's tables [24].

To determine the second constant of galactic rotation B, the values of A obtained using the radial velo-

TABLE 1

	Using V_r	Using spatial velocities	Using V_l	Using V_b	Average
X	$+16.0\pm0.2$	$+16.3\pm0.6$	—	—	$+16.0\pm0.2$
Y	$+7.2\pm0.2$	$+6.3\pm0.6$	—	—	$+7.1\pm0.2$
Z	$+6.7\pm0.8$	$+5.6\pm0.2$	—	$+7.7\pm0.3$	$+6.3\pm0.2$
P	$+12.3\pm0.2$	—	—	—	—
Q	-7.2 ± 0.2	—	—	—	—
$A\bar{r}$	$+7.6\pm0.2$	—	—	—	$+7.6\pm0.2$
$K\bar{r}$	-2.7 ± 0.2	—	—	—	-2.7 ± 0.2
A	$+12.3\pm0.3$	—	—	—	$+12.3\pm0.3$
K	-4.4 ± 0.3	—	—	—	-4.4 ± 0.3
B	—	—	-11.9 ± 0.7	—	-11.9 ± 0.7
l_0	$324°.0\pm0.°7$	—	—	—	$324°.0\pm0°.7$
$\bar{r}$	580	—	—	—	—

cities and the mean values of X and Y obtained using the radial and spatial velocities (given in the column headed "average") were substituted into the conditional equations of the form:

$$V_l = X \sin l - Y \cos l + A\bar{r} \cos 2\,(l - l_0) \cos b + B\bar{r} \cos b,$$

Similarly Z was determined from the conditional equations

$$V_b = X \cos l \sin b + Y \sin l \sin b - Z \cos b - A\bar{r} \sin 2\,(l - l_0) \sin b \cos b.$$

From the data of Table 1, the velocity of the sun and the coordinates of the apex are found to be

$$V_\odot = 18.6 \pm 0.2 \ \text{km/sec}, \qquad L = 24°.0 \pm 0°.7, \qquad B = +19°.8 \pm 0°.6,$$

sufficiently close to the standard values of these quantities.

The constant A is considerably smaller than is usually accepted for the objects of the disc subsystems. This result is in agreement with the majority of the previous determinations, as well as with the most recent data [25, 26].

TABLE 2

$\sigma_1 = 5.76 \pm 0.50$ km/sec
$\sigma_2 = 8.91 \pm 0.50$ "
$\sigma_3 = 9.94 \pm 0.50$ "
$L_2 = 8°.0 \pm 17°.0$
$B_2 = -4°.0 \pm 7°.0$
$L_3 = 278°.0 \pm 17°.0$
$B_3 = +6°.0 \pm 5°.8$

The elements of the velocity ellipsoid were obtained from the spatial velocities. The calculations were made according to the method described in [27]. The components of the spatial velocities were corrected for the motion of the sun, the galactic rotation, and the K-effect using the data of Table 1. The semiaxes of the ellipsoid and their directions are given in Table 2. The effects of errors in the velocity components were eliminated from these values. For the ratio of the axes we obtain 1:0.90:0.58 with an error of ±0.07.

These results therefore lead to the conclusion that for B stars:

1. The galactic rotation constants A and B are low.

2. The ratio of the velocity-ellipsoid axes lying in the galactic plane is close to unity. However, the ratio σ_1/σ_3 does not differ from that usually accepted for the disc-subsystem objects.

3. There is a considerable deviation of the direction of the velocity-ellipsoid major axis from the direction to the center of rotation.

4. As regards the other constants characterizing the motion, there are no differences between B stars and the other objects belonging to the disc subsystem.

4. On the Peculiarities of B Stars

In the paper of Torondzhadze [16] already mentioned the following kinematic peculiarities of B stars are listed:

1. The K-effect.

2. The abnornal values of the Oort coefficients A and B and of the longitude of the galactic center.

3. The tendency of O-B stars to form star streams.

4. The disagreement between the values of the velocity dispersions and the velocity of the sun relative to the bright O-B stars.

5. The negligible elongation of the velocity ellipsoid.

The peculiarities which require explanation must be established with sufficient confidence. Otherwise, there will always be a danger of explaining nonexistent peculiarities. On closer investigation it is found that some of the kinematic features listed above are classed as peculiarities without sufficient reasons. Let us consider them closer.

The K-effect is treated as a peculiarity because large positive values were obtained. It was pointed out above that the numerical values obtained for the K-effect are highly uncertain and, therefore, there are no reasons for ascribing to it a high positive value. In our solution, based on more material, K was found to be negative and of the order of −3 km/sec. Running somewhat ahead, let us remark that a number of variants of the solutions, obtained using radial velocities, will be given below and K remains negative in all cases. Consequently, there are no reasons for considering the K-effect to be a peculiarity, particularly since our results are in good agreement with the values of K obtained for the other objects of the disc subsystems, for example, the long-period cepheids [28, 29] or the dispersed stellar clusters [30, 31].

The abnormal value of the galactic-center longitude (center of rotation l_0). The longitude of the center of rotation has been determined by a number of investigators, but the majority of these determinations (a detailed review of them is given in [16]) are so uncertain that it is impossible to draw any conclusion from them as to the magnitude of l_0. From all the known determinations only seven (including ours), where the errors did not exceed ±5°, were selected. Their weighted mean value is

$$l_0 = 320^\circ.8 \pm 0^\circ.6,$$

which differs by only 4°.2 from the value $l_0 = 325^\circ$, accepted as the mean value for stars of other spectral classes. The difference is not sufficiently large to be considered anomalous.

The tendency of B stars to form star streams. This peculiarity is doubtful for the following reasons. First, the identification of small star streams was not carried out for stars of later spectral types, as was done by Markovich [32] for B stars,and it is unknown whether this is a tendency of B stars only. Second, among the large, well-defined streams, the stream in Ursa Major [33] and the Hyades [34] do not contain B stars. Consequently, there are no reasons to believe that the tendency to form streams is a characteristic of only the B stars.

From the above arguments, however, we cannot conclude that these three kinematic features are definitely not peculiarities. We can only say that at the present time there are no sufficient reasons for any kind of a definite conclusion.

Therefore, the following can be classed as kinematic peculiarities of B stars:

1. The abnormal value of the galactic-rotation constants A and B.

2. The negligible elongation of the velocity ellipsoid.

3. The disagreement between the values of the velocity dispersion and the velocity of the sun relative to the bright B stars. This peculiarity, however, is not independent of the others and may be a consequence of the preceding one.

4. The north-south asymmetry in the proper motions and radial velocities.

The latter peculiarity, investigated in detail by R.B. Shatsova [3, 4], for some reason or other is not contained in the list given in [16].

The abnormal values of A and B obtained from observation do not show that B stars actually participate in the galactic rotation. From the data of Table 1 the angular velocity at a distance R_0 from the galactic center is

$\Omega_0 = 24.2$ km/sec/kps. If $R_0 = 7.2$ kps, then the linear velocity is $v_0 = 174$ km/sec, i.e., the centroid of the B stars must move relatively to the sun with a velocity of the order of 60 km/sec but this is not observed. Consequently, the B stars participate in the galactic rotation in the same way as the other objects of the disc component and the reasons for the anomalies in the constants A and B, as well as the reasons for the other peculiarities, are not associated with galactic rotation.

Let us now investigate some general causes which can influence to some extent the values of the kinematic constants. None of them had been investigated in detail before.

We will restrict ourselves to the investigation of the influence of these factors on the value of A, since it is pointless to explain the other peculiarities if the anomaly in A cannot be explained.

5. Motion Along a Spiral Arm

It is known that stars of the early spectral classes are situated along the spiral arms of galaxies. In addition to the general motion because of galactic rotation, internal motions within the spiral arm itself may exist. The most probable is motion along the spiral arm. This motion has been considered as a possible reason for the rather complicated behavior of the K-effect [35].

Let us assume that a group of neighboring B stars is moving with a velocity V_1 along a tangent to the spiral arm in a direction opposite to the direction of galactic rotation (Figure 1). S is the sun, S_1 a star, V_0 and V are the velocities of the sun and the star, respectively, as the result of galactic rotation, C is the center of the Galaxy in the direction l_0. The sun does not take part in this motion. Let us assume that the spiral is a logarithmic one

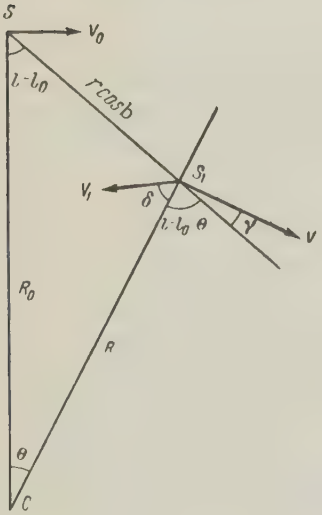

Fig. 1.

$$R = ae^{b\varphi},$$

where a is a constant and arc cot b = δ is the angle between the radius vector and the tangent to the spiral. Projecting all velocities in the line of sight, we obtain

$$\Delta V_r = V\cos\gamma\cos b - V_0\sin(l-l_0)\cos b + \\ + V_1\cos[(l-l_0)+\theta]\cos b.$$

The first two terms give the effect of galactic rotation $Ar\sin 2(l-l_0)\cos^2 b$. The last term, in view of the fact that

$$\cos\theta = \frac{R_0 - r\cos(l-l_0)\cos b}{R}$$
$$\sin\theta = \frac{r\sin(l-l_0)\cos b}{R},$$

can be transformed into the form

$$V_1\frac{R_0}{R}\left[\cos(l-l_0+\delta) - \frac{r}{R_0}\cos\delta\cos b\right]\cos b.$$

Let us expand R_0/R as a series and keep only the terms to the first order in r/R_0. Then

$$\frac{R_0}{R} = 1 + \frac{r}{R_0}\cos(l-l_0)\cos b.$$

After performing all the substitutions, we find that

$$\Delta V_r = -\frac{1}{2}\frac{V_1\sin\delta}{R_0}r\sin 2(l-l_0)\cos^2 b + V_1\cos(l_0-\delta)\cos l\cos b + \\ + V_1\sin(l_0-\delta)\sin l\cos b - \frac{V_1\cos\delta}{R_0}r\sin^2(l-l_0)\cos^2 b$$

and the radial velocity is

$$V_r = -[X - V_1 \cos(l_0 - \delta)] \cos l \cos b - [Y - V_1 \sin(l_0 - \delta)] \sin l \cos b -$$
$$- Z \sin b + \left[A - \frac{1}{2}\,\frac{V_1 \sin \delta}{R_0}\right] r \sin 2(l - l_0) \cos^2 b - \frac{V_1 \cos \delta}{R_0}\, r \sin^2 (l - l_0) \cos^2 b.$$

As can be seen from this expression all of the constants are altered and in addition a term appears, proportional to the distance. If we take $\delta = 82°$ (which corresponds to $b = 0.2$) and $l_0 = 330°$, then $\sin(l_0 - \delta) = -0.93$, and the biggest change should occur in y. Actually, this does not happen. Consequently, if there is motion along the spiral arm, the motion must be small. In this case, however, all the other corrections are also small and the constants are practically unchanged.

6. Admixture of Stars of the Spherical Component

The objects belonging to the spherical subsystems are characterized by a small velocity of galactic rotation and an almost spherical distribution of velocities. Therefore, if among the neighboring stars there is a fraction belonging to the spherical component, the value of the constant A will be decreased and the velocity distribution will tend to a spherical one. The fact that B stars exist with large z coordinates can be the basis for such an assumption. It is possible that some of them belong to the spherical component. Seventy-one such stars with $|z| > 300$ ps have been found and because of this, 150 stars can be taken to belong to the spherical component.

The approximate number of spherical-component stars required can be evaluated in the following way. We assume that in a certain region there is a mixture of stars of the disc and spherical components. Let n_1 be the number of the former, n_2 that of the latter. Let us assume that their mean distances from the sun are the same, $\bar{r}_1 = \bar{r}_2 = \bar{r}$. Let A_1 be the galactic-rotation constant for the disc component, A_2 be that for the spherical component and A be the observed value. Let us assume further that the stars are uniformly distributed with longitude. Then the absolute value of the mean radial velocity (corrected for the solar motion and the K-effect) in the direction (l, b) will be

$$\frac{n_1 A_1 \bar{r}\, |\sin 2(l - l_0)| \cos^2 b + n_2 A_2 \bar{r}\, |\sin 2(l - l_0)| \cos^2 b}{n_1 + n_2} =$$
$$= A\bar{r}\, |\sin 2(l - l_0)| \cos^2 b.$$

If we take a small volume and average this equation over all directions (in doing this we can assume that the average value of $\cos^2 b$ is the same for both groups), we will obtain

$$A = \frac{A_1 k + A_2}{k + 1},$$

where $k = n_1/n_2$. If we take $A_1 = +20$ km/sec/kps and $A_2 = +5$ km/sec/kps, the observed value $A = +12.3$ km/sec/kps will be obtained with $k = 1$, i.e., the stars of the two components must be present in equal numbers. If we take into account the inequality of the mean values of $\cos^2 b$, then k increases to 1.3. k can be as high as 2 if other differences are taken into account. But even if $k = 3$, 320 of the 1270 stars taken must belong to the spherical component. Actually, as we have seen, there are considerably fewer of them. Further, according to P.G. Shnirel'man [36] for B stars $\beta = 49$ ps, which also points to the very small admixture of spherical-component stars. Finally, the latter have a very high dispersion of velocities and a considerable admixture of them would have resulted in an increase of the velocity dispersion of all the stars considered. As can be seen from Table 2, their actual dispersion is less than that normally observed for objects of the disc subsystems.

Only a very small part of the decrease of the galactic-rotation constant A can therefore be explained by the influence of stars of the spherical component.

7. Incorrect Value of the Mean Absolute Magnitude of B Stars

The anomaly in the galactic-rotation constants can be associated with an error in the determination of the mean distance of B stars which can be produced by an uncertainty in the mean absolute magnitude and an error in the value of the mean absorption. Let us investigate the influence of these errors on the magnitude of A.

We introduce the following notation: $\overline{r}_H$ is the mean distance determined with an error in the mean absorption $\overline{\Delta}_H$, and $\overline{r}'_H$ is the corrected mean distance determined using the corrected value for the mean absorption $\overline{\Delta}'_H$. Let us use the well-known relations*

$$\lg \overline{r}'_{\mathrm{H}} = 0.2\,(\overline{m} - \overline{M} - \overline{\Delta}'_{\mathrm{H}}) + 1 + \lg C,$$

$$\lg \overline{r}_{\mathrm{H}} = 0.2\,(\overline{m} - \overline{M} - \overline{\Delta}_{\mathrm{H}}) + 1 + \lg C,$$

where $\log C$ is the correction for the dispersion of the absolute magnitudes. Subtracting the second equation from the first, we find

$$\lg \overline{r}'_{\mathrm{H}} = \lg \overline{r}_{\mathrm{H}} + 0.2\,\overline{\Delta}_{\mathrm{H}}\,(1 - q),$$

where $q = \overline{\Delta}'_H / \overline{\Delta}_H$. Since the B stars are situated near the galactic plane, we can take $\overline{\Delta}_H = \overline{a}_0 \overline{r}_H$, where $\overline{a}_0$ is the mean absorption per unit distance in the galactic plane. The above expression can now be written as

$$\lg \overline{r}'_{\mathrm{H}} = \lg \overline{r}_{\mathrm{H}} + 0.2\,\overline{a}_0\,\overline{r}_{\mathrm{H}}\,(1 - q). \tag{I}$$

If the mean absolute magnitude has also been incorrectly determined, then we can write

$$\lg \overline{r}'_{\mathrm{H}} = 0.2\,(\overline{m} - \overline{M}_{\mathrm{H}} - \overline{\Delta}'_{\mathrm{H}}) + 1 + \lg C,$$

$$\lg \overline{r}_{\mathrm{B}} = 0.2\,(\overline{m} - \overline{M}_{\mathrm{B}} - \overline{\Delta}_{\mathrm{B}}) + 1 + \lg C.$$

Here, $\overline{M}_B$ and $\overline{M}_H$ are the corrected and uncorrected values of the mean absolute magnitudes, respectively, and $\overline{r}_B$ and $\overline{\Delta}_B$ the mean distance and the mean absorption after correction of the zero point. From these equations we find

$$\lg \frac{\overline{r}'_{\mathrm{H}}}{\overline{r}_{\mathrm{B}}} = 0.2\,(\overline{M}_{\mathrm{B}} - \overline{M}_{\mathrm{H}}) - 0.2\,(\overline{\Delta}'_{\mathrm{H}} - \overline{\Delta}_{\mathrm{B}}),$$

from which

$$\overline{M}_{\mathrm{B}} - \overline{M}_{\mathrm{H}} = 5 \lg \frac{\overline{r}'_{\mathrm{H}}}{\overline{r}_{\mathrm{B}}} + \overline{a}_0\,(\overline{r}'_{\mathrm{H}} - \overline{r}_{\mathrm{B}}).$$

From Equation (I) we find

$$\overline{r}'_{\mathrm{H}} = \overline{r}_{\mathrm{H}} \cdot 10^{0.2\overline{a}_0\overline{r}_{\mathrm{H}}\,(1-q)}; \quad \lg \frac{\overline{r}'_{\mathrm{H}}}{\overline{r}_{\mathrm{B}}} = \lg \frac{\overline{r}_{\mathrm{H}}}{\overline{r}_{\mathrm{B}}} + 0.2\overline{a_0}\,\overline{r}_{\mathrm{H}}\,(1 - q).$$

Substituting this into the preceding equation and keeping in mind that

$$\frac{\overline{r}_{\mathrm{H}}}{\overline{r}_{\mathrm{B}}} = \frac{A_{\mathrm{B}}}{A_{\mathrm{H}}},$$

where A_B and A_H are the corrected and uncorrected values of the galactic-rotation constant, we find

$$\overline{M}_{\mathrm{B}} - \overline{M} = 5 \lg \frac{A_{\mathrm{B}}}{A_{\mathrm{H}}} + \overline{a}_0\,\overline{r}_{\mathrm{H}}\,(1 - q) + \overline{a_0\,r}_{\mathrm{H}} \left[10^{0.2\overline{a_0 r}_{\mathrm{H}}\,(1-q)} - \frac{A_{\mathrm{H}}}{A_{\mathrm{B}}} \right].$$

In the present case $A_H = +12.3$ km/sec/kps, $A_B = 19.5$ km/sec/kps, $\overline{r}_H = 0.6$ kps, $\overline{a}_0 = 3^m$ per kiloparsec, and $q = 0.8$ since there are reasons for believing that the absorption determined by the method of P.P. Parenago is overestimated by approximately 20%. Substituting these values into the last equation, we obtain

---

* 'lg' ≡ 'log' — Publisher.

$$\Delta\overline{M} = \overline{M}_B - \overline{M}_H = +1^m.7.$$

The correction is too high, and, of course, not acceptable. In fact it hardly can exceed $+0.^m5$ and the decrease of the galactic-rotation constant can only be partially explained. Thus, we cannot explain the peculiarities of B stars by the causes investigated. To establish the actual causes it is necessary to study in greater detail the neighboring group of B stars. In the following paragraphs we will consider the problem of the nonuniformity of the B-star system and the behavior of the Kamm function.

8. Nonuniformity of the B-Star System

Numerous investigations of the spatial distribution of B stars have established the nonuniformity of the B-star system. Therefore, it is natural to assume that there will also be a kinematic nonuniformity. Two versions of the calculations using radial velocities were carried out with the aim of establishing, even if approximately, the nature of this nonuniformity. In one case the calculations were carried out for a group of stars with different distances, in the other for stars of various spectral subclasses. The conditional equations of the form

$$-X\cos l\cos b - Y\sin l\cos b - Z\sin b + A\bar{r}\sin 2(l - l_0)\cos^2 b + K\bar{r}\cos^2 b - V_r = 0.$$

were solved. l_0 was taken equal to 330°. The results are given in Tables 3 and 4.

TABLE 3

Limits of r	n	$\bar{r}$	X	Y	Z	A	K
⩽200	110	154	+15.3±0.2	+10.1±1.0	+12.9±0.9	—17.5±7.8	+3.2±5.3
200—400	401	304	+18.0±0.5	+ 4.2±0.6	+ 9.6±1.0	+13.8±1.6	—4.9±1 3
400—600	263	502	+16.0±0.5	+ 2.3±0.7	+ 9.6±2.2	+10.8±1.2	—8.4±1.0
600—800	162	711	+13.5±0.5	+ 6.2±0.8	+10.0±2.4	+10.5±1.1	—5.1±0.7
800—1000	146	918	+ 7.7±0.9	+ 4.6±1.5	—20.5±5.4	+28.5±1.6	—7.4±1.0
1000—1400	126	1204	+15.4±1.1	+10.7±2.2	—15.6±6.7	+12.0±1.4	—6.3±1.1
1400—2000	69	1670	+10.4±2.4	+ 7.9±3.9	+ 9.3±12.2	+14.0±2.2	—3.5±1.4

TABLE 4

Sp	n	$\bar{r}$	X	Y	Z	A	K
B0	96	944	+17.8±2.8	+ 9.5±2.8	—14.9±18.2	+24.4±3.4	—4.5±2.3
B1	84	872	+14.6±2.6	+ 7.7±2.7	—15.6±10.7	+25.2±3.2	—3.9±2.2
B2	183	724	+16.6±0.3	+ 9.6±0.4	— 1.6±2.8	+10.5±0.3	—1.4±0.3
B3	434	557	+16.9±0.4	+ 8.8±0.5	+10.1±2.1	+10.6±0.8	—0.9±0.8
B4	149	777	+15.1±0.8	+12.8±1.3	+ 8.2±4.5	+ 7.2±1.4	—4.1±1.0
B5	318	460	+16.6±0.2	+ 6.4±0.6	+ 6.4±1.4	+ 6.7±1.4	—4.6±0.2

TABLE 5

	B0—B1	B2—B3			B4—B5		
	Using V_r	Using V_r	Using V_l	Average	Using V_r	Using V_l	Average
X	+15,2±0.7	+17.5±0.3	+12.2±0.5	+16.0±0.3	+14,2±0.4	+14.4±0.5	+14.3±0.3
Y	+ 8.5±0.7	+ 7.7±0.4	+ 5.3±0.5	+ 6.8±0.3	+ 9.3±0.5	+ 5.2±0.5	+ 7.2±0.4
Z	(+7.0)	+ 6.0±1.3	—	+ 6.0±1.3	+ 6.1±1.4	—	+ 6.1±1.4
$A\bar{r}$	+21.4±0.8	+ 6.3±0.4	—	+ 6.3±0.4	+ 3.6±0.4	—	+ 3.6+0.4
$K\bar{r}$	— 4.9±0.5	— 1.8±0.3	—	— 1.8±0.3	— 2.5±0.3	—	— 2.5±0.3
A	+23.2±0.9	+10.4±0.6	—	+10.4±0.6	+ 6.5±0.7	—	+ 6.5±0.7
B	—	—	—11.8±1.6	—11.8±1.6	—	— 7.9±1.6	— 7.9±1.6
K	— 5.3±0.5	— 3.0±0.4	—	— 3.0±0.4	— 4.4±0.5	—	— 4.4±0.5
n	180	620	182	—	467	130	—
$\bar{r}$	911	606	272	—	561	225	—

TABLE 6

$\sigma_1 = 4.7 \pm 1.2$ km/sec
$\sigma_2 = 7.5 \pm 1.2$ "
$\sigma_3 = 10.6 \pm 1.2$ "
$L_3 = 292° \pm 10°$
$B_3 = -10° \pm 11°$

Table 3 shows that the values of the velocity components of the sun vary considerably; this may be associated with a nonuniform distribution of the stars with galactic longitude and with various local irregularities. The values of A and K, on the other hand, are more alike, although anomalies are also observed here (the results for the group with $r \leq 200$ ps are not to be included, since they are highly uncertain).

From Table 4 it is immediately seen that the value of the constant A depends on the spectral subclass taken. The stars can be divided into three groups according to the value of A: B0-B1, B2-B3, and B4-B5. The results for each of these groups are given in Table 5.

For the group B0-B1, the solution was obtained using only the radial velocities since there are only 24 stars with a reliable value of the proper motion; Z was not determined at all, but was set equal to +7.0 km/sec. For the groups B2-B3 and B4-B5, the solutions were obtained using V_r and V_l. In the last case A was not determined, but the value determined from the radial velocities was used.

The constant A for the B0-B1 stars came out somewhat high. However, if the mean absorption is decreased by 20%, A is found to be very close to the usual value: +19.5 km/sec/kps. Taking $q = 0.8$, we obtain, from Equation (I) and $\bar{r}_H = 0.911$ kps, the mean distance as 1.171 kps; with the observed value $A\bar{r} = +21.4$ km/sec we then get

$$A = +18.3 \pm 0.7 \text{ km/sec/kps.}$$

It is obvious that the constant B must also have the normal value.

Similar results are obtained in the case of the velocity distribution. The semiaxes of the ellipsoid were determined using only 24 stars. Clearly, this is insufficient, but there is no point in using other stars with proper motions less reliably known, since the result obtained in this case could be even more uncertain. Table 6 gives the magnitudes of the ellipsoid semiaxes and the direction of the longer one for the B0-B1 stars. The ratio of the axes is 1 : 0.70 : 0.45. After the mean distance is corrected, the value of K is found to be (-4.2 ± 0.4) km//sec/kps.

TABLE 7

	B2—B3	B4—B5
σ_1	6.52 ± 0.35 km/sec	6.13 ± 0.70 km/sec
σ_2	9.54 ± 0.35 »	8.50 ± 0.70 »
σ_3	10.20 ± 0.35 »	9.74 ± 0.70 »
L_3	$274\overset{\circ}{.}1 \pm 46.2$	$276\overset{\circ}{.}3 \pm 22\overset{\circ}{.}4$
B_3	$+10\overset{\circ}{.}0 \pm 9\overset{\circ}{.}2$	$6\overset{\circ}{.}7 \pm 9\overset{\circ}{.}1$
Ratio of axes	1 : 0.94 : 0.64	1 : 0.87 : 0.63

Thus, the B0-B1 stars do not differ from the other elements of the disc subsystem as regards their motion. According to [36] B0-B1 stars, with rare exceptions, do not belong to the Local System. Consequently, there are reasons to believe that the kinematic peculiarities are somehow connected with the Local System.

The majority of the B2-B5 stars belong to the Local System and in their case the peculiarities are well defined. As regards the differences between B2-B3 and B4-B5 stars, they are not sufficiently marked and we cannot assume that there is a lack of uniformity here also, particularly since the velocity distributions of the stars are almost the same for the two groups. Therefore, no distinction was made below and the groups B2-B5 were investigated as a whole. Table 7 gives the results of the determination of the velocity-ellipsoid parameters.

9. The Kamm Function

With the help of the function

$$f(R, R_0) = R_0 [\Omega - \Omega_0] = V'_r \csc (l - l_0) \sec b,$$

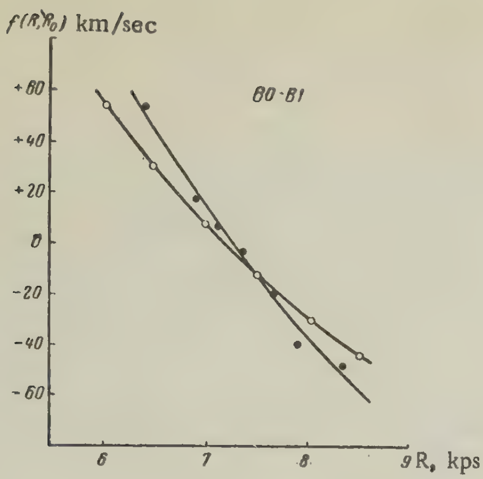

Fig. 2.

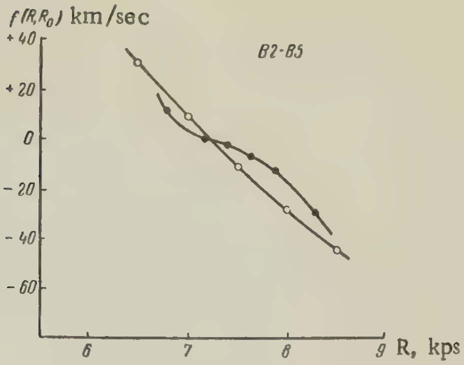

Fig. 3.

called the Kamm function, we can study the galactic rotation without any limitations on the distance. Here V'_r is the stellar radial velocity from which all motions, with the exception of galactic rotation, have been eliminated, Ω is the angular velocity at a distance R from the galactic center, and Ω_0 is the angular velocity at a distance R_0.

The Kamm function for B0-B1 stars is given in Table 8 and Figure 2. The data of Table 5 were used in calculating it. Since for stars with $l - l_0$ nearly equal to 0° or 180° the function $f(R, R_0)$ is strongly affected by the large values of csc $(l - l_0)$ sec b, values of the Kamm function were multiplied by the weighting factor

$$W = |\sin(l - l_0)\cos b|.$$

Only those values of $f(R, R_0)$ were used for which $W \geq 0.3$. The points give the observed values of $f(R, R_0)$, the open circles the theoretical values calculated from the following equation [21]:

$$f(R, R_0) = V_0\left[\frac{\alpha}{\alpha_0} - 1\right],$$

where $\alpha_0 = (h/k)^2$ is the square of the ratio of the velocity-ellipsoid semiaxes lying in the galactic plane, $V_0 = 233$ km/sec is the velocity of galactic rotation at a distance $R_0 = 7.2$ kps from the galactic center, and

$$\frac{\alpha}{\alpha_0} = \frac{1}{\alpha_0 + (1 - \alpha_0)\left(\frac{R}{R_0}\right)^2}.$$

α_0 was taken equal to 0.4.

TABLE 8

$\bar{R}$	n	$f(R, R_0)$	ΣW	σ_f
6.37	11	+54.0	5.66	±2.6
6.91	28	+18.3	21.85	1.3
7.09	9	+ 7.3	7.17	2.3
7.36	27	— 3.3	21.90	1.3
7.65	19	—19.0	14.32	1.6
7.88	15	—39.3	13.03	1.7
8.33	17	—47.1	13.47	±1.7

TABLE 9

$\bar{R}$	n	$f(R, R^0)$	ΣW	σ_f
6.77	116	+11.6	77.02	±0.6
7.14	226	+ 0.2	197.00	0.4
7.37	266	— 2.4	199.17	0.4
7.63	118	— 6.8	71.57	0.6
7.88	77	—12.1	52.37	0.7
8.27	58	—28.6	36.80	±0.8

Tables 8-11 were constructed in the same way and do not require explanation, except that the last column gives the mean errors of the mean values of the Kamm function. In calculating the errors, we assumed that

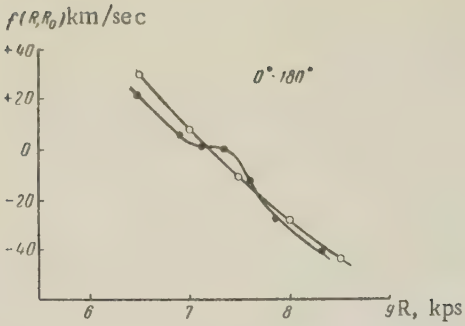

Fig. 4.

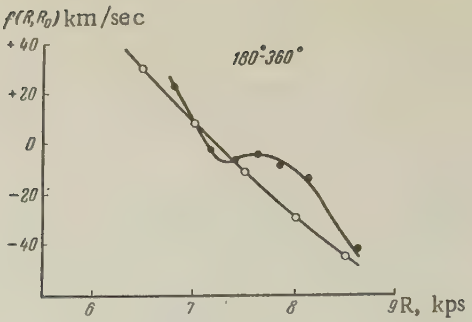

Fig. 5.

weight 1 corresponds to an error which is equal to the mean proper radial velocity; for B0-B1 stars this is +6.2 km/sec and for B2-B5 stars +5.0 km/sec.

The systematic discrepancy between the theoretical and observed curves of Figure 2 can be completely explained if the distances of B0-B1 stars are underestimated, which, as we have seen, is related to the inaccuracy in the determination of the absorption.

The Kamm function for the B2-B5 stars is given in Table 9 and Figure 3. It is seen that there is an obvious discrepancy between theory and observation, particularly for values of R between R = 7.3 kps and R = 8.3 kps, i.e., for a comparatively close neighborhood of the sun. Judging from the appearance of the curve, we see that the observed values must coincide with the theoretical ones for distances R > 8.4 kps and R < 6.8 kps.

The results presented definitely indicate that the kinematic peculiarities of B stars are associated with the Local System. It is known that the Local System is situated asymmetrically relative to the line joining the sun to the galactic center. The majority of stars are found between $l - l_0 = 180°$ and $l - l_0 = 360°$. Consequently, if the behavior of the Kamm function is really affected by the Local-System stars, then for $l - l_0$ in the range 0-180° there must be a better agreement between the theoretical and experimental curves than for $l - l_0$ in the range 180-360°. This behavior can be seen well in Figures 4 and 5 and Tables 10 and 11 corresponding to them.

TABLE 10

(Interval 0-180°)

$\bar{R}$	n	$f(R, R_0)$	ΣW	σ_f
6.47	31	+22.2	16.46	±1.2
6.90	69	+ 5.9	49.75	0.7
7.12	132	+ 1.6	116.81	0.5
7.36	129	+ 0.5	102.70	0.5
7.61	33	−12.0	22.77	1.0
7.86	17	−27.2	12.25	1.4
8.28	19	−40.7	12.83	±1.4

TABLE 11

(Interval 180-360°)

$\bar{R}$	n	$f(R, R_0)$	ΣW	σ_f
6.81	16	+22.8	10.83	±1.5
7.16	93	− 1.6	80.18	0.6
7.38	138	− 5.5	96.40	0.5
7.63	86	− 3.5	48.80	0.7
7.85	62	− 8.2	39.46	0.8
8.09	25	−13.4	16.45	1.2
8.60	14	−41.1	7.52	±1.8

Therefore, the assumption that there is a connection between the Local System and the kinematic peculiarities of B stars is confirmed as the result of the above analysis. The supporting evidence may be summarized as follows:

1. The B0-B1 stars that do not belong to the Local System do not show any anomalies.

2. The change in the appearance of the Kamm function is associated with the peculiarities of the spatial distribution of B stars, determined by the Local System.

3. The north-south asymmetry in the proper motions and the radial velocities is adequately explained by the rotation of the Local System.

LITERATURE CITED

[1] B.A. Vorontsov-Vel'iaminov, Astron. J. (USSR) 28, 43 (1951).

[2] K.F. Ogorodnikov, Uchenye Zapiski Leningrad Gosudarst. Univ. 15, 22, 3 (1950).

[3] R.B. Shatsova, Uchenye Zapiski Leningrad Gosudarst. Univ. 15, 22, 113 (1950).

[4] R.B. Shatsova, Uchenye Zapiski Leningrad Gosudarst. Univ. 16, 25, 67 (1952).

[5] E.B. Frost and W.S. Adams, Publ. Univ. Chicago 8, 247 (1904).

[6] J.C. Kapteyn and E.B. Frost, Astrophys. J. 32, 83 (1910).

[7] E. Freundlich and E. v.d. Pahlen, Astronomische Nachrichten 218, 369 (1923).

[8] I.F. Polak, Astron. J. (USSR) 13, 19 (1936).

[9] J.S. Plaskett and J.A. Pearce, Monthly Notices Roy. Astron. Soc. 94, 679 (1934).

[10] K.F. Ogorodnikov, Astron. J. (USSR) 21, 47 (1944).

[11] K. Pilowski, Z. Astrophys. 3, 53 (1931).

[12] W.W. Campbell, Lick Observatory Bull. 8, 82 (1914).

[13] S. Albrecht, Astrophys. J. 40, 473 (1914).

[14] V.V. Radzievskii, Biull. VAGO No. 6, 16 (1949).

[15] P. Bourgeois and R. Coutres, Ann. l'Obs. Roy. Belge 3, ser. 3, 4 (1948).

[16] A.F. Torondzhadze, Biull. Abast. obs. No. 15, 115 (1953).

[17] A. Ali, Monthly Notices Roy. Astron. Soc. 101, 324 (1941).

[18] P. Pismis and A. Prieto, Astrophys. J. 101, 314 (1945).

[19] P.N. Kholopov, Problems of Cosmogony, Vol. 1 [in Russian] (Izd. AN SSSR, Moscow, 1952), p. 195.

[20] B.A. Vorontsov-Vel'iaminov, Proceedings of the Fourth Conference on Cosmogony [in Russian] (Izd. AN SSSR, Moscow, 1955), p. 197.

[21] P.P. Parenago, Course in Stellar Astronomy [in Russian] (GTTI, Moscow, third edition, 1954), p. 452.

[22] P.P. Parenago, Astron. J. (USSR) 22, 129 (1945).

[23] P.I. Bakulin, Trudy GAISh 26, 124 (1955).

[24] J. Ohlsson, Ann. Obs. Lund. 1932, No. 3.

[25] P.I. Bakulin, Trudy GAISh 26, 124 (1955).

[26] H. Weaver, Astron. J. 60, 208 (1955).

[27] P.P. Parenago, Trudy GAISh 20, 26 (1951).

[28] P.P. Parenago, P. 3, 6, 102 (1948).*

[29] O.A. Mel'nikov, Trudy GAO 64, 5 (1950).

[30] R.J. Trümpler, Astrophys. J. 91, 186 (1940).

[31] K.A. Barkhatova, Astron. J. (USSR) 26, 256 (1949).

[32] W.M. Markowitz, Astron. J. 53, 217 (1948).

[33] E.D. Perepelkina, Astron. J. (USSR) 28, 49 (1951).

---

*As in Original – Publisher's note.

[34] P.P. Parenago and A.G. Masevich, Astron. J. (USSR) 28, 466 (1951).

[35] G.A. Shain and V.F. Gaze, Astron. J. (USSR) 30, 130 (1953).

[36] P.G. Shnirel'man, Astron. J. (USSR) 29, 179 (1952).

Received December 7, 1956

Stalinabad Astronomical Observatory
Academy of Sciences Tadzhik SSR

A PHOTOMETRIC INVESTIGATION OF THE ENERGY DISTRIBUTION IN THE CONTINUOUS SOLAR SPECTRUM IN ABSOLUTE UNITS

E. A. Makarova

An investigation of the energy distribution in the continuous spectrum of the center of the solar disc in absolute units has been carried out using a method involving a photographic comparison with the spectrum of a standard lamp in the region λ3700-8000. The work was carried out at the Kuchino Observatory using its solar installation, the solar diameter being 14 cm and the dispersion in the second-order spectrum 1.6 A/mm. The energy distribution obtained in this way shows an anomaly in the region λ 4400-5600, which supports the data of Wilsing [2], as well as an increase in the intensity in the region λ6800-7400. The absolute values of the energy, determined photographically, lie between those found by Abbot in 1902-1910 and in 1920-1922[1]; they are in good agreement with Wilsing's results, and, within the errors of observation, with the data of G.F. Sitnik [11]. The maximum of the energy distribution curve is at 4300 A.

Two series of observational data, namely the energy distribution in the continuous spectrum of the center of the solar disc in absolute units and the darkening of the solar disc towards the limb, are at the basis of the solution of one of the main problems of astrophysics, i.e., the determination of the temperature, pressure, density and other physical characteristics as functions of depth in the solar photosphere or, in other words, the construction of a model of the solar atmosphere. The model of the atmosphere is of great importance in the interpretation of absorption lines in the solar spectrum. Finally, information on the energy distribution in the solar spectrum is of purely practical importance, for example, in actinometry.

The range and importance of problems in which it is necessary to apply data on the energy distribution in the solar spectrum naturally require reliable and sufficiently accurate information, but unfortunately the accuracy of existing data is insufficient. Up to the present time three independent determinations of the energy distribution in the continuous spectrum of the whole solar disc in absolute units have been carried out: by Abbot and his collaborators in 1902-1910 and 1920-1922 [1], and by Wilsing [2]. All the subsequent determinations, namely, those by Plaskett [3], Pettit [4], Chalonge and Canavaggia [5, 6] and others, were carried out in relative units and in relatively narrow spectral bands. In absolute units, the data were expressed simply as an addition to the 1920-1922 Abbot distribution and can neither support nor contradict absolute determinations. The agreement of these results among themselves is well illustrated in Figure 8. The discrepancy between the two series of observations carried out by Abbot is up to 25-30%.* Furthermore, detailed studies of the distribution of energy with wavelength have recently become necessary in connection with studies of the origin of absorption in the solar photosphere. Such studies cannot be carried out on the basis of Abbot's data, or the data of subsequent observers, since these data were obtained with instruments having small resolving powers. The work of Peyturaux [9] and Pierce [10], carried out at about the same time, has shown that in the infrared region there is a relatively narrow band near 1.6μ in which the intensity of the solar radiation is anomalously high. It is of great interest to discover the presence of such regions in the photovisual region of the spectrum.

---

*It must be pointed out that the work of Abbot and Wilsing was concerned with the solar disc as a whole, and the reduction to the center which was carried out by Minnaert [7] and Milne [8] was based on a law of darkening towards the limb which was not very well known. The results are further distorted by absorption line effects and the corresponding reduction is not very reliable.

Studies of the continuous solar spectrum in absolute units were undertaken at the Kuchino Astrophysical Observatory under the direction of G.F. Sitnik, using the blackbody source of the solar spectrograph at this observatory, the resolving power of the latter being sufficiently high for this purpose. The work was carried out by two methods in parallel: photoelectrically by G.F. Sitnik and his collaborators, and photographically by us. Results of the photoelectric studies are given in G.F. Sitnik's dissertation [11]. The parallel work using the photographic method was undertaken in spite of the obvious difficulties and sheer bulk of the work. To begin with, the bulk of the work requires constant control which would guarantee freedom from accidentally introduced systematic errors which would distort the final result. Thus, for example, Abbot's data based on very considerable observational material clearly show a systematic discrepancy between the two series of observations, i.e., those of 1902-1910 and those of 1920-1922. Abbot, in spite of his experience as a first-class observer, could not explain this discrepancy; this serves to indicate the kind of difficulties which face the experimenter in this field. Our own work has once more confirmed the necessity for independent control and has helped to prevent the introduction of appreciable systematic errors into the photoelectric data. Second, and this in our opinion is the main point of this work, we were interested in the detailed distribution of energy in the continuous spectrum of the center of the solar disc as a function of wavelength or, in other words, the coefficient of continuous absorption as a function of wavelength. The photographic method ensures that the maximum resolving power of the instrument is being used and this is very important in view of the distorting effect of absorption lines on the continuous spectrum, particularly in the ultraviolet, and thus leads to quite reliable information on anomalies in the energy distribution. Some evidence of the existence of such anomalies has apparently been uncovered (see below).

1. Method of investigation. Observations. In order to obtain the energy distribution in the continuous solar spectrum in absolute units it is necessary to take into account, and do so quantitatively, all losses along the path of the solar light. At the Kuchino Observatory this was done by comparing the solar spectrum with the spectrum of a standard lamp which in turn was compared with the spectrum of a perfect blackbody at a known temperature. The work on the development of the model of a blackbody and the standard filament lamp (which was very difficult and troublesome) was described in detail in G.F. Sitnik's dissertation ([11], Chapters II-VI). The energy distribution in the spectrum of the filament lamp in absolute units (erg/cm^2·sec, with $\Delta\lambda = 1$ cm) is shown in Figure 1.

In the determination of the energy distribution in the continuous spectrum of the center of the solar disc in absolute units by the above method, which employs a comparison with the spectrum of a standard source, the following four problems must be solved: 1) light losses in the terrestrial atmosphere must be taken into account; 2) a similar correction must be made for those parts of the optical system in which the path of the solar radiation differs from that of the radiation from the comparison source; 3) a method must be found for equating the bright-

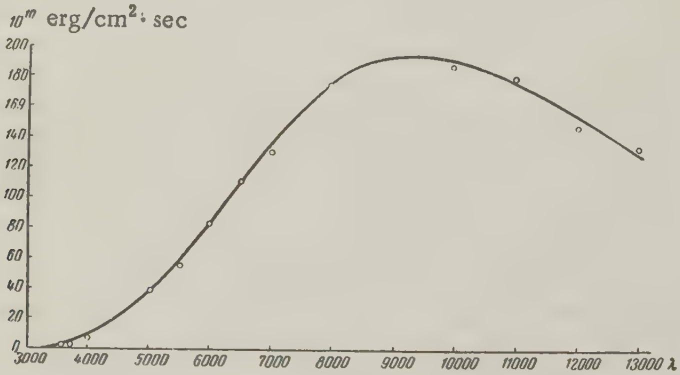

Fig. 1. Energy distribution in the spectrum of a Phillips filament lamp.

ness of the sun and the terrestrial comparison source which always differ considerably in the ultraviolet; 4) the solar spectral regions must be chosen so as to exclude the distorting effect of absorption lines. In those parts of the spectrum where the distortion is inevitable (ultraviolet end of the spectrum) one must estimate the necessary corrections for the effect of absorption lines. The solution of all these problems in our own case is described below.

The work on the photographic investigation of the continuous solar spectrum, briefly, consisted of the following. The comparison of the spectrum of the solar disc with the emission spectrum of a Phillips lamp was carried out photographically on the solar spectrograph of the Kuchino Observatory in the spectral region λ3700-8000. The work was so designed that the number of reductions in the comparison of the solar spectra and the lamp spectra was cut down to a minimum; the optical paths for the sun and the lamp differed by one mirror and a step-wedge. The losses in the earth's atmosphere were taken into account using the Bouguer methodand a simultaneous control of the constancy of the transparency of the earth's atmosphere was maintained. The slit of the spectrograph was chosen sufficiently narrow so that corrections for the absorption lines, at the dispersion and resolving power of our instrument, was in practice necessary only in the ultraviolet where one cannot choose parts of the continuous spectrum because of the natural blending of Fraunhofer lines in the solar spectrum.

a) The instrument. The horizontal solar telescope and diffraction spectrograph of the Kuchino Observatory, whose optical scheme is shown in Figure 2, was described in detail in the dissertations of I.S. Shcherbina-Samoilova [12] and G.F. Sitnik [11]. We shall merely describe their main characteristics. The reflecting solar telescope gives an image of the solar disc, 140 mm in diameter, at the focus of the spherical mirror C_1 (Figure 2) which coincides with the slit K of the spectrograph. The spectrograph is an autocollimating two-lens Zeiss O objective with a focal length of 5 m and the aperture reduced to 60 mm. The diffraction grating G has 600 lines per mm. The slit and the plate holder were in the same plane.

An additional part of the solar installation was the standard lamp with its reflecting mirror (Figure 2). The lamp L was placed near the focus of the reflecting mirror ($f = 120$ cm) at a small angle to the optical axis of the mirror. The light from the lamp after reflection from this mirror falls on the main mirror T_1 and then traverses a path identical with that traversed by the solar radiation.

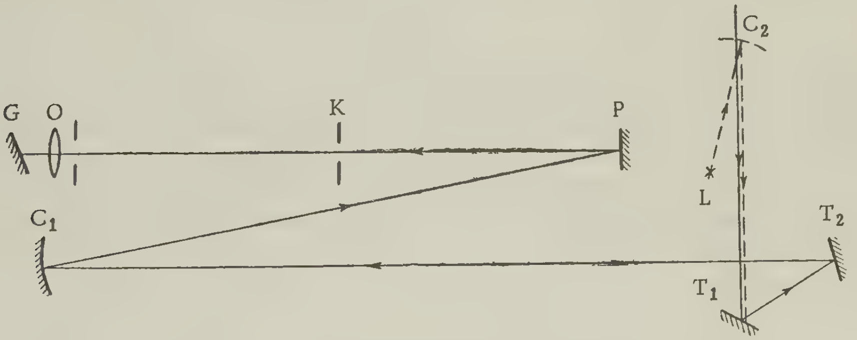

Fig. 2. The optical scheme of the horizontal solar telescope and diffraction spectrograph of the Kuchino Observatory.

Studies of the continuous solar spectrum, particularly in the ultraviolet where one measures narrow intervals between absorption lines, require the use of the maximum possible resolving power of the instrument. To achieve this, a special calibration and a series of tests were carried out on the instrument. 1)The focal curve of the spectrograph was determined by Hartmann's method for two working temperatures: 5° and 20°C. 2) A detailed study was made of the linear dispersion as a function of wavelength. The dispersion was somewhat lower in the ultraviolet and was about 3.25 A/mm in the first order in the region λ5000-8000 and 1.60 A/mm in the second order in the region λ3500-5000. 3) The instrumental profile was determined by I.S. Shcherbina-Samoilova [12]. Near 6000 A its half-width was 0.165 and 0.088 A in the first and second order, respectively. The profile is clearly asymmetric and has, on the violet side, a companion having an intensity of 16% of the maximum intensity while the wings are weak. 4) The scattered light was investigated photographically in the fall of 1953, using the method of Plaskett [13], in collaboration with V.Ia. Alduseva. According to measurements in the region λ4000 and λ6000 in 1953, the amount of scattered light did not exceed the limits of accuracy of photographic photometry and was 2-3%, which was confirmed by the absence of a measurable background on photographs taken in the ultraviolet in 1954 (for example, August 29, 1954). 5) The polarization properties of the solar spectrograph at the Kuchino Observatory were investigated by Iu.N. Lipskii [14]. It turned out that the degree of polarization of the light transmitted by the spectrograph depends strongly on wavelength. In the work involving a comparison with radiation from a standard source the polarization properties of the spectrograph do not enter if the light incident on the slit is unpolarized. Iu.N. Lipskii [15] showed that in the relatively wide spectral region λ4000-7700 the coefficient of depolarization of light incident on the slit of the spectrograph is equal to unity within the limits of experimental error.

b) Observations were carried out in the summer of 1954. The solar spectrum was photographed on clear days for different air masses beginning with 4-7 and up to 2-1.5 in 3 to 6 series of photographs. A visual check was made of the absence of disturbed regions near the center of the solar disc from the form of the H_α line before the beginning of the observations. The solar spectrum was photographed using a step-wedge filter with slit widths close to normal (from 0.03 to 0.07 mm in the various spectral regions) in the region λ3600-5000 in the second order, and in the region λ5000-8000 in the first order. The spectrum of the lamp was photographed using slits 0.3 to 3.7 mm wide without the filter, either on the day during which the observations of the sun were carried out, or on the following day. The exposure times for the sun and the lamp were the same (from 15^s to 2^m in the various parts of the spectrum). The zero point of the slit was determined visually under a magnifying glass at the end of the observations.

Altogether during the summer of 1954 18 days of observations were possible. Of these, eight days were chosen as suitable for further treatment. During the remaining days the transparency of the terrestrial atmosphere was not sufficiently steady (see below).

c) The treatment of the spectrograms. All the plates were developed in a fine-grain developer D-76 simultaneously with the corresponding spectrum of the lamp.

Measurements on the spectrograms were carried out on the self-recording microphotometer MF-4. The slit width of the microphotometer corresponded to 0.03 A in the ultraviolet to 0.2 A in the red on the spectrogram. Thus, the slit of the microphotometer was always a few times narrower than the width of the chosen spectral region (Table 1).

2. The effect of extinction in the earth's atmosphere. a) Criterion for the constancy of the transparency of the earth's atmosphere. Light losses in the earth's atmosphere were taken into account by the classical method of Bouguer; this method was used only in the determination of the coefficient of transparency of the atmosphere whose properties are constant in time. A criterion suggested by V.G. Fesenkov was used to check the constancy of the transparency. V.G. Fesenkov [16] has shown that if one confines one's attention to first-order scattering one obtains the following expression:

$$\frac{F_{\mathrm{H}}}{F_{\odot} m_z} = \mu, \tag{1}$$

where F_H and $F_\odot$ are the radiation fluxes received by the detector from the aureole and from the sun (at the given wavelength) respectively, m_z is the mass of air corresponding to the zenith distance z, and μ is the intensity of light scattered by all the earth's atmosphere in the given direction. Since μ is determined only by the scattering properties of the earth's atmosphere, Expression (1) has a constant value provided the optical properties of the earth's atmosphere remain constant. Judging by the data of V.G. Fesenkov and E.V. Piaskovskaia-Fesenkova [16-18] one may evidently consider that up to 6-7 air masses Expression (1) holds in the photovisual region of the spectrum (i.e., second-order scattering may be neglected). For larger air masses, and particularly in the blue-violet region of the spectrum, deviations from the linear law are possible and the Criterion (1) must be checked. On the basis of results obtained with an aureole photometer, and using the Criterion (1), we chose those days and hours during which the relative aureole divided by the air mass is represented by a straight line parallel to the axis of the abscissae (m_z). The selection was made by G.F. Sitnik and R.N. Khmeleva and deviations up to 9% were admitted. We estimated that if the Criterion (1) is satisfied to within 9%, then the accuracy of the coefficient of transparency is about 3% (the values of μ were taken from the paper by E.V. Piaskovskaia-Fesenkova [18]). The following days in 1954 were chosen as suitable: May 30th, June 28th, July 3rd, 8th and 10th, August 7th, 17th and 29th.

b) Bouguer's method. The coefficient of transparency of the earth's atmosphere for the chosen days was determined by Bouger's method. Using the coefficient of transparency obtained for different spectral regions a smooth curve was constructed representing the dependence of the coefficient of transparency on wavelength. Such a smoothing out is necessary because of the small number of series of observations (essentially three series), and this means that it was impossible to obtain Bouguer lines for separate wavelengths. Figure 3 shows the results of a photographic determination of the coefficient of transparency for different wavelengths (crosses) and the smoothed curve for three days of observations in 1954 (with noticeably different transparency). The data obtained with the aureole photometer are shown as open circles. The dotted curve in Figure 3 shows the coefficient of transparency as a function of wavelength calculated after Rayleigh for a pure molecular scattering at Kuchino. The tables of van de Hulst ([19], page 58) were used in this calculation.

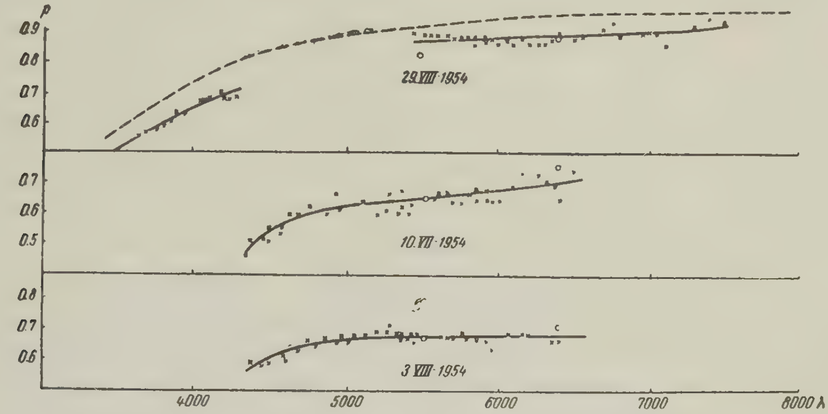

Fig. 3. Coefficients of transparency. Kuchino 1954. ××) Photographic observations; ○) observations on aureole photometer; ——) calculated after Rayleigh.

Using the coefficient of transparency taken from the smoothed curve for each part of the continuous spectrum, we determined the logarithm of the intensity of the solar radiation beyond the earth's atmosphere.

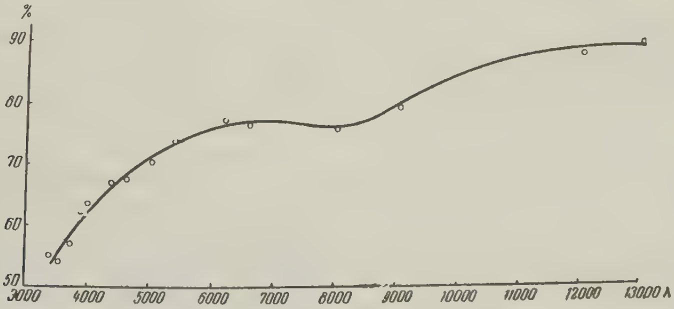

Fig. 4. Coefficients of reflection of the projector mirror.

3. Light losses in the optics of the receiving instrument. In our work the optical paths of the radiation from the sun (after passing through the earth's atmosphere) and the radiation from the standard lamp differed only by two elements. The radiation from the lamp suffered some losses on reflection from the projector mirror, while the solar radiation was reduced by the steps of the platinum filter.

a) The reflecting power of the aluminum-coated projector mirror was studied by G.F. Sitnik ([11], Chapter 8, Section 3) and is given by him in his dissertation. Figure 4 shows a plot of the reflecting power q_λ of the mirror in percent as a function of wavelength. The dip in the reflecting power near λ8000, which is characteristic for aluminum coatings, can be clearly seen.

b) Investigation of the step absorber. We have used a platinum on quartz absorber from an ISP-22 spectrograph. Results of studies of it are given in [20]. It must be noted that a check made using a laboratory monochromator has shown that as a result of a combination of polarization properties of the light, the absorber, the spectral apparatus, and the aperture of the beam of light which illuminates the slit of the instrument, the transmission of the steps of the absorber as a function of wavelength is different for different instruments. For this reason the absorber was investigated on the same instrument on which all the observations were carried out. Figure 5 shows a plot of the optical density of the steps as a function of wavelength. The mean square error of this determination is ~0.004 of the density, or not more than 1% in the estimate of the intensity. The transmission of the steps of the platinum absorber changes with wavelength, the more so the thicker the layer of platinum (for the densest steps this change is up to 15% in the region λ3500-5500). For comparison, in the case of the densest step, the dotted line shows the density of the step as a function of wavelength obtained for the same absorber on a monochromator. This comparison shows quite clearly that in both absolute and relative photometry one must use only those absorber data which were obtained on the same instrument on which the absorber was used to obtain the photographs.

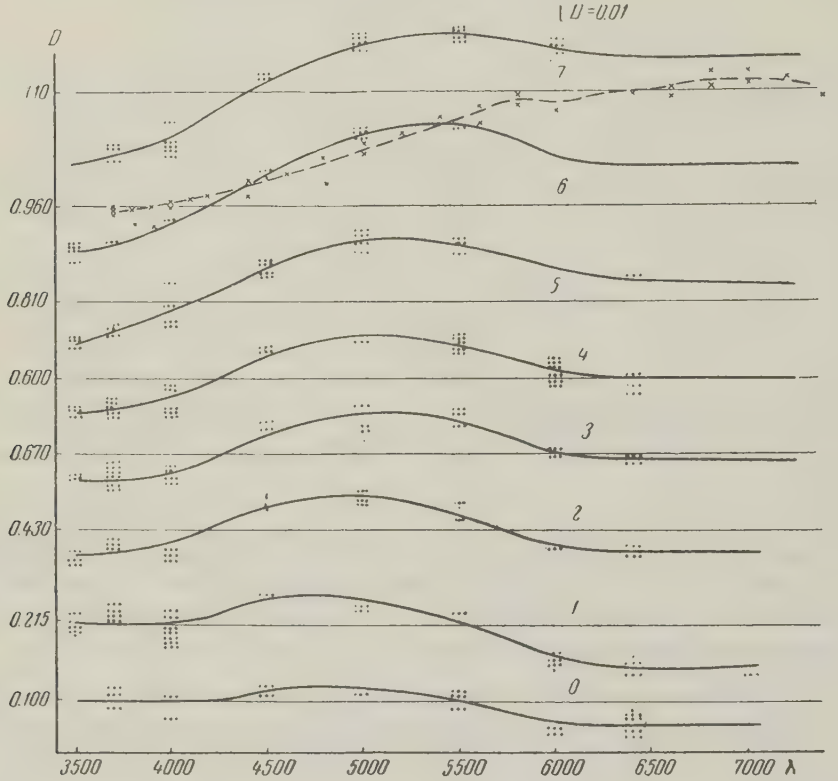

Fig. 5. Optical density of the steps of the quartz absorber as a function of wavelength obtained from a study with the solar spectrograph. 0, 1, 2, 3, 4, 5, 6, 7 are the numbers of the steps.

4. The method for equalizing the brightness of the sun and the standard lamp. The brightness of the Phillips filament lamp and the brightness of the center of the solar disc (at the bottom of the earth's atmosphere) differ from each other in the different spectral regions by factors of 100-5000. Equalization of brightness was carried out by increasing (by a factor of 100) the slit width for photographs of the spectra of the lamp. Since the solar spectrum was photographed with a very narrow slit (close to normal) a detailed study of the spectrograph slit was necessary.* Within the limits of measurements (0.001 mm, with the divisions on the drum equal

---

*The method and results of this check are reported in detail in our paper in Soobshchenia GAISh (in press).

to 0.01 mm) the slit is parallel and its edges are uniform. As the temperature increases the slit width decreases by 0.002 mm for every 10°. Since the maximum temperature changes during the observations are up to 10° no corrections for the heating of the slit were made (the correction is outside the limits of accuracy of the determination of the slit width).

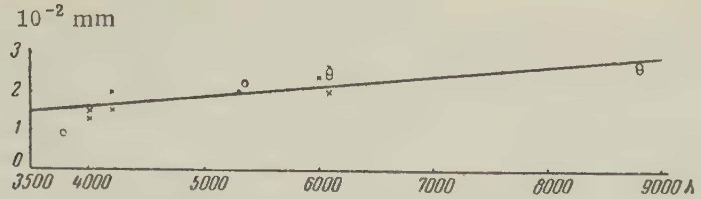

Fig. 6. Proportionality between light flux and slit width. Correction for diffraction as a function of wavelength.

The dependence of the light flux on the slit width was checked experimentally on the solar spectrograph in the region λ3800-8800 A, using a photomultiplier and a photocell. Both the sun and the filament lamp were used as the sources of light. Measurements were carried out for slit widths between the minimum at which measurements are possible and the widest possible. As a result of diffraction at the slit direct proportionality between the light flux and the width of the slit begins at some value of the slit width near the normal. The straight line does not pass through the true zero point of the slit but is displaced, the more so the greater the wavelength, and the point of intersection of the straight line with the axis of abscissa will be called the new zero point. A correction must be introduced for the displacement of the new zero point relative to the true one when the known slit widths are used in the determination of the ratio of intensities from the photographs of the spectra of the sun and the lamp. If for a given wavelength the slit widths for the lamp and the sun are s_l and $s_\odot$ respectively, then the true ratio of intensities corresponding to these slit widths is equal to

$$\frac{s_l - \Delta_\lambda}{s_\odot - \Delta},$$

where Δ_λ is the distance between the new and the true zero point (in the same units in which the quantities $s_\odot$ and s_l are measured).* Using the method of least squares, we fitted a straight line to the results of observations giving the best representation of Δ_λ as a function of λ (Figure 6); the error in Δ_λ is relatively large and is about 0.3 of a slit division.

In his dissertation G.F. Sitnik did not correct for the diffraction at the slit, and since the required brightness of the sun is directly proportional to the ratio $s_l/s_\odot$ of the slit widths ([11], p. 352, Equation (10,6)) it follows that his data on the distribution of energy in the continuous spectrum of the solar disc ([11], Table 44, Figure 49) are all low by a factor of ~15% (ultraviolet) to ~20% (red) in the case of measurements with the photomultiplier, and ~10% (λ5500) to ~15% (λ12000) in the case of measurements with a photocell. This explains the discrepancy, which exceeds experimental errors, between the results obtained with the photomultiplier and the photocell ([11], Figure 49). This error was corrected by G.F. Sitnik in a recent paper [21] in which the correct data on the distribution of energy in the continuous spectrum of the sun were given.

5. The choice of intervals in the continuous spectrum and the effect of absorption lines. Without exception all the investigations of the continuous spectrum of the sun which have been carried out up to now in the region $\lambda < 5500$ [1-6] are to a considerable degree subject to the effect of absorption lines since both the dispersion and the resolving power of the spectral instruments used in these investigations were small (at best, lower by one order than the dispersion and the resolving power of the spectrograph at the Kuchino Observatory). Any correction for the absorption lines is difficult and unreliable, and hence in our own work we tried to use to the full the advantages of the high-resolution spectrograph and used a slit width close to normal, which, of course, introduces the difficulties associated with work with narrow slits.

---

* The true zero point is defined as that corresponding to a source with an infinite brightness and a receiver with an infinite sensitivity. With our accuracy the sun and the eye fully satisfy these conditions.

TABLE 1

Intervals of the Continuous Spectrum and Results of Observations

Ilford Ordinary No. 30

№	Wave-length at midpoint of interval	Width of interval, A	Intensity of lines within the interval (according to Rowland)	Correction for absorption lines, %	Distorting effect of the wings of Balmer lines, %	Total correction, %	30.V	28.VI	7.VIII	17.VIII	29.VIII	Mean J	Mean square error		$B_\odot$ 10^{-14}	$B'_\odot$ 10^{-14}
							J						abs.	rel., %		
1	2	3	4	5	4'	5*	6					7	8	9	10	11
1	3501.31	0.2	—3, —2	3	—	3	—	7075	13800	6920	11210	9751	1489	15	1.07	1.10
2	3557.53	0.05	—	—	—	—	19900	6310	15820	9336	13800	13033	2343	17	1.60	1.60
3	3652.90	0.40	—3,3, (—3), (—3), (+3), (+1)	2	—	?	19500	11490	19040	14460	12300	15360	1660	10.8	2.64	?
4	3678.45	0.30	—3,—3,(—3),(+4),(+1)	5	$H_{21}\sim8$; $H_{22}\sim3$	16	19010	12010	15820	11490	11210	13909	1520	10.9	2.82	3.33
5	3698.85	0.20	—2,—2,(—1),(—1),(+4)	10	$H_{16}\sim1$; $H_{17}\sim4$	15	16600	12010	16220	12300	10220	13740	1260	9.3	2.98	3.51
6	3755.65	0.10	—1,(—1),(—1),(—2),(+1)	5	$H_{12}\sim2$	7	18620	—	—	—	9550	14690	1510	10.3	3.47	3.73
	»						19010	12590	—	12890	15490					
7	3811.52	0.12	—2,(—2), (+2), (+2)	7	$H_{10}\sim2$	9	17000	9330	17370	12600	12020	13660	1540	11.3	3.52	3.87
8	3851.98	0.20	0,(—1), (—1)	5	—		14800	9780	13800	10480	10970	11966	980	8.2	3.61	3.80
9	3999.80	0.20	—2,—3 (0), (—1)	6	—		12300	7079	10970	8511	7600	9292	1010	10.9	4.07	4.33
10	4050.575	0.07	—1,(0), (+3), (—1)	7	—		10700	6607	10220	7943	7762	8646	775	9.0	4.37	4.70
11	4069.85	0.20	—2,(—2), (+1), (0)	5	—		9120	6760	9550	6918	1413	7952	578	7.2	4.29	4.51
12	4117.13	0.20	—2,(—1), (+1)	5	—		10000	6310	8710	6607	7762	7878	685	8.7	4.65	4.90
13	4185.28	0.15	—1,(—1), (+2)	3	—		9120	6026	8320	5495	6761	7144	682	9.6	5.09	5.25
14	4234.9	0.2	—2, —2	4	—		5750	4790	7090	5129	5625	5677	400	7.1	4.45	4.65
15	4283.6	0.2	—2	2	—		5010	4677	7410	5012	5370	5496	500	10	4.88	5.00
16	4316.38	0.5	—2	2	—		5500	4898	6760	4467	5500	5425	393	7.2	5.02	5.12

TABLE 1 (continued)
Ilford F.P. 4

1	2	3	4	5	30.V	28.VI	3.VII	8.VII	10.VII	29.VIII	7	8	9	10	11
					6										
17	4349.45	0.3	—	—	4580	4580	4900	4790	5370	—	4835	119	5.5	4.98	4.98
18	4364.95	0.3	—2, —2	2	4080	5130	4790	4790	5010	—	4760	184	3.9	4.98	5.08
19	4448.6	0.2	—	—	3900	4070	3550	3900	4270	—	3938	189	3.0	4.77	4.77
20	4493.1	0.4	—2	2	3240	3550	3720	3720	3900	—	3626	111	3.1	4.74	4.84
21	4543.45	0.3	—3	0.5	3100	3310	3310	3390	3900	—	3400	134	3.9	4.86	4.86
22	4573.35	0.7	—3	0.5	2700	3310	3090	2690	3310	—	3032	132	4.4	4.49	4.49
23	4627.85	0.3	—3	0.5	3020	2810	3160	2820	2750	—	2887	51	4.7	4.70	4.70
	»				—	2950	2820	3090	2750	—	—				
24	4689.85	0.3	—2	2	2240	2630	2450	2630	2750	—	2540	108	4.4	4.49	4.60
25	4747.0	1.0	—		2140	2340	2290	2240	2340	—	2210	49	2.2	4.35	4.35
26	4795.45	0.5	—		2089	—	2390	2089	2291	—	2217	86	3.8	4.50	—
27	4879.25	0.4	—		1995	2180	2344	—	2089	—	2154	75	3.5	4.78	—
28	4931.35	0.3	—		2040	2240	1660	1740	2000	—	1947	76	3.8	4.71	—
	»				—	—	—	1860	2090	—					
29	4955.4	0.6	—		1950	1950	1698	1862	1820	—	1832	52	2.8	4.56	—
30	5010.6	0.2	—		1950	1995	1820	1585	1585	—	1787	87	4.9	4.72	—
31	5055.1	0.4	—		1739	1820	1739	1780	1739	—	1763	48	2.7	4.80	—
32	5096.5	0.4	—3, —3	1	1621	1698	1513	1739	1739	—	1662	43	2.6	4.78	—
33	5130.95	0.5	—3	0.5	1480	1621	1739	1513	1621	—	1592	46	2.9	4.71	—
34	5199.25	0.5	—		1318	1622	1585	1445	1433	—	1447	56	3.8	4.71	—
35	5256.4	0.8	—		1288	1479	1698	1288	1318	—	1414	79	5.6	4.74	—
36	5290.35	0.7	—		1202	1549	1445	1142	1259	—	1321	71	5.4	4.57	—
37	5299.35	0.7	—		1122	1549	1349	1175	1288	—	1297	74	5.7	4.55	—
38	5330.9	0.8	—3	0.5	1175	1514	1259	1072	1288	—	1261	73	5.8	4.53	—
39	5358.5	0.6	—3, —3, —3,	1	1047	1479	1148	—	1380	—	1248	64	5.1	4.57	—
	»				—	—	1202	—	1230						
40	5417.6	0.4	—	—	1148	1380	1047	1096	1259	1202	1130	39	3.4	4.33	—
	»				1000	1023	1148	—	1000	—					
41	5450.05	1.1	—	—	955	1349	955	975	1175	1096	1061	51	4.4	4.24	—
	»		—	—	1000	1000	1000	—	1047	—					
42	5502.45	0.3	—3	0.5	891	933	1047	1000	955	1000	971	25	2.6	4.14	—
43	5541.3	0.2	—3	0.5	891	912	871	851	955	912	899	15	1.7	3.88	—
44	5604.45	0.9	—3	0.5	912	759	759	894	871	851	824	26	3.2	3.72	—
45	5656.7	1.0	—3	0.5	851	661	776	759	794	724	761	26	3.4	3.61	—
46	5695.6	0.4	—	—	776	631	759	759	724	631	713	27	3.8	3.48	—
47	5665.0	2.0	—	—	646	617	724	724	708	689	668	25	3.6	3.43	—
48	5847.65	0.7	—	—	575	603	708	725	725	537	650	23.7	3.6	3.56	—
	»				—	549	660	759	708	603					
49	6006.8	0.6	—	—	478	467	575	646	616	426	535	36.6	6.7	3.32	—
50	6050.1	1.3	—	—	501	490	589	589	537	436	524	24.5	4.7	3.36	—
51	6250.5	1.0	—	—	398	363	467	389	416	550	430	27.9	6.5	3.14	—
52	6313.5	0.8	—3	0.5	331	331	436	389	380	479	404	23.8	5.9	3.02	—
53	6356.7	1.0	—	—	389	380	427	380	347	—	404	22	5.5	3.12	—
54	6401.7	1.0	—3	0.5	354	—	—	—	—	—					

TABLE 1 (continued)

Agfa Infrarotplatten 700

1	2	3	4	5	6				7	8	9	10	11
					30.V	7.VIII	17.VIII	29.VIII					
52	6313.5	0.8	—3	0.5	—	—	479	—	—	—	—	—	—
53	6356.7	1.0	—	—	—	—	501	—	—	—	—	—	—
54	6401.7	1.0	—3	0.5	—	363	436	—	384	26	6.8	3.04	—
55	6447.2	1.1	—	—	—	372	426	—	399	27	6.8	3.24	—
56	6589.75	0.5	—	—	—	347	372	331	335	12.5	3.7	2.91	—
	»					—	331	295					
57	6659.4	0.6	—	—	—	339	372	324	316	19.5	6.2	2.82	—
	»					—	276	269					
58	6699.75	0.5	—	—	—	309	363	316	309	15.6	5.0	2.81	—
	»					—	288	269					—
59	6765.5	1.0	—	—	—	309	316	246	290	22.2	7.6	2.71	—
60	6808.5	2.5	—3, —3, —3	1	—	309	309	251	290	19.2	6.6	2.75	—
61	6849.85	0.7	—3	0.5	—	316	295	269	293	13.6	—	2.83	—
62	6950.2	0.4	—	—	—	339	316	224	291	20.3	7.0	2.92	—
	»		—	—	—	—	309	269					
63	6995.7	1.0	—	—	295	331	309	240	295	13	4.6	3.00	—
	»		—	—	—	339	276	276					
64	7049.7	1.0	—	—	269	331	295	269	291	14.7	5.0	3.03	—
65	7104.7	1.0	—	—	246	282	282	246	264	10.4	4.0	2.79	—
66	7203.35	0.5	—	—	234	276	240	—	250	13	5.2	2.73	—
67	7307.05	0.4	—	—	209	263	255	—	242	16.7	6.9	2.71	—
68	7404.60	1.0	—	—	—	257	224	195	219	11.9	5.4	2.51	—
69	7506.75	0.5	—	—	—	219	191	195	193	7.6	3.9	2.29	—

Agfa Infrarotplatten 750

1	2	3	4	5	6		7	8	9	10	11
					7.VIII	17.VIII					
68	7405	—	—	—	229	191	—	—	—	—	—
69	7507	—	—	—	177	182	—	—	—	—	—
70	7584.85	0.9	—	—	191	191	191	0	0	2.31	—
71	7700.4	1.0	—	—	—	170	170	—	—	2.12	—
72	7794.0	6.0	—	—	162	170	166	4	2.4	2.12	—
73	7914.55	1.1	—	—	151	174	162	11	6.7	2.12	—
74	8001.85	0.7	—	—	155	138	146	8	5.5	1.95	—
75	8047.25	0.3	—	—	158	138	148	10	6.8	2.07	—

The existing discrepancy between the theoretical values for the coefficient of continuous absorption for negative hydrogen ions and the experimental data in the visible part of the spectrum (cf., for example, [22]) may be explained, as was pointed out by Minnaert ([23], p. 105), either by insufficient accuracy of the observational data, or by the fact that in the formation of the continuous spectra other absorbing atoms play a significant part as was suggested, for example, by Mishar. It is therefore of interest to investigate the continuous spectrum first from the point of view of careful exclusion of the effect of absorption lines and, second, by choosing spectral intervals sufficiently close to each other.

a) The choice of the intervals in the continuous spectrum which are free, or almost free, of absorption lines, and which are convenient in studies of the energy distribution in the solar spectrum in the region 3500-8000 A in steps of 50 A, was carried out using the Utrecht atlas of the solar spectrum [24]. The resolving power of the Utrecht spectrograph was a little greater than that of our instrument, the half-width of the instrumental profile in the second order in the region λ6000 being 0.06 and 0.09 A in the two cases,respectively. It follows that almost all the spectral intervals which are free of the effects of the absorption lines in the Utrecht atlas are also free of this effect in our own case. The absence of absorption lines in a given interval was verified against the corrected Rowland tables of solar lines [25]. The 75 intervals which were finally chosen are given in Table 1,in which the second column gives the wavelength of the midpoint of the interval, followed by the widths of the intervals in A and the intensities of the spectral lines in each interval according to Rowland. The quantities in brackets correspond to lines whose centers do not lie in the given interval but whose wings distort the continuous spectrum in the interval under consideration.

b) The distorting effect of absorption lines. With our resolving power, for wavelengths > λ4200 there are no intervals which are undistorted because of the blending of the lines in the solar spectrum. We note that further increase of the resolving power will not be advantageous since the half-width of the instrumental profile approaches the Doppler half-width for lines in the solar spectrum. Thus, in the case of sodium the Doppler half-width is ~0.07 A, while the instrumental half-width in our case is 0.09 A. In the first and rough approximation a graphical estimate was made of the effect of absorption lines in the following way. Our list (Table 1) does not include intervals bounded by strong lines with intensities according to Rowland greater than 3 or 4; the profile of such lines is determined by the instrumental profile of the spectrograph and may be obtained if their equivalent width is known. (The equivalent width, and not the residual intensity, since the latter is determined by the instrumental profile in the case of weak lines.) The equivalent widths for lines of given Rowland intensity in the ultraviolet region of the solar spectrum were taken from Wempe's paper [26]. For points No. 3 to No. 13 (Table 1) profiles were constructed for lines lying within the chosen interval and the lines whose wings distort the interval. Examples of such profiles are shown in Figure 7, in which the Rowland intensity is given above each line. By adding the ordinates of the profiles of the separate lines within the interval we obtain the resultant profile. The correction for the effect of absorption lines (in %, Column 5, Table 1) was determined

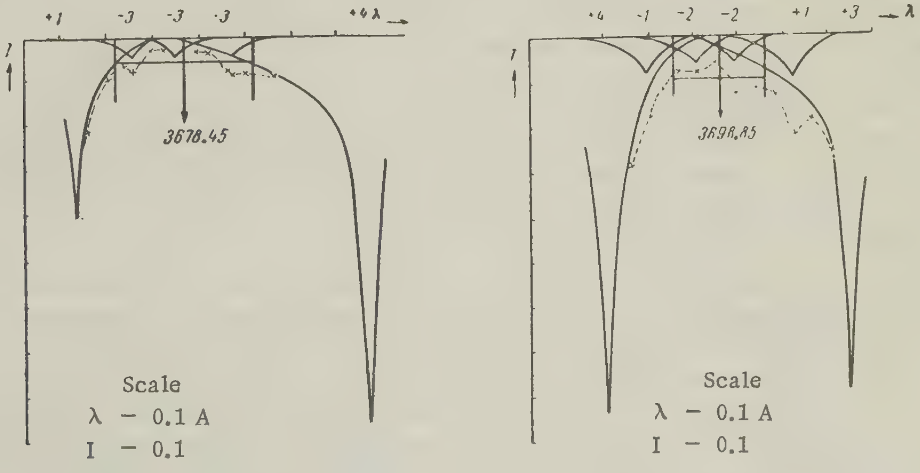

Fig. 7. Graphical method for taking into account the effect of absorption lines.

directly from the graph. It was found that the calculated and observed profiles agreed quite well.

Beginning with λ3811 A all the chosen intervals (up to the series limit) are distorted by the wings of hydrogen lines. This effect was estimated from the data of Jager [27]. Column 4' in Table 1 gives the number of the member of the series which has an effect on the given interval and the correction in percent. The only line for which the correction cannot be made is the line λ3659.90 which is close to the Balmer limit λ3645.98. The total correction for absorption lines is given in Column 5' (or in Column 5 for $\lambda > 3811$) of Table 1 and it does not exceed 10% in the case of two intervals, it is between 5 and 10% for seven intervals, 4-5% in the case of three intervals, 2% for eight intervals and not more than 0.5% for the rest.

In connection with the estimate of the effect of absorption lines let us consider the disadvantages and the advantages of working with a narrow slit close to normal. An estimate of the errors thus introduced (error in the determination of the zero point, the corrections Δ_λ, etc.) shows that in the region λ3500 to λ4500 we cannot, with our accuracy, obtain the energy distribution with an error in the final result less than 8 to 10% near λ3500, and ~5% near λ4500. This disadvantage is in our opinion compensated by the fact that we are able to correct for the effect of absorption lines. According to our estimates, already for slit widths of the order of three times normal, in the majority of intervals in the region under consideration, it is difficult to estimate the distorting effect of lines because of the presence of deeper lines within the intervals and the distorting effect due to the wings of strong lines whose profiles are difficult to compute. Evidently it is more difficult to obtain the coefficient of absorption as a function of wavelength in the case of a wide slit than in the case of a narrow slit.

6. Results of studies of the continuous spectrum of the center of the solar disc. The calculation of the monochromatic brightness of the center of the solar disc as a function of wavelength $B_\odot(\lambda, 0)$ in absolute units was carried out using the following formula:

$$B_\odot(\lambda, 0) = \frac{I_\odot(\lambda, m_z)p^{-m_z}}{I_l(\lambda)} \frac{s_l - \Delta_\lambda}{s_\odot - \Delta_\lambda} q_\lambda B_l(\lambda) = J(\lambda) q_\lambda B_l(\lambda), \tag{2}$$

where B_l is the brightness of the lamp in absolute units, $I_\odot(\lambda, m_z)$ the intensity of the solar emission for a given air mass m_z, p the coefficient of transparency of the earth's atmosphere (the quantity $I_\odot(\lambda, m_z)p^{-m_z}$ is determined graphically by Bouguer's method), $I_l(\lambda)$ is the intensity of the radiation from the lamp, s_l and $s_\odot$ are the slit widths used in the photography of the spectra of the sun and the lamp, respectively, Δ_λ is the correction for defraction at the slit, and q_λ is the reflecting power of the projector mirror.

a) Results of observations are given in Table 1 in which the 6th column gives the values of J_λ, the 7th column gives the mean value of J_λ, the 8th and the 9th give the mean square error in J_λ, both the relative and the absolute (in percent), and the 10th column gives the quantity $B'_\odot(\lambda)$ which is equal to the monochromatic brightness of the center of the solar disc in absolute units, i.e., erg/cm²·sec for $\Delta\lambda = 1$ cm. In the case of intervals distorted by the effect of absorption lines the corrected value of $B_\odot(\lambda)$ is given in the last column of the table. The dependence of the monochromatic brightness of the center of the solar disc on wavelength is shown in Figure 8. Table 2 gives the results taken from a smoothed curve representing the distribution of energy in the continuous spectrum of the sun in absolute units in the region λ3700-8000 according to photographic data. The region λ3500-3650 is not represented because of the small transmission of the instrument and the earth's atmosphere, and the rapid fall in the brightness of the lamp, in this part of the spectrum, which meant that the results were obtained by extrapolation and were therefore unreliable.

b) Accuracy of the results. The error in the monochromatic brightness of the center of the solar disc $B_\odot(\lambda, 0)$ in absolute units is due to the combined effect of the errors in the ratio of intensities of the sun and the lamp, the standardization of the lamp, and the reflecting power of the projector mirror. The mean square errors for the various spectral intervals are given in Table 3 in which the last column shows the error in the determination of the brightness of the sun by the photoelectric method ([11], Table 45). The error is greatest in the ultraviolet (the narrowest slit, brightness of the sun and lamp very different, the coefficient of transparency of the atmosphere falls rapidly beginning with ~λ4300). In the long-wavelength region $\lambda > 4300$ the error in the photographic method is fully acceptable and even somewhat lower than the error in the photoelectric determination, which, in our opinion, is due mainly to the advantages of using a smoothed curve in determining the coefficient of transparency of the earth's atmosphere. It is appropriate to emphasize once again that our main aim was a detailed study of the energy distribution in the continuous solar spectrum as a function of wavelength while the errors shown in Table 3 characterize the accuracy of the determination of the absolute values of energy and to a considerable extent are due to the use of a narrow slit. For a single plate obtained with a single setting of the slit the distribution of energy and the anomalies in it can be obtained with greater accuracy than is shown in Table 3 (in Figure 8 the spectral regions photographed on a single plate are separated by vertical lines).

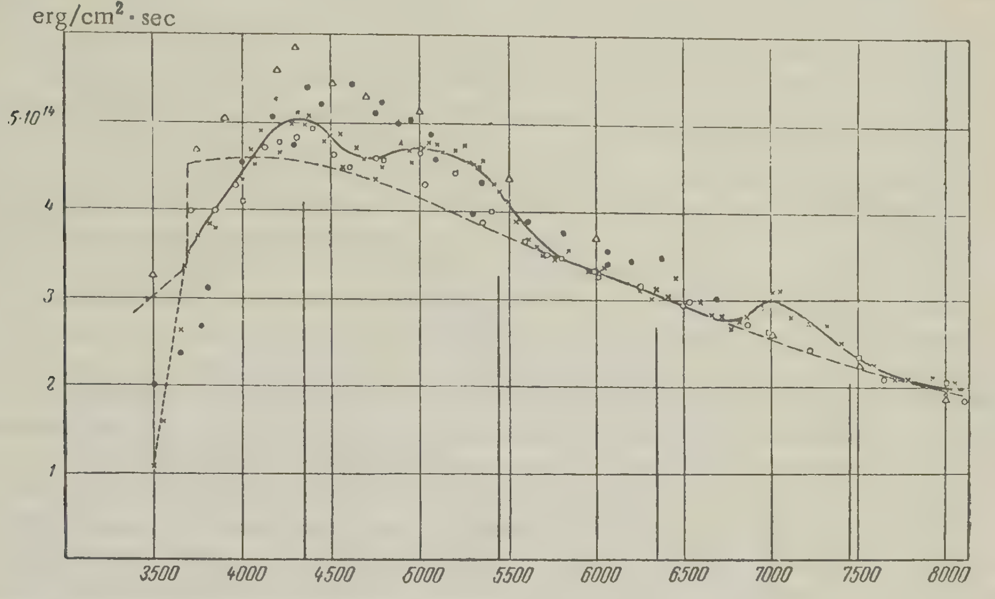

Fig. 8. Distribution of energy in the continuous spectrum of the center of the solar disc: △) Abbot's data 1902-1910; ○) Abbot's data 1920-1922; □) Wilsing's data; x) photographic data; --) contemporary data (Minnaert); •) photoelectric data of G.F. Sitnik.

c) Comparison with the results of other workers. In Figure 8 in addition to the results of the photographic investigation we plot also the data of Abbot [1] and Wilsing [2] reduced to the center of the sun by Minnaert [7] and Milne [8],respectively, and the most recent data of Wempe [26] corrected by us for the effect of absorption lines. The distribution of energy in the continuous spectrum of the solar disc which is accepted at the present time and is given in Minnaert's paper ([23], p. 88) is shown by the dotted line ,while the photoelectric results obtained by G.F. Sitnik are shown as points.

TABLE 2

Distribution of Energy in the Continuous Spectrum of the Center of the Solar Disc in Absolute Units (erg/cm²·sec per $\Delta\lambda = 1$ cm)

λ	$B_\odot \cdot 10^{-14}$	λ	$B_\odot \cdot 10^{-14}$	λ	$B_\odot \cdot 10^{-14}$
3700	3.46	4800	4.68	6600	2.88
3800	3.79	5000	4.72	6800	2.78
3900	4.10	4200	4.64	7000	2.98
4000	4.42	5400	4.38	7200	2.80
4100	4.70	5600	3.84	7400	2.50
4200	4.96	5800	3.46	7600	2.24
4300	5.10	6000	3.34	7800	2.08
4400	5.00	6200	3.20	8000	2.00
4600	4.70	6400	3.04		

The energy distribution obtained by the photographic method is somewhat different from the usual smoothed curve as given by Mulders [28] or Minnaert [23]. A dip in the intensity curve is found to be present in the region λ 4400-4700 and an increase in the region λ4800-5600. A somewhat smaller increase in the intensity is noticeable near λ6500-7400. Is there a confirmation of the anomalous behavior in the region λ4400-5600 in the work of other observers? Abbot's results obtained from observations with a spectrobolometer are strongly averaged with respect to wavelength but some indication of the presence of the anomalous behavior seems to be present (Figure 8). Mulders' distribution was obtained by a "best" combination of the data of Fabry [29] and Plaskett [3] with the results of Abbot of 1920-1922. Such a method of averaging smooths out any detailed structure in the energy distribution. Pettit's results [4] for the region in question were obtained for points separated by 500 A, which also does not lead to any information about details of the distribution. The results of Chalonge and Canavaggia [5, 6] are distorted by a considerable systematic error.* G.F. Sitnik's results for wavelengths less than 4600 A are not corrected for the effect of absorption lines, and, furthermore, his points are not sufficiently close to each other, so that, in our opinion, photoelectric studies can neither confirm nor contradict the existence of the anomaly in the region in question (Figure 8). A comparison with the results of Wilsing was the most interesting. Wilsing [2] studied the region λ4000-6600 by a photographic method (in the long-wavelength region up to λ23000 measurements were carried out using a spectrobolometer). In spite of the fact that the correction for the effect of absorption lines was carried out by a different method compared with that used in our work (since the dispersion of Wilsing's instrument was much lower than ours), nevertheless the dependence on wavelength of the monochromatic brightness of the center of the sun in the region λ4000-6600 in Wilsing's case was very similar to that obtained by us. Wilsing's data confirmed the existence of an anomalous behavior of the energy distribution curve in the region λ4400-5600. Unfortunately, no data are available to confirm the existence of the increase in intensity in the region λ6800-7400. Wilsing's and Abbot's results were obtained with a spectrobolometer which masked all the details. (A good example is the region of increased intensity near 1.6μ which "disappears" in the spectrobolograms of Abbot and Wilsing but which is found with instruments of higher dispersion which were used by Peyturaux [9] and Pierce [10].) Peyturaux [9] carried out measurements at λ6790 and λ7805 and the region which interests us here was not studied. Pierce [10] studied the energy distribution from λ10000 onwards. For technical reasons G.F. Sitnik could not study the region in question. The anomalies in the energy distribution in the continuous spectrum of the solar disc are interesting and require a theoretical interpretation, but above all, further experimental verification is, of course, necessary.

TABLE 3

Mean Square Error in the Determination of the Monochromatic Brightness of the Center of the Solar Disc

Wavelength interval	Error in the determination of the ratio of the intensities of the emission from the sun and the lamp, %	Error in the determination of the brightness of the filament lamp, %	Error in the determination of the reflectivity of the projector mirror, %	Error in the determination of the monochromatic brightness of the center of the solar disc by the photographic method, %	Error in the determination of the monochromatic brightness of the center of the solar disc by the photoelectric method, %
3700-4300	9.2	5.2	2.0	10.7	9
4300-6400	4.1	3.5	1.3	5.5	9
6400-8000	5.5	2.6	0.7	6.1	7

On the basis of a comparison of the absolute values of energy obtained by the photographic method with the results of other studies it is possible to draw the following conclusion. The absolute values of energy in the region under investigation lie between the data of Abbot obtained in 1902-1910 and those obtained in 1920-1922 and are in best agreement with the data of Wilsing. The results are in agreement with the absolute values obtained photoelectrically by G.F. Sitnik within the limits of experimental error. Contemporary data on the energy distribution in the region λ4000-6000 based on the work of Chalonge and Canavaggia are clearly low.

According to all the data the maximum of the energy distribution curve occurs in the region near λ4300.

---

*Chalonge and Canavaggia in their comparison of the solar spectrum with the spectrum of a lamp did not take into account the variation of the slit width with wavelength which considerably distorted the energy distribution. The problem was considered in detail in [30].

It should be noted that photographic results in the region below 3700 A, although not very reliable, are nevertheless in agreement with photoelectric data inasmuch as they indicate a rapid fall in the intensity of the solar radiation beyond the Balmer series limit. This fall in the intensity is much more rapid and deep than was assumed up to now. This conclusion is in good agreement with rocket data [31].

In conclusion it is my pleasant duty to express deep gratitude to all the workers at the Kuchino Observatory for their help, to my supervisor G.F. Sitnik for his interest and advice, and to Iu.N. Lipskii for a number of valuable suggestions.

LITERATURE CITED

[1] C.G. Abbot, F.E. Fowle and L.B. Aldrich, Smithson. Ann. 2 (1908); 3 (1913); 4 (1922); Smithson. Misc. Coll. 74, No. 7 (1923).

[2] J. Wilsing, Publ. Astroph. Obs. zu Potsdam 22, No. 66 (1913); 23, No. 72 (1917).

[3] H.H. Plaskett, Publ. Dom. Astr. Obs. 2, 242 (1923).

[4] E. Pettit, Astrophys. J. 75, 185 (1932); 91, 159 (1940).

[5] R. Canavaggia and D. Chalonge, Ann. Astrophys. 9, 143 (1946).

[6] R. Canavaggia, D. Chalonge, M. Egger-Moreau and H. Oziol-Peltey, Ann. Astrophys. 13, 355 (1950).

[7] M. Minnaert, Berliner Astronomische Nachrichten 2, 75 (1924).

[8] E.A. Milne, Phil. Trans. Roy. Soc. London A, 223, 201 (1922).

[9] R. Peyturaux, Ann. Astrophys. 15, 302 (1952).

[10] A.K. Pierce, Astrophys. J. 119, 312 (1954).

[11] G.F. Sitnik, Dissertation (MGU, Moscow, 1955).

[12] I.S. Shcherbina-Samoilova, Dissertation (MGU, GAISh, Moscow, 1952).

[13] H.H. Plaskett, Monthly Notices, Roy. Astron. Soc. 112, 177 (1952).

[14] Iu.N. Lipskii, Vestnik MGU No. 2, 41 (1955).

[15] Iu.N. Lipskii, Astron. Tsirkular No. 163 (1955).

[16] V.G. Fesenkov, Astron. J. (USSR) 10, 249 (1933).

[17] E.V. Piaskovskaia-Fesenkova, Astron. J. (USSR) 24, 119 (1947).

[18] E.V. Piaskovskaia-Fesenkova, Doklady Akad. Nauk SSSR 61, 1035 (1948).

[19] Atmospheres of the Earth and the Stars [Russian translation], edited by G.P. Kuiper (IL, Moscow, 1951).

[20] E.A. Makarova, Astron. Tsirkular No. 176 (1957).

[21] G.F. Sitnik, Doklady Akad. Nauk SSSR 110, No. 2 (1956).

[22] D. Chalonge and V. Kourganoff, Ann. Astrophys. 2, 69 (1946).

[23] The Sun, edited by G.P. Kuiper (Chicago, 1954).

[24] M. Minnaert, G.F.W. Mulders and J. Hautgast, Photometric Atlas of the Solar Spectrum (Amsterdam, 1940).

[25] E. St. John, C.E. Moore, L.M. Ware, E.F. Adams and H.D. Babcock, Revision of Rowland's Preliminary Table of Solar Spectrum Wavelengths (Washington, 1928).

[26] J. Wempe, Astronomische Nachrichten 275, 3, 97 (1947).

[27] C. Jager, Rech. Astr. de l'Observ. d'Utrecht 13, part 1 (1952).

[28] G.F.W. Mulders, Z. Astrophys. 11, 132 (1935).

[29] Ch. Fabry and H. Buisson, Compt. Rend. 175, 156 (1922).

[30] E.A. Makarova, Astron.Tsirkular No. 175 (1957).

[31] N.L. Wilson, R. Tousey, J.D. Purcell, F.S. Johnson and C.E. Monore, Astrophys. J. 119, 590 (1954).

Received November 1, 1956

P.K. Shternberg State Astronomical
Institute

ON THE ROLE OF TRUE ABSORPTION IN THE MARTIAN ATMOSPHERE

V. V. Sharonov

It is shown that if in the Martian atmosphere there exists a "violet layer" consisting of particles which preferentially absorb, but do not scatter, rays corresponding to the violet end of the spectrum, then condensations in this layer should appear as dark, rather than light, spots on violet-sensitive photographs. There are no facts at the present time which cannot be explained by ascribing purely scattering properties to the Martian atmosphere, the more so since it is difficult to point to any gas or aerosol which could cause absorption with the necessary variation along the spectrum.

It is well known that in the earth's atmosphere extinction, in the visible part of the spectrum, is almost exclusively due to scattering, since true absorption is concentrated in relatively few and not very deep telluric bands, and plays a very small part in reducing the total luminous flux. In the visual part of the spectrum of Mars no absorption bands due to the atmosphere of this planet have so far been discovered, and it is therefore natural to expect that the importance of true absorption in this atmosphere is even smaller than in the earth's atmosphere. Bearing this in mind, a number of authors have published [1-4] calculations of the optical thickness and density of the Martian atmosphere in which only scattering was taken into account and absorption was neglected. Such calculations were successful in the sense that they gave a representation of results of photometric observations with the necessary degree of accuracy.

On the other hand, in many papers concerned with the interpretation of photographic and photometric observations of Mars, the opinion was expressed that the atmosphere of this planet is optically quite different from the earth's atmosphere because of the presence of noticeable, or even considerable, absorption in it. In this category belong the many papers on the so-called "violet layer" in the Martian atmosphere. The work on the "violet layer" was started off by V.G. Fesenkov's discussion [5] of the effect reported by Wright [6] who discovered that the diameter of the Martian disc on violet-sensitive photographs is greater than on red-sensitive photographs. In his paper V.G. Fesenkov showed that even a very high and dense Rayleigh atmosphere, by which Wright initially tried to explain the effect discovered by him, cannot lead to the observed difference in diameters, and it is therefore necessary to assume the presence of a thin violet layer situated at great height and separated from the surface by a thick layer of the atmosphere which is optically not very noticeable. Subsequently, N.P. Barabashev [7], and also the author of the present paper [8], showed that Wright's effect can most naturally be explained by some sort of a photographic effect. If, however, one considers that the observed difference in diameters is a real one and due to the atmosphere, the assumption of the presence of a violet layer becomes inevitable.

Supporters of the violet-layer hypothesis usually assume that this layer produces a screening effect which prevents us from observing details of the Martian surface on violet photographs. Furthermore, these "violet clouds" which are sometimes visible on such photographs are taken as condensations, or regions of increased density, in this layer. In addition, in some papers, considerable absorption is ascribed to this layer.

I note that the term "absorption" and terms equivalent to it in foreign languages are sometimes used as synonymous with "extinction." It is therefore useful to emphasize that many authors ascribe true short wavelength absorption to this layer and not merely extinction. In order to show this, it is sufficient to quote the following passages in Vaucouleur's book [4] (my translation – V.Sh.): "In conclusion, it is necessary to assume the existence of a layer which preferentially absorbs but does not scatter short-wavelength radiation" (p. 51 in the Russian edition, p. 62 in the French edition). "This violet layer has no appreciable effect on long-wavelength radiation but weakly scatters and very strongly absorbs blue, violet, and ultraviolet rays" (p. 275 of the Russian edition, p. 323 of the French edition).

One notes that authors who ascribe very unusual optical properties to the violet layer, produce hypotheses as to the nature of the particles in this layer which completely contradict these properties. Thus, Vaucouleur agrees with Hess's opinion [9] that the particles which make up the violet layer are crystals of solid carbon dioxide, but also admits as probable the explanations of Kuiper [10] and Schatzmann [11] who consider that these particles are ice crystals and water drops, respectively. However, these substances, being dielectrics, cannot give noticeable absorption in the ultraviolet. Many authors have mentioned dust as a possible cause of the turbidity of the various layers in the Martian atmosphere and have suggested that this dust is of surface (Fournier [12] and others), vulcanic (McLaughlin [13]), or meteoric (Link [14], N.N. Sytinskaia [15]) origin. However, such dust clouds, well known on the earth, are not optically similar to the material of which the violet layer is supposed to be composed. Thus, the only hypothesis which is self-consistent is that due to Rosen [16], according to which the violet layer consists of melting carbon dioxide particles. Other authors (Wildt [17], Martz [18]) have tried to explain the violet veil and the violet clouds by intense daily aurorae polaris. However, atmospheric luminescence thus produced should lead to the appearance of absorption bands in the spectrum of the planet but this is, in fact, not observed.

Some authors have gone even further and have assumed that absorption predominates over scattering not only in the violet and the ultraviolet but over the whole visible part of the spectrum, and even ascribe the red hue of Mars to this process. The latter viewpoint is a new development of the hypothesis suggested in the 19th century according to which the color of Mars is due to the optical properties of the Martian atmosphere and not to the selective reflection by the surface of the planet. To begin with the red hue was thought to be due to selective extinction of radiation reflected by the surface, which in the case of Rayleigh scattering would reduce the intensity of short-wavelength rather than long-wavelength radiation. In a special paper on this subject [19] we showed that this is in principle possible, but only if a certain relation, which is improbable in the case of Mars, holds between the reflecting power of the surface and that of the atmosphere. Later, taking into account V.G. Fesenkov's criticism, Wright [6] suggested a double-layer model of the Martian atmosphere. The lower layer is assumed to absorb, the absorption increasing from the red to the violet, so that the layer acts in effect as an orange filter. This explains the reddish color of the various surface details and, in particular, of the low-lying clouds and some parts of the polar cap. The upper layer scatters according to Rayleigh's law, which leads to a screening effect and the appearance of violet clouds and, together with the yellow hue due to the lower layer, produces the greenish tint of the "seas" on the Martian disc.

Recently N.A. Kozyrev came out in support of the hypothesis of the atmospheric origin of the red hue of Mars and reported his spectrophotometric observations of the Martian disc, carried out with the 50" reflector of the Crimean Observatory in the year 1954. Since it is difficult to find a substance which would have the necessary, for this hypothesis, optical properties (as has been pointed out by Menzel [21]) the suggestion that one deals here with mineral dust cannot be accepted, and for this reason N.A. Kozyrev [22] in his subsequent work suggested life processes in the Martian atmosphere as the cause of the unusual absorption.

In the present paper we shall discuss the suggested solutions of the above problem from the photometric point of view, and shall try to discover to what extent they are in agreement with the observed distribution of brightness over the Martian disc.

In our study of the distribution of brightness over the Martian disc during true opposition, we shall use the simple formula suggested by N.N. Sytinskaia [3]

$$\rho = \frac{B}{B_0} = r \cos^q i e^{-2\tau \sec i} + \varkappa \left(1 - e^{-2\tau \sec i}\right), \qquad (1)$$

where ρ is the so-called apparent albedo (intensity factor) which is given by the ratio of the brightness B at a given point to the brightness B_0 of a perfectly white surface placed at the same distance from the sun but perpendicular to the rays, $\underline{i}$ is the angle of incidence of the rays, which in opposition is equal to the angle of reflection ϵ and the planetocentric angle between the direction towards the given point of the surface and that towards the observer, $\underline{r}$ is the surface luminosity of the planet with $i = \epsilon = 0$, $\underline{q}$ is the smoothness factor and τ is the optical thickness of the atmosphere.

We may put

$$\tau = \alpha H, \tag{2}$$

where α is the attenuation coefficient (coefficient of extinction) and H is the linear thickness of a uniform atmosphere.

Equation (1) is based on a simple calculation of the luminous intensity of a scattering medium based on Lambert's theory [23] in which higher-order scattering and light exchange between the surface and the atmosphere, as well as refraction and curvature of the atmospheric layers,are neglected. However, this approximation will be sufficient for our purposes if one assumes that the Martian atmosphere has purely scattering properties so that the surface reflectivity for violet rays is low, the optical thickness of the atmosphere is small [1-4], and hence the rejected components of intensity are unimportant. If, on the other hand, the Martian atmosphere is assumed to absorb, then the rigorous theory of scattering developed by V.A. Ambartsumian [24] shows that higher-order scattering is unimportant even for relatively large optical thicknesses.

The difference between the two models of the atmosphere may be reduced to a relative difference between the components α_s and α_a of the absorption coefficient $\alpha = \alpha_s + \alpha_a$ which are determined by scattering and absorption,respectively. This property of a scattering layer is usually expressed by the quantity

$$\eta = \frac{\alpha_s}{\alpha_s + \alpha_a}, \tag{3}$$

which we shall call the "luminosity factor." The component α_s may be expressed in terms of the scattering coefficient $\sigma = \sigma_0 f(\vartheta)$ by means of the formula

$$\alpha_s = 2\pi\sigma_0 \int_0^\pi f(\vartheta) \sin\vartheta \, d\vartheta = \pi\sigma_0\gamma, \tag{4}$$

where

$$\gamma = 2\int_0^\pi f(\vartheta) \sin\vartheta \, d\vartheta. \tag{5}$$

For spherical symmetry ($\sigma = \sigma_0 = \text{const}$) $\gamma = 4$, and for scattering according to Rayleigh's law $f(\vartheta) = 1 + \cos^2\vartheta$, which gives $\gamma = {}^{16}/_3$. We shall take σ_0 to be the value of σ corresponding to $\vartheta = \pi$, i.e., the direction towards the source of light. We then have

$$\varkappa = \frac{\pi\sigma_0}{2\alpha} = \frac{\eta}{2\gamma}. \tag{6}$$

Let us consider the following special cases:

$\underline{1.\ \tau = 0,}$ atmosphere absent. Hence

$$\rho_0 = r \cos^q i. \tag{7}$$

$\underline{2.\ \tau > 0,\ \sigma_0 = \kappa = 0,}$ no scattering, purely absorbing atmosphere, and hence:

$$\rho = r \cos^q i \, e^{-2\tau \sec i}. \tag{8}$$

For $q \geq 0$ the intensity decreases monotonically with the angle i; therefore the edge of the disc will always be darker than its center and the degree of this darkening monotonically increases with optical thickness τ. At the edge itself $i = 90°$ and $\rho = 0$, a result which is not in accordance with reality and reflects the approximate character of Equation (1) which is based on the inaccurate $\sec i$ and $\cos^q i$ laws. The effect of the atmosphere on the apparent brightness of the disc may be expressed by

$$\Delta = \rho - \rho_0 = -r\cos^q i\,(1 - e^{-2\tau \sec i}) < 0. \tag{9}$$

This means that an absorbing atmosphere always has the opposite effect, i.e., it lowers the apparent brightness of the disc.

If at an equal distance from the center of the disc there are regions of the atmosphere having different optical thicknesses $\tau = \tau_1$ and $\tau = \tau_2$, then the corresponding values of ρ_1 and ρ_2 will also be unequal, and the contrast K will be given by

$$K = \frac{B_2}{B_1} = e^{-2(\tau_2 - \tau_1)\sec i}. \tag{10}$$

If $\tau_2 > \tau_1$ then $K < 1$, i.e., regions of high optical thickness will appear as dark spots on the disc.

3. $\tau > 0,\ 1 \geq \eta > 0,\ \kappa > 0$, both absorption and scattering are present. The value of ρ is given by the general expression (1) and the effect of the atmosphere on the brightness is given by

$$\Delta = (\varkappa - r\cos^q i)\,(1 - e^{-2\tau \sec i}). \tag{11}$$

Depending on the sign of the first term, Δ can be either positive or negative, i.e., depending on the relation between the luminosity of the surface and of the atmosphere, the atmospheric layer may either increase or decrease the apparent brightness of the disc. If $r = \rho_0 = 0$ (black surface) the value of $\Delta = \rho$ monotonically increases along the radius of the disc from $\kappa(1 - e^{-2\tau})$ at the center to κ at the edge. If $r > 0$, then with $q > 0$ and $\kappa > r$ the effect of the atmosphere will lead to the illumination of the whole disc. The quantity ρ increases with distance from the center, reaches a maximum at some value $i = i_m$, and thereafter falls off towards the value κ at the edge. On differentiating Equation (1) we find that the position of the maximum may be obtained from the equation

$$rqz^{q+1} + 2r\tau z^q - 2\varkappa\tau = 0, \tag{12}$$

where $z = \cos i_m$. In the special case of $q = 1$ (Lambert's law) we have a quadratic equation which, remembering that in our case $\cos i_m$ should be positive, yields

$$\cos i_m = -\tau + \sqrt{\tau(\tau + 2\varkappa/r)}. \tag{13}$$

If $\kappa < r$ and $q > 0$, then for the values $i < i_p$, where i_p is given by $\rho_0 = r\cos^q i_p = \kappa$, the difference Δ will be negative, i.e., the atmosphere reduces the brightness. If $i > i_p$ the atmosphere has an illuminating effect. The quantity ρ decreases with distance from the center, at $i = i_p$ passes through a value κ, and at a value determined by Equation (12) reaches a minimum and thereafter increases again towards the value κ at the edge of the disc. Finally, if $q = 0$, then for $\kappa > r$ the atmosphere illuminates the disc, and for $\kappa < r$ it darkens it, and the zones of maximum and minimum brightness lie at the values of i_m given by $\cos i_m = \kappa/r$ while if $\kappa = r$ the brightness remains constant over the whole disc.

Consider now the dependence of the darkening towards the edge on the optical thickness τ in the case of an atmosphere in which scattering predominates. The edge of the disc will be defined as that zone for which the angle $i = i_k$ has a sufficiently large value; we shall write the ratio of the brightness of this zone to the brightness at the center, i.e., at $i = 0$, in the form

$$K = \frac{B_k}{B_c} = \frac{\rho_k}{\rho_c} = \frac{(r\cos^q i_k - \varkappa)\,e^{-2\tau\sec i_k} + \varkappa}{(r - \varkappa)\,e^{-2\tau} + \varkappa}. \tag{14}$$

It is easy to see that if $\kappa > r$, i.e., in the case of an illuminating atmosphere, and for small values of τ, we shall have $K > \cos^q i_k$, i.e., the presence of a thin, illuminating atmosphere reduces the darkening towards the edge. We cannot use our formulas to study this problem for an optically thick illuminating atmosphere since as τ increases in such an atmosphere the importance of higher-order scattering grows, and the result of such a calculation would be unreliable. However, such a calculation can be carried out for a strongly absorbing atmosphere within certain known limits of τ. It follows from Equation (14) that if $r > \kappa$ the value of K at first decreases as τ increases, i.e., the darkening towards the edge of the disc increases, but at some value $\tau = \tau_m$ the value of K passes through a minimum and then increases again. The latter is clear from the fact that if τ tends to infinity then ρ_c and ρ_k tend to κ and their ratio K tends to unity. If we put $r \cos^q i - \kappa = a$, $r - \kappa = b$, $\sec i = p$, and $e^{-2\tau_m} = y$ for brevity, we obtain the following equation which gives the optical thickness corresponding to the greatest darkening towards the edge:

$$ab(1-p)\,y^p - ap\varkappa y^{p-1} + b\varkappa = 0. \tag{15}$$

In practice, photometric measurements of discs of planets are only carried out up to 0.9 of the radius since beyond this various edge effects affect the result. This corresponds to $i_k = 60°$ which gives $\cos i = 0.5$ and $p = \sec i = 2$. If we assume the latter values then Equation (15) goes over into a quadratic form and can be easily solved. In particular, if $q = 0$, then $a = b$ which gives

$$y = \frac{\varkappa - \sqrt{\varkappa r}}{\varkappa - r}. \tag{16}$$

Two parts of the disc, at the same distance from the center and characterized by equal values of r (same surface) and κ (atmosphere of the same composition) but different values of τ (different atmospheric density), will have albedoes ρ_1 and ρ_2 whose ratio is given by:

$$K = \frac{\rho_2}{\rho_1} = \frac{\varkappa + (r\cos^q i - \varkappa)\,e^{-2\tau_2 \sec i}}{\varkappa + (r\cos^q - \varkappa)\,e^{-2\tau_1 \sec i}}. \tag{17}$$

It is easy to see that if $\tau_2 > \tau_1$ then $K > 1$ for $\kappa - r\cos^q i > 0$ and $K < 1$ for $\kappa - r\cos^q i < 0$. In other words, if the atmosphere in the given zone of the disc has an illuminating effect then the more dense regions in it will come out as bright spots, and if it has a darkening effect then these spots will be dark. As the ratio τ_2/τ_1 increases, the value of K at a given value of i departs more and more from unity. For a given value of τ_2/τ_1 the contrast K at first departs from unity as τ_1 increases, at some value of the latter quantity it passes through a maximum or a minimum, and then asymptotically tends to unity. For $q = 0$ there will be an analogous dependence on sec i, i.e., on the distance from the center of the disc, so that spots which represent regions of increased density in the atmospheric aerosol will be most sharply defined in a certain zone lying between the center of the disc and its limb.

The problem of the violet layer is in reality much more complex than the above formulas would suggest, since these formulas are strictly applicable only to an optically uniform atmosphere. It is well known that a real atmosphere of a heavenly body can only be replaced by such a model if the factors η and γ (and consequently the form of the scattering characteristic remain constant throughout the atmosphere. However, the violet-layer hypothesis admits the presence of a layer which is optically quite different from a pure atmosphere so that in this case it is necessary to consider a three-layer model. Within the limits of applicability of Equation (1), i.e., by neglecting the curvature of the atmospheric layers, refraction, the effect of self-illumination, and the exchange of light between the surface and atmosphere, each of the three layers may be taken as optically uniform. If this is assumed it is easy to obtain an expression for ρ. Denoting the optical characteristics of the lower, intermediate, and upper layers by τ_1, κ_1; τ_2, κ_2; τ_3, κ_3 respectively, we have

$$\rho = \frac{B}{B_0} = \{[r\cos^q i e^{-2\tau_1 \sec i} + \varkappa_1(1 - e^{-2\tau_1 \sec i})]\,e^{-2\tau_2 \sec i} + \\ + \varkappa_2(1 - e^{-2\tau_2 \sec i})\}\,e^{-2\tau_3 \sec i} + \varkappa_3(1 - e^{-2\tau_3 \sec i}). \tag{18}$$

Without introducing a general and relatively cumbersome analysis of this expression we shall consider the following special cases which are of interest from the point of view of the problem under consideration.

If we neglect the optical effect of the third layer and consider only the two lower layers (a scheme close to that suggested by Wright) then the theory given above will be fully applicable, with the difference that the second layer will play the role of the atmosphere while the apparent surface will be replaced by the solid surface together with the first layer. Algebraically this means that the parameter $r \cos^q i$ in Formula (1) must be replaced by

$$[r \cos^q i e^{-2\tau_1 \sec i} + \varkappa_1 (1 - e^{-2\tau_1 \sec i})]. \tag{19}$$

If the lower layer is considered as optically thin and scattering, then it will produce an illuminating effect on the dark Martian surface and therefore the fall of brightness towards the edge as given by Formula (14) will be reduced and, with the suitable combination of numerical parameters, an increase in the brightness towards the edge may even be obtained. If the brightness, represented by Formula (19), is empirically expressed in the form (7), then the latter case corresponds to negative value of the parameter q.

If the third layer is brought in as well, then the line of reasoning remains the same except that the underlying surface is the solid surface together with the two lower layers, while the atmosphere is taken as the third (upper) layer. If the optical parameters of the solid surface and the three atmospheric layers are suitably chosen, the latter scheme can be used to represent any observed variation of brightness along the radius since the number of arbitrary parameters is large. In practice, the problem will have a multiplicity of solutions among which solutions assuming predominance of true absorption in any or all of the layers may be made to agree with observational data. However, regions of increased density in such strongly absorbing layers should, in the case of a multilayer atmosphere, appear as dark spots on the disc if the lower layers do not produce too dark a background for the illuminating effect produced by the upper absorbing layers having a lower value of the parameter η. The same result is valid if some of the approximations are removed, for example, if the exchange of light between the surface and the atmosphere is taken into account, or if higher-order scattering is brought in. It is quite clear that in any model of the atmosphere the presence of a layer in which absorption is stronger than at other levels always leads to a reduction in the brightness of the disc and never to an increase.

The formulas obtained above will be applied in a discussion of the absorbing-atmosphere hypothesis from the photometric point of view. Because of the approximate nature of these formulas the results obtained below will be qualitative rather than quantitative.

As was shown above, authors who look upon the "violet layer" as consisting of a substance which predominantly absorbs rather than scatters, at the same time consider that the luminous cloud formations obtained on violet photographs are parts of the Martian atmosphere corresponding to increased optical density of the violet layer. But, as can be seen from Equation (17), such regions would come out as luminous only if the atmospheric layer has an illuminating effect, i.e., if $\kappa > r \cos^q i$. The values of κ should be very low for absorbing media. It follows that an absorbing atmosphere can only have an illuminating effect, and at the same time give luminous formations, if the underlying surface of the planet has an exceptionally low albedo. One can easily verify that such a value for the albedo is inconsistent with the relatively high values of ρ in the ultraviolet which are indicated by observations of Mars. In fact, measurements by N.N. Sytinskaia, N.P. Barabashov and others show that the value of ρ is of the order of 0.1 at 400 mμ. Such a value cannot be obtained in conjunction with κ of the order of 0.05, say, and an even lower value of r. This value of ρ is only possible in the case of a low κ if the atmosphere covers a luminous surface having a high r. However, if this is so then the atmosphere will have a darkening effect and its denser parts will appear as dark spots on the disc. It follows that if one looks on the violet clouds as regions of increased density in the violet layer than the only admissible hypothesis is that this layer consists of a strongly scattering and weakly absorbing substance having a high value of κ. For example, a model with a value of κ of the order of 0.1-0.2 and r of the order of 0.03-0.05 (which, according to the data of E.L. Krinov [25], is in sufficient agreement with spectrophotometric studies of red-colored specimens of eroded terrestrial crust) may give an agreement with the phenomena observed on Mars. This was shown by N.N. Sytinskaia [3], using observations obtained in 1939. We are led to the same conclusion by a study of the distribution of brightness along the radius. It follows from Equation (14) that, in the case of an atmosphere producing a darkening effect and having a small optical thickness, the reduction of the brightness at the limb of the disc produced by oblique incidence of solar rays on the solid surface ($\cos^q i$ law) is greater the greater the optical thickness of the atmospheric layer. Thus, if the atmospheric absorption on Mars increases towards the violet end of the spectrum, then the darkening towards the end of the disc should be greater for violet and ultraviolet rays then for red and infrared. In fact, as is well known, the opposite is observed: the ratio ρ_k/ρ_c falls off monotonically with λ as is illustrated by the following readings obtained at Tashkent in 1939 [3] which correspond to $i_k = 60°$:

λ (mμ)	380	430	560	630	730
ρ_k/ρ_c	0.97	0.92	0.66	0.54	0.47

In order to reproduce this dependence on λ it is necessary either to turn to the double-layer model of the type suggested by Wright, in which the upper layer has purely scattering properties and is chosen so that its optical effect just compensates the fall in brightness towards the edges produced by absorption in the lower layer, or to assume a single-layer model in which the optical thickness τ of the absorbing atmospheric layer exceeds the value τ_m given by Formula (15).

As an example, let us consider the single-layer model of the atmosphere which was assumed by N.A. Kozyrev for the purposes of interpretation of his spectrophotometric measurements [20]. In this case we have $r = 0.45$ and $\kappa = 0.05$. Assuming $q = 1$ (Lambert's law) and $p = \sec i = 2$, we obtain from Equation (15) $\tau_m = 0.43$ which corresponds to $\rho_k/\rho_c = 0.36$. In Kozyrev's case this value of τ corresponds to 570 mμ. We would thus have an increase in the darkening at the limb of the disc from the infrared to the yellow-green, and a reduction towards the ultraviolet. If the latter corresponds with reality (for example, for 440 mμ Kozyrev's model gives $\rho_k/\rho_c = 0.85$ which is sufficiently close to the above quantities) then, on the whole, the behavior of the darkening along the spectrum as given by this scheme is in conflict with observations since the observed behavior is monotonic. This conclusion was to be expected since it was assumed that τ increases from very small values in the far red to very large values in the ultraviolet, and therefore in the visible region it must pass through the value $\tau = \tau_m$. In order to obtain a monotonic behavior for the darkening as a function of λ the scheme must be modified so that the condition $\tau > \tau_m$ is satisfied for all λ. At the same time it is necessary to bear in mind that for larger values of τ higher-order scattering begins to come in, in the case of an absorbing atmosphere, and hence the accuracy of our formulas may turn out to be insufficient.

The following remarks must be made in relation to Kozyrev's calculations. Having obtained the monochromatic value of ρ (denoted by $\overline{I}(\lambda)$ in [20]) for the continents and the seas at the center of the disc and combining them in pairs, N.A. Kozyrev was able to set up a set of two equations of type (1) in four unknowns for each λ, the four unknowns being $\underline{r}$ for the seas and the continents, τ and κ, where instead of the latter he used the quantity $A = \kappa(1 - e^{-2\tau})$. Such a scheme is indeterminate and it is therefore necessary to bring in a number of hypothesis which can be reduced to the assumption of neutral reflection by the continents and the seas while the value of $\underline{r}$, assumed to be independent of λ, is taken as 0.45 for the continents and 2.15 times smaller for the seas. This reduces the number of unknowns to two, namely, A and τ, and these were found. Of course, such a scheme is as good as any other and each author can choose those assumptions which appear to him the most probable. However, one cannot agree with the statement of the above author who considers that the curves obtained by him "show that the seas and the continents on Mars have the same natural color" and "the observed difference in color is due entirely to the properties of the atmosphere" ([20], p. 147) so that as a result of the observations and calculations "one obtains a remarkable confirmation of the opinion expressed above according to which the Martian hue is due to spectral properties of the Martian atmosphere" ([20], p. 149). As was shown above, the neutral reflection by the continents and the seas does not come out of the calculations but is assumed at the very outset so that the system of equations could be solved. Thus, the only conclusion of these calculations is that the model involving neutral surfaces and an absorbing atmosphere is not in conflict with observed spectral curves; but then, the infinite number of other models are not in conflict with these curves either. Kozyrev's curves can of course be represented by a model assuming a purely scattering atmosphere, in particular, a Rayleigh atmosphere, due to the very low luminosity and low intensity contrast between the seas and the continents in the ultraviolet.

As a proof of applicability of his model Kozyrev quotes the curves of reflecting power as a function of wavelength for the continent and the sea which were obtained by him and which are very similar and show the same secondary waves and curvatures. However, the author upsets his own proof by assuming that the coloring of the sea is analogous to that of the continent and differs only by the presence of dark spots which take up about half of the area. It is obvious that for such a scheme the curves will be parallel independently of atmospheric effects. In addition, the reality of the secondary waves on these curves which were determined from only two negatives is subject to doubt.

In conclusion to our discussion of the probable role of true absorption in the Martian atmosphere and, in particular, of the existence of the so-called high-altitude violet layer, we may list the following results:

1. The hypothesis according to which there exists in the Martian atmosphere an absorbing layer of variable optical density such that areas of increased density appear as luminous clouds observable on violet photographs is in conflict with facts, since for any model of the atmosphere such increases in density in the most absorbing layer can only appear as dark and not luminous spots on the disc.

2. The hypothesis according to which absorption predominates over scattering throughout the Martian atmosphere and increases towards the ultraviolet end of the spectrum cannot in the case of a single layer atmosphere of small optical thickness be brought to agreement with the observed distribution of brightness along the radius of the disc, since for this model of the atmosphere the darkening at the limb of the disc should increase from the red to the violet while the opposite is observed. The observed behavior of this darkening as a function of wavelength may be obtained either from a model involving an absorbing atmosphere of high optical thickness or from a double or multilayer atmosphere in which the upper layer is purely scattering.

3. The weakness of the hypotheses which assume the predominance of absorption over scattering is that it is impossible to point to any gas or natural aerosol which has the optical properties ascribed to the Martian atmosphere.

4. There is no necessity for the absorption hypothesis since the phenomena observed on Mars, as well as results of photometric and spectrophotometric measurements, can be fully interpreted assuming a purely scattering atmosphere in which Rayleigh scattering, as well as neutral scattering, takes place.

5. The appearance in the Martian atmosphere of steady intensely yellow patches which were observed, for example, in 1956 opens up the problem of the possible nature of aerosols with such specific coloring. It is widely believed that the dispersive phase of such an aerosol is in the form of a mineral dust taken up by wind from the surface of the planet, but this belief must be critically examined since it is necessary to explain the origin of such large quantities of dust, their prolonged existence in the suspended state in a rarefied atmosphere, and the characteristic coloring which does not correspond to anything observed in terrestrial dust clouds. Experimental studies of the latter, particularly over deserts, may bring in new data in this connection. It is also necessary to take into account scattering by particles of atmospheric plankton having dimensions which would give rise to a dependence on wavelength opposite to that expected for Rayleigh scattering and which would therefore lead to a yellow coloring of the scattered light and a bluish coloring for the direct light. This problem was studied in the terrestrial case by V.V. Shuleikin [26] and by Schatzmann [11] in application to Mars.

6. If one agrees that the difference in the diameters of the Martian disc in the different part of the spectrum is not real but is due to photographic effects then there is no reason for bringing in the high-altitude violet-layer hypothesis. It is not possible to study photometrically the distribution with height of the scattering material above the surface of the planet. The main argument produced by Vaucouleur in reply to the criticisms of the violet-layer hypothesis, which quotes the variability of the screening effect of the Martian atmosphere for blue rays ([4], p. 47 of the Russian edition, p. 56 of the French edition) as the proof of the existence of such a layer cannot be accepted since it is not at all necessary for the formation and break-up of the aerosol particles to occur in the high-altitude layer; it can equally successfully occur in any part of the atmosphere, including the layer next to the surface of the planet. Thus, there are no definite proofs for or against the existence of a special high-altitude scattering layer in the Martian atmosphere at the present time.

LITERATURE CITED

[1] N.P. Barabashev, Tsirk. Khar'k. obs. No. 8, 3 (1951); No. 9, 3 (1952); No. 11, 3 (1953); Astron. J. (USSR) 23, 321 (1946).

[2] V.G. Fesenkov, Astron. J. (USSR) 21, 257 (1944).

[3] N.N. Sytinskaia, Doklady Akad. Nauk SSSR 43, 4, 151 (1944); Vestnik Leningrad Univ. No. 4-5, 3 (1946); Tr. Iubil. sessii LGU, sekts. astron. (1948), p. 24.

[4] G. Vaucouleur, Physics of the Planet Mars [Russian translation] (IL, Moscow, 1956).

[5] V.G. Fesenkov, Astronomische Nachrichten 228, 5420, 25 (1926).

[6] W.H. Wright, Lick Obs. Bull. 12, 366, 48 (1925); 13, 389, 50 (1927).

[7] N.P. Barabashov, Tsirk. Khar'k. obs. No. 6, 1 (1950).

[8] V.V. Sharonov, Tsirk. GAO, Vol. 32, 62 (1941); Astron. J. (USSR) 26, 116 (1950).

[9] S.J. Hess, Meteorology 7, 1 (1950).

[10] G. Kuiper (ed.), Coll: Atmospheres of the Earth and the Planets [Russian translation] (IL, Moscow, 1951) p. 382.

[11] E. Schatzmann, Compt. Rend. 232, 692 (1951).

[12] G. Fournier, Astronomie 55, 58 (1941).

[13] D.B. McLaughlin, Publs. Astron. Soc. Pacific 66, 391, 161; 392, 221 (1954); 68, 71 (1956); Astron. J. 69, 261 (1955).

[14] F. Link, Bull. Astron. Inst. Czechoslovakia 2, 1, 1 (1950).

[15] N.N. Sytinskaia, Tr. Stalinabadsk. Obs. 20, 106 (1954).

[16] B. Rosen, Ann. Astrophys. 16, 4, 288 (1953).

[17] R. Wildt, Astrophys. J. 86, 323 (1937).

[18] E.P. Martz, Astron. J. 58, 1212, 221 (1953); Publs. Astron. Soc. Pacific 66, 389 (1954).

[19] V.V. Sharonov, Izv. AN Kaz SSR 90, 62 (1950).

[20] N.A. Kozyrev, Izv. Krymskoi Astrofiz. Obs. 15, 147 (1955).

[21] D.H. Menzel, Astrophys. J. 63, 48 (1926).

[22] N.A. Kozyrev, Izv. Krymskoi Astrofiz. Obs. 16, 215 (1956).

[23] J.H. Lambert, Photometria (1760); German translation (1892) 930, 946, 947.

[24] V.A. Ambartsumian, et al., Theoretical Astrophysics [in Russian] (Gostekhizdat, 1952), Chapter VIII.

[25] E.L. Krinov, Spectral Reflecting Power of Natural Formations [in Russian] (Izd. AN SSSR, 1947).

[26] V.V. Shuleikin, Physics of the Sea [in Russian] (Izd. AN SSSR, 1941), pt. 6; Coll. in Memory of P.P. Lazarev [in Russian] (Izd. AN SSSR, 1956), p. 222.

Received December 14, 1956

A.A. Zhdanov Astronomical Observatory of the Leningrad University

THE DISTRIBUTION OF ORBIT ELEMENTS IN THE EJECTION THEORY

S. K. Vsekhsviatskii and O. I. Meshcheriakova-Babich

It is shown that P. G. Dukhnovskii's results [5] on the distribution of elements of cometary orbits on the ejection theory are incorrect because of a number of fundamental errors made by him.

Approximate distributions of elements of cometary orbits have been found assuming that the initial velocities on the surface of the sphere of influence of Jupiter are distributed uniformly with respect to magnitude and direction. The distributions have been calculated for different limiting values of velocity, taking into account visibility conditions, and have turned out to be in good general agreement with the observed distributions of elements of short-period comets of the Jupiter family. The best correspondence was achieved for limiting velocities on the boundary of the sphere of influence equal to 6.9 km/sec. This corresponds to an ejection velocity of 7-9 km/sec on the surface of the satellites.

Using the ejection theory, it is estimated that the total number of ejections from Jupiter's satellite system over the last two centuries is 600-800. It was found that the number of short-period comets as a function of perihelion distance increases in proportion to $q^{0.9}$, and for $r > 4$ AU it rapidly increases towards the orbit of Jupiter. It is shown that the hypothesis of condensation of short-period comets in the zone of motion of Jupiter (A. D. Dubiago [9]) is erroneous.

1. It is well known that peculiarities of motion in the system of short-period comets in the Jupiter and Saturn families are not in agreement with the hypothesis that these bodies were captured from the field of long-period and parabolic comets [1]. The considerable discrepancy between the distributions of semiaxes, eccentricities and perihelion distances actually observed and those resulting from the hypothesis of major perturbations and capture, together with the estimated small probability of conversion and the small growth of comets, may be considered as evidence against the capture hypothesis. These problems were thoroughly reexamined in [2].

On the basis of the ejection idea first suggested by Lagrange and developed and popularized by Proctor, and particularly Crommelin, it was possible to obtain a natural explanation of the properties of orbits of short-period and periodic comets. This was shown as far back as 1932 [3]. Later, in [4], the existence of a remarkable correspondence between the distribution of inclinations and other orbital characteristics of short-period comets was established using the ejection theory.

For this reason the appearance of the paper by P. G. Dukhnovskii [5] in which diametrically opposite conclusions were reached was very surprising. However, the latter conclusions were a result of elementary mistakes. It was stated in this paper that Soviet astronomers have only worked out the plane case, while as far back as 1934 S. K. Vsekhsviatskii considered the spatial problem [4] and obtained results which were in favor of the ejection theory. The fact that this was ignored in [5] is very strange since in his investigation of the origin of comets

Woerkom [6] considered kinematic consequences of the ejection theory and in his account of the results given in [4] wrote that he is in "agreement with Vsekhsviatskii that in this way almost all properties of short-period comets can be explained".

In 1949, using the fact that retrograde motions are absent in the system of short-period comets, S. K. Vsekhsviatskii concluded that the short-period comets which are now being observed should have been formed in Jupiter's system of satellites, and that at present no ejections from the planet itself leading to heliocentric orbits are evidently taking place, since it is not very probable that the initial velocities could lie within such narrow limits (58.3-60.1 km/sec) as are required for the formation of orbits with only direct motion. In [5] the latter conclusion is quoted as if it was due to its author and it is even stated that the presence of only direct motions is not explained on the ejection theory and that "the available data speak against this hypothesis quite conclusively".

The author of [5] does not discuss contemporary ideas of the ejection theory (ejection from the surface of statellites) but calculates heliocentric orbits for some quite artificial conditions on Jupiter's surface and compares the distribution of these elements with observations, treating this as a verification of " the ejection hypothesis". The paper does not indicate how the theoretical distributions were obtained but it is clear that a quite erroneous procedure was employed. The elements of heliocentric orbits were calculated as functions of planetographic coordinates for only two values of initial velocity on Jupiter, namely, 58.0 and 59.0 km/sec. The summing over the corresponding element intervals was carried out for only two values of velocity, and since for the initial velocity of 58.0 km/sec the resulting perhelion distances were all greater than 2 AU and were excluded in accordance with the accepted selection criterion, it follows that, in the calculation of the distribution with $\underline{q}$, only orbits corresponding to the velocity of 59.0 km/sec were included, which completely distorted the theoretical distribution.

This was the reason for the considerable difference between the distribution with $\underline{q}$ as obtained in [5] and that actually observed. This would not have been the case had the intermediate values of velocity been used (for example 58.1, 58.2 etc). The distributions of other elements in [5] are also incorrect but they were not as strongly distorted as the distribution of perihelion distances. Despite the intentions of the author of [5], they confirm the conclusion made a long time ago that there exists a remarkable correspondence between the kinematic consequences of the ejection theory and the observed properties of short-period comets. It follows that all the conclusions reached in [5] and the statement that "the ejection hypothesis is incorrect" are a result of a misunderstanding.

2. The present work was undertaken in order to obtain theoretical distributions of orbit elements for short-period comets on the basis of the kinematic scheme of the ejection theory. It was decided not to use the procedure given in [5], not only because of the errors in that paper, but also because of the considerable complexity of the scheme, and the fact that it is completely unsubstantiated. The method of calculation used in [5] was used by S. K. Vsekhsviatskii as far back as 1930-1931. It was, however, used formally. Eruptions on Jupiter, leading to the emission of products normally to the surface of the planet were considered. The planetocentric motion was determined using the initial velocity and the planetographic coordinates of the point of exit, and then from the velocity on the boundary of the sphere of influence of the planet the elements of the heliocentric orbit were determined. However, it was not taken into account that there may be nonradial ejections, deviation of the surface of a planet from a sphere, and a complete uncertainty as to the correctness of the hypothesis that the distribution of centers of volcanic activity over the surface of the planet is uniform, etc. The main point, however, as was argued above, is that there are many reasons for supposing that the source of the short-period comets in the Jupiter family is not the planet itself but the bigger satellites of Jupiter.

Ejections take place at different angles to the surface apparently on only some of the satellites. At least three of the larger satellites of Jupiter have a considerable albedo and may be covered by solidified methane-ammonia compounds, and during volcanic eruptions they may form comets whose characteristic property is the presence of these solids. With different velocities, and different directions of velocities, of the products of eruptions on the surfaces of the satellites and the planet, we shall have on the boundary of the sphere of influence of the planet conditions which are close to a uniform distribution of the magnitudes and directions of the relative velocity vectors. In fact, if one remembers that ejection may take place both during the time of transit of the satellite in front of the planet (when the orbital velocity of the planet and the orbit velocity of the satellite subtract) and during the time when the satellite moves behind the planet (when orbital velocities add), it will be obvious that there is a considerable diversity in the distribution of the velocity vectors on the boundary of the sphere of action of the planet. The most natural approach is to assume that the distribution of the directions and magnitudes of the relative velocities is uniform, taking into account the diversity of the initial conditions and the existence of few centers of activity producing Jupiter's comets. If this were not so, and, for example, the velocity vectors would tend to lie close to the plane of the orbit of the planet, because of the greater activity in the equatorial zone of the planet and satellites, then this would only lead to a more pronounced concentration towards the principal plane of the solar system which is already characteristic of the distributions of orbital elements for short-period comets.

Below we list some data for Jupiter and its satellites which will be useful in what follows.

	Equa. radius, AU.	Mass ($M_\odot = 1$)	Escape velocity, km/sec	Albedo	Orbital velocity, km/sec
Jupiter	$4.75 \cdot 10^{-4}$	$0.95 \cdot 10^{-3}$	48.0—61.0	0.42	13.0
I Io	$1.24 \cdot 10^{-5}$	$4.28 \cdot 10^{-8}$	2.42	0.53—0.69	17.0
II Europa	$1.07 \cdot 10^{-5}$	$2.41 \cdot 10^{-8}$	1.98	0.55—0.76	13.7
III Ganymede	$1.72 \cdot 10^{-5}$	$7.60 \cdot 10^{-8}$	2.79	0.35—0.45	10.8
IV Callisto	$1.72 \cdot 10^{-5}$	$4.29 \cdot 10^{-8}$	2.09	0.14—0.16	8.2

The linear velocity of rotation of a point on Jupiter's equator is 12.6 km/sec. The parabolic relative velocity on the boundary of the sphere of influence of the planet ($\rho = 0.32$ AU) is equal to 25 km/sec.

3. In accordance with the above, we considered the following problems. It is required to find the visible distributions of orbit elements of the products of eruptions, which have a uniform distribution of directions and magnitudes of the relative velocity vectors on the boundary of the sphere of influence of Jupiter, if these vectors lie within given limits. The lower limit must clearly be assumed to be zero while the upper limit may be obtained from the condition that orbits with a retrograde motion and parabolae are absent. This corresponds to a relative velocity of about 8.5 km/sec, or 0.29 in the units of $\underline{k}$. The center of the distribution of the relative velocities was assumed to coincide with the center of the planet (i. e., the dimensions of the sphere of influence were considered to be small compared with the distance of the planet from the sun). The planet was assumed to be moving in a circle of radius D. Beyond the sphere of influence the attraction due to the planet was considered to be small and was neglected. These simplifications, which were also used in the statistical capture theory, do not introduce important distortions into the required distributions of elements.

On the basis of these assumptions it is possible to obtain the following expressions for the elements of heliocentric orbits, as was already shown earlier in [4].

Let H be the relative velocity of ejection on the boundary of the sphere of influence of the planet. At the initial instant of time the position of the point at which the ejection takes place, and which has a velocity H relative to the planet, coincides with the position of the planet. We choose a system of coordinates with the sun at the origin and such that the x-axis is in the direction towards the planet at the initial instant of time, the y-axis lies in the plane of the orbit and is in the direction of motion, while the z-axis passes through the pole of the orbit of the planet. Denoting by ξ, η, ζ the components of H, we have for t = 0 ($h = 1/\sqrt{D}$ is the velocity of the planet in its orbit)

$$\begin{gathered} x_0 = D; \quad y_0 = 0; \quad z_0 = 0; \\ (x')_0 = \xi; \quad (y')_0 = h + \eta; \quad (z')_0 = \zeta. \end{gathered} \tag{1}$$

Introducing spherical coordinates λ and β, we have

$$\begin{aligned} \xi &= H \cos\lambda \cos\beta, \\ \eta &= H \sin\lambda \cos\beta, \\ \zeta &= H \sin\beta, \end{aligned} \tag{2}$$

TABLE 1

$H = 0.05$

λ	0°	30°	60°	90°	120°	150°	180°	210°	240°	270°	300°	330°
$\beta = 0$												
a	5.27	5.96	6.59	6.86	6.59	5.96	5.27	4.72	4.39	4.28	4.39	4.72
q	4.66	5.01	5.16	5.18	5.16	5.01	4.66	4.07	3.55	3.35	3.55	4.07
e	0.115	0.159	0.217	0.244	0.217	0.159	0.115	0.138	0.191	0.216	0.191	0.138
i	0°00	0°00	0°00	0°00	0°00	0°00	0°00	0°00	0°00	0°00	0°00	0°00
$\beta = \pm 15°$												
a	5.27	5.93	6.51	6.79	6.51	5.93	5.27	4.74	4.41	4.31	4.41	4.74
q	4.70	5.05	5.16	5.20	5.160	5.05	4.70	4,09	3.65	3.41	3.65	4.09
e	0.107	0.148	0.207	0.233	0.207	0.148	0.107	0.138	0.172	0.210	0.172	0.138
i	1°68	1°60	1°55	1°52	1°55	1°60	1°68	1°78	1°87	1°90	1°87	1°78
$\beta = \pm 30°$												
a	5.27	5.86	6.38	6.59	6.38	5.86	5.27	4.79	4.49	4.39	4.49	4.79
q	4.76	5.02	5.17	5.18	5.17	5.02	4.76	4.21	3.76	3.58	3.76	4.21
e	0.097	0.143	0.190	0.213	0.190	0.143	0.097	0.121	0.163	0.185	0.163	0.121
i	3°27	3°12	3°00	2°97	3°00	3°12	3°27	3°32	3°62	3°62	3°62	3°32
$\beta = \pm 50°$												
a	5.27	5.86	6.05	6.19	6.05	5.86	5.27	4.89	4.67	4.59	4.67	4.89
q	4.87	4.72	5.16	5.19	5.16	4.72	4.87	4.51	4.10	3.98	4.10	4.51
e	0.075	0.194	0.147	0.161	0.147	0.194	0.075	0.078	0.122	0.132	0.122	0.078
i	4°98	4°80	4°70	4°65	4°70	4°80	4°98	5°18	5°32	5°38	5°32	5°18
$\beta = \pm 90°$												
a							5.27					
q							5.27					
e							0.000					
i							6°50					

TABLE 2

$H = 0.15$

λ	0°	30°	60°	90°	120°	150°	180°	210°	240°	270°	300°	330°
$\beta = 0°$												
a	5.89	9.53	17.94	26.23	17.94	9.53	5.89	4.25	3.53	3.32	3.53	4.25
q	3.87	4.75	5.09	5.20	5.09	4.75	3.87	2.55	1.70	1.44	1.70	2.55
e	0.342	0.502	0.716	0.802	0.716	0.502	0.342	0.400	0.519	0.568	0.519	0.400
i	0°00	0°00	0°00	0°00	0°00	0°00	0°00	0°00	0°00	0°00	0°00	0°00
$\beta = \pm 15°$												
a	5.89	9.42	16.78	23.48	16.78	9.42	5.89	4.29	3.57	3.37	3.57	4.29
q	3.93	4.74	5.09	5.20	5.09	4.74	3.93	2.66	1.80	1.53	1.80	2.66
e	0.382	0.496	0.696	0.778	0.696	0.496	0°382	0.380	0.496	0.545	0.496	0.380
i	5°05	4°35	3°93	3°80	3°93	4°35	5°05	4°35	7°07	7°53	7°07	4°35
$\beta = \pm 30°$												
a	5.89	8.87	14.08	17.94	14.08	8.87	5.89	4.41	3.72	3.53	3.72	4.41
q	4.11	4.81	5.10	5.20	5.10	4.81	4.11	2.96	2.11	1.85	2.11	2.96
e	0.303	0.458	0.637	0.710	0.637	0.458	0.303	0.330	0.434	0.476	0.434	0.330
i	9°70	8°47	7°75	7°52	7°75	8°47	9°70	8°47	12°95	13°65	12°95	8°47
$\beta = \pm 50°$												
a	5.89	7.85	10.37	11.85	10.37	7.85	5.89	4.72	4.12	3.92	4.12	4.72
q	4.50	4.92	5.14	5.20	5.14	4.92	4.50	3.66	2.92	2.65	2.92	3.66
e	0.237	0.373	0.505	0.561	0.505	0.373	0.237	0.226	0.291	0.323	0.291	0.226
i	14°65	13°28	12°42	12°10	12°42	13°28	14°65	13°28	17°93	18°60	17°93	13°28
$\beta = 90°$												
a							5.89					
q							5.20					
e							0.116					
i							18°88					

TABLE 3

$H = 0.250$

λ	0°	30°	60°	90°	120°	150°	180°	210°	240°	270°	300°	330°
β = 0°												
a	7.71	49.63	—16.61	—11.16	—16.61	49.63	7.71	4.18	3.13	2.86	3.13	4.18
q	3.31	4.50	5.04	5.20	5.04	4.50	3.31	1.66	0.76	0.53	0.76	1.66
e	0.571	0.909	1.303	1.466	1.303	0.909	0.571	0.603	0.758	0.815	0.758	0.603
i	0°00	0°00	0°00	0°00	0°00	0°00	0°00	0°00	0°00	0°00	0°00	0°00
β = ± 15°												
a	7.71	42.05	—18.61	—12.18	—18.61	42.05	7.71	4.24	3.19	2.93	3.19	4.24
q	3.42	4.53	5.04	5.20	5.04	4.53	3.42	1.80	0.90	0.65	0.90	1.80
e	0.557	0.892	1.271	1.427	1.271	0.892	0.557	0.575	0.719	0.777	0.719	0.575
i	8°38	6°58	5°70	5°43	5°70	6°58	8°38	11°50	15.75	18°17	15°75	11°50
β = ± 30°												
a	7.71	28.78	—28.75	—16.61	—28.75	28.78	7.71	4.45	3.29	3.13	3.29	4.45
q	3.70	4.63	5.06	5.20	5.06	4.63	3.70	2.26	1.34	1.06	1.34	2.26
e	0.521	0.839	1.176	1.313	1.176	0.839	0.521	0.493	0.594	0.662	0.594	0.496
i	15°92	12°88	11°28	10°80	11°28	12°88	15°92	20°73	26°45	29°38	26°45	20°73
β = ± 50°												
a	7.71	16.89	131.4	—88.73	131.4	16.89	7.71	5.00	3.97	3.69	3.97	5.00
q	4.29	4.83	5.11	5.20	5.11	4.83	4.29	3.31	2.45	2.15	2.45	3.31
e	0.444	0.714	0.961	1.059	0.961	0.714	0.444	0.338	0.382	0.416	0.382	0.338
i	23°60	20°27	18°33	17°72	18°33	20°27	23°60	28°22	32°58	34°60	32°58	28°22
β = ± 90°												
a							7.71					
q							5.20					
e							0.326					
i							29°68					

where β is the angle between the relative velocity vector and the plane of the orbit and lies between + 90° and − 90°; λ is measured from the radius vector in a counterclockwise direction and lies between 0° and 360°. Using well-known relations we obtain

$$y_0 z_0' - z_0 y_0' = \sqrt{p}\sin i_p \sin \Omega_p = 0; \tag{3}$$

$$x_0 z_0' - z_0 x_0' = \sqrt{p}\sin i_p \cos \Omega_p = DH \sin\beta; \tag{4}$$

$$x_0 y_0' - y_0 x_0' = \sqrt{p}\cos i_p = D\left(\frac{1}{\sqrt{D}} + H\sin\lambda\cos\beta\right). \tag{5}$$

From Expressions (4) and (5) (assuming Ω_p = 0° or 180°) we have

$$\tan\, i = \frac{H\sin\beta}{\frac{1}{\sqrt{D}} + H\sin\lambda\cos\beta} = \frac{\zeta}{h+\eta}, \tag{6}$$

$$p = D^2\left(H^2\sin^2\beta + H^2\sin^2\lambda\cos^2\beta + \right.$$
$$\left. + \frac{2H}{\sqrt{D}}\sin\lambda\cos\beta + \frac{1}{D}\right) = D^2\,[\zeta^2 + (h+\eta)^2]. \tag{7}$$

Furthermore, since the heliocentric velocity $\underline{v}$ is given by

$$v^2 = h^2 + H^2 + 2hH\sin\lambda\cos\beta + \frac{1}{D} + \frac{2H}{\sqrt{D}}\sin\lambda\cos\beta, \tag{8}$$

it follows that

$$\frac{1}{a} = \frac{1}{D} - H^2 - \frac{2H}{\sqrt{D}}\sin\lambda\cos\beta. \tag{9}$$

Knowing $\underline{p}$ and $\underline{a}$ we obtain

$$e = \left(1 - \frac{p}{a}\right)^{1/2} \tag{10}$$

and also

$$q = a(1-e). \tag{11}$$

4. Using the assumption that the magnitudes and directions of the velocities are distributed uniformly, we calculated the elements of heliocentric orbits for various values of λ and β corresponding to values of H between 0.01 and 0.29 (in units of $\underline{k}$) in steps of 0.02. The values of λ were λ = 0, 30, 60, 90, 120, 150, 180, 210, 240, 270, 300, 330° and for each of these β = 0, ± 15, ± 30, ± 50 and ± 90° which corresponds to a uniform distribution of directions. Thus for each value of H we calculated 60 orbits, so that altogether 720 orbits were calculated; this makes it possible to obtain some general results on the properties of theoretical distributions of elements. As an example we give the results of calculation for H = 0.05 (1.5 km/sec), 0.15 (4.5 km/sec) and 0.25 (7.5 km/sec).

5. In order to obtain distributions which can be compared with observations one must take into account the effect of observational selection. To do this one could use the distribution of absolute magnitudes of short-period comets, taking into account the conditions of detection of comets. However, for the approximate theory which we have used it was sufficient, as is usual, to consider as visible only those orbits whose perihelion distances are less than a certain limiting value. In the statistical theory of the origin of comets it was assumed that q < 2 AU. We have calculated the number of theoretical orbits, within the corresponding intervals of values of elements, under two assumptions:

I. All comets which have perihelion distances q < 2 AU may be detected.

II. All comets with q < 3 AU may be detected.

TABLE 4

Theoretical and Observed Distributions of Perihelion Distances of Orbits ($q < 2$)

q	0.41—0.60	0.61—0.80	0.81—1.00	1.01—1.20	1.21—1.40	1.41—1.60	1.61—1.80	1.81—2.00	2.01—2.20	2.21—2.40	2.41—1.60
Boundary value of H											
0.23	0	3	6	15	10	19	11	18	—	—	—
0.25	1	7	10	17	14	19	17	18	—	—	—
0.27	4	13	12	17	18	21	21	18	—	—	—
Observed distribution	3	3	6	8	13	7	8	7	3	3	2

TABLE 5

Theoretical and Observed Distribution of Eccentricities ($q < 2$)

e	0.101—0.20	0.201—0.30	0.301—0.40	0.401—0.50	0.501—0.60	0.601—0.70	0.701—0.80	0.801—0.900
Boundary value of H								
0.23	0	0	0	16	40	20	6	0
0.25	0	0	0	16	48	24	14	1
0.27	0	0	0	16	48	36	20	4
Observed distribution	2	0	6	7	23	14	9	4

TABLE 6

Theoretical and Observed Distribution of Major Semiaxes of Orbits ($q < 2$)

a	2.11—2.60	2.61—3.10	3.11—3.60	3.61—4.10	4.11—4.60	4.61—5.10	5.11—6.40
Boundary value of H							
0.23	0	7	59	8	8	0	—
0.25	0	10	71	8	14	0	—
0.27	0	17	79	8	20	0	—
Observed distribution	2	9	27	19	4	3	1

Tables 4-7 show the theoretical distributions of the different elements in the case $q < 2$ AU. In order to obtain an idea as to the stability of the characteristic properties of the distributions, results are given for the three boundary values of H, namely, H = 0.23, 0.25 and 0.27. The observed distributions for short-period comets are also shown. The values of the elements were taken for first-apparition orbits. Of the total number of 68 short-period comets detected up to 1956 ($P < 11$ years, the comet of Schwassmann-Wachmann 1, 1925II, is included since it has undoubtedly a relation to the Jupiter system), the comet of Encke, as well as the comets of 1946 (Johnson) and 1949g (Wilson Harrington) are apparently unrelated to Jupiter's system. The observed distributions include all short-period comets, including those which have $q > 2$.

Figures 1-4 show a comparison between the observed and theoretical distributions of elements corresponding to H = 0.23. The distributions are given on a unified scale. Figures 5-7 show curves corresponding to the condition $q < 3$.

TABLE 7

Theoretical and Observed Distribution of the Inclinations $(q < 2)$

i	0—5°.0	5.01—10°.0	10.01—15°.0	15.01—25°.0	20.01—25°.0	25.01—30°.0	30.01—35°.0	35.01—40°.0	40.01—45°.1
Boundary value of H									
0.23	22	18	18	10	10	4	0	0	0
0.25	27	18	22	16	10	10	0	0	0
0.27	32	18	26	20	12	14	2	0	0
Observed distribution	11	15	20	10	3	2	3	0	0

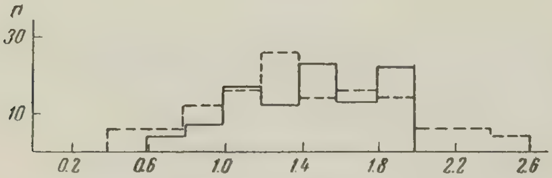

Fig. 1. Distribution of perihelion distances $q(q < 2)$; continuous line — theoretical distribution, dotted line — observed distribution.

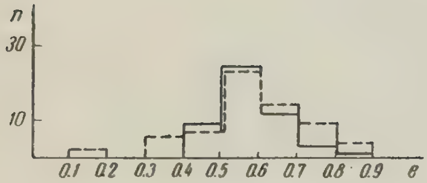

Fig. 2. Distribution of eccentricities $e(q < 2)$; continuous line — theoretical distribution, dotted line — observed distribution.

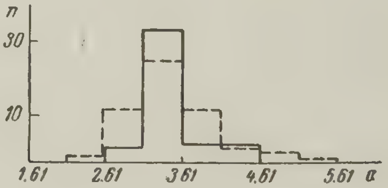

Fig. 3. Distribution of semiaxes $a(q < 2)$; continuous line — theoretical distribution, dotted line — observed distribution.

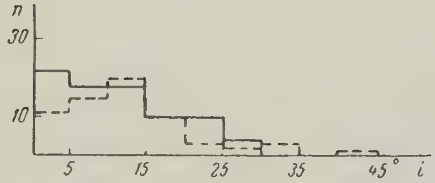

Fig. 4. Distribution of inclinations $i(q < 2)$; continuous line — theoretical distribution, dotted line — observed distribution.

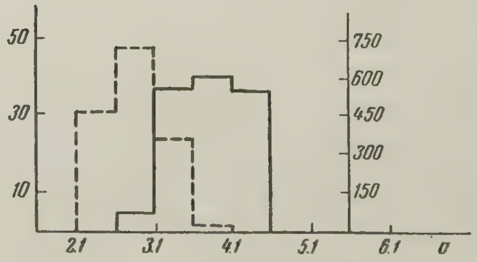

Fig. 5. Distribution of semiaxes $a(q < 3)$; continuous line — theoretical distribution, dotted line — observed distribution.

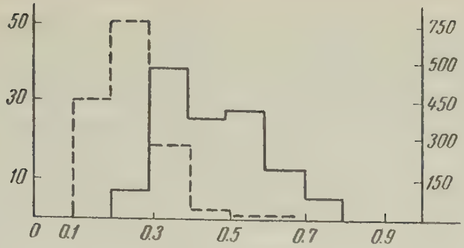

Fig. 6. Distribution of eccentricities e(q < 3); continuous line — theoretical distribution, dotted line — observed distribution.

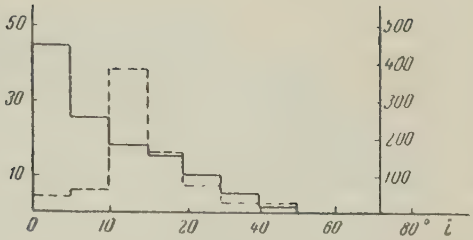

Fig. 7. Distribution of inclinations i(q < 3); continuous line — theoretical distribution, dotted line — observed distribution.

6. In considering Figures 1-4 we should note (as was already done earlier in [4]) the good agreement between orbital characteristics obtained from ejection theory and those actually observed. It must be pointed out that the effect of observational selection is accounted for in a very approximate manner (by the introduction of the condition $q < 2$). The observed distribution should reflect the inequality of absolute magnitudes of comets which for first apparitions lie between $H_{10} = 4^m2$ (Faye's comet) and $H_{10} = 13\text{-}14^m$ (Neujmin-Jackson and 1953e).

We have already pointed out that the above scheme for calculating theoretical distributions is only approximate and does not take into account the size of the sphere of influence of the planet and the effect of subsequent perturbations, but these cannot alter the general picture. One could consider other distributions of the vectors H also. In the calculations the values of λ and β varied by 30-40°, i. e., quite considerably, which led to a relatively small number of cases in the different element intervals and was the reason for the appearance of fluctuations in the theoretical distributions which can, for example, be seen in the q distribution. But all this could not have an effect on the essential features of the obtained distributions. For this reason, and in spite of all the noted effects, one must admit the striking and almost complete similarity between theoretical and observed distributions of elements of short-period comets. It is impossible to attribute to coincidence the correspondence between the maxima in the distributions of eccentricities and semiaxes of orbits with the simultaneous and excellent agreement of the character of distributions of perihelion distances and inclinations. The best correspondence is obtained, as can be seen, for the boundary value $H = 0.23$. The simultaneous agreement of the distributions of eccentricities, semiaxes, and the values of the greatest angles of inclination of orbits in the Jupiter family of comets, obtained on the basis of the most natural assumptions about the uniform distribution of the relative velocity vectors and the existence of a limiting value of H, may be looked upon as very convincing evidence in favor of the ejection theory. On the other hand, no kind of modification of the capture theory will, as was shown by G. Newton, B. M. Shchigolev and others, lead to a distribution observed in the system of short-period comets. The discrepancy in the distribution of inclinations which consists in the predominance of orbits with small inclinations (near 0-5°) in the theoretical, as compared with observed, distributions, may be due to the fact that the true inclination of the plane of motion of the producing Jupiter system to the ecliptic was not taken into account. On the other hand, it is very probable that the conditions of visibility have an effect, since the detection of comets with small i is less probable, other things being equal, because of interference produced by the sunset cones. All this may affect the observed distribution of inclinations. An even better agreement is obtained between the theoretical and observed distribution when comets with $q > 2$ are excluded.

However, we are not concerned in the present paper with discussing the separate properties of the distributions of elements of short-period comets which may form the subject of an independent interesting problem. We merely note the striking general agreement between theoretical and observed distributions, while the special descrepancies between them may also be a result of an insufficient number of objects which enter into our statistics.

The distributions for $q < 3$ differ considerably from the distributions for short-period comets although they retain their general form. One notes the considerable predominance of large perihelion distances. The maximum of the distribution of eccentricities is shifted towards lower values of e (0.3-0.4). The predominance of small inclinations is even more pronounced. The maximum of the distribution of semiaxes is displaced towards larger values of a (3-4 AU).

It must be noted that the properties of the distributions which are related to the conditions of visibility and observational selection (and which more closely correspond to the conditions of detection of asteroids) correspond precisely to that character of the distributions of elements of asteroids which has often been noted on comparison with cometary distributions (cf. [4] and [7]). In Figures 5-7 we show, in addition to the theoretical distribution, the observed distribution for asteroids and the general agreement between them which serves as a further confirmation of the similarity between both groups of minor planets and an indication of the general way of their formation in the solar system. We shall not attempt, in the present paper, to discuss the various problems connected with the latter proposition and shall refer the reader to the general discussions given in [8], and also in [2], which treat the problems associated with asteroids.

However, in connection with the statistics of comets and asteroids it is necessary to consider whether the explanation of the origin of observable short-period comets which was given by A. D. Dubiago in a recent paper [9] is possible. It is assumed in the latter paper that comets condense in the zone of motion of Jupiter, and that, as a result of perturbations due to the planet, they move into the region of visibility in the form of short-period comets.

However, this explanation does not take into account the following facts. In the zone of motion of Jupiter, and even further away from the sun, masses of dust and gas cannot occur permanently since under the action of solar radiation, corpuscular bombardment and effects of bremsstrahlung, etc., they should be "swept out" from this region of the solar system. Gases in a frozen state cannot occur at this distance since they are subject to dissociation and ionization which is in fact observed in comets. Thus, if gas-dust medium exists at Jupiter's distance it should continuously be filled up, and moreover, this should occur very rapidly. In fact, however, it does not exist in sufficient quantities in order to ensure condensation, and this is very satisfactorily shown by the absence of gaseous and dust atmospheres on many distant asteroids. Such large bodies as the Trojans, for example, should condense gases and transform into comets much faster than ordinary objects of this kind. Finally, if these condensation effects were taking place, one should be able to see a gradual increase in the luminosity of comets, at least in some cases. In fact one observes a rapid disintegration of short-period comets. For this reason, the above explanation, which ignores the known physical processes in the solar system, turns out to be quite incorrect.

The remarkable correspondence between theoretical and observed distributions of orbital characteristics of short-period comets leads to the conclusion that we deal here with a young formation just being produced in Jupiter's system, which move in orbits as yet not very distorted by perturbations, and which therefore are related to the orbit of this planet.

The Jupiter family of comets is not the only one in the solar system. The properties of cometary groups of Saturn, Uranus and Neptune can be explained in a similar way [2].

7. We now formulate the results of the present work:

a) It is shown that P. D. Dukhnovskii's results are incorrect and his attempt to discredit the ejection theory must be rejected.

b) By assuming uniform distribution of the initial velocity vectors, theoretical distributions of elements of short-period comets were obtained and are in good agreement with observed distributions. A comparison of the theoretical and observed distributions shows that during the last few centuries short-period comets were formed as a result of eruptive processes in the Jupiter system, the value of the relative velocity on the boundary of the sphere of influence being, on the average, not more than $H = 0.23$ (i. e., 6.9 km/sec). This corresponds to a maximum possible velocity on the surface of the satellites of the order of 9 km/sec (Io) and 7 km/sec (Callisto).

c) The distributions of the elements of the products of eruptions, which correspond to the conditions of visibility and observational selection characteristic for the detection of asteroids, agree with the properties of the observed distributions in the asteroid system. The latter serves as a serious argument in favor of the hypothesis that short-period comets and minor planets in the solar system are related and were formed in a similar way.

d) Using the short-period comets of the Jupiter family (65 comets) which are known at present, it is estimated that the total number of cometary objects ejected from Jupiter's system is of the order of 600-800. The variation of the real number of comets in Jupiter's family as a function of the perihelion distance q may be represented by $n = 6.0, q^{0.9}$ (between 1 and 4 AU) and $n = 1.45 \cdot 10^{-5}, q^{10.2}$ (between 4 and 5.3 AU), which give magnitudes calculated in steps of 0.2 AU. It follows that in Jupiter's system 3-4 eruptions occur per year, and these produce a sufficient amount of matter to form an average short-period comet.

e) It is shown that the hypothesis of condensation of short-period comets in the zone of motion of Jupiter (A. D. Dubiago [9]) is completely self-inconsistent and incorrect.

Department of Astronomy of the Kiev State University

Received September 17, 1956

LITERATURE CITED

[1] S. K. Vsekhsviatskii, Astronomische Nachrichten, 243, 281 (1931); Astron. J. (USSR) 10, 18 (1933); 29, 63 (1952).

[2] S. K. Vsekhsviatskii, Publication of Kiev Observatory 5 (1953).

[3] S. K. Vsekhsviatskii, Astron. J. (USSR) 10, 37 (1933).

[4] S. K. Vsekhsviatskii, Astron. J. (USSR) 11, 450 (1934).

[5] P. G. Dukhnovskii, Publication of Kiev Observatory 6 (1954).

[6] A. J. J. Woerkom, Bull. Astron. Inst. Netherl. 399 (1948).

[7] N. Richter, Statistik u. Physik d. Kometen (Leipzig, 1954) p. 17.

[8] S. K. Vsekhsviatskii, Astron. J. (USSR) 32, 432 (1955).

[9] A. D. Dubiago, Astron. J. (USSR) 33, 390 (1956).

THE RESTRICTED PROBLEM OF TWO BODIES OF VARIABLE MASS *

V. V. Radzievskii and B. E. Gel'fgat

The restricted problem of two bodies, for the case when the mass (m) of the central body varies with time (t) as $dm/dt = -\alpha m^n$, is investigated. It is proved that for any value of n, the problem is reduced to the problem of two bodies with constant mass moving under the influence of their mutual gravitational attraction whose motion is perturbed by a quasi-elastic force and a force of friction. The values of these perturbing forces remain very small even if the mass of the central body decreases by a factor of two.

It is shown that the exact solution for $+\infty \geq n \geq -\infty$ can easily be found if all the solutions for $3 \geq n \geq 1$ are known.

New individual cases have been found of the integrability of the differential equations of motion of a mass point in the gravitational field of a central body (whose mass varies with time) surrounded by a gravitating and resisting atmosphere. It is proved that a periodic motion along a conic section is possible if the mass of the central body varies according to an exponential law and the resisting medium has a constant density.

In recent years, more and more attention has been drawn in the literature [1-3] to the considerable role played by the corpuscular emission from the sun. It is proposed that in the time during which the planetary system has been in existence, the mass of the sun could have decreased several times and the resulting increase of the major semiaxis a of the planetary orbits is taken by some authors as the basis for developing various theories of cosmogony. At the same time, it is well known that the dependence of the osculating elements of the planetary orbits on the magnitude of the solar mass, in the general case of the variation of the latter, has not, as yet, been determined. Therefore, we do not have any assurance that such a substantial change of the solar mass is not in contradiction with the fact, that at present the planetary orbits are almost circular.

It is true that in the well-known monograph of Jeans [4] an argument has been presented, which has been widely accepted as a theorem, according to which for any law of variation of the solar mass the following relations must hold:

$$ma = \text{const}, \tag{1}$$

$$e = \text{const}. \tag{2}$$

However, this result of Jeans is based on an assumption whose validity is not obvious.

In fact, in deriving Equations (1) and (2) Jeans assumed that for one revolution $1/r = 1/a$, where r is the modulus of the radius vector of the planet. In reality, this will only be the case for unperturbed Kepler motion

---

* The mass of the satellite is taken to be zero.

of the planet. The actual orbit, in the problem of two bodies with variable masses, can have no relation at all to conic sections and the representation of it by an osculating conic section must be treated carefully.

The exact solution of the problem has so far only been obtained by I. V. Meshcherskii [5] for two particular laws of the variation of the mass (the first and second law of Meshcherskii) and the investigation of the evolution of the osculating orbits, carried out for these cases by a number of authors [6-9], has shown that with existing rates of change of the stellar masses the Jeans relations (1) and (2) are practically satisfied.

At the present time, it is accepted that the mass of a star changes according to the law

$$\frac{dm}{dt} = -\alpha m^n, \tag{3}$$

where α is a constant coefficient, and the value of the exponent $\underline{n}$ is within the limits $3.5 \le n \le 4$ for stars of the main sequence. The first and second law of Meshcherskii are obtained by integrating (3) with $n = 2$ and $n = 3$, respectively. The possibility that with another value of $\underline{n}$ the eccentricity of the osculating orbit will rapidly increase with decreasing mass has not been excluded. At any rate, the presence of the well-known correlation between the periods and orbit eccentricities of double stars is in favor of this possibility. Therefore, the solution of the problem considered for two particular cases of the law of mass variation does not decrease the importance of investigating this problem in the general case.

1. Transformation of the Differential Equations of Motion

The differential equations of planetary motion with any law for the variation of the solar mass have the form

$$\ddot{x} = -\frac{Gm}{r^3}x, \quad \ddot{y} = -\frac{Gm}{r^3}y, \tag{4}$$

since the central nature of the force guarantees the planar character of the trajectories.

Let us introduce the following space-time transformations which, in contrast to the transformations of Meshcherskii, preserve the dimensions of space and time:

$$\xi = \nu^q x, \qquad \eta = \nu^q y, \qquad \rho = \nu^q r, \qquad d\tau = \nu^k dt, \tag{5}$$

where

$$\nu = \frac{m}{m_0}. \tag{6}$$

With the help of (6), the Equation (3) can be written as

$$\frac{d\nu}{dt} = -\beta\nu^n, \tag{7}$$

where

$$\beta = \frac{\dot{m}_0}{m_0} = \alpha m_0^{n-1}.$$

With the new variables the differential equations (4) take the form

$$\begin{aligned} \xi'' &= -\frac{Gm_0}{\rho^3}\xi\nu^{3q-2k+1} - (2q-k)\beta\xi'\nu^{n-k-1} + (n-q-1)\,q\beta^2\xi\nu^{2(n-k-1)}; \\ \eta'' &= -\frac{Gm_0}{\rho^3}\eta\nu^{3q-2k+1} - (2q-k)\beta\xi'\nu^{n-k-1} + (n-q-1)\,q\beta^2\nu^{2(n-k-1)}, \end{aligned} \tag{8}$$

where the prime denotes differentiation with respect to τ.

In order to free Equations (8) from the factor which depends on the variation of mass, it is sufficient to put $3q - 2k + 1 = 0$ and $n - k - 1 = 0$ or, which is the same,

$$k = n - 1, \quad q = \frac{2n-3}{3}. \tag{9}$$

Substituting (9) into (8), we find

$$\xi'' = -\frac{Gm_0}{\rho^3}\xi - \left(\frac{n}{3} - 1\right)\beta\xi' + \frac{n(2n-3)}{9}\beta^2\xi,$$

$$\eta'' = -\frac{Gm_0}{\rho^3}\eta - \left(\frac{n}{3} - 1\right)\beta\eta' + \frac{n(2n-3)}{9}\beta^2\eta. \tag{10}$$

As can be seen from (10), for any value of $\underline{n}$ the problem being investigated can be reduced to the problem of two bodies with constant masses whose motion is perturbed by two very small (because of the smallness of β) forces. One of these forces (per unit mass) is proportional to the velocity $\underline{v}$

$$F_1 = -\left(\frac{n}{3} - 1\right)\beta v \tag{11}$$

and acts as a force of friction for $n > 3$. This force is zero for $n = 3$ and the Equations (10) reduce to the integrable equations of Meshcherskii. Finally, for $n < 3$ the force (11) produces an acceleration. The other perturbing force

$$F_2 = \frac{n(2n-3)}{9}\beta^2\rho \tag{12}$$

is a quasi-elastic central force which is attractive (for $n < 3/2$) or repulsive (for $n > 3/2$). This force is absent if $n = 0$ or $n = 3/2$. Both of the perturbing forces are negligibly small compared with the main force of quasi-Newtonian attraction during the whole period of the motion. As is easily shown, these forces become comparable for a planet moving around the sun only when the radius of the orbit exceeds the radius of the Galaxy.

Therefore, applying the classical theory of perturbation to the Equations (10), we are able to obtain with high accuracy, and for a sufficiently long period in advance, the osculating elements of the orbit which for unperturbed motion has the form

$$\rho = \frac{C^2 / Gm_0}{1 + \varepsilon\cos(\vartheta - \omega)}. \tag{13}$$

Here, the actual calculation of the elements ϵ and ω is simplified by the fact that the small parameter β, or β^2, appears in the perturbation functions as a simple multiplier. Finally, the fact that for $n = 2$ the differential equations of motion can be reduced, either to the Equations (10) or to Meshcherskii's equations which are integrable in their final form, makes it possible to check the accuracy of the approximate solutions of the problem in the case of the particular examples taken.

To conclude the description of this method, we point out that, mathematically, it consists in approximating the actual trajectory of the body by the osculating orbit (13) which represents, so to say, a "quasi-conic section" with a variable parameter. The orbit (13) accurately describes the motion when $n = 2$, while for $n \neq 2$ it gives a better description of the motion than the osculating conic section with a constant parameter normally used in celestial mechanics in the presence of a perturbing central force. In fact, when the mass varies considerably, the elements of such a conic section corresponding to the initial, i. e., constant value of the mass will not have anything in common with the elements of the osculating orbit corresponding to the instantaneous value of the mass.

The second method proposed by us for the investigation of the problem consists in reducing the differential equations (4) to the differential equations for the unperturbed motion of two bodies whose masses vary according to some law which is different from the mass-variation law of Equations (4). With this in view, in Equation (8) we put $n - q - 1 = 0$ and $2q - k = 0$ or, which is the same,

$$q = n - 1, \quad k = 2(n - 1). \tag{14}$$

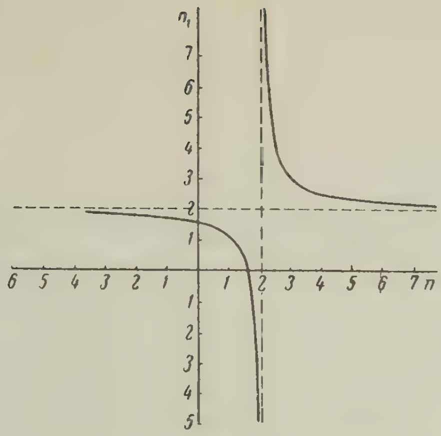

Equations (8) then take the form

$$\xi'' = -\frac{GM}{\rho^3}\xi, \quad \eta'' = -\frac{GM}{\rho^3}\eta, \tag{15}$$

where

$$M = m_0 \nu^{2-n}. \tag{16}$$

In the Equations (15) the "mass" M changes with the "time" τ according to the law

$$\frac{dM}{d\tau} = \frac{dM}{dt}\frac{dt}{d\tau} = -(2-n)\beta m_0 \nu^{3-2n} = -\beta_1 M^{n_1}. \tag{17}$$

Thus, if we have a solution of the differential equations (8) for some value of n, then for the value n_1, related to n by the equation

$$n_1 = \frac{3 - 2n}{2 - n}, \tag{18}$$

the solution can be obtained after a preliminary transformation of equations of the type (15) to the equations of the type (8).

As can be seen from (18), $n = \frac{3 - 2n_1}{2 - n_1}$, i. e., n_1 is an invertable, single-valued function of n. Therefore each known solution of the Equations (8) (for any value n) generates only one new solution (for n_1). The cases $n = 1$ and $n = 3$ are exceptions, since they do not give new solutions because in these cases $n = n_1$. The dependence of n_1 on n is presented graphically in the figure. As can be seen from the graph, for any value $3 \leq n \leq \infty$, the value of n_1 is within the limits $2 \leq n_1 \leq 3$, while for $-\infty \leq n \leq 1$, n_1 lies within the limits $1 \leq n_1 \leq 2$.

It follows from this, however, that to obtain a solution of Equations (8) for any value of n within the limits $-\infty \leq n \leq \infty$, it is sufficient to know the solutions with the values of n_1 lying within the limits $1 \leq n_1 \leq 3$. Thus, the result obtained by us immediately introduces a considerably simplification into the investigation of the problem.

In view of the above, the search for new solutions in quadratures of the Equations (18) acquires considerable importance. In a following paper, one of the authors will show a new solution of these equations for the case $n = 0$ and, consequently, for $n = 3/2$.

2. Some Particular Examples of the Integrability of the Differential Equations in the Presence of a Retarding and Gravitating Medium

As we have already seen in the preceding paragraph, Equations (4) corresponding to the case of variable mass can be transformed into Equations (10) which correspond to the case of constant mass and the presence of forces of friction and quasi-elastic attraction. It is clear that the inverse problem can also be set.

Suppose that we have a central body of constant mass surrounded by a spherical dust cloud of constant density. Then the gravitational interaction between this cloud and a moving mass point will be quasi-elastic, while the frictional force will only depend on the velocity; as a result of this, the differential equations of motion of the mass point will be identical with the Equations (10) if in these equations the parameters n and β satisfy the condition

$$n \leqslant \frac{3}{2}, \quad \beta < 0.$$

In the case considered, the differential equations of motion of the mass point have the form

$$\ddot{x} = -\frac{Gm_0}{r^3} x - b\dot{x} - ax, \qquad \ddot{y} = -\frac{Gm_0}{r^3} y - b\dot{y} - ay, \tag{19}$$

where b > 0 and a > 0 are the specified coefficients of friction and elasticity.

Assuming that

$$\left(\frac{n}{3} - 1\right)\beta = b; \qquad -\frac{n(2n-3)}{9} = a, \tag{20}$$

we can determine the values of n and β for which this problem reduces to the problem of two bodies of variable mass moving under the action of only the force of mutual gravitational attraction. In view of this result, it appears to us to be particularly important to investigate the problem of two bodies of variable mass for values of n within the limits 1 ≤ n ≤ 2. Knowing all the solutions for the interval indicated, we would be able to integrate Equations (19) for any values of the coefficients a and b.

Let us now investigate the more complicated problem of the motion of a mass point near a central body of variable mass surrounded by a gravitating and retarding medium of constant density.

The differential equations of motion in this case will have the form

$$\ddot{x} = -\frac{Gm}{r^3} x - b\dot{x} - ax, \qquad \ddot{y} = -\frac{Gm}{r^3} y - b\dot{y} - ay. \tag{21}$$

Using the transformation (5), we find

$$\xi'' = -\frac{Gm_0}{\rho^3} \xi \nu^{3q-2k+1} - [(2q-k)\beta\nu^{n-k-1} + b\nu^{-k}]\xi' - [(1+q-n)q\beta^2\nu^{2(n-k-1)} + bq\beta\nu^{n-2k-1} + a\nu^{-2k}]\xi \tag{22}$$

and the analogous equation for η.

Assuming that in (22)

$$n = 1, \quad 3q - 2k + 1 = 0, \tag{23}$$

we obtain

$$\xi'' = -\frac{Gm_0}{\rho^2}\xi - \left[\frac{1}{2}(q-1)\beta + b\right]\nu^{-k}\xi' - [q^2\beta^2 + bq\beta + a]\nu^{-2k}\xi, \tag{24}$$

from which it follows that for

$$b = \frac{1}{2}(1-q)\beta \text{ and } \quad a = -\frac{q\beta^2}{2}(1+q) \tag{25}$$

the complete solution can be obtained: the representative point will move along the conic section

$$\rho = r\nu^q = \frac{C^2/Gm_0}{1+\varepsilon\cos\vartheta}. \tag{26}$$

It must be pointed out, however, that for the conditions b > 0 and a > 0 to be satisfied, the values of q must lie within very narrow limits. As can be seen from (25), these conditions impose the following limits on q:

$$-1 \leq q \leq 0. \tag{27}$$

Therefore, the solution of the problem in the form (26) can only be obtained in the case when the coefficients b and a are related by the equation which follows from (25) and (27) for a given value of β.

The most interesting particular case of the problem investigated is that of the motion of a mass point in a retarding but not gravitating medium. Assuming that in (25) $a = 0$, we obtain $q = 0$, $b = {}^1/_2\,\beta$, as the result of which the equation of the orbit (26) will have the form

$$r = \frac{C^2/Gm_0}{1+\varepsilon\cos\vartheta}\,. \tag{28}$$

Therefore, if the mass of the central body surrounded by a retarding medium of constant density is decreasing exponentially,

$$m = m_0 e^{-\beta t},$$

and if the coefficient of friction for motion of the mass point in this medium under the influence of the gravitational attraction towards the central body satisfies the condition $b = {}^1/_2\,\beta$, then for any initial conditions the motion of the point will be along an unperturbed conic section but with decreasing sector velocity.

On the other hand, if $b > {}^1/_2\,\beta$ and the retarding force is greater than the accelerating force (11), the mass point (with $\epsilon_0 \leq 1$) will gradually approach the central body along a spiral. Finally, if $b < {}^1/_2\,\beta$ then, despite the presence of retardation, the dimensions of the mass-point orbit will experience a secular increase, whatever the initial conditions of its motion.

K. D. Ushinskii
Iaroslav State Pedagogical Institute

Received November 1, 1956

LITERATURE CITED

[1] D. Ia. Martynov, Doklady Akad. Nauk SSSR 60, 1149 (1948).

[2] V. G. Fesenkov, Doklady Akad. Nauk SSSR 64, 795 (1949).

[3] V. A. Krat, Voprosy Kosmogonii Akad. Nauk SSSR 1, 34 (1952).

[4] J. Jeans, Astronomy and Cosmogony (Cambridge, 1929).

[5] I. V. Meshcherskii, On the Mechanics of Bodies of Variable Mass [in Russian] (GITTL, Moscow-Leningrad, 1949).

[6] J. Jeans, Monthly Notices Roy. Astron. Soc. 85, 2 (1924).

[7] A. A. Batyrev, Astron. J. (USSR) 18, 343 (1941).

[8] G. Armellini, Atti accad. naz. Lincei, Rend. Classe sci. fis., mat. e natur. 15, 345 (1953).

[9] V. V. Radzievskii, Problems of Photogravitational Celestial Mechanics [in Russian] (Dissertation) (State Astronomical Observatory, 1954).

SOME METHODS OF PLOTTING AN INTERMEDIATE ORBIT FOR ASTEROIDS OF THE TROJAN GROUP. II.

Iu. A. Riabov

A method of computing an intermediate orbit for the "Trojans" without the use of mechanical quadratures or numerical harmonic analysis is considered. The final expressions for the major axis, the longitude of the perihelion and the difference of longitude between Jupiter and a "Trojan" are given in the form of a general solution of differential equations for the intermediate orbit and contain three arbitrary constants. They can conveniently be used in a development of a more accurate theory of motion of the "Trojans".

The method of computing an intermediate orbit described in [1] suffers from the disadvantage that it involves mechanical quadratures and so it is necessary to compute an intermediate orbit for each "Trojan" separately. Furthermore, in order to carry out these mechanical quadratures it is necessary to have numerical values for the initial osculating elements, so that one obtains not the general solution of the equations for the intermediate orbit which contains arbitrary constants of integration, but a particular solution determined by the initial conditions.

The latter is of course a drawback when one attempts to improve the intermediate orbit and to use it in a further development of an accurate analytical theory of motion of the "Trojans". In view of all this it appears to us that it would be expedient to introduce an additional simplification of the right-hand sides of the differential equations which determine the intermediate orbit and so avoid the necessity for numerical integration.

§ 1. Differential Equations for the Intermediate Orbit

We shall retain in the right-hand sides of Equation (16) of the previous paper [1] only terms of zero order in e, i. e., we shall reject terms of the order of e^2, e^4, . . . etc. (the equations do not contain terms of odd order in e).

As a matter of fact, the intermediate orbit obtained as a result of these simplifications should coincide with the orbits obtained by Thüring [2, 3] and Brown [4, 5] since these workers neglected analogous terms in their equations for the intermediate orbit. However, Thüring and Brown used mechanical quadratures or methods of numerical harmonic analysis. We, on the other hand, obtain explicit expressions which represent the general solution of the differential equation of the intermediate orbit.

We note that, in the derivation of Equations (16) in [1], we used a simplified method of averaging, as a result of which the perturbation function did not contain a whole series of constants and long-period terms of the order of e^2 or higher. This leads us to suppose that the rejection of all the terms of (16) depending on e will not produce a marked deterioration of the final results.

Replacing the mean anomaly M by the Delaunay anamoly D and rearranging, we can write down the equations which determine our intermediate orbit in the form

$$\begin{aligned}
\frac{da_*}{dt} &= m2a_*\sqrt{a_*}\,[1-(1+\rho)^{-3/2}]\sin D_*;\\
\frac{d\bar{\omega}_*}{dt} &= m\frac{1}{\sqrt{a_*}}\left\{\frac{1}{a_*}-a_*^2+[1-(1+\rho)^{-3/2}]\left(\frac{3}{2}\,a_*^2+a_*\cos D_*\right)\right\};\\
\frac{dD_*}{dt} &= \frac{1}{a_*\sqrt{a_*}}-1-2\sqrt{a_*}m\left\{\frac{1}{a_*^2}-a_*\,[1-(1+\rho)^{-3/2}]\,(a_*-\cos D_*)\right\};\\
\frac{de_*}{dt} &= \frac{d\Omega_*}{dt}=\frac{di_*}{dt}=0,
\end{aligned}\tag{1}$$

where $\rho=a_*^2-2a_*\cos D_*$, $D_*=\bar{\omega}_*+M_*-\lambda'$.

§ 2. Solution of the Equations of the Intermediate Orbit

Equations (1) have the following Jacobi integral

$$\frac{1}{2a_*}+\sqrt{a_*}+m\left(-\frac{1}{a_*}-\frac{1}{2}\,a_*^2\right)+m\left(\frac{1}{\sqrt{1+\rho}}-1+\frac{1}{2}\,\rho\right)=C,\tag{2}$$

where C is a constant.

Having obtained this integral, which relates a_* and D_*, we need only, in the solution of Equations (1), find a_* and ω_* as functions of time.

We shall express integral (2) in the form

$$\frac{1}{\sqrt{1+\rho}}-1+\frac{1}{2}\,\rho=q^2,\tag{3}$$

where

$$q^2=\frac{1}{m}\left[C-\frac{3}{2}+\frac{3}{2}\,m-\frac{1}{a_*}-\sqrt{a_*}+\frac{3}{2}+m\left(\frac{1}{a_*}+\frac{1}{2}\,a_*^2\right)-\frac{3}{2}\,m\right].\tag{4}$$

In considering (3) as an equation determining ρ as a function of $\underline{q}$ we shall rewrite it in the form (introducing a common denominator and removing the irrational term)

$$\rho^3-\rho^2(3+4q^2)+\rho(4q^2+4q^4)+8q^2+4q^4=0.\tag{5}$$

This equation has, in general, three roots but we are only interested in two of them, namely, those that are zero for q = 0. Equation (5) may be solved in a closed form by means of well-known algebraic methods. The roots which vanish at q = 0 are the following:

$$\begin{aligned}
\rho_1 &= -\sqrt[3]{r}\left(\cos\frac{\varphi}{3}+\sqrt{3}\sin\frac{\varphi}{3}\right)+1+\frac{4}{3}\,q^2,\\
\rho_2 &= -\sqrt[3]{r}\left(\cos\frac{\varphi}{3}-\sqrt{3}\sin\frac{\varphi}{3}\right)+1+\frac{4}{3}\,q^2,
\end{aligned}\tag{6}$$

where

$$r=\sqrt{1+4q^2+\frac{20}{3}\,q^4+\frac{416}{81}\,q^6+\frac{80}{27}\,q^8+\frac{64}{81}\,q^{10}+\frac{64}{729}\,q^{12}},$$

$$\sin\varphi=\pm\frac{q\sqrt{8}}{r}\sqrt{1+\frac{2}{3}\,q^2+\frac{4}{81}\,q^4}.$$

It is easy to see that

$$\rho_1(+q)=\rho_2(-q),$$

so that Equations (6) may be combined and written in the form

$$\rho = -\sqrt[3]{r}\left(\cos\frac{\varphi}{3} + \sqrt{3}\sin\frac{\varphi}{3}\right) + 1 + \frac{4}{3}q^2, \tag{6*}$$

where q can assume positive and negative values.

If

$$4q^2 + \frac{20}{3}q^4 + \frac{416}{81}q^6 + \frac{80}{27}q^8 + \frac{64}{81}q^{10} + \frac{54}{729}q^{12} \leqslant 1,$$

i. e., if the absolute magnitude of q does not exceed about 0.43, then r and all the quantities which enter into (6*) can be developed into series of integral powers of q. When this is carried out we obtain

$$\begin{gathered}\rho = \sqrt{\frac{8}{3}}\,q + \frac{10}{9}q^2 + \frac{40}{81}\sqrt{\frac{3}{8}}\,q^3 - \frac{8}{243}q^4 - \\ - \frac{28}{729}\sqrt{\frac{3}{8}}\,q^5 + \frac{64}{6561}q^6 + \frac{670}{177147}\sqrt{\frac{3}{8}}\,q^7 + \ldots.\end{gathered} \tag{7}$$

If the values of $|q|$ do not exceed 0.25 then it is possible to show that the inclusion of terms up to and including terms of the seventh order in q ensures that ρ will be accurate to within $5 \cdot 10^{-8}$.

We note that when q is close to $\pm$ 0.43, or even when $q = \pm$ 0.45 and the series (7) in general diverge, the family of terms written down above can still be used for approximate calculations of ρ for given q.

Starting with the expression

$$1 - (1+\rho)^{-3/2} = 1 - \left(1 + q^2 - \frac{1}{2}\rho\right)^3,$$

which can be obtained using the integral (3) and the formulas

$$\sin D_* = \pm\sqrt{1 - \cos^2 D_*} = \pm\sqrt{\frac{4 - a_*^2}{4}(1+p)},$$

where

$$p = \frac{4}{4 - a_*^2}\left(\frac{1}{2}\rho - \frac{1}{4}\frac{\rho^2}{a_*^2}\right),$$

we shall write the equation for a_* in the following form:

$$\frac{dt}{da_*} = \pm\frac{1}{m2\sqrt{6}\,q}\,\frac{1}{a_*\sqrt{a_*}}\sqrt{\frac{4}{4 - a_*^2}}\,(1+v)^{-1}(1+u)^{-1/2}, \tag{8}$$

where

$$\begin{gathered}1 + u = (1+s)^2(1+p), \quad s = q^2 - \frac{1}{2}\rho - \frac{1}{3}\left(q^2 - \frac{1}{2}\rho\right)^2, \\ 1 + v = \sqrt{\frac{3}{8}}\,\frac{\rho}{q} - 2\sqrt{\frac{3}{8}}\,q,\end{gathered}$$

and the negative sign corresponds to the case $D_* < 0$, the positive sign to the case $D_* > 0$.

We note that when $|q| < 0.25$ the quantities u and v do not, in their absolute magnitude, exceed about 0.15, and the product

$$(1+v)^{-1}(1+u)^{-1/2}$$

can be developed as a series of integral powers of q which converges quite rapidly.

Let us now consider Expression (4) for q^2, which can be written, assuming

$$a_* = 1 + x$$

and expanding $\frac{1}{a_*}$, $\sqrt{a_*}$ into power series in x, in the following form:

$$q^2 = \frac{1}{m}\left\{\beta - \left(\frac{3}{8} - \frac{3}{2}m\right)x^2 + \left(\frac{7}{16} - m\right)x^3 - \right.$$
$$\left. - \left(\frac{59}{128} - m\right)x^4 + \left(\frac{121}{256} - m\right)x^5 - \frac{491}{1024}x^6 + \dots\right\}, \tag{9}$$

where β is an arbitrary constant.

The error in q^2, if one retains terms up to the sixth order in x inclusive, is not more than

$$\left|\frac{x^5}{1+x}\right| + \frac{1}{2}\left|\frac{x^7}{m}\right|,$$

i. e., for $|x| < 0.01$ it is of the order of 10^{-10} or less.

Let us try and express q^2 in the form

$$q^2 = \frac{1}{m}(\mu^2 - z^2)\varphi(z), \tag{9*}$$

where $\varphi(z)$ is the following series in z:

$$\varphi(z) = a_0 + a_1 z + a_2 z^2 + \dots, \quad z = x - \varepsilon,$$

and μ, ϵ, a_0, a_1 are constants depending on β and the coefficients of the series (9).

Substituting $x = z + \epsilon$, removing the brackets in (9*), and equating the coefficients of the same powers of z, we obtain for μ^2, ϵ, a_0, a_1, . . ., a_4 the following series (the value of m was assumed equal to 0.9838753):

$$\begin{aligned}
\mu^2 &= 2.676\,880\,36\,\beta + 3.408\,414\,\beta^2 + 1.594\,\beta^3 + \dots,\\
\varepsilon &= 0.584\,290\,87\,\mu^2 - 0.210\,887\,78\,\mu^4 + \dots,\\
a_0 &= 0.373\,569\,18 - 0.305\,226\,\mu^2 + 0.317\,\mu^4 + \dots,\\
a_1 &= -0.436\,546\,12 + 0.602\,401\,\mu^2 - 0.311\,\mu^4 + \dots,\\
a_2 &= 0.459\,983\,6 - 0.901\,35\,\mu^2 + \dots, \quad a_3 = -0.473 + \dots, \quad a_4 = 0.479 + \dots
\end{aligned} \tag{10}$$

In carrying out these calculations it is easy to see that the above formulas determine $\varphi(z)$ with an error of the order of μ^4 and q^2 with an error of the order of μ^6/m. We shall meet values of μ of the order of 10^{-2}, so that the errors in $\varphi(z)$ and q^2 will be of the order of 10^{-8} and 10^{-9}, respectively.

Starting with (9*), the expression for q may be put into the form

$$q = \pm\sqrt{\frac{\mu^2 - z^2}{m}}\,[\varphi(z)]^{1/2},$$

where $[\varphi(z)]^{1/2}$ is expressed in the form of a series of integral powers of z.

Let us now put

$$z = \mu\cos\theta$$

so that q can be written in the form

$$q = \frac{\mu}{\sqrt{m}}\sin\theta f(\theta), \tag{11}$$

where $f(\theta)$ is a trigonometric series in cosines and sines of multiples of θ and whose coefficients are functions of μ.

We shall transform Equations (8) by expanding $(1 + v)^{-1} (1 + u)^{-1/2}$ into a series of powers of q, and the coefficients of this series which depend on a_*, and the general coefficient

$$\frac{1}{a_* \sqrt{a_*}} \sqrt{\frac{4}{4 - a_*^2}}$$

into a series of powers of z, assuming that

$$z = \mu \cos \theta$$

and substituting Expression (11) for q. After rearranging and replacing the variable a_* by θ we have

$$\frac{dt}{d\theta} = \mp \frac{1}{n} \Phi(\theta), \tag{12}$$

where

$$\begin{aligned}
\Phi = (&1 + 0.16714774\, d^2 + 0.13045513\, d^4 + 0.07538668\, d^6 + \\
&+ 0.06085488\, d^8 + 0.04531851\, d^{10} + \dots) + \\
&+ (-0.02942819\, d - 0.01665890\, d^3 - 0.01304962\, d^5 - \\
&- 0.00912281\, d^7 - 0.00727964\, d^9 + \dots) \cos \theta + \\
&+ (0.81649658\, d + 0.22573245\, d^3 + 0.17608226\, d^5 + \\
&+ 0.13068943\, d^7 + 0.10265826\, d^9 + \dots) \sin \theta + \\
&+ (-0.16548816\, d^2 - 0.17284799\, d^4 - 0.11204271\, d^6 - \\
&- 0.09653187\, d^8 - 0.07511448\, d^{10} + \dots) \cos 2\theta + \\
&+ (-0.03323611\, d^2 - 0.02059516\, d^4 - 0.01723384\, d^6 - \\
&- 0.01390422\, d^8 - 0.00917894\, d^{10} + \dots) \sin 2\theta + \\
&+ (0.01671045\, d^3 + 0.01959950\, d^5 + 0.01635803\, d^7 + 0.01457483\, d^9 + \dots) \cos 3\theta + \\
&+ (-0.07471112\, d^3 - 0.08677621\, d^5 - \\
&- 0.07745402\, d^7 - 0.06776725\, d^9 + \dots) \sin 3\theta + \\
&+ (0.04239866\, d^4 - 0.04362053\, d^6 + 0.04701662\, d^8 + \\
&+ 0.04222108\, d^{10} + \dots) \cos 4\theta + \\
&+ (0.01028603\, d^4 - 0.01372675\, d^6 + \\
&+ 0.01383869\, d^8 + 0.01051178\, d^{10} + \dots) \sin 4\theta + \\
&+ (-0.00648901\, d^5 - 0.00900722\, d^7 - 0.01046271\, d^9 + \dots) \cos 5\theta + \\
&+ (0.01684887\, d^5 + 0.02524602\, d^7 + 0.02800918\, d^9 + \dots) \sin 5\theta + \\
&+ (-0.00696457\, d^6 - 0.01283351\, d^8 - 0.00038722\, d^{10} + \dots) \cos 6\theta + \\
&+ (-0.00341095\, d^6 - 0.00593244\, d^8 - 0.00590323\, d^{10} + \dots) \sin 6\theta + \\
&+ (0.00169059\, d^7 + 0.00369076\, d^9 + \dots) \cos 7\theta + \\
&+ (-0.00338194\, d^7 - 0.00661138\, d^9 + \dots) \sin 7\theta + \\
&+ (0.00170541\, d^8 - 0.00330034\, d^{10} + \dots) \cos 8\theta + \\
&+ (0.00079156\, d^8 + 0.00176054\, d^{10} + \dots) \sin 8\theta + \\
&+ (-0.00042051\, d^9 + \dots) \cos 9\theta + (0.00078051\, d^9 + \dots) \sin 9\theta + \\
&+ (-0.000363\, d^{10} + \dots) \cos 10\theta + (-0.00010927\, d^{10} + \dots) \sin 10\theta + \dots,
\end{aligned} \tag{12*}$$

$$n = \sqrt{18\left(\frac{3}{8} - \frac{3}{2} m\right) m} = 0.080\,080\,023,$$

where d is a constant which depends on μ in the following way:

$$d^2 = \frac{\mu^2}{m}\left(\frac{3}{8} - m\right). \qquad (12^{**})$$

The negative sign on the right-hand side corresponds to the case $D_* > 0$, the positive sign to the case $D_* < 0$.

Integrating (12) we obtain an equation which determines θ as a function of t:

$$(t - t_0)\,n = \pm\int \Phi\, d\theta - \bar{C}, \qquad (13)$$

where $\bar{C}$ is an arbitrary constant and the unit of time is 689$^{\mathrm{d}}$.5503.

The equation for $\bar{\omega}_*$ can be expressed in the following form by transforming to a new independent variable θ and expressing the right-hand side in the form of a trigonometric series of cosines and sines of multiples of θ:

$$\frac{d\bar{\omega}_*}{d\theta} = \pm\Phi_1(\theta), \qquad (14)$$

where

$$\begin{aligned}\Phi_1 = {} & (-0.02779473\,d^2 - 0.00341885\,d^4 + \\ & + 0.00044948\,d^6 - 0.00026030\,d^8 + \ldots) + \\ & + (-0.00180553\,d + 0.00035897\,d^3 + 0.00003422\,d^5 + \ldots)\cos\theta + \\ & + (0.05834850\,d + 0.02029708\,d^3 + 0.00106335\,d^5 + \ldots)\sin\theta + \\ & + (0.02784016\,d^2 + 0.00453226\,d^4 - 0.00006618\,d^6 + \ldots)\cos 2\theta + \\ & + (-0.00024570\,d^2 - 0.00040521\,d^4 + \ldots)\sin 2\theta + \\ & + (-0.00036232\,d^3 - 0.00005133\,d^5 + \ldots)\cos 3\theta + \\ & + (-0.00670161\,d^3 - 0.00048261\,d^5 + \ldots)\sin 3\theta + \\ & + (-0.00111341\,d^4 + 0.00026447\,d^6 + \ldots)\cos 4\theta + \\ & + (0.00020622\,d^4 + \ldots)\sin 4\theta + \\ & + (0.00001711\,d^5 + \ldots)\cos 5\theta + (0.00007689\,d^5 + \ldots)\sin 5\theta + \ldots\end{aligned} \qquad (14^*)$$

On integrating, we have

$$\bar{\omega}_* = \pm\int \Phi_1\, d\theta + B, \qquad (14^{**})$$

where B is an arbitrary constant.

It is not necessary to integrate the expression for D_* since D_* is related to a_* and ρ by the relation

$$\cos D_* = \frac{1}{2}a_* - \frac{1}{2a_*}\rho,$$

and ρ may be expressed in terms of θ by means of Equations (7) and (11).

Let us now express the formulas which determine our intermediate orbit in the following form:

$$\begin{aligned}& (1 + 0.16714774\,d^2 + 0.13045513\,d^4 + 0.07538668\,d^6 + \\ & + 0.06085488\,d^8 + 0.04531851\,d^{10} + \ldots)\,\theta = \mp n(t - t_0) + \bar{C} + \\ & + (0.81649658\,d + 0.22573245\,d^3 + 0.17608226\,d^5 + \\ & + 0.13068943\,d^7 + 0.10265826\,d^9 + \ldots)\cos\theta + \\ & + (0.02942819\,d + 0.01665890\,d^3 + 0.01304962\,d^5 + \\ & + 0.00912281\,d^7 + 0.00727964\,d^9 + \ldots)\sin\theta + \\ & + (-0.01661806\,d^2 - 0.01029758\,d^4 - 0.00861692\,d^6 - \\ & - 0.00695211\,d^8 - 0.00458947\,d^{10} + \ldots)\cos 2\theta + \\ & + (0.08274408\,d^2 + 0.08642400\,d^4 + 0.06602136\,d^6 + \\ & + 0.04826594\,d^8 + 0.03755724\,d^{10} + \ldots)\sin 2\theta +\end{aligned}$$

$$
\begin{gathered}
+(-0.02490371\,d^3 - 0.02892540\,d^5 - \\
-0.02581801\,d^7 - 0.02258908\,d^9 + \ldots)\cos 3\theta + \\
+(0.00557015\,d^3 - 0.00653317\,d_5 - \\
-0.00545268\,d^7 - 0.00485828\,d^9 + \ldots)\sin 3\theta + \\
+(0.00257151\,d^4 + 0.00343169\,d^6 + \\
+0.00345967\,d^8 + 0.00262795\,d^{10} + \ldots)\cos 4\theta + \\
+(-0.01059966\,d^4 - 0.01090513\,d^6 - \\
-0.01175416\,d^8 + 0.01055527\,d^{10} + \ldots)\sin 4\theta + \\
+(0.00336977\,d^5 + 0.00504920\,d^7 + 0.00560184\,d^9 + \ldots)\cos 5\theta + \\
+(0.00129780\,d^5 + 0.00180144\,d^7 + 0.00209254\,d^9 + \ldots)\sin 5\theta + \\
+(-0.00056849\,d^6 + 0.00098874\,d^8 + \ldots)\cos 6\theta + \\
+(0.00116076\,d^6 - 0.00213892\,d^8 + \ldots)\sin 6\theta + \\
+(-0.00048313\,d^7 - 0.000944\,d^9 + \ldots)\cos 7\theta + \\
+(-0.00024151\,d^7 - 0.00052725\,d^9 + \ldots)\sin 7\theta + \ldots
\end{gathered}
\tag{15_1}
$$

$$
\begin{gathered}
\bar{\omega}_* = B \pm \{(-0.02779473\,d^2 - 0.00341885\,d^4 + \\
+0.00044948\,d^6 + 0.00026030\,d^8 + \ldots)\theta + \\
+(-0.00180553\,d + 0.00035897\,d^3 + 0.00003422\,d^5 + \ldots)\sin\theta + \\
+(-0.05834850\,d - 0.02029708\,d^3 - 0.00106335\,d^5 + \ldots)\cos\theta + \\
+(0.01392008\,d^2 - 0.00226613\,d^4 - 0.00003309\,d^6 + \ldots)\sin 2\theta + \\
+(0.00012285\,d^2 - 0.00020260\,d^4 + \ldots)\cos 2\theta + \\
+(-0.00012077\,d^3 - 0.00001711\,d^5 + \ldots)\sin 3\theta + \\
+(0.00223387\,d^3 + 0.00016087\,d^5 + \ldots)\cos 3\theta + \\
+(-0.00027835\,d^4 + 0.00006612\,d^6 + \ldots)\sin 4\theta + (-0.00005156\,d^4 + \ldots)\cos 4\theta + \\
+(0.00000342\,d^5 \ldots)\sin 5\theta + (-0.00001538\,d^5 + \ldots)\cos 5\theta - \ldots;
\end{gathered}
\tag{15_2}
$$

$$
a_* = 1 + 0.00149193\,d^2 - 0.00000137\,d^4 + \ldots + 0.05053127\,d\cos\theta; \tag{15_3}
$$

$$
\begin{gathered}
\frac{1}{2}\rho = (0.27777778\,d^2 - 0.00653402\,d^4 + 0.00154058\,d^6 + \ldots) + \\
+(-0.00820138\,d^3 + 0.00026057\,d^5 - 0.00006832\,d^7 + \ldots)\cos\theta + \\
+(0.81649658\,d + 0.11278249\,d^3 + \\
-0.00759001\,d^5 + 0.00002571\,d^7 + \ldots)\sin\theta + \\
+(-0.27777778\,d^2 + 0.00880998\,d^4 - 0.00231693\,d^6 + \ldots)\cos 2\theta + \\
+(-0.01205351\,d^2 - 0.00332807\,d^4 + 0.00028130\,d^6 + \ldots)\sin 2\theta + \\
+(0.00820138\,d^3 - 0.00038775\,d^5 + 0.00012301\,d^7 + \ldots)\cos 3\theta + \\
+(-0.03756885\,d^3 + 0.00384971\,d^5 - 0.00002237\,d^7 + \ldots)\sin 3\theta + \\
+(-0.00227595\,d^4 + 0.00093292\,d^6 + \ldots)\cos 4\theta + \\
+(-0.00166917\,d^4 - 0.00022466\,d^6 + \ldots)\sin 4\theta + \\
+(0.00012717\,d^5 - 0.00006836\,d^7 + \ldots)\cos 5\theta + \\
+(-0.00079183\,d^5 + 0.00001206\,d^7 + \ldots)\sin 5\theta + \\
+(-0.00015764\,d^6 + \ldots)\cos 6\theta + (0.00005601\,d^6 + \ldots)\sin 6\theta + \ldots;
\end{gathered}
\tag{15_4}
$$

$$
e_* = e_0; \quad \Omega_* = \Omega_0; \quad i_* = i_0,
$$

where e_0, Ω_0, i_0 are the initial values of the eccentricity, the longitude of the node, and the inclination; $\underline{d}$, $\bar{C}$, B are constants which depend on the initial values of the major semiaxes the Delaunay anomaly, and the longitude of the perihelion; the positive sign in front of $n(t - t_0)$ in (15_1) and in front of the brace in (15_2) corresponds to $D_* < 0$, and the negative sign to $D_* > 0$.

We have thus obtained the solution of the initial equations (1) in the form of series, in general, expanded in integral positive powers of the constant $\underline{d}$. It is easy to see, on analysis of the above developments, that these series will converge if ρ can be developed into the series (7) in powers of $\underline{q}$ (i. e., if $\underline{q}$ does not exceed, in its absolute magnitude, about 0.43) and if the quantities x and z are small in their absolute magnitudes compared with unity. The limits for q, z, and x are determined, as can be seen from (9) and (9*), by the inequalities

$$q^2 \leqslant \frac{\beta}{m}, \qquad |z| < \mu, \qquad |x| < \mu + \varepsilon,$$

where the constants β, μ, ϵ are interdependent among themselves and depend on d in the way given by (10) and (12*). If one of these constants is known the others can, in general, be calculated.

The absolute values of q will not exceed 0.43 if the constant β is not greater than $1.8 \cdot 10^{-4}$ (to two significant figures). With this limiting value of β the constants μ, ϵ, d are given to the same accuracy by

$$\mu = 2.2 \cdot 10^{-2}, \qquad \varepsilon = 2.8 \cdot 10^{-4}, \qquad d = 0.43.$$

The condition that x, z should be small is satisfied and our series converges if $\beta < 1.8 \cdot 10^{-4}$ i. e., if $d < 0.43$.

We have determined only the first few terms of these series as given in Equations (15). We shall now estimate the error which we allow by limiting ourselves to only those terms which are given in Equations (15). Since it is difficult to find a general expression for the residual term we shall carry out this estimate of accuracy under the condition that $\beta \leqslant 0.0625\, m$, i.e., $|q| \leqslant 0.25$, $d \leqslant 0.2500$, $\mu \leqslant 1.263 \cdot 10^{-2}$, $|z| \leqslant 1.263 \cdot 10^{-2}$, $|x| \leqslant 1.263 \cdot 10^{-2}$ (with an accuracy of up to four significant figures).

As was shown above, Expressions (7) and (9*) for ρ and q^2 determine these quantities with an accuracy of up to $5 \cdot 10^{-8}$ and 10^{-9}, respectively, if $|q| \leq 0.25$ and $|z| \leq 0.01$. In our case $|z|$ may exceed 0.01 somewhat but this, in any case, does not change the order of the error in (9*).

In carrying out the above calculations we assumed that Expressions (7) and (9*) for ρ and q^2 are accurate if we limit ourselves to the terms written down above. Using these expressions for ρ and q^2 we carried out all the calculations in such a way that the rejected terms in the corresponding series and polynomials did not altogether exceed 1-2 digits in the 8th decimal place (if $|q| \leq 0.25$, $|z| \leq 0.01$). However, remembering that Expressions (7) and (9*) determine ρ and q^2 with an accuracy of up to $5 \cdot 10^{-8}$ and 10^{-9}, respectively, for $|q| \leq 0.25$, $|q| \leq 0.01$, it is easy to estimate that the error in the function Φ on the right-hand side of Equation (12) does not exceed $\pm\, 4 \cdot 10^{-7}$ if we limit ourselves to the terms written down above, and the error in the right-hand side of Equation (14) does not exceed $\pm\, 2 \cdot 10^{-8}$.

We shall express the functions Φ and Φ_1 in the form

$$\Phi = \bar{\Phi} + \Delta\Phi, \qquad \Phi_1 = \bar{\Phi}_1 + \Delta\Phi_1,$$

where $\bar{\Phi}$, and $\bar{\Phi}_1$ is the family of terms included in Formulas (12*) and (14*), and $\Delta\Phi$, $\Delta\Phi_1$ is the sum of rejected terms, where

$$|\Delta\Phi| < 4 \cdot 10^{-7}, \qquad |\Delta\Phi_1| < 2 \cdot 10^{-8}.$$

We shall denote by α the constant term and by $\bar{\bar{\Phi}}$ the aggregate of terms which depend on θ as a function of $\bar{\Phi}$. The solution of Equation (12) can then be written down in the form

$$\mp n(t - t_0) = \int_{\theta_0}^{\theta} (\alpha + \bar{\bar{\Phi}} + \Delta\Phi)\, d\theta$$

or

$$\alpha(\theta - \theta_0) = \mp n(t - t_0) - \int_{\theta_0}^{\theta} \bar{\bar{\Phi}} d\theta - \int_{\theta_0}^{\theta} \Delta\Phi\, d\theta,$$

where θ_0 is the initial value of θ.

Comparing this exact equation, which determines θ as a function of $\underline{t}$, with the approximate one which does not take into account the aggregate of terms $\Delta\Phi$:

$$\alpha(\bar{\theta}-\theta_0) = \mp n(t-t_0) - \int_{\theta_0}^{\bar{\theta}} \bar{\bar{\Phi}} d\theta,$$

we find that

$$\alpha(\bar{\theta}-\theta) = \int_{\bar{\theta}}^{\theta} \bar{\bar{\Phi}} d\theta + \int_{\theta_0}^{\theta} \Delta\Phi \, d\theta$$

or

$$\Delta\theta = \bar{\theta} - \theta = \frac{1}{\alpha + \bar{\bar{\Phi}}(\tilde{\theta})} \int_{\theta_0}^{\theta} \Delta\Phi \, d\theta,$$

where $\theta < \tilde{\theta} < \bar{\theta}$ or $\bar{\theta} < \tilde{\theta} < \theta$.

Since, for given θ, $\bar{\bar{\Phi}}$ is a relatively small quantity and α is close to unity, it follows that the error in the required and unknown θ, which is determined by Expression (15_1), does not exceed a quantity of the order of $4 \cdot 10^{-7} \mid \theta - \theta_0 \mid$. With $\mid \theta - \theta_0 \mid = 2\pi$, i. e., over a period of changes in a_* and D_* equal to, say 150 years, the error $\Delta\theta$ is not more than $3 \cdot 10^{-6}$ (in radians). From the expressions for a_* and ρ we may conclude that the errors Δa_* and $\Delta\rho$ do not exceed $\pm\, 3 \cdot 10^{-8}$ and $\pm\, 1.2 \cdot 10^{-6}$, respectively during this period of time, and the error in D_* is $\sim \pm\, 1''$.

The solution of Equation (14) may be written down in the form

$$\bar{\omega}_* - \bar{\omega}_0 = \pm \int_{\theta_0}^{\theta} (\bar{\Phi}_1 + \Delta\Phi_1) \, d\theta,$$

where $\bar{\omega}_0$ is the initial value of $\bar{\omega}_*$.

Comparing this exact expression with the approximate one in which the aggregate of terms $\Delta\Phi_1$ was not taken into account, and in which instead of the exact value of θ an approximate value $\bar{\theta}$ is used, we find that the error in $\bar{\omega}_*$ for $\mid \theta - \theta_0 \mid = 2\pi$ does not exceed

$$\max \mid \Delta\Phi_1 \mid 2\pi + \max \mid \Phi_1 \mid \Delta\theta,$$

i. e., in any case it does not exceed 10^{-6} (in radians) or 0.1 sec of arc.

Thus if the constant $\underline{d}$ does not exceed 0.25 then the accuracy of our formulas is quite sufficient if we limit ourselves to the number of terms written down above.

§ 3. Application of the Formulas Obtained to Numerical Calculations

We shall now carry out a comparison between the osculating elements given by Equations (15) and the elements obtained by observations for the minor planet No. 884.

To begin with, we note that in Part I [1] we used orbital elements referred to the plane of the ecliptic and have simply neglected the inclination i' of the orbit of Jupiter. However, it is easy to see that all the above equations and formulas retain their form if i' is not neglected and the osculating elements of the orbit of the asteroid are referred to the plane of Jupiter's orbit. Taking the ascending node of Jupiter's orbit as the starting point of our calculations and using Table 3 of [1], we obtain the values given in Table 1 for the osculating elements ω, Ω, $\underline{i}$, D of the minor planet No. 884 (the elements $\underline{a}$, $\underline{e}$, M remain essentially unchanged).

To begin with, we note that the osculating eccentricity, longitude of the node, and inclination change very slowly, as can be seen from observational data. For our intermediate orbit these elements are taken as constant, which, in view of the latter fact, is fully admissible.

TABLE 1

	t_0	t_{-1}	t_{-2}	t_{-3}	t_{-4}	t_{-5}
	1948, VII, 28.0	1940, VII, 31.0	1938, II, 1.0	1931, III, 10.0	1925, I, 1.0	1917, IX, 25.0
$\bar{\omega}$	172.128	171.644	171.164	170.949	170.769	170.924
☊	198.447	198.489	198.490	198.457	198.519	198.534
i	10.120	10.103	10.102	10.114	10.090	10.088
D	—72.744	—71.238	—70.683	—68.548	—66.458	—63.151
a	1.002613	1.005477	1.006015	1.008533	1.010301	1.011340
e	0.12052	0.12007	0.12072	0.11896	0.11808	0.11946

We shall now consider osculations of the major semiaxis, longitude of the perihelion, and the Delaunay anomaly.

Starting with the values of these elements at the instant 1948, VII, 28.0 we recalculate the constants β, μ and $\underline{d}$

$$\beta = 0.475995\cdot 10^{-4}; \qquad \mu = 0.011\,288, \quad d = 0.223\,392,$$

and then the coefficients in Formulas (15) and the constants $\bar{C}$, B*. As a result of calculations we obtain the following formulas:

$$\begin{aligned} \theta = \tau + 74^\circ\!.099 + 10^\circ\!.510\cos\theta + 0^\circ\!.384\sin\theta + \\ - 0^\circ\!.049\cos 2\theta + 0^\circ\!.247\sin 2\theta + \\ - 0^\circ\!.017\cos 3\theta - 0^\circ\!.004\sin 3\theta + \\ - 0^\circ\!.002\sin 4\theta + \ldots; \\ a_* = 1.00007 + 0.01129\cos\theta; \\ \bar{\omega}_* = 172^\circ\!.284 - 0.00139553\,\theta - 0^\circ\!.760\cos\theta - 0^\circ\!.023\sin\theta + \\ + 0^\circ\!.040\sin 2\theta + \\ + 0^\circ\!.001\cos 3\theta \pm \ldots; \end{aligned} \tag{16}$$

$$\begin{aligned} \frac{1}{2}\rho = 0.013846 - 0.000091\cos\theta + 0.183652\sin\theta + \\ - 0.013841\cos 2\theta - 0.000610\sin 2\theta + \\ + 0.000091\cos 3\theta - 0.000417\sin 3\theta + \\ - 0.000006\cos 4\theta + 0.000004\sin 4\theta + \ldots, \end{aligned}$$

where

$$\tau = 0^\circ\!.006597395\,(t - t_0)$$

and $\underline{t}$ is expressed in mean solar days.

A comparison of the osculating major axis, longitude of the perihelion, and the Delaunay anomaly calculated from these formulas and those observed for the minor planet No. 884 has lead to the following result:

	t_0	t_{-1}	t_{-2}	t_{-3}	t_{-4}	t_{-5}
$10^4\,\Delta a_*$	0	—7	—24	—5	+9	+8
$\Delta\bar{\omega}_*$	0	—0°.183	—0°.628	—0°.726	—0°.823	—0°.621
ΔD_*	0	—0°.110	—0°.271	—0°.576	—1°.155	—1°.373

---

[*] In calculating all these constants we ascribed to the osculating elements for the instant 1948, VII, 28.0 a much greater accuracy than that indicated above in the tables, since otherwise $\underline{d}$, $\bar{C}$, B are determined only very approximately. However, such an operation is fully admissible if the obtained values of the constants $\underline{d}$, $\bar{C}$, B are looked upon as very approximate and their values are then improved by comparing the theory with observations.

where $\Delta a_* = a_H = a_*$, $\Delta\bar{\omega}_* = \bar{\omega}_H - \bar{\omega}_*$, $\Delta D = D_H - D_*$; a_H, $\bar{\omega}_H$, D_H are observed and a_*, $\bar{\omega}_*$, D_* are calculated.

We see that comparison of the intermediate orbit with the observed one for the minor planet No. 884 gives a satisfactory result (and even somewhat better than that obtained in [1]).

It is easy to show that for the planets No. 588, 659, 1143 the constants β and α, calculated from the values of the osculating elements for any instant, are even smaller than for the planet No. 884. Thus Formulas (15) determine the intermediate orbit for these minor planets with the same accuracy. At the same time, in the case of the minor planet No. 1173 the quantity $\underline{d}$ is about 0.40-0.41 and the series (15) converge slowly and determine the intermediate orbit to a low accuracy only.

From a comparison of the results of calculations with observational data for the minor planet No. 884 we 4 note that the results could, of course, be improved by calculating the integration constants $\underline{d}$, $\bar{C}$, B in Formulas 5) (15) using the osculating elements observed during the whole interval of time under consideration rather than those given for a single instant of time.

This method of calculating the constants is also better because by using a single system of osculating elements they are only determined very approximately. Thus, for example, if the major semiaxis is known to an accuracy corresponding to the fourth decimal place and the Delaunay anomaly with an accuracy of up to 0°.001 (which is the case in our calculations) then the constants $\bar{C}$, B do not contain more than 2 or 3 significant figures.

Let us make the following substitution in the Formulas (15):

$$\begin{aligned} d &= d_0 + \Delta d, & a_* &= a_*^0 + \Delta a_*, \\ \bar{C} &= \bar{C}_0 + \Delta\bar{C}, & \rho &= \rho^0 + \Delta\rho, \end{aligned}$$

where $\Delta a_* = a_H - a_*^0$, $\Delta\rho = \rho_H - \rho^0$; d_0, $\bar{C}_0$ are the values used in obtaining (16) and are equal to 0.223392, and 74°.742, respectively; a_*^0, ρ_0 are the values calculated from these formulas and a_H and ρ_H are the observed values. We shall denote by ΔD the differences between the observed and the calculated (by means of Formulas (16)) Delaunay anomaly. Using (15), and by limiting our attention to terms of the first order in Δd, $\Delta\bar{C}$, ΔD, Δa, it is possible to obtain simple relations connecting these quantities. Using these relations and the data given in the table on Page 583 we determine the corrections Δd and $\Delta\bar{C}$ so as to make the differences ΔD for the instants of time under consideration as small as possible and unsystematic. We found that

$$\Delta d = -0.006\,465, \qquad \Delta\bar{C} = 7^\circ.254$$

and set up formulas determining a_*, $\bar{\omega}$, ρ, θ using the new values of $\underline{d}$ and $\bar{C}$

$$\begin{aligned} \theta = 0^\circ.00660077\,(t - t_0) + 81^\circ.332 + 10^\circ.202 \cos\theta + 0^\circ.373 \sin\theta &+ \\ - 0^\circ.046 \cos 2\theta + 0^\circ.233 \sin 2\theta &+ \\ - 0^\circ.015 \cos 3\theta - 0^\circ.003 \sin 3\theta &+ \\ - 0^\circ.001 \sin 4\theta &+ \ldots \end{aligned}$$

$$a_* = 1.00007 + 0.01096 \cos\theta,$$

$$\begin{aligned} \bar{\omega}_* = B - 0.0013152\,\theta - 0^\circ.737 \cos\theta - 0^\circ.022 \sin\theta &+ \\ + 0^\circ.037 \sin 2\theta &+ \\ + 0^\circ.001 \cos 3\theta &+ \ldots, \end{aligned}$$

$$\begin{aligned} \frac{1}{2}\rho = 0.013057 - 0.000084 \cos\theta + 0.178268 \sin\theta &+ \\ - 0.013052 \cos 2\theta - 0.000574 \sin 2\theta &+ \\ + 0.000084 \cos 3\theta - 0.000382 \sin 3\theta &+ \\ - 0.000005 \cos 4\theta - 0.000004 \sin 4\theta &+ \ldots \end{aligned}$$

The constant B we assume to be equal to 171°.957, in order to reduce the absolute values of the differences $\bar{\omega}_H - \bar{\omega}_*$, and the elements e_*, Ω_*, i_* as equal to 0.1200, 301°.049 and 8°.890, respectively.

Using these formulas we determine the quantities a_*, D_*, $\overline{\omega}_*$, and comparing with observations we have the following results:

	1917, IX, 25.0	1925, I, 1.0	1931, III, 10.0	1938, II 1.0	1940, VII 31.0	1948, VII, 28.0
$a_H - a_*$	$+0.0041$	$+0.0056$	$+0.0051$	$+0.0037$	$+0.0056$	-0.0063
$D_H - D_*$	$-0\overset{\circ}{.}046$	$-0\overset{\circ}{.}064$	$+0\overset{\circ}{.}248$	$+0\overset{\circ}{.}209$	$+0\overset{\circ}{.}237$	$-0\overset{\circ}{.}089$
$\overline{\omega}_H - \overline{\omega}_*$	$-0\overset{\circ}{.}279$	$-0\overset{\circ}{.}483$	$-0\overset{\circ}{.}390$	$-0\overset{\circ}{.}310$	$-0\overset{\circ}{.}114$	$+0\overset{\circ}{.}400$

We have also carried out calculations of the equatorial coordinates α, δ for the same instants of time using the new osculating elements for the intermediate orbit (α_*, δ_*) and the observed osculating elements (a_H, δ_H). The differences $a_H - a_*$ and $\delta_H - \delta_*$ are given below:

	1917, IX, 25.0	1925, I, 1.0	1931, III, 10.0	1938, II, 1.0	1940, VII, 31.0	1948, VII, 28.0
$\alpha_H - \alpha_*$	$-.0\overset{m}{.}27$	$+0\overset{m}{.}24$	$+0\overset{m}{.}48$	$+1\overset{m}{.}12$	$+1\overset{m}{.}10$	$-0\overset{m}{.}30$
$\delta_H - \delta_*$	$-5\overset{\prime}{.}3$	$-1\overset{\prime}{.}6$	$+2\overset{\prime}{.}1$	$-1\overset{\prime}{.}7$	$+8\overset{\prime}{.}5$	$+2\overset{\prime}{.}9$

One could hardly expect of the intermediate orbit a better representation of observational data.* We note by the way, that when the accuracy of the constants $\underline{d}$, $\overline{C}$, B and the quantities e_*, Ω_*, i_* is improved, in order to obtain a good representation of observations, it would be more correct to use the method of least squares, which we did not do. However, our calculations must be considered as preliminary and were carried out in order to show that, even with our relatively rough intermediate orbit, obtained from considerably simplified differential equations, it is possible to represent observations of the minor planet No. 884 quite well. We consider that further work on the intermediate orbit should be concerned with taking into account those terms in the perturbation function which were neglected in the above treatment, and only after this has been done should the constants of integration be made more accurate.

If the above intermediate orbit is to be used to obtain a more accurate theory of motion of the "Trojans", which would take into account the neglected terms in the perturbation function, it would be useful to have D_* and a_* as explicit functions of $\underline{t}$, and to exclude the auxiliary variable θ. To do this it is first necessary to express θ in terms of $\underline{t}$ using (15_1). This equation, which expresses θ as an implicit function of $\underline{t}$, belongs to the type of the so-called generalized Lagrange equations. Denoting the coefficient of θ on the left side of (15_1) by α, and the aggregate of terms on the right-hand side of (15) which depend on θ by $\overline{f}(\theta, d)$, we can write this equation in the form

$$\theta = \tau + f(\theta, d), \tag{17}$$

where

$$\tau = \mp \frac{n}{\alpha}(t - t_0) + C, \qquad f(\theta, d) = \frac{1}{\alpha}\overline{f}(\theta, d),$$

and C is an arbitrary constant.

---

*The "Trojans" unfortunately experience the greatest perturbations, as compared with other minor planets, which is due to a resonance of the lowest order. For example, if one takes a "normal planet" such as Ceres, then it is possible to choose unperturbed orbit elements which represent the motion of Ceres over a hundred to a hundred and fifty years with an accuracy of a few minutes of arc. In the case of the "Trojans", whatever unperturbed elements we choose, the deviations from unperturbed motion will reach, over 150 years, a quantity of the order of $1/2(D_{max} - D_{min})$ or more. For the "Trojan" No. 884 this quantity is about 13°. For this reason it is difficult to obtain an accurate representation of the motion of the "Trojans". Thus the above differences would not be acceptable in the case of Ceres, but for the "Trojans" they must be considered as very moderate.

The function $f(\theta, d)$ may be expanded into a series of powers of the parameter $\underline{d}$ (in order to do this $1/\alpha$ must be expanded into such a series) where $f(\theta, 0) \equiv 0$.

We may use the well-known expression for the solution of Equation (17):

$$\Phi(\theta) = \sum_{n=0}^{\infty} \frac{1}{(n+1)!} \left\{ \frac{d^n}{d\theta^n} \left[f^{(n+1)}(\theta, d) \right] \right\}_{\theta=\tau}. \tag{18}$$

We shall also have to calculate the functions $\cos k\theta$ and $\sin k\theta$ ($k = 1, 2, 3, \ldots$). For these calculations we use the formula

$$\Phi(\theta) = \Phi(\tau) + \sum_{n=0}^{\infty} \frac{1}{(n+1)!} \left\{ \frac{d_n}{d\theta^n} \left[\Phi'(\theta) f^{(n+1)}(\theta, d) \right] \right\}_{\theta=\tau}, \tag{18*}$$

where $\Phi(\theta)$ is an arbitrary analytical function of θ.

In the expression for the function $f(\theta, d)$ we shall only consider terms up to the 5th order in $\underline{d}$, inclusively. For this reason, in Formulas (18), (18*) we shall confine our attention to terms of the same order.

Having carried out all these calculations, we obtained the following formula for θ:

$$\begin{gathered}
\theta = \tau + (0.816497\, d + 0.055200\, d^3 + 0.067211\, d^5) \cos\tau + \\
+ (0.029428\, d + 0.014851\, d^3 + 0.007835\, d^5) \sin\tau + \\
+ (0.007410\, d^2 + 0.005207\, d^4) \cos 2\tau + (-0.250156\, d^2 + 0.011500\, d^4) \sin 2\tau + \\
+ (-0.127627\, d^3 + 0.002713\, d^5) \cos 3\tau + \\
+ (-0.003626\, d^3 - 0.007883\, d^5) \sin 3\tau + 0.001269\, d^4 \cos 4\tau + \\
+ 0.075721\, d^4 \sin 4\tau + 0.047020\, d^5 \sin 5\tau + 0.001123\, d^5 \sin 5\tau + \ldots
\end{gathered} \tag{19}$$

We then calculated $\cos k\theta$ and $\sin k\theta$ ($k = 1, \ldots, 5$) and, on substituting into the expressions which determine a_* and $\cos D_*$, we finally obtained the following result:

$$\begin{gathered}
a_* = 1 + 0.000747\, d^2 - 0.000298\, d^4 - 0.000274\, d^6 + \\
+ (0.050531\, d - 0.006318\, d^3 + 0.001949\, d^5) \cos\tau + \\
+ (-0.000116\, d^3 - 0.000112\, d^5) \sin\tau + \\
+ (0.000744\, d^2 + 0.000314\, d^4 + 0.000343\, d^6) \cos 2\tau + \\
+ (-0.020629\, d^2 + 0.001692\, d^4 - 0.001285\, d^6) \sin 2\tau + \\
+ (-0.010526\, d^3 + 0.001660\, d^5) \cos 3\tau + \\
+ (-0.000491\, d^3 - 0.000234\, d^5) \sin 3\tau + \\
+ (-0.000323\, d^4 - 0.000231\, d^6) \cos 4\tau + \\
+ (0.006375\, d^4 - 0.001252\, d^6) \sin 4\tau + \\
+ 0.004206\, d^5 \cos 5\tau + 0.000202\, d^5 \sin 5\tau + 0.000061\, d^6 \cos 6\tau - \\
- 0.002875\, d^6 \sin 6\tau + \ldots
\end{gathered} \tag{20}$$

$$\begin{gathered}
\cos D_* = 0.5 - 0.610737\, d^2 - 0.100327\, d^4 - 0.042231\, d^6 + \\
+ (0.025266\, d + 0.031728\, d^3 + 0.009038\, d^5) \cos\tau + (-816497\, d - \\
- 0.170216\, d^3 + 0.065221\, d^5) \sin\tau + (-0.055193\, d^2 - 0.127965\, d^4 - \\
- 0.024256\, d^6) \cos 2\tau + (0.010354\, d^2 - 0.012221\, d^4 - 0.012331\, d^6) \sin 2\tau + \\
+ (0.006448\, d^3 + 0.002955\, d^5) \cos 3\tau + (-0.019267\, d^3 + 0.036461\, d^5) \sin 3\tau + \\
+ (-0.011131\, d^4 + 0.010929\, d^6) \cos 4\tau + (-0.001719\, d^4 - \\
- 0.006231\, d^6) \sin 4\tau + 0.000458\, d^5 \cos 5\tau + 0.003678\, d^5 \sin 5\tau + \\
+ 0.000727\, d^6 \cos 6\tau + 0.000700\, d^6 \sin 6\tau + \ldots
\end{gathered} \tag{20*}$$

Formulas (20)(20*) determine a_* and $\cos D_*$ with an accuracy corresponding to terms of the 6th order in d inclusively.

If the mean solar day is chosen as the unit of time (for this n must be divided by 689.5503) then the variable τ will depend on t in the following way:

$$\tau = \mp 0^\circ.0066546328\,(1 - 0.167148\,d^2 - 0.102517\,d^4 - \\ - 0.036447\,d^6 - 0.028248\,d^8 + \ldots)\,(t - t_0) + C.$$

The above expressions for the intermediate orbit were calculated for use in the case of those "Trojans" for which the parameter does not exceed about 0.25 (planets No. 588, 659, 884, 1143). With such values of d one may guarantee that the above formulas give 5 significant figures. As far as the convergence of the series (19) and the series (20)(20*) are concerned it can be shown that they converge in the same region in which the series used to represent the right-hand side of (8), and to obtain (15), converge i. e., when d is less than about 0.43.

The radius of convergence of the solution $\theta = \theta(d)$ of Equation (17) expanded as a series in powers of d may, in general, be found by simultaneously solving in the complex plane Equations (17) and

$$1 - f_0'(\theta,\ d) = 0. \tag{21}$$

The general roots of these equations determine singular points of the function $\theta = \theta(d)$ considered as a function of a complex variable. If $\bar{d}$ is the root having the smallest modulus, then $|\bar{d}|$ gives the required radius of convergence for $\theta(d)$.

In our case it was not necessary to find the radius of convergence in this way since the problem can be solved in a simpler way. In fact, the function $f(\theta,\ d)$ in Equation (17) is only considered for $d < 0.43$ (i. e., inside the circle C which has radius $|d| = 0.43$ in the complex plane) for which it is expanded into a series of powers of d. However, the function $\theta = \theta(d)$ does not have singular points within this circle. We shall express the derivative $f_\theta'(\theta,\ d)$ in a closed form which is possible since we obtained the function, $f(\theta,\ d)$ on integrating Equation (11), the right-hand side of which is expressed through the right-hand side of (8). It turns out that, to within a constant multiplier, the expression $1 - f_\theta'(\theta,\ d)$ is equal to the right-hand side of (8) multiplied by $\sin\theta$:

$$1 - f_\theta'(\theta,\ d) = L\,\frac{1}{(1+\varepsilon+\mu\cos\theta)^{3/2}} \cdot \frac{2}{\sqrt{4-(1+\varepsilon+\mu\cos\theta)^2}} \cdot \frac{1}{\sqrt{\varphi(\mu\cos\theta)}}\,\frac{1}{(1+v)}\,\frac{1}{\sqrt{1+u}},$$

where L is a constant and the remaining quantities are determined by the formulas given above. In any case, in the region in which the functions f, f_θ' and $\theta(d)$ were considered, the above expression (in which θ is a complex function of d determined by (17)) does not vanish. It follows that within the circle C the function $\theta = \theta(d)$ does not have singular points and is an analytical function of d for $|d| < 0.43$. The radius of convergence of the series (20), (20*) is clearly identical. For $|d| > 0.43$ all the series considered above diverge.

In conclusion we wish to express our deep gratitude to the staff of the Department of Celestial Mechanics of the Moscow State University for their valuable advice and suggestions which helped us to carry out the present work.

P. K. Shternberg State Astronomical Institute

Received April 19, 1956

LITERATURE CITED

[1] Iu. A. Riabov, Astron. J. (USSR) 34, 276 (1957). *

[2] B. Thüring, Astron. J. 238, 357 (1930).

[3] B. Thüring, Astron. J. 243, 182 (1931).

[4] E.W. Brown, Trans. Astron. Obs. Yale University 3 (1923).

[5] E.W. Brown, Astron. J. 35, 69 (1923).

---

*[Soviet Physics – Astronomy, p. 268.]

AUTOMODEL MOTION OF A GAS WITH SPHERICAL SYMMETRY IN THE FIELD OF A GRAVITATING CENTER

M. L. Lidov

The problem of a central explosion in the Roche model was solved in [1] for the adiabatic coefficients $\gamma = 5/3$ and $\gamma = 3/2$.

A more general formulation of automodel problems involving nonstationary motion of a gas in the field of a gravitating center is given below starting with results of dimensional analysis.

Two integrals of the system of ordinary equations corresponding to the problem considered in [1] are given for an arbitrary value of the adiabatic coefficient. For $\gamma = 4/3$ an exact solution of this problem is obtained involving quadratures.

The method of formulation of automodel problems used below is based on analogous solutions given in L. I. Sedov's book [2].

The problem of a central explosion in the Roche model was solved in [1] for the adiabatic coefficients $\gamma = 5/3$ and $\gamma = 3/2$. The authors found a particular solution which depends essentially on a single independent variable (automodel solution). The automodel formulation made it possible to go over from a system of equations involving partial differentials to ordinary equations, the complete system of which was integrated numerically.

A more general formulation of automodel problems involving nonstationary motion of gas in the field of a gravitating center is given below on the basis of the theory of dimensions. Two integrals of the system of ordinary equations corresponding to an arbitrary value of the adiabatic coefficient are given for the problem considered in [1]. For $\gamma = 4/3$ an exact solution of this problem is obtained involving quadratures. The method of formulating automodel problems employed in the present paper is based on the analogous solution given in L. I. Sedov's book [2].

1. Roche's model consists of a gas distributed with spherical symmetry round a nucleus having a large mass. It is assumed that the gravitating effect of the gas itself can be neglected compared with the attraction of the nucleus. If the gas is at rest the distributions of density ρ_0 and pressure p_0 satisfy the equilibrium equation

$$\frac{1}{\rho_0}\frac{dp_0}{dr} + \frac{\mu}{r^2} = 0, \tag{1}$$

where r is the distance from the center of symmetry, $\mu = fM$, f being the gravitational constant and M the mass of the gravitating center.

Using the theory of dimensions [2] it is possible to state at the outset that any problem involving one-dimensional nonstationary motion of the gas will be of the automodel type, and the corresponding system of equations involving partial differential coefficients may be reduced to a system of ordinary equations, if the equations and the initial and the boundary conditions contain only two constant parameters having independent dimensions. Thus the automodel formulation of problems involving nonstationary motion in the Roche model assumes that the equilibrium characteristics may, in addition to r and μ, depend on a further constant parameter A whose dimensions can, without loss of generality, be written in the form $[A] = ML^kT^s$.

Hence, using dimensional analysis and Equation (1) it is easy to find uniquely (to within constant parameters) the values of density and pressure which in equilibrium lead to automodel solutions:

$$\rho = \frac{A\mu^{s/2}}{r^{3/2 s+k+3}}, \quad p_0 = \frac{1}{\frac{3}{2}s + k + 4}\,\frac{A\mu^{s/2+1}}{r^{3/2 s+k+4}}. \tag{2}$$

2. Nonstationary adiabatic motion of a gas with spherical symmetry in a field of a gravitating point is described by the system of equations

$$\begin{gathered}\frac{\partial u}{\partial t} + u\frac{\partial u}{\partial r} + \frac{1}{\rho}\frac{\partial p}{\partial r} + \frac{\mu}{r^2} = 0,\\ \frac{\partial \rho}{dt} + u\frac{\partial \rho}{\partial r} + \rho\,\frac{\partial u}{\partial r} + \frac{2u\rho}{r} = 0,\\ \frac{\partial}{\partial t}\left(\frac{\rho}{\rho^{\gamma}}\right) + u\,\frac{\partial}{\partial r}\left(\frac{p}{\rho^{\gamma}}\right) = 0,\end{gathered} \tag{3}$$

where t is the time and u is the velocity.

For automodel problems the required characteristics may be represented in the following form [2]:

$$\begin{gathered}u = \mu^{1/3}t^{-1/3}V(\lambda),\\ \rho = A\mu^{-\left(1+\frac{k}{3}\right)}t^{-s-2/3k-2}R(\lambda),\\ p = A\mu^{-(k+1)/3}t^{-s-2/3k-8/3}p(\lambda),\end{gathered} \tag{4}$$

where $\lambda = \mu^{-1/3}rt^{-2/3}$ is a dimensionless parameter; V, R, p are dimensionless functions. On substituting (4) into (3) we obtain a system of ordinary equations which describe automodel nonstationary motion:

$$\begin{gathered}\left(V - \frac{2}{3}\lambda\right)\frac{dV}{d\lambda} - \frac{1}{3}V + \frac{1}{R}\frac{dp}{d\lambda} + \frac{1}{\lambda^2} = 0,\\ \frac{dR}{d\lambda}\left(V - \frac{3}{2}\lambda\right)\lambda + R\lambda\frac{dV}{d\lambda} + 2R\left(V - \frac{s + 2/3 k + 2}{2}\lambda\right) = 0,\\ \left(V - \frac{3}{2}\lambda\right)\frac{d}{d\lambda}\left(\frac{p}{R^{\gamma}}\right) + \left[2\gamma - \frac{8}{3} - \left(s + \frac{2}{3}k\right)(1-\gamma)\right]\frac{p}{R^{\gamma}} = 0.\end{gathered} \tag{5}$$

3. In the majority of problems involving nonstationary motion of a gas with spherical symmetry the boundary conditions are prescribed on the shock wave. In the case where the gas in front of the shock wave is at rest these conditions are

$$\begin{gathered}u^* = \frac{2}{\gamma+1}c(1-q),\\ \rho^* = \frac{\gamma+1}{\gamma-1}\rho_0\left(1 + \frac{2}{\gamma-1}q\right)^{-1},\\ p^* = \frac{2}{\gamma+1}\rho_0c^2\left(1 - \frac{\gamma-1}{2\gamma}q\right),\end{gathered} \tag{6}$$

where $q = \frac{a_0^2}{c^2} = (\gamma p_0/\rho_0)/c^2$, a_0 is the velocity of sound in front of the shock wave, and c is the speed of propagation of the discontinuity. We shall indicate quantities relating to motion immediately behind the shock wave by an asterisk.

The automodel conditions [2] can be used to determine the law of motion of the shockwave $r^*(t)$ and its velocity of propagation $c = dr^*/dt$ to within a dimensionless multiplier λ^* in the form

$$r^{*}(t) = \mu^{1/3} t^{2/3} \lambda^{*}, \quad C = \frac{dr^{*}}{dt} = \frac{2}{3} \mu^{1/3} t^{-1/3} \lambda^{*}. \tag{7}$$

The boundary conditions for the dimensionless functions which enter into (5) are obtained by substituting (2), (4) and (7) into (6):

$$\begin{aligned} V^{*} &= \frac{4}{3(\gamma+1)} \lambda^{*}(1-q), \\ R^{*} &= \frac{\gamma+1}{\gamma-1} \frac{1}{\lambda^{*3/2s+k+3}} \left(1 + \frac{2}{\gamma-1} q\right)^{-1}, \\ p^{*} &= \frac{8}{9(\gamma+1)} \frac{1}{\lambda^{*3/2s+k+1}} \left(1 - \frac{\gamma-1}{2\gamma} q\right), \\ q &= \frac{9\gamma}{4(3/2s+k+4)\lambda^{*3}}. \end{aligned} \tag{8}$$

4. Using the automodel formulation suggested above it is possible to treat a number of problems, for example, the problem of nonstationary motion of a gas in front of a spherical piston expanding according to the law

$$r = \mu^{1/3} t^{2/3} \alpha, \tag{9}$$

and the problem of motion of a gas in the case when, at the center of symmetry, energy is being liberated according to the law

$$E = A \mu^{\frac{2-k}{3}} t^{-\left(s + \frac{2}{3}k + \frac{2}{3}\right)} \beta, \tag{10}$$

where α and β are dimensionless constants. Since the conditions are adiabatic we can in all cases obtain an integral of the system (5) as shown in [3],which in our notation has the form

$$\left(\frac{p}{R^{\gamma}}\right)^{z^{*}} R \left(V - \frac{2}{3}\lambda\right) \lambda^{2} = C_1, \tag{11}$$

where

$$z^{*} = -\frac{2k+3s}{3s(1-\gamma) + 2k(1-\gamma) + 8 - 6\gamma}.$$

5. The problem of a sudden explosion which was solved in [1] is a special case of the motion which results when energy is liberated according to (10). In the case considered in [1], and which we shall discuss in what follows, we must put $k = 2$ and $s = -2$, i. e., we assume that the parameter A has the dimensions of energy.

At the same time, another integral of the system of equations (5) which was not mentioned in [1] may be obtained.

The total energy (kinetic + internal + gravitational) of the gas contained between the two moving surfaces

$$r_1 = \mu^{1/3} t^{2/3} \lambda_1, \quad r_2 = \mu^{1/3} t^{2/3} \lambda_2,$$

(λ_1, λ_2 are dimensionless constants) may be represented in the form of the integral

$$E = \int_{r_1}^{r_2} \left(1/2 \rho u^2 + \frac{p}{\gamma-1} - \frac{\rho\mu}{r}\right) 4\pi r^2 dr. \tag{12}$$

It follows from the theory of dimensions [2] that this integral should be constant and independent of time for any fixed values of λ_1 and λ_2.

Differentiating (12) with respect to time, and using the law of conservation of energy, we obtain a relation between the required characteristics, which for the dimensionless functions has the form

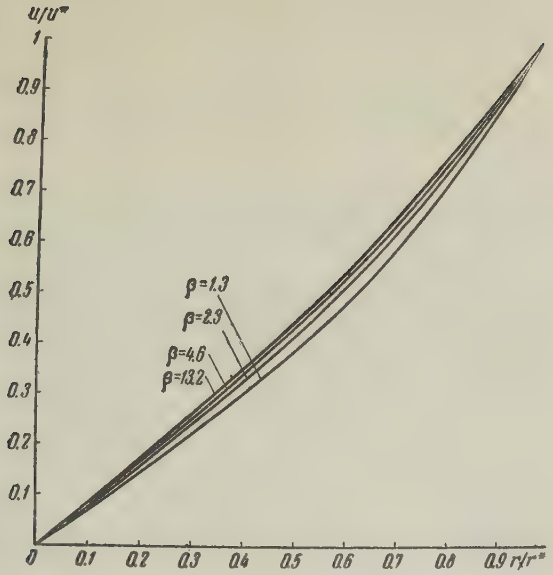

Fig. 1.

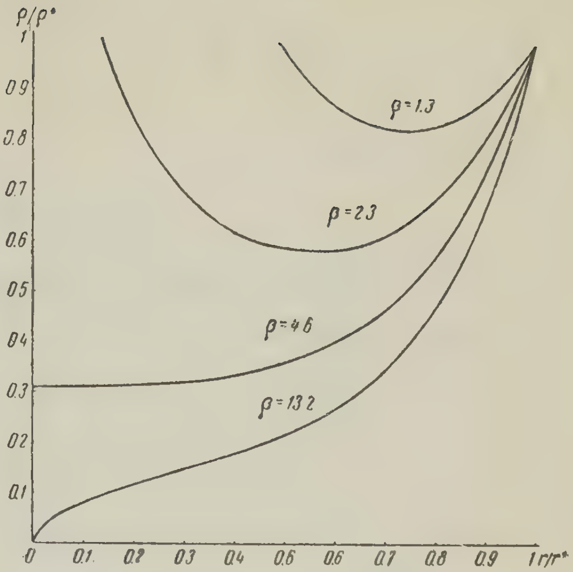

Fig. 2.

$$\lambda^2\left[\left(\frac{1}{2}RV^2+\frac{p}{\gamma-1}-\frac{R}{\lambda}\right)\left(\frac{3}{2}\lambda-V\right)-pV\right]=C_2. \tag{13}$$

The values of the constants C_1 and C_2 are determined by substituting Expressions (8) into (11) with $k = 2$ and $s = -2$. As a result, we obtain

$$C_1=\left[\frac{8}{9(\gamma+1)}\left(1-\frac{3}{8}\,\frac{\gamma-1}{\lambda^{*3}}\right)\right]^{\frac{1}{3-2\gamma}}\left[\frac{\gamma-1}{\gamma+1}\left(1+\frac{3}{2}\,\frac{\gamma}{\gamma-1}\,\frac{1}{\lambda^{*3}}\right)\right]^{\frac{\gamma}{3-2\gamma}}\frac{2}{3}\,\lambda^{*\frac{3}{3-2\gamma}}. \tag{14}$$

$$C_2=\frac{2}{9}\,\frac{4-3\gamma}{\gamma-1}. \tag{15}$$

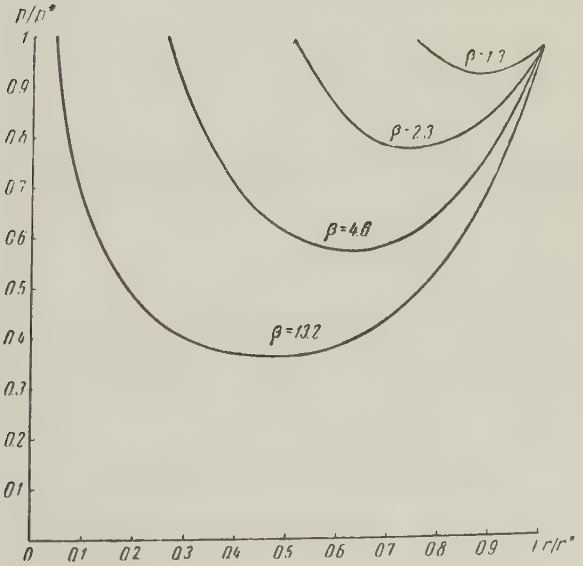

Fig. 3.

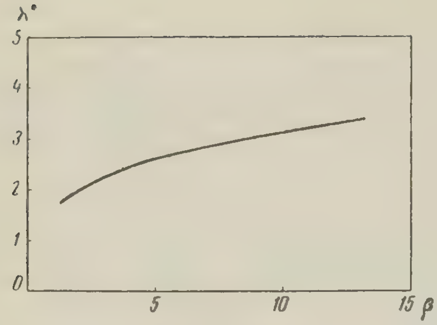

Fig. 4.

6. With the adiabatic coefficient $\gamma = 4/3$, the solution of the problem of a sudden explosion is substantially simplified. In this case

$$C_2 = 0, \qquad C_1 = \frac{2^{10}}{3^4 \cdot 7^7} \lambda^{*9} \left(1 - \frac{1}{8\lambda^{*3}}\right)^3 \left(1 + \frac{6}{\lambda^{*3}}\right)^4. \tag{16}$$

the integrals (11) and (13) give the following simple relations:

$$\lambda^3 = 2\,\frac{(2/3 - V_1)^{4/3} - 2C_1^{1/3}(1 - 2V_1)}{(2/3 - V_1)^{4/3} V_1^2}, \tag{17}$$

$$z_1 = \frac{C_1^{1/3}}{(2/3 - V_1)^{1/3}}, \tag{18}$$

where

$$V_1 = \frac{V}{\lambda}, \quad z_1 = \frac{p}{R}\lambda. \tag{19}$$

An expression for the dimensionless density may be obtained from the second equation of the system (5) in the form

$$R = \frac{R^* \lambda^{*3}}{\lambda^3} \exp\left\{-\int_{V^*}^{V} \frac{dV}{V - 2/3\,\lambda}\right\}. \tag{20}$$

It follows from an analysis of the solution that the motion is continuous up to the center of symmetry and the asymptotic dependence of V_1 and the velocity V on the dimensionless coordinate λ can be easily obtained from (17):

$$V = k\lambda + \frac{3}{4} k\left(\frac{2}{3} - k\right)(1 - 2k)\lambda^4 + 0(\lambda^7). \tag{21}$$

Relation (17) also gives the connection between C_1 and k

$$C_1^{1/3} = \frac{\left(\frac{2}{3} - k\right)^{4/3}}{2(1 - 2k)}, \tag{22}$$

and, through (16), the dependence of k on λ*. Since physically we must have $C_1 > 0$ it follows that $k < 1/2$. Using (20) we obtain an asymptotic expression for the density distribution corresponding to $\lambda \to 0$

$$R \approx \frac{C}{\lambda^{2 + k/(k - 2/3)}}, \tag{23}$$

i.e., for $k = 4/9$ the density at the center of symmetry is finite, for $1/2 > k > 4/9$ it is zero, and for $k < 4/9$ it is infinite. For $\gamma = 4/3$ the sum of internal and gravitational energy of the gas in equilibrium is zero. It follows that the total energy of a moving gas should be equal to the energy E_0 which is liberated initially at the center, i.e., we have

$$E_0 = \int_0^{r^*} \left(\frac{1}{2}\rho u^2 + \frac{p}{\gamma - 1} - \frac{A\rho}{r}\right) 4\pi r^2 dr. \tag{24}$$

Using the latter relation we obtain

$$\beta = \frac{E_0}{4\pi A} = \int_0^{\lambda^*} \left(\frac{1}{2} R V^2 + 3p - \frac{R}{\lambda}\right) \lambda^2 d\lambda. \tag{25}$$

This equation determines the connection between β and λ^* and consequently also the relation between β and k.

Figures 1 to 3 show the distribution of velocity, density and pressure for a number of values of β, These curves show various characteristic cases of the possible form of the distribution of density near the center. Figure 4 shows a graph of λ^* as a function of β using the four calculated cases.

Received January 23, 1957

LITERATURE CITED

[1] P. Carrus, P. Fox, F. Haas and Z. Kopal, Astrophys. J. 113, 1 (1951).

[2] L. I. Sedov, Similarity and Dimensional Analysis in Mechanics [in Russian] (GTTI, Moscow, 1951).

[3] M. L. Lidov, Doklady Akad. Nauk SSSR 103, 1 (1955).

AN ELECTRONIC-MECHANICAL COMPUTER FOR DETERMINING THE MEAN TIMES OF STELLAR TRANSITS DURING THE OBSERVATIONS

V. G. Kruchinenko, Iu. P. Platonov, and V. B. Sukhov

In the astronomical laboratory of the Main Astronomical Observatory at Pulkovo (GAO) a device was designed and constructed which provides for the calculation of mean times of stellar transits during observations by averaging the contact times of a photoelectric amplifier or contact micrometer. Here the chronograph tape does not have to be measured at all, so that the time required for reducing the observations is shortened considerably.

1. Theoretical Basis of Operation

As a star passes across the reticle of a transit instrument we obtain signals of rectangular form (contacts) at the output of the photoelectric amplifier. The instant of the star's transit across the center of the reticle is the arithmetic mean of the central instants of all the contacts.

To provide for measurement of these instants, pulses from the working clock are usually superimposed on the record of the contacts. They serve as reference points for measuring the stellar contacts on the comparator. In the method we have adopted for measuring these instants it is necessary that at least one time pulse arrive in the course of a contact from the star. With the minimum contact duration of $1^s.5$ available on the photoelectric equipment of the Pulkovo Time Service, it is sufficient to use one-second clock pulses.

The proposed arrangement allows for the measurement of the duration of the two parts of a contact (C and B, Figure 1) into which it is divided by the seconds pulses. Obviously, the distance from the center of the contact to the clock pulse is equal to (B − C)/2. To obtain the correct fractional parts of a second in the final result it is necessary to specify the numbers of those seconds with respect to which the centers of the contacts are calculated.

If the numbers of the seconds are not specified, i.e., if we take $T = \sum_{i=1}^{n} \frac{B_i - C_i}{2}$, there will be an uncertainty in the result equal to $1^s/n$, where n is the number of contacts. The uncertainty indicates that the result given by the counter differs from the true result by an amount $\pm K \frac{1^s}{n}$, where K is an unknown whole number. For example, for n = 8 the uncertainty is $0^s.125$, which is completely inadmissible with a scatter in clock corrections for a single star within the limits of $0^s.1$-$0^s.2$.

In order to increase the size of the uncertainty it is necessary to record and sum up the numbers of the seconds with which the instants of contact are connected. By numbering the seconds with a period N the uncertainty is increased to N/n.

It is convenient to have this value equal to the entire number of seconds. Therefore, for n = 8, as assumed in our arrangement, it is convenient to take N as a multiple of 8. We have chosen N = 24 so that the uncertainty is $N/n = 3^s$.

This implies that we cannot distinguish the 4th, 7th, 10th, etc. seconds from the first second; therefore, having obtained the result of the calculation, i.e., the preliminary clock correction, we may add to it ±3K in such a way that the result is $\geq 0^s$ and $< 3^s$.

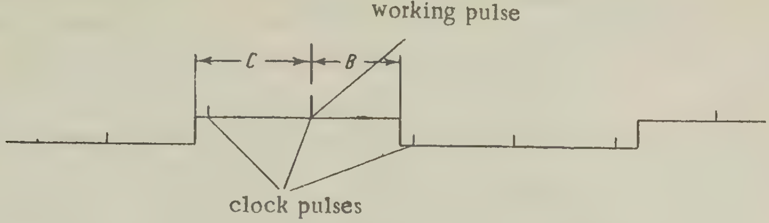

Fig. 1.

It is easily shown that the result obtained will be correct to the same degree of uncertainty in the usual system of numbering seconds (from 0 to 59), if the zeros of both numbering systems once coincide. This holds not for just any values of N/n, but only when the magnitude of the uncertainty is evenly divisible by 60.

Thus, under the conditions given, namely when $n = 8$ and $N = 24$, the formula for calculating the instant of transit has the following form:

$$T^s = \frac{\sum\limits_1^8 A_i^s + \frac{\sum\limits_1^8 (B_i^s - C_i^s)}{2} \pm 24\,K}{8} = \frac{1}{8}\sum_1^8 A_i^s + \frac{1}{16}\sum_1^8 B_i^s - \frac{1}{16}\sum_1^8 C_i^s \pm 3K \qquad (K = 1, 2, 3, \ldots). \tag{1}$$

Here A_i^s is the number of the second with which the ith contact is connected; B_i^s and C_i^s are the corresponding parts of the ith contact (in accordance with Figure 1).

For the measurements of the intervals B_i and C_i we used high-speed electromechanical counters SB-1 M, which in the course of the measured intervals count pulses at a frequency of 100 cps; thus, one pulse corresponds to a time interval of $0^s\!.01$. For summing the numbers of seconds A_i we used a similar counter, connected at required moments to a numbering mechanism that yields a number of pulses each second corresponding to the numbering of the seconds in our chosen system of counting. An electronic circuit, built around 22 tubes, serves principally for the commutation of pulses to counters A, B and C in accordance with the chosen calculation scheme.

2. Operation of the Device

In the absence of a signal from the star, pulses are not fed to any of the counters. The moment a contact begins, pulses at 100 cps are sent to counter C. At the next pulse from the clock, counter C is switched out, and counter B is switched in.

At this moment counter A is connected to the numbering mechanism for 1^s so that the following seconds-pulse disconnects it. At the end of the contact from the star, counter B is switched off. At all subsequent contacts these same operations are repeated. The prepared model of the device is suitable for operation with a reticle that gives six contacts before and after reversal of the instrument.

Since the correct result can be obtained only for a given number of contacts, the device has a counter for the number of contacts recorded. Before the star enters the reticle, and during reversal of the transit, false contacts often occur, hence the first and seventh contacts are not recorded but are used to shift the counter from the starting to the operating position, i.e., only the 2nd, 3rd, 4th and 5th contacts are recorded before reversal, and only the 8th, 9th, 10th and 11th after reversal. The 6th and 12th contacts are not recorded either, in order to preserve the symmetry of the system of contacts. Thus, out of twelve contacts yielded by the star, only eight are used for the calculation.

3. Block Diagram of the Device

After preamplification an alternating voltage at 100 cps obtained from a quartz sidereal clock is fed into a power amplifier which drives the synchronous motor of the numbering mechanism (Figure 2). This frequency goes through a pulse-shaper to electronic relay II, which is controlled by signals from the star so that it passes the frequency only for the duration of a contact. After this relay, the 100-cycle pulses go to two electronic relays which are controlled by voltages of opposite phases from the anodes of the clock trigger.

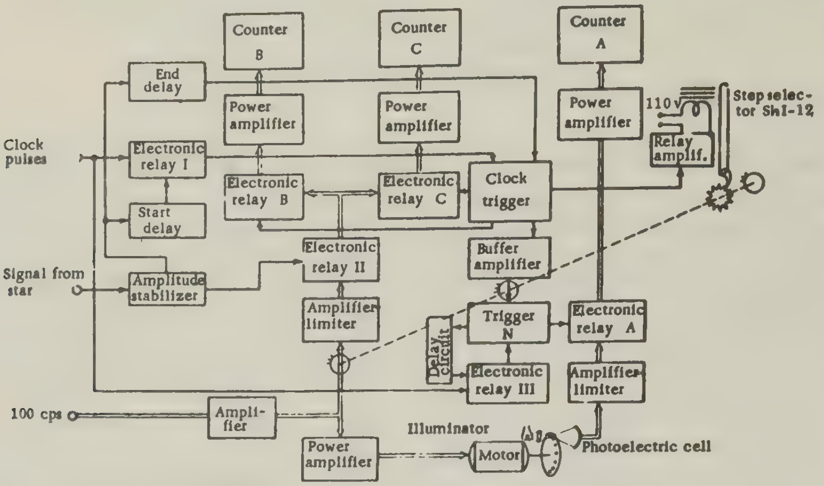

Fig. 2.

In the operating condition, pulses go through the relay C to counter C; at the start of a contact through the start delay circuit, electronic relay I releases, passing the clock pulses to the trigger. Thus, the seconds pulse immediately following the start of a contact trips the trigger, relay C shuts off, and the pulses go through relay B to counter B. At the end of a contact, relay II shuts off and counter B ceases operating, while the return of the clock trigger to its original condition takes place somewhat later through the end-of-contact delay circuit.

The result of the calculations will be correct even if the edge of the contact is irregular, which is usually the case with photoelectric observations of faint stars. Because of the delay circuits the clock trigger will be tripped only during the smooth portion of the contact and its operation will thus be more clearly defined. When the edges of a contact are irregular they are stored with the corresponding part of the smooth contact. For this reason it is necessary to select the proper time delays at the beginning and end of contacts, and they must be varied in proportion to secδ. In this device switching is provided for three different delays, corresponding to the equatorial, zenith and polar zones.

The number of contacts is counted with the aid of a 12-position telephone step selector. An operation of the step selector takes place on each return of the clock trigger, which is caused by a pulse from the end-of-contact delay. After the 6th and 12th contacts, pilot lamps light up to indicate, respectively, the time for reversal of the transit instrument and the end of a stellar observation.

To indicate the number of a second, a disc is used which is divided into 24 equal sectors around the circumference and which is rotated at a speed of 1 revolution in 24 seconds by the motor SD-2 through a 15:24 gear reduction. In each sector is drilled a number of holes equal to the number of the second from 0 to 23. An illuminator is located on one side of the disc, a photoelectric cell on the other. As the disc rotates, light passing through the holes produces pulses of current at the output of the photoelectric cell. After the pulses have been amplified and shaped they proceed to electronic relay A, which passes them on through a power amplifier to counter A for just 1^s following the working clock pulse. Thus, a record is provided of the number of the second with respect to the beginning of which the location of the center of the contact is determined.

Relay A is turned on by trigger N, which is released by the working pulse of the clock trigger through the buffer amplifier fed through the contacts of the step selector. This is necessary in order to cut off the starting pulses on unrecorded contacts (1, 6, 7 and 12). The trigger N must be brought to its original condition by the clock pulses which follow the working pulse. The delay circuit activates electronic relay III a few (3-5) milliseconds after the working pulse, thereby permitting the clock pulse which follows the working pulse to return the trigger to its original condition.

4. Test of the Device and Prospects for Development

a) A model of the device was made up according to the circuit described above. The tests conducted gave positive results.

b) In order to increase the operating efficiency of the device, an electromechanical computing and printing block is being prepared to complete the calculation of T by Formula (1) and to send the result after completion to a printing or perforating mechanism.

The computing block will be made up of decimal trochotrons (type LP-4) according to the following scheme: for counting the pulses referred to above, two scaling circuits having a period of 200 N are used; by means of a suitable phase shift it is possible to feed one of the circuits with A and B pulses simultaneously. In the other scaling circuit, which sums up the C pulses, an addition to the scaling period is computed and sent to the first circuit, which sums up A and B. The final result obtained is read from the vanes of the trochotrons by a step selector having a numbered printing wheel. The numbering mechanism is a scaler of period N, to which N + 1 pulses are sent each second. To simplify the device it is proposed that $n = 10$, $N = 20$.

c) The proposed device is also adaptable to operation with a transit micrometer. The arrangement is thereby simplified somewhat, since there is no need of delays for the start and end of the signal or for counter B.

d) The choice of n, and corresponding N, is determined by the number of contacts that it is required to record, and is therefore not critical.

Received December 14, 1956

The Main Astronomical Observatory
Academy of Sciences, USSR

A CATALOG OF RIGHT ASCENSIONS OF 203 STARS BASED ON OBSERVATIONS WITH A NEW PHOTOELECTRIC TRANSIT INSTRUMENT

P. M. Afanas'eva

Results of observations with the photoelectric transit instrument of the Pulkovo Time Service during 1955-1956 are given in brief. The Φ2 catalog of right ascensions of 203 stars, compiled on the basis of these observations, may be considered absolute with regard to $\Delta\alpha_{\delta}$ in the declination zone −10° to +78° and with regard to $\Delta\alpha_{\alpha}$ only in the declination zone +50° to +70°.

The Φ2 catalog is compared with the FK3, N30 and Pu α1 catalogs and with the mean system proposed by Soviet astronomers [11], and the comparison shows that the adoption of the latter system for reduction of observations would make possible an increase in accuracy of the work of the Time Services during the International Geophysical Year.

In recent years at Pulkovo N.N. Pavlov has developed and successfully employed a new improved method of photoelectric recording of stellar transits by the use of a reflecting reticle and two photomultipliers. With the employment of the new method photoelectric recording became less dependent on variations in sky background; at the same time the general sensitivity of the method was considerably increased, as well as the accuracy of the recording in an incidental respect.

Interest was shown in applying the new method to compiling the most accurate possible catalog of right ascensions of stars, since a comparison of the principal fundamental systems of star positions revealed significant systematic discrepancies among them [1-3].

In particular, on the basis of these comparisons, and also as a result of comparisons of the newest catalogs with the FK3 [4] and from observations of the Time Services [5, 6], it was found that the FK3 system adopted as the international standard has large systematic errors of the form $\Delta\alpha_{\alpha}$ and $\Delta\alpha_{\delta}$ in the right ascensions of stars in the declination zone +40° to +80°.

Observations for the new catalog were made on the Zeiss reversible transit instrument No. 14546 from January, 1955, to May, 1956. 203 stars in the declination zone −10° to +78° were included in the program. P.M. Afanas'eva, M.I. Esipova, N.N. Pavlov, Iu.P. Platonov and G.V. Staritsyn took part in the observations. In all, 4770 observations were used. Each star in the program was observed an average of 22 times.

The resulting catalog of right ascensions of 203 stars is designated Φ2 (to distinguish it from the first photoelectric catalog of the Pulkovo Time Service [4]). This catalog is being published in the Bulletin (Izvestiia) of the Main Astronomical Observatory.

In connection with the work of compiling the Φ2 catalog an investigation of the pivots of the transit instrument was carried out with the aid of a level. The pivots proved to be of very good quality and the influence of their errors on the results of observation may be considered hardly appreciable.

The accuracy of recording the instant of a stellar transit was estimated according to the well-known formula for determining the error of a single contact:

$$\varepsilon_{K}^{2} = a^{2} + b^{2}\sec^{2}\delta. \tag{1}$$

The coefficients a and b in Equation (1), which we calculated from the results of 2450 observations of stars closer to the zenith, proved to be equal to

$$\begin{array}{cc} a = 0^{\mathrm{s}}.026, & b = 0^{\mathrm{s}}.012, \\ \pm 4 & \pm 1 \end{array}$$

whereas for visual observations according to M.S. Zverev's data [7]

$$a \approx b \approx 0^{\mathrm{s}}.036,$$

i.e., for photoelectric observations the coefficients a and b proved to be considerably smaller than for ordinary visual observations.

As our experiment showed, recording a large number of contacts does not in a practical sense increase the accuracy of observations. For this reason the number of paired contacts recorded was small, 6 to 7, which considerably reduced the time spent on observation and reduction.

The first reduction of observations was performed on the system of Morgan's N30 catalog. The instrumental azimuth was determined by combining a group of reference stars near the zenith with each equatorial star. The mean error in determining the azimuth from one equatorial star was found to be $\pm 0^{\mathrm{s}}.022$.

It is well known that in first-class longitude determinations the error in determining the azimuth from one star near the pole is approximately $\pm 0^{\mathrm{s}}.040$ [8].

As reference stars we chose 51 zenith stars. As is well known, errors in the azimuth, the pivots, etc. are practically eliminated in observing these stars. The right ascensions of these reference stars were subjected to cyclical smoothing by Cohn's simplified method (without accounting for terms of diurnal period).

In connection with the fact that the azimuth of the instrument was determined from a combination of zenithal and equatorial stars, and the right ascensions of the zenithal stars in the original catalog contain significant errors, the cyclical smoothing of the right ascensions of the reference stars had to be carried out in two approximations. It was not necessary to make a third approximation, since the corrections in the second approximation changed the azimuth by only $0^{\mathrm{s}}.001$-$0^{\mathrm{s}}.002$.

After the corrections of the first and second approximations had been entered into the right ascensions of the reference stars, the instrumental azimuths were computed anew.

From the deviations of individual azimuths from the mean for the night, the accidental errors in the positions of the azimuthal stars were determined and taken into account in the course of further reduction.

The corrections to the right ascensions of the stars for which positions were being determined were found on the basis of the deviations of the errors for each star from the error computed for the group of reference stars.

The mean error for a single observation of a star for which the position was being determined was calculated from the deviations of the individual differences for each star from the mean. In Table 1 we give this mean error for a single observation, reduced to the equator.

TABLE 1

δ	ε_1	n
10—20°	$\pm 0^{\mathrm{s}}.013$	407
20—30°	± 0.013	604
30—40°	± 0.014	478
40—50°	± 0.011	795
50—60°	± 0.009	436
60—70°	± 0.010	305
70—80°	± 0.010	160

In this table n stands for the number of observations made on a star of a given group.

The mean error for a single observation of a reference star was derived from the deviations in the differences of clock corrections for adjacent reference stars from their common mean difference. This error, reduced to the equator, was found to be $\pm 0^{\mathrm{s}}.0085$.

The mean error, reduced to the equator, in the right ascension of each star in our catalog is characterized by the following figures:

δ	15°	25°	35°	45°	55°	65°	75°
ε	$\pm 0^{s}.003$	$\pm 0^{s}.003$	$\pm 0^{s}.003$	$\pm 0^{s}.002$	$\pm 0^{s}.002$	$\pm 0^{s}.002$	$\pm 0^{s}.002$

To make possible a determination of the absolute instrumental azimuth, we observed 18 zenithal stars at lower culmination. These observations allow us to obtain the absolute difference of errors of the form $\Delta\alpha_{\delta}$ in the original N30 catalog between the zenithal and equatorial zones which are symmetrically located with respect to the zenith and the stars at lower culmination. This difference is obtained free from the effect of inaccuracies in the pivots. In fact, in observation of zenith stars on reversible transit instruments, the effect of pivot inaccuracies is eliminated [9, 10]. As N.N. Pavlov has shown, the relative influence of pivot errors on the inclination and azimuth being determined may also be eliminated for stars symmetrically located with respect to the zenith.

In fact, let us suppose that the pivot errors produce an error in azimuth Δa_z and an error in inclination Δb_z. In this case Mayer's formula for reduction of meridian observations may be written in its general form as

$$\Delta T_z = a \sin z \sec \delta + b \cos z \sec \delta + \Delta a_z \sin z \sec \delta + \Delta b_z \cos z \sec \delta. \tag{1'}$$

Let us introduce the notation

$$\Delta T'_z = \Delta T_z - b \cos z \sec \delta,$$
$$A_z = \sin z \sec \delta,$$

and let us represent $\Delta b_z \cos z \sec\delta$ in the form $\Delta b_z \cot z \sin z \sec\delta$. Then Formula (1') takes the form (2) for stars observed south of the zenith

$$\Delta T'_z = (a + \Delta a_z + \Delta b_z \cot z)\, A_z, \tag{2}$$

and form (2') for stars observed north of the zenith

$$\Delta T'_{-z} = [a + \Delta a_{-z} + \Delta b_{-z} \cot(-z)]\, A_{-z}, \tag{2'}$$

but, as is well known [9], for a reversible transit instrument, the following relations hold:

$$\Delta a_z = \Delta a_{-z}; \quad \Delta b_z = -\Delta b_{-z}. \tag{3}$$

Having made use of the Equalities (3), it is easy to obtain

$$\Delta T'_{z-} = (a + \Delta a_z + \Delta b_z \cot z)\, A_{-z},$$

i.e., the effect of pivot errors on the inclination and azimuth is the same for symmetrical zenith distances and may be represented in the form of an azimuth correction. From this it follows that, if one determines the azimuth from zenithal stars at upper and lower culmination, and then, with this azimuth, computes the clock correction from equatorial stars which are symmetrically located with respect to the zenith and stars at lower culmination, then these corrections will be free from the effect of pivot inaccuracies.

Therefore, the systematic difference of the clock corrections determined from zenithal and equatorial stars in the present case may be considered to be a difference in errors of the form $\Delta\alpha_{\delta}$ between the zenithal and equatorial zones of the original catalog.

From our observations it was found that

$$\Delta\alpha_{\sigma=60^\circ} - \Delta\alpha_{\delta=6^\circ} = -0^s.012.$$

Hence the azimuths which we determined earlier from stars near the zenith and near the equator will for this reason be in error by the amount

$$\Delta a = \frac{\Delta\alpha_{\delta_z} - \Delta\alpha_{\delta_s}}{\bar{A}_z - \bar{A}_s} = \frac{-0^s.012}{-0.828} = +0^s.014,$$

where $\bar{A}_z - \bar{A}_s$ is the difference in the mean values of the azimuthal coefficients in Mayer's formula for zenithal and nearly equatorial stars. Therefore all the corrections obtained earlier for the right ascensions of the stars were adjusted for the effect of this azimuth error.

Our observations, of course, do not permit us to find the correction to the equinox of the original N30 catalog. From our point of view, it would be most correct to bring our derived system into conformity in the near-equatorial zone with the FK3 system, which is the international standard, since it is known that the fundamental systems are most reliable with respect to $\Delta\alpha_\delta$ precisely in the near-equatorial zone. Besides, the Puα1 system recently derived by A.A. Nemiro at Pulkovo was reduced to the equinox of the FK3 [1].

TABLE 2

Systematic Differences of the Form $\Delta\alpha_\delta$ Between Catalogs (in $0^s.001$)

δ	Φ2—N30	n	Puα 1— N30	n	Φ2 — FK3	Puα 1 — FK3
0°	—9	7	—16	42	+3	—4
10	—11	17	—10	46	—1	0
20	—13	19	—6	43	—1	+6
30	—9	30	—11	44	+1	—1
40	—7	16	—10	21	+9	+5
45	—20	14	—14	17	—8	—2
50	—11	21	—15	17	+3	—2
55	—22	26	—18	14	+5	+8
60	—24	23	—20	14	+12	+14
65	—16	17	—13	8	+30	+30
70	—28	7	—27	11	+20	+17

TABLE 3

δ	10—40°						40—60°						60—80°					
α	Φ2 — N30	n_Φ	Puα 1 — N30	Φ2 — FK3	Puα 1 FK3	n_Φ	Φ2 — N30	n_Φ	Puα 1 — N30	Φ2 — FK3	Puα 1 — FK3	n_Φ	Φ2 — N30	n_Φ	Puα 1 — N30	Φ2 — FK3	Puα 1 — FK3	n_Φ
0	+3	9	+1	0	—2	15	+4	11	+12	—1	+7	10	+7	4	+10	+5	+8	5
3	+3	5	+4	+2	+3	18	+3	14	+8	+4	+9	13	+11	4	+11	+28	+28	4
6	+1	14	+3	+2	+4	17	+1	9	—4	+9	+4	3	—3	3	—1	+26	+28	2
9	+1	7	0	+4	+3	12	—3	12	—10	+3	+1	8	—9	6	—3	+10	+16	3
12	0	9	0	+1	+1	10	—7	8	—9	+1	—1	7	—13	5	—15	—6	—8	4
15	—4	6	—1	—5	—2	17	—5	10	—5	—6	6	10	2	5	—10	—21	—29	6
18	—3	12	—4	—5	—6	19	0	8	+1	—8	—7	11	0	6	—2	—30	—32	6
21	0	7	—3	—1	—4	18	+6	10	+5	—1	—2	7	+11	4	+5	—8	—14	6

For conversion to the equinox of the FK3 catalog it was necessary to add the amount $-0^s.023$ to all our calculated corrections to the right ascensions, this being the value obtained as a mean of the differences between the FK3 and our own system in the near-equatorial zone.

Following this, the final system of corrections to the original N30 catalog was obtained, with the aid of which the Φ2 catalog was produced.

In Table 2 we present the results of a comparison of the Φ2 catalog with the N30 and the FK3 with respect to errors of the form $\Delta\alpha_\delta$. Also listed in it are the results of a comparison of the fundamental catalog Puα1 with these same catalogs. We obtained the differences Φ2 − N30 and Puα1 − N30 directly from the original material, and compared Φ2 and Puα1 with FK3 through the differences N30 − FK3 taken from the work of Kopff [2]. It should be borne in mind that the comparison of the Φ2 with the N30 and FK3 was made in 1955, and Puα1 in 1950.

TABLE 4

Systematic Differences of the Form $\Delta\alpha_\alpha$ Between Catalogs (in $0\overset{s}{.}001$)

δ	40—60°		60—80°	
α	$\frac{N30 + Pu\alpha 1}{2} - FK3$	Φ2 − FK3	$\frac{N30 + Pu\alpha 1}{2} - FK3$	Φ2 − FK3
0^h	+1	—1	+9	+5
3	+6	+4	+25	+28
6	+7	+9	+29	+26
9	+6	+8	+19	+10
12	0	+1	—3	—6
15	—5	—6	—25	—21
18	—9	—8	—30	—30
21	—4	—1	—13	—8

As is evident from Table 2, in the most reliably determined zenith zone 55-65° the Φ2 catalog lies between the N30 and the FK3 and practically coincides with the independent system of the Puα1.

We carried out a comparison of the Φ2 with the FK3 and N30 with respect to $\Delta\alpha_\alpha$ according to declination zones 10-40°, 40-60° and 60-80°. The results of the comparison are given in Table 3. Also listed here are the differences Puα1 − FK3 and Puα1 − N30, taken from the work of A.A. Nemiro [1] already mentioned. In this table n_Φ stands for the number of stars of a given group in the Φ2 catalog, n_Φ likewise for the Puα1 catalog.

TABLE 5

Systematic Differences of the Form $\Delta\alpha_m$ Between Catalogs

m	Φ2 − N30	Φ2 − FK3	n	Nik. 30 − FK3	Pul. 30 − FK3	$W2_{50}$ − FK3
0—2	$-0\overset{s}{.}011$	$-0\overset{s}{.}014$	14	$-0\overset{s}{.}007$	$-0\overset{s}{.}011$	$-0\overset{s}{.}007$
2—3	—0.004	—0.005	25	—0.004	—0.008	—0.006
3—4	—0.005	—0.003	55	—0.003	—0.005	—0.005
4—5	0.000	0.000	77	0.000	0.000	0.000
5—6	—0.003	0.000	28	+0.004	+0.006	+0.007

The data of Table 3 indicate that in the zone 10-40° the discrepancies among all the catalogs are small. It is interesting to note that the final positions of the Φ2 in this zone proved to be closest to the Puα1, in spite of the fact that we used the initial positions of the N30.

In the zone 40-60° the discrepancies among all the catalogs increase considerably, so that Φ2 is somewhat closer to N30 here.

In the zone 60-80° the FK3 shows very large departures from the other catalogs, which confirms the existence in it of large systematic errors of the form $\Delta\alpha_\alpha$.

Better agreement in the trend of the differences Φ2 − N30 and Puα1 − N30 indicates that catalog N30 also may be suspected of errors of the form $\Delta\alpha_\alpha$ in the declination zone 60-80°.

In connection with the fact that the FK4 catalog will not have been completed by the beginning of the In-

Differences Φ2 — N30 for Individual Stars for 1955

№	№ KG3	№ FK3	№ 30	Φ2—30 0.001	№	№ KG3	№ FK3	№ 30	Φ2—30 0.001
1	2	3	4	5	1	2	3	4	5
1	15	2	17	—33	65	1021	282	1656	—10
2	21	7	32	—6	66	1031	286	1675	—4
3	28	—	46	—5	67	1045	1196	1703	—1
4	37	1009	63	—6	68	1059	292	1737	+1
5	43	—	—	—28	69	1070	295	1758	—11
6	55	16	100	—2	70	1081	1207	1801	+8
7	72	21	133	—31	71	1100	—	1856	—9
8	97	1021	169	—2	72	1118	—	1907	—11
9	112	32	187	—2	73	1128	—	—	—24
10	121	—	—	+3	74	1143	317	1971	—27
11	145	—	—	—17	75	1149	—	—	—28
12	161	45	269	—7	76	1159	—	—	—36
13	173	48	290	—12	77	1200	335	2113	—15
14	180	50	309	—13	78	1208	341	2136	—12
15	193	52	331	—10	79	1218	—	—	—30
16	208	57	355	—16	80	1226	—	2183	—59
17	221	63	389	—6	81	1243	1244	2237	—7
18	242	70	418	—8	82	1253	355	2258	—31
19	257	75	439	—6	83	1267	—	2281	—23
20	275	79	463	—8	84	1278	1250	2309	—8
21	285	—	—	—8	85	1288	367	2334	—16
22	294	85	501	—7	86	1294	368	2355	—26
23	314	91	534	+4	87	1301	—	—	—6
24	326	93	554	—16	88	1321	380	2414	—24
25	343	103	591	—6	89	1332	383	2442	—22
26	354	—	608	—17	90	1343	387	2464	—29
27	368	108	628	—23	91	1356	394	2495	—38
28	376	111	636	—6	92	1363	398	2508	—38
29	385	114	648	—4	93	1368	1275	—	—37
30	402	—	675	—19	94	1411	417	2598	—46
31	415	120	690	—8	95	1421	420	2626	—26
32	422	122	703	—21	96	1426	422	2637	—15
33	433	125	714	—26	97	1435	425	2653	—21
34	440	—	—	—27	98	1455	433	2699	—48
35	453	131	753	—2	99	1483	444	2755	—18
36	496	—	810	—34	100	1488	447	2769	—31
37	508	—	—	—29	101	1499	—	—	—30
38	522	152	848	+2	102	1501	450	2799	—12
39	540	—	877	—15	103	1514	456	2835	—37
40	605	168	962	—20	104	1538	—	2879	—5
41	630	175	1015	—35	105	1552	472	2904	—53
42	641	178	1036	—5	106	1566	478	2929	—14
43	657	181	1053	—13	107	1587	483	2976	—54
44	665	182	1069	—13	108	1604	488	2999	—14
45	678	185	1083	—4	109	1606	1337	3007	—7
46	702	193	1121	—21	110	1618	492	3027	—19
47	722	—	—	—22	111	1629	494	3049	—21
48	736	202	1163	—7	112	1638	—	—	—4
49	755	1151	1186	—1	113	1646	500	3080	—29
50	780	211	1208	—12	114	1654	—	3095	—19
51	802	220	1242	—1	115	1665	—	—	—29
52	820	1157	1261	—17	116	1678	509	3141	—33
53	826	225	1275	—39	117	1690	513	3162	—14
54	842	1163	1300	—16	118	1702	521	3202	—25
55	849	232	1313	—7	119	1707	522	3215	—10
56	879	237	1355	—18	120	1718	526	3229	—20
57	913	1174	1420	+1	121	1734	531	3272	—45
58	924	251	1440	—22	122	1744	535	3291	—10
59	935	252	1460	—15	123	1757	543	3317	—5
60	948	—	1481	—18	124	1779	550	3361	—72
61	969	—	—	—12	125	1798	555	3392	—19
62	979	269	1536	—9	126	1834	569	3464	—52
63	988	—	—	—5	127	1841	571	3475	—36
64	1005	—	—	—4	128	1858	578	3502	—16

(continued)

№	№ KG3	№ FK3	№ 30	Φ2—30 0.001	№	№ KG3	№ FK3	№ 30	Φ2—30 0.001
1	2	3	4	5	1	2	3	4	5
129	1886	590	3547	—43	166	2358	733	4326	—14
130	1889	1416	3571	—4	167	2369	—	4338	—13
131	1918	598	3605	—19	168	2389	742	—	+12
132	1931	601	3625	—17	169	2397	745	4388	—20
133	1941	603	3639	—9	170	2416	—	—	+4
134	1954	608	3664	—47	171	2428	752	4417	—20
—	—	—	—	—	172	2459	756	4459	—12
135	1965	615	—	—10	173	2470	758	4472	—27
136	1974	618	3696	—11	174	2481	—	—	+14
137	1985	621	3710	—17	175	2491	765	4504	—10
138	1999	C_4	3744	—59	176	2505	767	4532	—22
139	2005	627	3747	—10	177	2523	1539	4559	—2
140	2027	—	3793	+23	178	2532	777	4579	—32
141	2028	634	3800	—15	179	2542	783	4593	—33
142	2037	635	3811	—11	180	2572	788	4639	—4
143	2047	639	3833	—22	181	2588	792	4658	—10
144	2055	643	3846	—10	182	2603	797	4690	—8
145	2068	—	—	—17	183	2615	803	4712	—25
146	2093	653	3903	—12	184	2641	809	4748	—33
147	2114	663	3932	—19	185	2657	—	4774	—13
148	2118	665	3943	—13	186	2670	815	4790	—16
149	2123	667	—	—37	187	2697	—	—	—30
150	2137	671	3981	—17	188	2723	831	4873	—7
151	2144	676	3992	—19	189	2733	836	4890	—38
152	2161	—	4008	—16	190	2746	—	—	—19
153	2175	681	4027	—20	191	2764	844	4934	+1
154	2189	685	4052	—12	192	2782	848	4963	+12
155	2209	695	4088	—22	193	2792	—	—	+30
156	2224	—	4121	—2	195	2815	867	5026	—22
157	2237	699	4138	—5	196	2827	—	—	+2
158	2243	—	—	—8	197	2842	869	5064	—2
159	2254	1491	4168	—22	198	2852	—	—	—38
160	2260	—	—	—16	199	2885	880	5129	+3
161	2287	713	4214	—11	200	2899	885	5158	+1
162	2302	716	4228	—27	201	2921	893	5198	+4
163	2318	723	4261	—13	202	2933	895	5218	—1
164	2337	—	4292	+10	203	2942	889	5236	—26
165	2343	730	4301	—10					

ternational Geophysical Year, Soviet astronomers have proposed that the FK3 be improved with respect to $\Delta\alpha_\alpha$ by means of corrections based on the mean system of the two catalogs (N30 + Puα1)/2 [11].

A comparison of this system with the FK3 and also of the Φ2 with the FK3 with respect to $\Delta\alpha_\alpha$ for the declination zones 40-60° and 60-80° is presented in Table 4.

As is apparent from Table 4, the differences agree well among themselves, a fact which favors adoption of the Pulkovo astronomers' proposals.

Experiments which we have conducted for investigation of the brightness equation in photoelectric observations have shown that on our instrument the observations are practically free of errors related to differences in stellar brightness.

A comparison of our catalog with the FK3 and N30 with respect to errors of the form $\Delta\alpha_m$ showed that for these catalogs there is a small residual brightness equation, more noticeable for the brightest stars (Table 5).

The large deviation of the Φ2 from the N30 and FK3 for 0^m-2^m stars cannot be explained by errors in the Φ2 catalog which depend on stellar brightness, since the introduction of the insignificant corrections of $0^s.001$-$0^s.002$ for the brightness equation increases this difference still further. Besides, a similar large difference for 0^m-2^m stars is obtained on comparing the Nikolaev 1930 [12], Pulkovo 1930 [13], and $W2_{50}$ [14] catalogs with the FK3 on the basis of the same material. For convenience in making the comparison, the differences between catalogs was taken to be zero for $4^m.5$ stars.

SUMMARY

1. As shown by comparison, the Φ2 catalog agrees best of all with the fundamental catalog Puα1, which

was derived from a hundred-year series of observations with the large transit instrument at Pulkovo. The conformity of the results obtained on different instruments by the use of dissimilar methods of recording the stellar transits implies that both of these catalogs are free of systematic errors to a considerable extent.

2. In view of the large systematic discrepancies in right ascensions among the existing fundamental catalogs it is necessary to invite new observations for the purpose of improving the precision of the fundamental systems.

The present work has shown that observation with the transit instruments of the Time Services may be used with success for this purpose. Therefore, we recommend the organization of catalog observations of a general list of stars at the Time Services by the use of a photoelectric method of recording stellar transits.

In conclusion, I consider it my duty to express my gratitude to Professor N.N. Pavlov for the valuable advice and direction which he gave in the course of this work, and also to A.A. Nemiro and M.S. Zverev, who made valuable critical comments upon it.

LITERATURE CITED

[1] A.A. Nemiro, Proceedings of the Eleventh All-Union Astronomical Conference [in Russian] (1955).

[2] A. Kopff, Monthly Notices Roy. Astron. Soc. 114, 4 (1954).

[3] H. Nowacki, Nachrichtenblatt der Astronomichen Zentralstelle 6 (August, 1953).

[4] N.N. Pavlov, Porownanie wynikow obserwacji usyskanych fotoelektrycznym narzedziem przej s ciowym z ukladem katalogu FKS Sprawozdania Polskiego Towarzystwa Astronomiahnego Lescyt 111 (1951).

[5] J. Heide, Astronomische Nachrichten 281 (1952).

[6] B. Gainot, Compt. Rend. 241, 20, 1387 (1955).

[7] M.S. Zverev, Trudy GAISh* 18, No. 2 (1950).

[8] P.N. Dolgov, Time Determination by Meridian Transit Instrument [in Russian](1952).

[9] S.N. Blazhko, Astron. J. (USSR) 22, 1 (1945).

[10] N.N. Pavlov, Izv. GAO** No. 146 (1951).

[11] A.A. Nemiro and N.N. Pavlov, Astron. J. (USSR) 33, No. 3 (1956).

[12] L.N. Semenov, Trudy GAO** Ser. II, 1, XIII (1949).

[13] A.A. Nemiro, Trudy GAO** Ser. II, 1, XIII (1949).

[14] F.A. Graf, Publ. U.S. Naval Obs., Ser. II, XVI, part III (Washington, 1952).

Received January 7, 1957

Main Astronomical Observatory
Academy of Sciences, USSR

---

*GAISh – P.K. Shternberg State Astronomical Institute.

**GAO – Main Astronomical Observatory (in Pulkovo).

EFFECTIVE SCATTERING CROSS SECTION OF A WEAKENED METEOR TRAIL

F. I. Peregudov

A fundamental characteristic of a radar target is its effective scattering cross section. A similar characteristic may also be given for a meteor trail. Most meteor trails are weakened trails which the incident radio wave penetrates without distortion.

The effective scattering cross section S_0 of a weakened meteor trail may be calculated by the well-known Lovell-Clegg formula. This formula, however, does not explain the sharp decrease in the value of S_0 for the meteor trail with decreasing wavelength.

A new formula suitable for a wider frequency band has been derived by taking into account phase differences inside the trail on the basis of Herlofson's work.

The detection of a meteoric body by radio means is possible because, in moving through the upper layers of the earth's atmosphere, the meteor creates in its path a column of ionized gas capable of scattering radio waves in a certain frequency band.

The scattering power of a meteor trail may be characterized by the effective scattering area.

From radar theory [1] it follows that

$$S_0 = 4\pi R^2\left(\frac{P_2}{P_1}\right) = 4\pi R^2\left(\frac{E_1}{E_2}\right)^2 = 4\pi R^2\left(\frac{H_1}{H_2}\right)^2, \tag{1}$$

where R is the distance from the radar station to the target; P_1 is the power flux density produced at the target position by the radar transmitter; P_2 is the power flux density of the secondary field at the location of the radar receiver; E_1, H_1 are, respectively, the electric and magnetic field intensities at the target; E_2, H_2 are, respectively, the electric and magnetic field intensities at the receiver.

In the theoretical consideration of scattering of radio waves by a meteor trail one studies the scattering of a plane monochromatic wave by an infinitely long dielectric cylinder with a permittivity $\epsilon(r)$ which varies along the radius of the cylinder.

The solution of the problem is reduced to finding the scattering coefficient g which characterizes the scattering properties of the cylinder at a great distance from it [2]:

$$g = \sqrt{\frac{\pi k R}{2}}\left(\frac{E_1}{E_2}\right), \tag{2}$$

where k is the wave number.

From (1) and (2), taking into account the sphericity of the incident wave, it is possible to determine the effective scattering surface

$$S_0 = \frac{4R}{k} g^2. \tag{3}$$

The value of S_0 for the meteor trail does not remain constant with time. This is explained by the fact that the meteor trail begins to decay right after its formation. The most important cause of the drop in volume ionization density $n(r)$ in the trail is ambipolar diffusion, which reduces the volume electron density, not affecting the linear electron density α.

If it is assumed that the volume electron density along the radius of the trail has a Gaussian distribution, then the volume density at a distance r from the axis of the column at the instant of time t will be [3]

$$n(r) = \frac{\alpha}{4\pi D(t+b)} e^{-\frac{r^2}{4D(t+b)}}, \tag{4}$$

where D is the ambipolar diffusion coefficient; $b = a^2/4D$ is a constant; a is the initial radius of the trail, which is determined by the mean free path of molecules in the meteoric zone and amounts to 10-100 cm.

The quantity $r_0 = \sqrt{4D(t + e)}$ defines the radius of the trail at the instant of time t. It denotes the distance from the axis of the column at which the volume electron density is e times smaller than the volume electron density on the axis.

The character of the variation of S_0 with time depends on the initial volume electron density. The results of numerous observations [4, 5] indicate that the largest number of reflections is obtained from so-called weakened trails, where the incident wave penetrates into the trail without distortion. This corresponds to the condition

$$1 - \varepsilon(r) \ll 1$$

or

$$\alpha \ll 3.5 \cdot 10^{13} \left(\frac{r_0}{\lambda}\right)^2 \frac{\text{el}}{\text{cm}}. \tag{5}$$

As follows from (5), with decreasing wavelength the great majority of meteor trails will belong to the class of weakened trails.

The well-known Lovell-Clegg formula for S_0 of a weakened trail [3] is derived on the assumption that the meteor trail represents a row of free electrons reflecting in the same phase:

$$S_0 = 2\pi R \lambda \alpha^2 \left(\frac{e^2}{mc^2}\right)^2, \tag{6}$$

where e is the charge of the electron; m is the mass of the electron; and c is the velocity of light.

It is evident that Formula (6) is suitable for calculating only the initial effective scattering cross section of a weakened column, where $r_0 \ll \lambda$. But this condition is violated either at once, if the initial radius of the column a is commensurate with the wavelength, or at some time after the expansion of the trail as a result of diffusion. In this case the condition of cophasal scattering by all the electrons in the trail is not fulfilled.

Consideration of the phase differences within a weakened meteor trail permitted Kaiser [2], on the basis of Herlofson's work [6], to obtain an expression for the scattering coefficient

$$g = \pi\alpha \left(\frac{e^2}{mc^2}\right) e^{-(2\pi r_0/\lambda)^2}. \tag{7}$$

Making use of (3) and (7), we find

$$S_0 = 2\pi R \lambda \alpha^2 \left(\frac{e^2}{mc^2}\right)^2 e^{-2(2\pi r_0/\lambda)^2}, \tag{8}$$

or, taking into account the dependence of r_0 on the time,

$$S_0 = \left[2\pi R \lambda \alpha^2 \left(\frac{e^2}{mc^2} \right)^2 e^{-2(2\pi a/\lambda)^2} \right] e^{-32\pi^2 Dt/\lambda^2} \tag{9}$$

The effective scattering cross section of the meteor trail decreases with time according to an exponent with the attenuation constant

$$T_3 = \frac{\lambda^2}{32\pi^2 D} \tag{10}$$

from an initial value of

$$2\pi R\alpha^2 \left(\frac{e^2}{mc^2} \right)^2 e^{-2(2\pi a/\lambda)^2}, \tag{11}$$

which agrees well with (6) for $a \ll \lambda$.

Formula (9) explains the sharp decrease in the value of S_0 for wavelengths shorter than 1.5-2 m.

It should be noted that (9) does not account for the additional reduction in S_0 with decreasing wavelength, which depends upon the final velocity of the meteor.

The use of (9) permits the introduction of a correction in the relation of hourly rate to wavelength [7]:

$$\frac{N_1}{N_2} = \left(\frac{P_{i_1} P_{r_2} \lambda_1^3}{P_{i_2} P_{r_1} \lambda_2^3} \right)^{(s-1)/2}, \tag{12}$$

where P_i is the transmitter pulse power; P_r is the receiver sensitivity; N is the hourly rate; s is the exponent characterizing the distribution of meteoric masses – for sporadic meteors $s \approx 2$.

The subscripts 1 and 2 refer to the two radar stations, working at wavelengths λ_1 and λ_2.

Formula (12) is derived on the assumption that the hourly rate is proportional to $\alpha_{\min}^{1-s}$, where $\alpha_{\min}$ is the minimum detected linear electron density in the trail at distance R from the radar station [7]. $\alpha_{\min}$ may be found from the radar range equation [1], after substituting in it (6):

$$P_r = \frac{P_i G^2 \lambda^3}{32\pi^2 R^3} \left(\frac{e^2}{mc^2} \right)^2 \alpha_{\min}^2, \tag{13}$$

where G is the directivity coefficient of the antenna system. However, taking (11) into account

$$P_r = \frac{P_i G^2 \lambda^3}{32\pi^2 R^3} \left(\frac{e^2}{mc^2} \right)^2 \alpha_{\min}^2 e^{-2(2\pi a/\lambda)^2}, \tag{14}$$

and consequently, for sporadic meteors

$$\frac{N_1}{N_2} = \left(\frac{P_{i_1} P_{r_1} \lambda_1^3}{P_{i_2} P_{r_2} \lambda_2^3} \right)^{1/2} e^{(2\pi a)^2 \left(\frac{1}{\lambda_2^2} - \frac{1}{\lambda_1^2} \right)}. \tag{15}$$

The results of observations by McKinley [5] at two wavelengths $\lambda_1 = 9.22$ m and $\lambda_2 = 2.83$ m give a significant discrepancy between the experimental result $N_1/N_2 = 104$ and the calculated value 48 obtained on the basis of (12).

Calculation according to Formula (15) for $a = 0.4$-0.5 m gives the value $N_1/N_2 = 90$-130, which agrees well with experiment [5].

LITERATURE CITED

[1] A.F. Bogoliubov, Radar Fundamentals [in Russian] (Soviet Radio Press, Moscow, 1954).

[2] T.R. Kaiser and R.L. Closs, Phil. Mag. 7, 43, 1 (1952).

[3] Vestnik Informatsii, Soviet Radio Press, No. 10, 1 (1952).

[4] T.R. Kaiser, J. Terrest. Phys., Special Suppl. 2 (1955).

[5] D.W.R. McKinley, Can. J. Phys. 29, 5, 403 (1951).

[6] N. Herlofson, Arkiv. Fysik 3, 247 (1951).

[7] T.R. Kaiser, J. Adv. Phys. 2, 8, 495 (1953).

Received December 1, 1956

The S.M. Kirov Tomsk Polytechnic
Institute

CALCULATION OF LATITUDE BY THE METHOD OF M. V. PEVTSOV

A. V. Butkevich

Dedicated to the memory of
Professor V.V. Kavraiskii

For field control of observations by M.V. Pevtsov's method a comparison of the time differences $\Delta T_i = (T_N - T_S)_i$ is recommended. Differential formulas are derived for correcting the latitude for variation of the chronometer correction (the mean hour angle of the pair), the difference of the hour angles, and also the effect of diurnal aberration in α and δ.

M.S. Molodenskii's method of latitude calculation is criticized for its complexity and lack of a control, and another method is proposed wherein, by a simple additional calculation, the latitude is obtained for each wire after it has been calculated for the mean instant, so that a control is provided and the bulk of the calculation is reduced.

1. Introduction

According to the "Instructions" of 1948 [1] and 1956 [2], the method of M.V. Pevtsov is recommended for use at 1st to 3rd class points at latitudes up to 65° together with Talcott's method. The publication in 1946 by the Main Administration of Geodesy and Cartography (GUGK) of new ephemerides for Pevtsov's method [3], extended for latitudes 59°45' to 64°45', in comparison with I.I. Seliverstov's obsolete 1912 ephemerides [4], ensured simplicity in preparing and carrying out observations by this method.

A.N. Kuznetsov in 1949 [5] employed for observations by Pevtsov's method an eyepiece shutter which increased the number of contacts and hence the accuracy of the observations.

Investigations of A.P. Kolupaev in 1950 [6] demonstrated the possibility of applying Pevtsov's method at latitudes up to 70° with a sufficient number of pairs not fainter than the 5th magnitude.

Thus, the problem of preparing and organizing observations for this method has been worked out in detail. This broadens the prospect for further application of Pevtsov's method, especially with the development of the geodetic network in the northern and eastern parts of the country. However, in the area of reduction of observations made by Pevtsov's method, not all the problems have yet been solved. Thus, a means is lacking for rapid and reliable field control of observations, such as N.Ia. Tsinger's method possesses. The questions of the need for taking account of the effect of diurnal aberration, of calculating the error in the chronometer correction, and of the control of latitude calculations, have been insufficiently investigated.

To these questions, therefore, the present paper is devoted.*

---

*In the preparation of this paper, a considerable amount of calculation was done by M.A. Ershova, graduate of the Novosibirsk Institute of Geodesy, Aerial Photography, and Cartography (NIGAIK), whom the author wishes to thank for her assistance.

2. Field Control of Observations in M.V. Pevtsov's Method

In all forms of astronomical observation a field control is carried out for which appropriate tolerances are usually quoted in the instructions. Thus, in azimuth determination by Polaris, tolerances are observed for horizon closure, variations of the collimation error, and the level zero point.

In time determination by the method of N.Ia. Tsinger, sufficient control is provided by:

a) convergence of the mean instants $\frac{1}{2}(T_W + T_0)_i$ for the individual wires, which must agree within the limits of observational error or (for large differences in declination) smoothly increase or decrease.

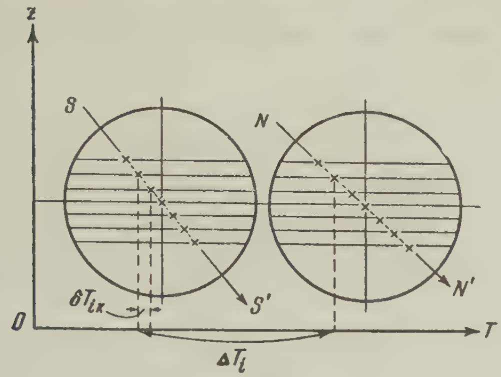

Fig. 1.

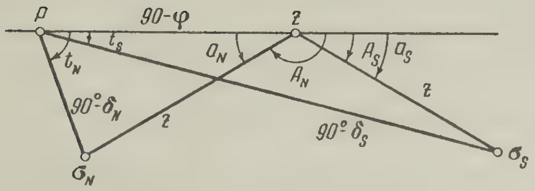

Fig. 2.

b) convergence to $0^{\rm m}\!.1$ of the chronometer corrections, computed according to the approximate formula

$$u_0 = S - T_m, \tag{1}$$

where S is the ephemeris time corrected for the epoch.

However, in Pevtsov's method there is no form of field control and no place is even provided for it in the observation journal. True, in the "Direction" [7] it is pointed out that for 1st-class points the values of the latitude calculated for observations on each of the seven wires must not differ by more than $2''\!.5$. But such a control is not well-timed and effective, since it is carried out not immediately after the observations but only after rather cumbersome calculations.

It might seem that a field control would not be possible for observations made by Pevtsov's method, since here, in contrast to Tsinger's method, both stars of a pair move in one direction with respect to altitude, i.e., either ascend or descend. Recording observations of the second star in reverse order does not help matters, since the distances between wires of the reticle are never ideally equal.

However, if we consider that the variation in zenith distance is expressed by the formula

$$\delta z = 15 \cos\varphi \sin A \delta T, \tag{2}$$

we obtain

$$\delta T = \frac{\delta z \sec\varphi}{15 \sin A}. \tag{3}$$

But in Pevtsov's method the stars are observed under the conditions

$$A_N \approx 180° - A_S \quad \text{or} \quad A_N \approx 540° - A_S. \tag{4}$$

Hence the time intervals

$$\delta T^{N}_{k,\,k-1} = T^{N}_{k} - T^{N}_{k-1} \quad \text{and} \quad \delta T^{S}_{k,\,k-1} = T^{S}_{k} - T^{S}_{k-1}$$

required for the passage of the stars between two adjacent horizontal reticle wires must be approximately equal (Figure 1).

Let us suppose that the northerly star crossed the first wire an interval of time ΔT_1 later than the southerly star; then for the second wire its retardation ΔT_2 will have the value

$$\Delta T_2 = T_2^N - T_2^S = \Delta T_1 + \delta T_{12}^N - \delta T_{12}^S \text{ etc.} \tag{5}$$

Thus, the differences in the times of transit of the stars across corresponding wires of the reticle must also be nearly the same. For field control it is simpler to calculate and compare the differences ΔT, not δT. Obviously, as parallel segments between the two nearly parallel straight lines SS' and NN' (Figure 1), they must behave like the mean instants of Tsinger's method, i.e., agree within the limits of observational error or (for considerable disparity in the azimuths of the stars) display a smooth increasing or decreasing trend.

Let us consider examples of field control for observations of three Pevtsov pairs taken from [7] and [8].

TABLE 1

Field Control of Observations

Wire No.	Pair № 232 ([8], p. 237)			Pair № 252 ([7], p. 92)			Pair № 184 ([7], p. 91)		
i	T_N	T_S	ΔT_i	T_N	T_S	ΔT_i	T_N	T_S	ΔT_i
	17^h	17^h		19^h	19^h		14^h	14^h	
1	$24^m44^s.5$	$16^m15^s.5$	$8^m29^s.0$	$35^m10^s.0$	$29^m35^s.0$	$5^m35^s.0$	$42^m37^s.0$	$34^m52^s.0$	$7^m45^s.0$
2	25 08.0	16 38.5	8 29.5	35 47.0	30 11.7	5 35.3	43 15.2	35 29.0	7 46.2
3	25 31.0	17 01.5	8 29.5	36 25.5	30 48.0	5 37.5	44 00.8	36 14.8	7 46.0
4	25 54.0	17 24.0	8 30.0	37 06.3	31 27.6	5 38.7	44 47.3	37 01.2	7 46.1
5	26 18.0	17 47.5	8 30.5	37 46.2	32 06.5	5 39.7	45 27.6	37 44.3	7 43.3
6	26 41.0	18 11.5	8 29.5	38 26.4	32 46.4	5 40.0	46 13.7	38 29.7	7 44.0
7	27 06.0	18 36.5	8 29.5	39 05.0	33 25.5	5 39.5	46 56.4	39 15.0	7 41.4
Mean	$25^m54^s.64$	$17^m25^s.00$	$8^m29^s.64$	$37^m06^s.63$	$31^m28^s.67$	$5^m37^s.96$	$44^m45^s.43$	$37^m00^s.86$	$7^m44^s.57$

Obviously, in these observations pair No. 232 exhibits the first kind of regularity, pair No. 252 the second kind, and pair No. 184 neither the first nor the second kind. And in fact, calculations of the latitude for each wire in the case of the latter pair gave intolerable discrepancies:

φ_i	Wire No.						
	1	2	3	4	5	6	7
55°45′	$38''.7$	$36''.9$	$37''.3$	$36''.2$	$40''.7$?	$36''.2$	$37''.8$

Thus, the value of the latitude does not satisfy the tolerance requirement for precisely that wire (the 6th) for which the field control fails.

Let us determine the size of a possible shift in the time differences ΔT_i for unequal azimuths of the stars. If we compare the time differences for wires i and k, in accordance with (5) we obtain

$$\Delta T_k - \Delta T_i = \delta T_{ik}^N - \delta T_{ik}^S, \tag{6}$$

or, according to (3),

$$|\Delta T_k| - |\Delta T_i| = \frac{\delta z_{ik} \sec \varphi}{15} \left(\frac{1}{\sin a_N} - \frac{1}{\sin a_S} \right), \tag{7}$$

where a, an acute angle, is the deviation of the star from the meridian (Figure 2). Hence,

$$|\Delta T_k| - |\Delta T_i| = \frac{\delta z_{ik} \sec\varphi\,(\sin a_S - \sin a_N)}{15 \sin a_N \sin a_S} \approx \frac{\delta z_{ik} \sec\varphi \sin(a_S - a_N) \cos a_m}{15 \sin^2 a_m}. \tag{8}$$

Let us determine the difference in zenith distances of the wires δz_{ik} from the difference in the times of transit of the star across the wires:

$$\delta z_{ik} = 15\,(T_k - T_i)_m \cos\varphi \sin a_m. \tag{9}$$

Then*

$$|\Delta T_k| - |\Delta T_i| \approx (T_k - T_i)_m \sin\Delta a \operatorname{ctg} a_m. \tag{10}$$

Thus, for example, for pair No. 252 with $A_S = 332°59'$ and $A_N = 206°19'$; $a_S = 27°01'$, $a_N = 26°19'$ and $(T_7 - T_1)_m = 3^m52\overset{s}{.}2 = 232\overset{s}{.}2$ we obtain $a_m = 26°40'$, $\Delta a = 0°42'$ and $\Delta T_7 - \Delta T_1 \approx 5\overset{s}{.}6$. In fact we obtain a maximum variation of $5\overset{s}{.}0$, which, in view of the observational errors, may be considered permissible.

The proposed field control appears to be simple and reliable enough, and requires merely the provision of an additional column in the observation journal.

3. Calculation of Errors in the Chronometer Correction and the Difference of the Hour Angles

This problem has been discussed in print [8, 7, 5], but there are no simple and convenient formulas for calculating the error in the chronometer correction or indications of the accuracy required in the chronometer correction in the textbooks and instructions.

K.A. Tsvetkov in 1934 [8], differentiating the fundamental formula of M.V. Pevtsov's method

$$\operatorname{tg}\varphi = \frac{\cos\delta_S \cos t_S - \cos\delta_N \cos t_N}{\sin\delta_N - \sin\delta_S} = (S - N)\,D, \tag{11}$$

where

$$t_S = T_S + u - \alpha_S;\quad t_N = T_N + u - \alpha_N, \tag{12}$$

and

$$D = \frac{1}{\sin\delta_N - \sin\delta_S}, \tag{13}$$

obtained the expression

$$d\varphi_u = 15\cos^2\varphi\, D\,(N' - S')\,du^s, \tag{14}$$

in which

$$N' = \cos\delta_N \sin t_N \quad \text{и} \quad S' = \cos\delta_S \sin t_S. \tag{15}$$

In the example cited by him the correction $d\varphi_u$ is obtained with the help of irrational six-place computations.

Another accurate, more convenient and descriptive formula for $d\varphi_u$ has been obtained by the author, the simple derivation of this formula is given below.

Let us make use of the well-known formula applied in studying the most favorable conditions of observation [9],

---

*'ctg' ≡ 'cot,' 'tg' ≡ 'tan,' 'lg' ≡ 'log' – Publisher.

$$d\varphi = \frac{(\sin A_N dt_N - \sin A_S dt_S)\cos\varphi}{\cos A_S - \cos A_N}, \tag{16}$$

where

$$dt_N = dT_N + du - d\alpha_N;\quad dt_S = dT_S + du - d\alpha_S. \tag{17}$$

Temporarily let us take $dT_S = dT_N = d\alpha_S = d\alpha_N = 0$; then with $dt_S = dt_N = du$ we shall have

$$d\varphi''_u = \frac{15\cos\varphi\,(\sin A_N - \sin A_S)\,du^s}{\cos A_S - \cos A_N}. \tag{18}$$

Transforming the numerator and denominator we obtain the simple formula

$$d\varphi''_u = 15\cos\varphi\,\mathrm{ctg}\,A_m du^s, \tag{19}$$

where

$$A_m = \frac{1}{2}(A_S + A_N).$$

In calculations based on Formula (19), the accuracy of ephemeris azimuths will be inadequate in individual cases, the more so since they are usually reduced to the first wire, and one is obliged to compute the azimuths A_S and A_N to 1' according to the formulas

$$\sin A_S = \cos\delta_S \sin t_S \operatorname{cosec} z, \tag{20}$$
$$\sin A_N = \cos\delta_N \sin t_N \operatorname{cosec} z, \tag{21}$$

using the ephemeris zenith distance. Even in this case Formula (19) is more reasonable than Formula (14), as the following example shows.

TABLE 2

Calculation of the Correction $d\varphi_u$ from Formula (19). Original Data: see [8], p. 402

Auxiliary calculations					Calculation of $d\varphi_u$			
formula	N	S	pair					
lg cos δ	9.5743	9.9867	z	40°57′	lg 15 $\cos^2\varphi$	0.927	du	—10s.50
lg sin t	9.9833	9.5761	A_S	31°09′	lg ctg A_m	7.560	φ'	55°39′ 38″87
lg cosec z	0.1509	0.1509	A_N	149°16′	lg du^s	1.021	$d\varphi_u$	+0.32
lg sin A	9.7085	9.7137	A_m	90 12′5	lg $d\varphi_u$	9.508	φ	55°39′ 39″19

For significant values of du, strictly speaking, the azimuth A_m should be taken as the mean of values calculated for u_0 and for u.

The importance of Formula (19) extends far beyond the calculation of the error in the chronometer correction. If we define

$$t_m = \frac{1}{2}(t_N + t_S), \tag{22}$$

then

$$dt_m = \frac{dt_N}{2} + \frac{dt_S}{2}. \tag{23}$$

If, however, as assumed above, $dt_S = dt_N = du$, then $dt_m = du$. Consequently, Formula (19) at the same time gives the correction to the variation of mean hour angle of the pair. This will be utilized below.

Since, according to Formula (17), the rounding error in the hour angles has the same effect as errors in the instants of observation and the chronometer correction, it would seem that in calculating it one may also use Formula (19). However, the error in the chronometer correction du always has the same sign for both stars of a pair, while the rounding errors in the hour angles have different signs. The least favorable case will be for $dt_S = -dt_N = -dT/2$. Substituting the values $dt_S = -dT/2$ and $dt_N = dT/2$ in Formula (16), we obtain

$$d\varphi_T = \frac{7.5 \cos\varphi (\sin A_N + \sin A_S)\, dT}{\cos A_S - \cos A_N}, \tag{24}$$

where $dT/2$ is the rounding error, or

$$d\varphi''_T = 7.5 \cos\varphi \operatorname{ctg} \frac{\Delta A}{2}\, dT^s, \tag{25}$$

where

$$\Delta A = A_N - A_S. \tag{26}$$

But half the difference in hour angles r is given by

$$r = \frac{1}{2}(t_N - t_S). \tag{27}$$

Therefore,

$$dr = \frac{dt_N}{2} - \frac{dt_S}{2}. \tag{28}$$

But if t_N varies by the amount $dT/2$ and t_S by $-dT/2$, as assumed in the derivation of Formula (25), then the quantity r will vary by $dr = dT/2$. Hence, Formula (25), derived on the condition that $dt_S = -dt_N$, simultaneously gives the correction for the variation in the difference of hour angles of the pair, if 2dr is substituted in it in place of dT.

4. Calculation of the Effect of Diurnal Aberration

At first-class points the latitude is calculated for each wire to $0''.1$, the right ascensions being written down to $0^s.01$, the chronometer correction and hour angles to $0^s.1$ and $0^s.05$, declinations to $0''.01$, and the effect of diurnal aberration being disregarded. At second-class points the latitude is calculated from the mean instant to $0''.1$, the right ascensions and hour angles being written down to $0^s.01$, and the declinations to $0''.1$ [7]. Let us inquire whether the accuracy of such observations is consistent.

In order to calculate the effect of diurnal aberration in right ascension, let us differentiate Formula (11) with respect to φ, t_S and t_N and obtain

$$\sec^2\varphi\, d\varphi_\tau = \frac{\cos\delta_N \sin t_N\, dt_N - \cos\delta_S \sin t_S\, dt_S}{\sin\delta_N - \sin\delta_S}. \tag{29}$$

Let us substitute herein

$$\begin{aligned} dt_N &= -d\alpha_N = -0''.32 \cos\varphi \sec\delta_N \cos t_N, \\ dt_S &= -d\alpha_S = -0''.32 \cos\varphi \sec\delta_S \cos t_S, \end{aligned} \tag{30}$$

and obtain

$$d\varphi''_{d\alpha} = \frac{0''.16 \cos^3\varphi (\sin 2t_S - \sin 2t_N)}{\sin\delta_N - \sin\delta_S}. \tag{31}$$

In the worst case, with $\sin 2t_S = 1$; $\sin 2t_N = -1$ and $\varphi = 45°$, we get

$$d\varphi''_{d\alpha} \approx \frac{0''.11}{\sin\delta_N - \sin\delta_S} > 0''.11.$$

Hence, at first-class points the effect of diurnal aberration in right ascension must be taken into account.

To calculate the effect of diurnal aberration in declination let us differentiate Formula (11) with respect to φ, δ_S and δ_N to obtain

$$\sec^2\varphi\, d\varphi_\delta = \frac{\sin\delta_N \cos t_N \cdot d\delta_N - \sin\delta_S \cos t_S\, d\delta_S}{\sin\delta_N - \sin\delta_S} - \\ - \frac{(\cos t_S \cos\delta_S - \cos t_N \cos\delta_N)(\cos\delta_N\, d\delta_N - \cos\delta_S\, d\delta_S)}{(\sin\delta_N - \sin\delta_S)^2} \tag{32}$$

or

$$d\varphi_\delta = \frac{\cos^2\varphi}{\sin\delta_N - \sin\delta_S}\,[(\cos\delta_S \operatorname{tg}\varphi - \sin\delta_S \cos t_S)\, d\delta_S - \\ - (\cos\delta_N \operatorname{tg}\varphi - \sin\delta_N \cos t_N)\, d\delta_N]. \tag{33}$$

But, according to [9],

$$\sin\delta_N - \sin\delta_S = 2\sin z \cos\varphi \cos a > 0, \tag{34}$$

where a is the acute azimuth (deviation of the star from the meridian), and

$$\sin z \cos q = \sin\varphi \cos\delta - \cos\varphi \sin\delta \cos t. \tag{35}$$

Therefore,

$$d\varphi''_\delta = \frac{1}{2\cos a}(\cos q_S\, d\delta''_S - \cos q_N\, d\delta''_N). \tag{36}$$

Let us substitute here

$$d\delta''_S = 0''.32 \cos\varphi \sin\delta_S \sin t_S, \\ d\delta''_N = 0''.32 \cos\varphi \sin\delta_N \sin t_N \tag{37}$$

and obtain

$$d\varphi''_{d\delta} = \frac{0''.16\cos\varphi}{\cos a}(\cos q_S \sin\delta_S \sin t_S - \cos q_N \sin\delta_N \sin t_N). \tag{38}$$

But

$$\sin t_S = \frac{\sin z\ \sin A_S}{\cos\delta_S}, \qquad \sin A_N \approx \sin A_S.$$

Therefore,

$$d\varphi''_{d\delta} = 0''.16 \cos\varphi \sin z\ \operatorname{tg} A_S (\cos q_S \operatorname{tg}\delta_S - \cos q_N \operatorname{tg}\delta_N). \tag{39}$$

Pevtsov pairs are observed at values of a from 6-40° and z from 15-60°, at latitudes from 45-65°. In the worst case, for $\varphi = 45°$, $z = 60°$ and $a = 40°$, we obtain

$$d\varphi_{d\delta} = 0''.08\,(\cos q_S \operatorname{tg}\delta_S - \cos q_N \operatorname{tg}\delta_N) > 0''.08 \ .$$

Hence, at first-class points a correction for the effect of diurnal aberration in declination must also be taken into account.

Since each Pevtsov pair handles a latitude zone of only 30′ − 1°00′ [3], the diurnal aberration corrections for each pair $d\varphi_{d\alpha} + d\varphi_{d\delta}$ may be considered constant and quoted directly in the ephemerides.

5. Accuracy Required in the Calculations

On the basis of Formula (19) we conclude that the accuracy required for the chronometer correction is not constant but depends on the latitude and the mean azimuth of the pair

$$m_u^s < \frac{m_\varphi'' \sec\varphi \operatorname{tg} A_m}{15} \ . \tag{40}$$

The closer the mean azimuth of the pair to 90° (270°), the less precisely can the chronometer correction be known. We list the data on the required accuracy of the chronometer correction in relation to the mean azimuth of the pair and the accuracy required in the latitude.

TABLE 3

Accuracy Required in the Chronometer Correction

φ	45°			55°			65°		
m_φ \ A_m	90°±15′	90°±30′	90°±45′	90°±15′	90°±30′	90°±45′	90°±15′	90°±30′	90°±45′
$0''.01$	$0^s.22$	$0^s.11$	$0^s.07$	$0^s.27$	$0^s.13$	$0^s.09$	$0^s.36$	$0^s.18$	$0^s.12$
0.05	1.08	0.54	0.36	1.33	0.67	0.44	1.81	0.90	0.60
0.50	10.8	5.4	3.6	13.3	6.7	4.4	18.1	9.0	6.0

Hence, for first-class points it is always possible to round off $\underline{u}$ to $0^s.1$ and for second-class points to $1^s.0$ (for $A_m < 90°30'$).

We ascertain the accuracy required in the half-differences of the hour angles (the accuracy of determination of the hour angles) arising from Formula (25) and list in Table 4

$$m_r^s < \frac{m_\varphi'' \sec\varphi \operatorname{tg}\frac{\Delta A}{2}}{15} = \frac{m_\varphi'' \sec\varphi \operatorname{ctg} a}{15} \ . \tag{41}$$

TABLE 4

Accuracy Required in the Half-Differences of the Hour Angles

φ	45°			55°			65°		
m_φ \ a	6°	20°	40°	6°	20°	40°	6°	20°	40°
$0''.01$	0.009	0.003	0.001	0.011	0.003	0.001	0.015	0.004	0.002
0.05	0.045	0.013	0.006	0.055	0.016	0.007	0.075	0.022	0.009
0.50	0.45	0.13	0.06	0.55	0.16	0.07	0.75	0.22	0.09

Hence, at first-class points, for calculation from the mean instant, it is necessary to compute t_S, t_N and $\underline{r}$ to $0^s.01$, and in the remaining cases to $0^s.1$.

The calculation of the latitude for each wire to 0".1 appears to be sufficient in all cases. Actually, at the same time the over-all rounding error in the latitude amounts to 0".05, and the mean square $\pm 0''.05/\sqrt{3} = \pm 0''.03$. For the mean of the seven wires this error is further reduced by a factor of $\sqrt{7}$ and amounts to $0''.05/\sqrt{21} = \pm 0''.01$.

In order to compare the logarithmic and nonlogarithmic methods of latitude calculation, let us suppose that we have tables of tan x and log tan x to the same number of decimal places, for example, six. It is well known [9] that in determining the angle x from tan x and $m_{\tan x} = 1 \cdot 10^{-6}$

$$m''_{x_1} = m_{\mathrm{tg}\, x} \frac{\rho'' \cos^2 x}{10^6} = 0''.206 \cos^2 x. \qquad (42)$$

Similarly [9], in determining the angle x from log tan x

$$m''_{x_2} = m_{\mathrm{lg\, tg}\, x} \frac{\rho'' \sin 2x}{2\mu \cdot 10^6} = 0''.237 \sin 2x. \qquad (43)$$

Evidently, $m_{x_1} < m_{x_2}$ for

$$x < \mathrm{arc\,tg}\, \mu \simeq 23°28'.5. \qquad (44)$$

Hence, beyond the limits of the tropical zone (beyond the limits of the "arctangent of the modulus") it is more advantageous to employ nonlogarithmic tables for computing the latitude.

For six-place tables with $m_{f(x)} = 1 \cdot 10^{-6}$ the following errors in the latitude are obtained.

TABLE 5

Accuracy of Latitude Calculations

m_φ \ φ	20°	23°30	30°	40°	50°	60°	70°
From tg φ	0".18	0".17	0".16	0".12	0".09	0".05	0".02
From lg tg φ	0.15	0.17	0.21	0.23	0.23	0.21	0.16

Thus, the six-place calculations from tan x provide the required accuracy for first-class points only at latitudes 60-70°. However, it must be borne in mind that in Peters' well-known tables (with an interval of 10") the values of tan x for angles greater than 60° are given only to five decimal places, while the tables of A.S. Filonenko (with an interval of 1') have six places, but are inconvenient for computation. Consequently, it is necessary to give tan x to six decimal places in Peters' tables within the range 60-70°, and until then to use the seven-place tables of the natural trigonometric functions by Professor L.S. Khrenov or seven-place logarithmic tables. Furthermore, it is desirable to have six- or seven-place tables of the natural functions for argument in time.*

6. Calculation of the Latitude from Mean Data

Several methods have been proposed by Russian and Soviet astronomers for calculating the latitude in the method of M.V. Pevtsov from the mean instants of observation. Such methods were proposed by Professor A.Ia. Orlov in 1909 [10], N.O. Shchetkin in 1924 [11], Professor N.A. Urmaev in 1925 [12], Professor V.V. Kavraiskii in 1926 [13], V.G. Shaposhnikov in 1930 [14].

All of these methods, which reduce the bulk of the calculations considerably (six-seven times), have nevertheless two intrinsic disadvantages:

---

*Such tables (by S.A. Angelov) are being prepared for publication at the GTTI.

a) They do not provide a control of the calculations, and b) they do not permit an estimate of convergence of the latitudes obtained from observations on the individual wires. Therefore they are employed only at second- and third-class points.

In 1931 M.S. Molodenskii [15] attempted to remove the latter disadvantage and "to obtain the value of the latitude from observations on each wire separately by means of a subsequent three-place calculation . . ." The essence of his method is as follows [16].

First, an auxiliary value of the latitude φ_0 is calculated from the formula*

$$\operatorname{tg} \varphi_0 = \operatorname{tg} \delta \cos h \sec g = \operatorname{tg} \delta \cos r \sec M, \tag{45}$$

where [9]

$$\operatorname{tg} g = \operatorname{tg} M = \operatorname{ctg} \varepsilon \operatorname{tg} h \operatorname{ctg} \delta = \operatorname{ctg} \varepsilon \operatorname{tg} r \operatorname{ctg} \delta. \tag{46}$$

Obviously, the latitude φ would have the value φ_0 if the angle $t - M$ were equal to zero. In this case we would have $A_m = 90°$ (270°) and $d\varphi/du = 0$.

Then three corrections are added to the value of the latitude φ_0: a) for acceleration in the interval $(\tau_{si})_0$

$$\mathrm{I} = \alpha (\tau_{si})_0^2, \tag{47}$$

where

$$\alpha = \frac{0.1148}{\Delta \lg \operatorname{tg} \varphi_0}; \; (\tau S_i)_0 = TS_i - (\alpha_S - u_S + g_0 - h_0) = T_{Si} - T_{S0}, \tag{48}$$

$$h_0 = r = \frac{(\alpha_S - \alpha_N) + (u_N - u_S) + (T_N - T_S)_0}{2};$$

$$(T_N - T_S)_0 = \frac{\Sigma (T_N - T_S)}{n}; \tag{49}$$

b) for the deviation of the hour angle differences from the mean

$$\mathrm{II} = \beta 2 \Delta z_i = \beta 2 \Delta r, \tag{50}$$

where

$$\beta = \left[7.5 \frac{\Delta \lg \cos h_0}{\Delta \lg \operatorname{tg} \varphi_0} + 7.5 \frac{\Delta \lg \sec g_0 \, \Delta \lg \operatorname{tg} h_0}{\Delta \lg \operatorname{tg} \varphi_0 \, \Delta \lg \operatorname{tg} g_0}\right], \tag{51}$$

$$2 \Delta z_i = (T_N - T_S)_i - (T_N - T_S)_0, \tag{52}$$

c) for the effect of second-order terms

$$\mathrm{III} = \gamma \, \mathrm{II} \, \tau_{si}, \tag{53}$$

where

$$\gamma = (\operatorname{ctg} t_N \sin 1^s). \tag{54}$$

Thus the value of the latitude for each wire is obtained from the formula

$$\varphi_i = \varphi_0 - \mathrm{I} + \mathrm{II} + \mathrm{III} + \delta\varphi_b, \tag{55}$$

---

*For conformity with the previous text we have converted M.S. Molodenskii's symbols to the usual ones.

where $\delta\varphi_b$ is a correction for inclination. The final value of the latitude is obtained as the mean

$$\varphi = \frac{[\varphi_i]}{n} . \tag{56}$$

It must be noted that Molodenskii's formulas were published in [16] without derivation, with an unusual notation and with a large number of misprints in the formulas and in the calculations. Besides, his supplementary calculations are far from simple and are not controlled in any way. To this must be added yet another substantial disadvantage – the basic calculations of the latitude φ_0 also are not controlled in any way, hence all the rest of the calculations are without control. All this makes utilization of this method difficult and is probably the reason why it has not been applied in practice.

The lack of a control for the calculations in Molodenskii's method may be removed in two ways:

a) If in calculating from the mean instant we allow for an acceleration correction (according to the deviations of τ from the mean instant) and log cos(t – M), the formulas will take the form:

$$\lg \operatorname{tg} \varphi' = \lg \operatorname{tg} \varphi_0 + \lg \cos(t - M) + \lg f, \tag{57}$$

$$\varphi = \varphi' + \delta\varphi_{b,m} = \frac{[\varphi_i]}{n} . \tag{58}$$

b) If we introduce into the latitude φ_0 an acceleration correction $\Delta\varphi_0$ calculated according to the deviations of τ_0 from the fictitious mean instant T_0, and, if necessary, a correction $\delta\varphi_T$ for rounding of the mean differences $(T_N - T_S)_0$, we obtain the formula

$$\varphi = \varphi_0 + \Delta\varphi_0 + \delta\varphi_T + \delta\varphi_{b,m} = \frac{[\varphi_i]}{n} . \tag{59}$$

As an example from [16] these calculations will have the following form.

TABLE 6

Control of Calculations for M.S. Molodenskii's Method (Original Data: see [16])

A) Control by Formula (57)				B) Control by Formula (59)			
τ_{si}	τ_{si}^2	calculation of φ		calculation of $\Delta\varphi_0$		calculation of $\delta\varphi_T$ and φ	
$-69^s.5$	4830	$t - M$	$-0^h00^m29^s.24$	$2\varphi_m$	$110°04'.2$	$(T_N - T_S)_0$	$8^m30^s.00$
-46.5	2162	$(t - M)^0$	$-0°07'18''.6$	$[\tau_0^2]:7$	3036	$(T_N - T_S)_m$	8 29.64
-23.5	552	$\lg \operatorname{tg} \varphi_0$	0.1553469	$\lg \frac{[\tau_0^2]}{7}$	3.482	dT	$-0^s.36$
-1.0	1	$\lg \cos(t - M)$	9.9999990	$\lg \frac{(-15\,\rho''^2)}{4\,\rho''}$	6.436	$\lg dT$	$9.556n$
$+22.5$	506	$\lg f$	25	$\lg \sin 2\varphi_m$	9.973	$\lg k_2$	$0.245n$
$+46.5$	2162	$\lg \operatorname{tg} \varphi'$	0.1553434	$\lg \Delta\varphi_0''$	$9.891\ n$	$\lg \delta\varphi_T$	9.801
$+71.5$	5112	φ'	$55°04'07''.21$			φ_0	$55°02'07''.37$
						$\Delta\varphi_0$	-0.78
0.0	15325	$\delta\varphi_{в, m}$	-0.26	Calculation of lg k_2 see Table 7		$\Delta\varphi_{T, m}$	$+0.63$
$[\tau^2]:7$	2189	φ	$55°02'06''.95$			$\Delta\varphi_{B, m}$	-0.26
						φ	$55°02'06''.96$

Using Formulas (19) and (25) derived above, it is possible to suggest another, simpler method of computing the latitude. First let us calculate the value of the latitude from the mean instant (without allowing for an acceleration correction) according to V.G. Shaposhnikov's formula [14]:

TABLE 7

Calculation of Latitude by a New Method (Original Data: see [16], p. 289)

Auxiliary calculations				No.	t_m	τ_i	τ_i^2	dT_i
$\alpha_S-\alpha_N+\Delta u$	$-1^h\,01^m\,37^s.50$	δ	$54^\circ13'\,58''.28$	1	$1^h\,03^m\,07^s.25$	$-69^s.82$	4875	$-0^s.64$
$(T_N-T_S)_m$	8 29.64	r	16 58 10.17	2	2 44.00	−46.57	2169	−0.14
$2r$	— 53 07.86	z	$18^\circ46'.0$*	3	2 21.00	−23.57	555	−0.14
r	— 26 33.93	A_S	337 38.1	4	1 58.25	− 0.82	1	+0.36
r°	$-6^\circ38'\,28''.95$	A_N	202 10.1	5	1 3.50	+22.93	526	+0.86
t_N	$-1^h28^m\,31^s.35$	A_m	269 54.1	6	1 11.00	+46.43	2156	−0.14
t_S	— 35 23.49	$\frac{\Delta A}{2}$	−67 44.0	7	0 46.00	+71.43	5102	−0.14
		$2\varphi_m$	110 04.2	Mean	$1^h\,01^m57^s.43$	−0.01	15384	0.00

Formulas	Calculation of φ_m
$\log\tan r$	9.0660865
$\log\operatorname{ctg}\delta$	9.8575444
$\log\operatorname{ctg}\varepsilon$	0.5154887
$\log\tan M$	9.4391196
M°	$-15^\circ22'08''.52$
M^h	$-1^h01^m28^s57$
t_m	−1 01 57.42
$t-M$	-0^m28^s85
$(t-M)^\circ$	$-0\ 07'\,12''.8$
$\log\sec M$	0.0158155
$\log\cos r$	9.9970758
$\log\tan\delta$	0.1424556
$\log\cos(t-M)$	9.9999991
$\log\tan\varphi_m$	0.1553460
φ_m	$55^\circ02'07''.79$
$\Delta\varphi_0$	−0.56
$\delta\varphi_{bm}$	−0.26
φ	55°02′06.97
	Control
$[\varphi_i]:n$	$55^\circ02'06''.97$
M_φ	±0.20

Formulas	Calculation of φ_i				
$\log\frac{15^2}{4\rho''}$	6.436	$[\tau^2]:7$	2198	log 15	1.176
$\log\sin 2\varphi_m$	9.973	log 7.5	0.875	$\log\cos\varphi$	9.758
$\log k_2$	6.409	$\log\cos A_m$	9.758	$\log\operatorname{ctg} A_m$	7.235
$\log\frac{[\tau^2]}{7}$	3.342	$\log\operatorname{ctg}\Delta A/2$	9.612	$\log k_3$	8.169
$\log\Delta\varphi_0''$	9.751	$\log k_2$	0.245		

Formulas \ No.	1	2	3	4	5	6	7
$\log\tau_i^2$	3.688	3.335	2.744	9.828	2.721	3.336	3.708
$\log \mathrm{I}'$	0.097	9.744	9.153	6.237	9.130	9.744	0.117
$\log dT$	9.806	9.146	9.146	9.556	9.934	9.146	9.146
$\log \mathrm{II}'$	0.051	9.391	9.391	9.801	9.170	9.391	9.391
$\log\tau_i$	1.844	1.668	1.372	9.914	1.369	1.667	1.854
$\log \mathrm{III}'$	0.013	9.837	9.541	8.083	9.529	9.836	0.023
$-\mathrm{I}'$	−1.25	−0.55	−0.14	0.00	−0.13	−0.55	−1.31
II'	+1.12	+0.25	+0.25	−0.63	−1.51	+0.25	+0.25
III'	−1.03	−0.69	−0.35	−0.01	−0.34	+0.69	+1.05
$\delta\varphi_{b,\,i}$	0.00	−0.03	0.20	−0.33	−0.33	−0.40	−0.50
$\Delta\varphi_i$	−1.16	−1.02	−1.44	−0.97	−1.63	−0.01	−0.51
φ_i	06.63	06.77	07.35	06.82	06.16	07.78	07.28
φ_i [8]	06.65	06.75	07.34	06.79	06.16	07.75	07.25
φ_i [16]	06.64	06.75	07.34	06.81	06.16	07.76	07.27

---

* Zenith distance and azimuths calculated from Formulas (20), (21).

$$\lg \operatorname{tg} \varphi_m = \lg \operatorname{ctg} \delta \operatorname{tg} r \sec M \cos (t - M). \tag{60}$$

Evidently,

$$\lg \operatorname{tg} \varphi = \lg \operatorname{tg} \varphi_m + \lg f. \tag{61}$$

Then let us obtain the value of the latitude for each wire, introducing into the value of φ_m three corrections:

a) For acceleration in the interval $\tau_i = (t_i - t_m)_m$ from the formula of A.Ia. Orlov [10]

$$I' = -[6.4361 \sin 2\varphi_m \tau_i^2 = -k_1 \tau_i^2; \tag{62}$$

b) For the deviation of the half-difference of the hour angles from the mean value, according to the author's Formula (25)

$$II' = 7.5 \cos \varphi \operatorname{ctg} \frac{\Delta A}{2} dT_i = k_2 dT_i, \tag{25'}$$

where

$$dT_i = (T_N - T_S)_i - (T_N - T_S)_m; \tag{63}$$

c) For the deviation of the hour angle from the mean according to the author's Formula (19)

$$III' = 15 \cos \varphi \operatorname{ctg} A_m \tau_i = k_3 \tau_i. \tag{19'}$$

Then

$$\varphi_i = \varphi_m - I' + II' + III' + \delta\varphi_b. \tag{64}$$

To calculate the deviations of the hour angles from the fictitious instant T_{S0}, as M.S. Molodenskii does, and not from the mean hour angle, is profitable only if at the same time $d\varphi/du = 0$, and it is not necessary to calculate the correction III' for deviation of the hour angles. But, in this case $[\tau_0] \neq 0$, which makes control of the calculation of τ_0 difficult. Besides, the calculation of τ in (19) is performed on the basis of the mean hour angles (not on the basis of the hour angles of the southerly star), which is more accurate, and in addition the corrections III are diminished and become symmetric with respect to the mean instant, so that their influence may be neglected.

Control of the calculations may also be realized here in two ways:

a) The mean of the values φ_i must agree with the value of φ_m, corrected for acceleration and inclination

$$\varphi = \frac{[\varphi_i]}{n} = \varphi' + \delta\varphi_{b,m}, \tag{65}$$

b) The mean of the values φ_i obtained, as in the method of Molodenskii, from the initial latitude φ_0, must equal the value of the latitude corrected for $\log \cos (t - M)$, for acceleration (according to τ_0), and for inclination [see Formula (57)].

Thus it is possible to draw the following conclusions:

1. Field control of observations in Pevtsov's method can be achieved through comparison of the differences $(T_N - T_S)_i$.

2. For calculating the error in the chronometer correction it is convenient to use Formula (19).

3. At first-class points it is most efficient to calculate the latitude from the mean instant, obtaining in addition the latitude for each wire from Formula (64). This provides an economy of 30-40% in comparison with

the usual method of calculation for all the wires, and ensures control of the calculations. At the same time, it is necessary to derive u to $0^s.1$, α, r and t to $0^s.01$, δ to $0''.01$, to use seven-place tables and to take into account the effect of diurnal aberration. It is expedient to give the corrections $d\varphi_{d\alpha} + d\varphi_{d\delta}$ in the ephemerides. At second- and third-class points the latitude is to be calculated from the mean instant, rounding u to $0^s.5$, and the corrections for diurnal aberration may be neglected.

LITERATURE CITED

[1] Instruction for Astronomical Determination of Points of Classes I, II, III and IV [in Russian] (Moscow, 1948) p. 14.

[2] Instruction for Triangulation of 1st, 2nd, 3rd and 4th Classes [in Russian] (Moscow, 1956).

[3] "Ephemerides for the determination of latitude from corresponding altitudes of stars," Trudy TsNIIGAiK 50, 1-5 (Moscow, 1946).

[4] I.I. Seliverstov, Ephemerides of Stars for the Determination of Latitude from Corresponding Altitudes [in Russian] (St. Petersburg, 1912).

[5] A.N. Kuznetsov, "The determination of latitude by Pevtsov's method with the use of a shutter," Trudy TsNIIGAiK 81 (Moscow, 1951).

[6] A.P. Kolupaev, "Latitude determinations by M.V. Pevtsov's method," Collection of papers of the Main Administration of Geodesy and Cartography [in Russian] (Moscow, 1950) 32.

[7] Directions for Reduction of Astronomical Determinations [in Russian] (Moscow, 1939) pp. 81, 91, 92.

[8] K.A. Tsvetkov, A Course in Practical Astronomy [in Russian] (ONTI, Moscow-Leningrad, 1934) pp. 237, 402.

[9] K.A. Tsvetkov, Practical Astronomy [in Russian] (Geodezizdat, Moscow, 1951) pp. 244, 253, 503.

[10] A.Ia. Orlov, Izv. Russk. Astr. Ob. (1909).

[11] N.O. Shchetkin, "Latitude determination from corresponding altitudes of two stars," Zapiski VTU RKKA Vol. LXXIII, part 2, No. 1 (Moscow, 1924).

[12] N.A. Urmaev, "The determination of geographic latitude from corresponding altitudes of two stars," Geodezist No. 6-7 (1925).

[13] V.V. Kavraiskii, Izv. Russk. Astr. Ob. 26 (1926).

[14] V.G. Shaposhnikov, "Latitude calculation from observations by Pevtsov's method," Geodezist No. 2-3 (1930).

[15] M.S. Molodenskii, Astron. J. (USSR) 3, No. 3-4 (1931).

[16] Geodesy, An Information Manual [in Russian] Vol. II (Izd. NKKh RSFSR, Moscow-Leningrad, 1940) p. 288.

Received August 10, 1956

Novosibirsk Institute of Engineers
of Geodesy, Aerial Photography
and Cartography

SOME RESULTS OF OBSERVATIONS OF THE VIBRATION OF IMAGES OF STARS AT THE MAIN ASTRONOMICAL OBSERVATORY OF THE ACADEMY OF SCIENCES OF THE UKRAINIAN SSR AT GOLOSEEVO

I. G. Kolchinskii

Results are given of measurements of the amplitudes and periods of vibration of the images of stars on plates obtained with the 400-mm astrograph of the Main Astronomical Observatory of the Academy of Sciences of the Ukrainian SSR at Goloseevo using a fixed tube. The observations were carried out during 1955-1956.

It is shown that the root-mean-square amplitudes of vibration are proportional to $L^{0.5}$ where L is the mass of the atmosphere and the principal periods of vibration are of the order of a few seconds. Large amplitudes correspond to smaller frequencies of vibration. The theoretical dependence of the root-mean-square amplitude of vibration on temperature is confirmed experimentally. It is shown that the distribution of amplitudes according to their magnitude is gaussian.

Observations of vibration of star images in telescopes are of great interest at the present time for the following reasons:

1. The amplitude of vibration of star images is one of the criteria of the suitability of a given place for an observatory.

2. The vibration of images, as well as the oscillations in the intensity of the stellar light (twinkling), are connected with turbulence in the terrestrial atmosphere. For this reason, observations of vibration of stellar images are valuable in that they provide information on the nature of the turbulent irregularities, their motion, size, height, etc.

3. Phenomena analogous to vibration of star images and twinkling are also observed in the propagation of radio waves in a defined frequency range in the atmosphere.

The general laws of propagation of electrical waves, and particularly radio waves, in a medium with random irregularities in the refractive index are the subject of many studies, both theoretical and experimental, at the present time. In a number of cases it is of great interest to compare the phenomena of vibration and twinkling observed at optical frequencies, with the analogous phenomena in the radio-frequency range, and also to compare observational data with theoretical results.

In view of the above it was decided to undertake observations of vibration of star images at the Main Astronomical Observatory of the Academy of Sciences of the Ukrainian SSR in order to obtain more detailed information than was obtained earlier at other observatories. The aim of the observations was to determine the character of the dependence of the amplitude of vibration on zenith distance, and to bring to light the existence of periods of vibration, if any, and the first results of these observations are published in the present paper.

1. Observations

Observations of the vibration of star images were carried out photographically on an astrograph ($D = 400$ mm, $F = 5.5$ m). The so-called "tracks" of the star images were obtained on photographic plates with the clock mechanism at rest. The astrograph was set up in a separate tower on a solid concrete base. The installation is very massive and its total weight probably exceeds 10 tons. Since this part of the observatory lies in a wood and is at a relatively large distance from a town (3-4 km from the outskirts) vibration of the base due to, for example, the motion of trams, heavy trucks etc. were not observed. A large number of observations of stars were carried out using the guide of the astrograph ($D = 300$ mm, $F = 5.5$ m) for different zenith distances and a magnification of 400, with the clock both going and at rest, and it was established that in the presence of a wind of force 3-4 directed at the open observational slit the tube begins to experience small vibrations. It was therefore decided to carry out observations only in the absence of wind or when the wind force does not exceed 1-2. The majority of observations were carried out in quiet weather.

One may therefore assume that the waviness of the tracks on photographic plates which were obtained by us is due to atmospheric microturbulence since the vibration of the instrument itself and the effect of wind are excluded. This was confirmed by the results obtained with the above apparatus (for example, from the dependence of the zenith distance).

The first plates containing tracks were obtained in 1949-1950 when the astrograph was just completed. Later, systematic observations were begun in January 1955 and are continuing at the present time. The plates employed were Ilford Ordinary No. 30 and, sometimes, Agfa-Astro (6 x 24) cut out from larger plates.

During each clear night one or a few plates were obtained and each plate contained a few tracks having an average length of 14 cm, which for a star with $\delta = 0°$ corresponds to a time interval of about six minutes. The range of zenith distances was 27-84°. Usually only stars having magnitudes of 2-3 were taken since they give tracks which are not too dense or wide, and which have a waviness which for large zenith distances is very noticeable even without a lens.

Altogether 134 plates containing 280 tracks were obtained in the period January 1956-May 1956.

2. The "Resolving Power" of the Method

The scale given by our astrograph is $37''\!.4$ per 1 mm. Thus, the speed with which the image of an equatorial star moves along the plate is 0.4 mm/sec, and for a star whose inclination is δ this speed is smaller by a factor of δ. We shall consider that the diameter of the "minimum circle of scattering" due to diffraction is $20\text{-}30\mu$. This distance is covered by an equatorial star in 0.05-0.08 sec. One may consider that this quantity determines the order of the exposure time for all the points of the plate traversed by the moving image. This is correct for the average line of the track. At the edges of the track the exposure time will be less.

Thus, with an exposure of the order of a fraction of a second the density of the image turns out to be sufficient for a reliable measurement in the case of stars whose magnitudes are 2-3. If the image deviates from the direction of the track during time intervals which are small compared with the exposure time then such deviations will not be very visible on the photographic plate. In addition, since the time of deviation is small compared with the time during which the image of the star covers a distance equal to its diameter, it follows that successive deviations will be difficult to separate. Thus, using the above method one may discover vibrations whose period is not less than 0.1 sec, or even of the order of a second.

It was therefore decided to measure deviations from the direction of the track at intervals not less than 50μ.

However, if one increases the speed with which the image of a star moves across the plate (i.e., if one increases its speed of "sweep"), and if one uses more sensitive plates, it is possible to detect periods less than 0.1 sec.

3. The Determination of the Amplitudes of Vibrations

By the "amplitude of vibration" we shall understand the root-mean-square value of the deviation from an imaginary track which would be obtained on the plate if the vibrations were not present. We shall measure these vibrations in a direction perpendicular to the direction of the track.

Generally speaking, the track is curved. By taking into account "curvature of the parallel" and the differential refraction, it is possible, as is well known, to represent the track by a second-degree curve.

In a number of papers, concerned with the determination of the amplitude of vibration, corrections were introduced which exclude these effects so that the track could be represented by a straight line. The small angle between this straight line and the direction of one of the axes of the coordinate system of the measuring instrument (the lining-up error) was found graphically by taking an average line through a number of points corresponding to the readings of the instrument into which the necessary corrections were introduced (cf. for example [1, 2]). The required deviations from this straight line were then found after a conversion into angles and thus gave the values of the amplitudes.

Since we had to deal with a possibly large number of tracks, and our main concern was to establish the presence of short-period vibrations, we introduced a simplified version of this method. In the present investigation all the track was divided into small sections each 5 mm long which corresponds to 12.5 sec in the case of an equatorial star. Our calculations have shown that such sections may, with accuracy sufficient for our purposes, be considered as straight. For stars whose inclination is about ±30°, the error is of the order of 0".01.

Measurements were carried out using the Repsol'd machine belonging to the Observatory of the Kiev State University. This machine has a micrometer which can be used to determine both X and Y coordinates. The length of the micrometer screw was such that measurements could only be carried out in the range ±5 mm (the same type of measuring machine was used in the measurement of the negatives of the "Chart of the Sky" and is provided with a Got'e grid). The size of one division on the micrometer drum is clear from the following data:

along the Y-axis: 5 mm — 10.168 turns,
along the X-axis: 5 mm — 10.198 turns.

Readings could be taken to about 0.001 of a turn, i.e., about 0.5μ which in angular measure, corresponding to the scale of the astrograph, is 0".018. The plate was placed in the machine so that the Y-axis was along the track. Beginning with the left-hand end of the track readings were taken along the X-axis in steps of 50μ. The double thread of the micrometer was placed in the middle of the track so that equal parts of it lay on either side. In order to simplify and speed up the measuring process, measurements were carried out without turning the plate through 180°. This could not introduce a systematic error if the thickness is constant along the entire track. However, parts of tracks show well-defined grain structure (strong twinkling). Between these grains the track is somewhat narrower than the grains themselves. In this case lining-up error depending on the width of the track is possible. A check on the results obtained by turning the plate through 180° showed that this error has almost no effect on the magnitude of the amplitude.

TABLE 1

No. of series	1	2	3	4	5	6	7	8	9
Root-mean-square amplitude	45.2	57.1	70.4	53.8	55.5	43.7	41.0	33.1	47.4
No. of series	10	11	12	13	14	15	16	17	
Root-mean-square amplitude	51.2	40.5	54.8	41.4	51.0	52.9	46.4	45.3	

Thus, the results of measurements on a track consisted of a number of series, 100 readings each, corresponding to 5-mm sections.

Further work was carried out as follows. The mean value of the X coordinate was calculated for each series, as well as the deviation of each reading from the mean with its sign. These deviations were at the basis of subsequent calculations. Next, using the method of least squares,we calculated the coefficients a and b in the

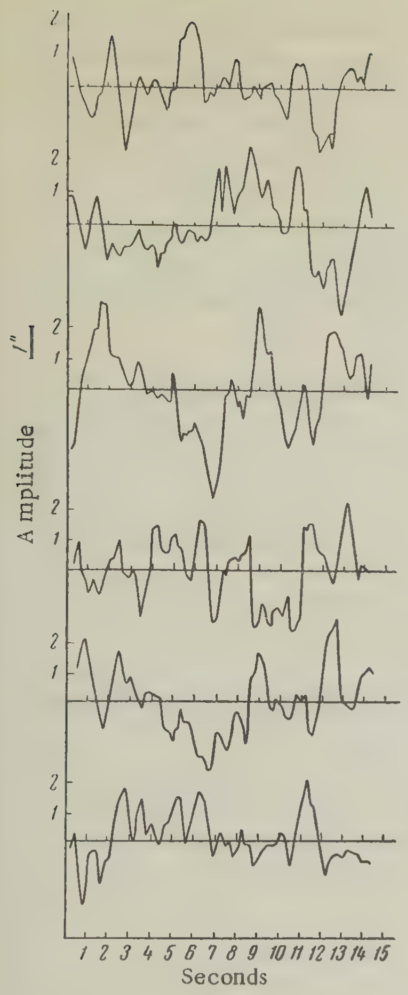

Fig. 1. Vibration amplitudes for some sections of track No. 2 plate 141 ($z = 80^\circ.3$).

linear equation $X = aY + b$ which best represents the points (X, Y). The coefficient $\underline{a}$ determines the angle between the track and the Y-axis. In the majority of cases this angle was about 1°.

We then determine the ordinate X_i for each of the 100 points in a series. The final amplitude was taken as equal to the difference between the values of the deviation from the mean and the quantity X_i. Strictly speaking, in order to obtain the amplitude in the direction perpendicular to the track it is necessary to multiply this difference by the cosine of the small angle of inclination to the Y-axis.

The root-mean-square values of the amplitude were then calculated for each series separately and for all the series for a given track together, first in thousandths of a turn of the micrometer screw and then in angular measure.

One must remember that the image of a star in the telescope vibrates in all directions and a measurement on the track yields only the component of these vibrations perpendicular to the track. If the star is in the meridian the track will be parallel to the horizon and one records the component directed towards the zenith. If one observes stars at larger angles, then one records the component of vibrations which is at an angle P to the direction towards the zenith, where P is the parallactic angle.

Without going into the problem of the "isotropy" of vibration we have confined our attention to a comparison of the amplitude obtained at different time angles and disregarding the direction of the vibrations.

We shall give here some data in order to estimate the accuracy of the amplitudes. Track No. 2 on plate 141, which was obtained during the night of September 15-16, 1950, was measured along its whole length of 8.5 cm ($z = 80^\circ.3$).

The root-mean-square error of a single sighting on the track obtained from the differences between pairs of successive sightings was calculated from the formula $m = \pm\sqrt{\Sigma v_i^2/2n}$, where v_i is the difference between the sightings, and $\underline{n}$ is the number of pairs ($n = 50$); it was found that the error was ±0.0022 of a micrometer turn, which corresponds to $0''.04$.

We give a table of the root-mean-square of the amplitudes (in thousandths of a micrometer turn) for the above track.

The root-mean-square of these values is 50.04 and was the final value of the amplitude for this track. The root-mean-square value of the deviations from this quantity is 6.6. Thus, the error in the amplitude will be approximately 0.0016 micrometer turns ($6.6/\sqrt{17}$) or $0''.03$, which is about 3%. It must be pointed out that the differences between the separate series can probably be explained not so much by the errors of measurement as by a real random change of the mean amplitudes from series to series.

The values of the amplitudes obtained at intervals of 50μ were plotted. Along the ordinate axis we plotted the amplitude in thousandths of a micrometer turn and along the abscissa axis the distances along the track in tenths of a micrometer turn. These distances give the time scale.

For a star whose inclination is δ one turn of the micrometer along the Y-axis corresponds to $1^s.23 \sec\delta$.

We give graphs for a number of series obtained for track No. 2 plate 141. These graphs show the oscillatory nature of the phenomenon and a tendency to an approximate periodicity (Figure 1).

In order to analyze statistically the data for a given track the separate series of readings were combined in the following way. In the measuring process there was a gap after each 50μ between the separate series since at these points the track was covered by a horizontal line of the Got'e grid. At these points between the series, an additional amplitude, equal to the mean of the last amplitude of the previous series and the first amplitude of the next one, was introduced. After this, the whole sequence of amplitudes from the first to the last series was rewritten in the usual order. Thus, in each separate series the obtained amplitudes were related to some, generally speaking, different level of "mean refraction."

4. The Dependence of Vibration Amplitudes on the Zenith Distance

To obtain this dependence, the root-mean-square amplitudes were measured at 400 points using 2-cm sections of each track.

Eighty-three amplitudes over 48 nights at different zenith distances were used. The aggregate of these values was represented by the formula

$$\Delta = \alpha L^{p}, \tag{1}$$

where L is the mass of the atmosphere, Δ is the amplitude and α and p are constants which were found by the method of least squares. For this purpose Formula (1) was put into the form

$$\log \Delta = \log \alpha + p \log L. \tag{2}$$

The normal equations were obtained from 83 equations of the above type and the following values were found for the two constants:

$$\log \alpha = 1.545 \pm 0.04 \text{ (mean error)},$$
$$p = 0.47 \pm 0.08 \text{ (mean error)}.$$

Thus,

$$\Delta = 0''.354 L^{0.47}. \tag{3}$$

Figure 2 shows the observed values of the amplitudes and the curve which represents them in accordance with (3).

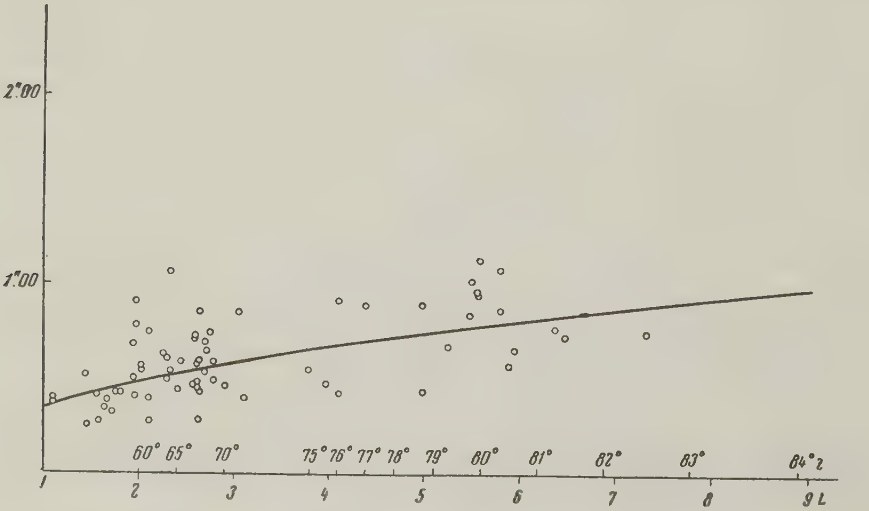

Fig. 2. The curve calculated from the formula $\Delta = 0''.35\ L^{0.47}$. The open circles represent the observed values of the root-mean-square amplitudes, L is the mass of the atmosphere.

It may be considered that the amplitudes of vibration are in fact proportional to $L^{0.5}$ as should be the case in accordance with the general theory (cf. [3]).

5. A Comparison With the Results of Analogous Observations at Other Observatories

Our earlier paper [4] gives results of a treatment of observations of vibration of stellar images at various z which were obtained by other observers. Generally speaking, they support the above result, namely, that the vibration amplitudes are proportional to $L^{0.5}$.

Let us consider certain other observations. E.K. Kharadze [5] gives data on the vibration of images at Abastuman (altitude of 1500 m). Observations were carried out visually in 1932-1933. A graphical representation of these results shows that they do not follow the law (1) but obey the following relation:

$$\Delta = \alpha \log \sec z + \beta, \tag{4}$$

where $\alpha = 3''.6$ and $\beta = 0''.40$.

On calculating the values of α and p according to Formula (1) as before, we obtain

$$\alpha = 0''.46, \ p = 1.44;$$

but this formula does not represent the observations so well.

We then used the considerable observational material obtained by the astronomers Coutrez and Bossy [6] during their expedition to Central Africa (Belgian Congo) in 1948. The aim of this expedition was to choose a site for an observation station. Observations were carried out at altitudes of 2100 to 4550 m. The vibrations of images were observed visually with the help of a reflector. Some hundreds of observations of amplitudes at various z were obtained. The authors considered that these observations show that the amplitudes are proportional to sec z (or L) but the problem is not discussed in detail. They determined the "turbulence angle" at the zenith using a "sec z" reduction, and to obtain this quantity they divided the observed amplitude by sec z. The observed values of the amplitude at the zenith are, in general, constant, as they should be if the amplitudes are proportional to sec z.

However, on analysis of these data one notes the following fact: when the zenith distance is large, and consequently sec z is also large, the amplitude at the zenith, obtained by dividing the amplitude at the given z by sec z, is much smaller than the same amplitude derived from observations at small z. For such days the "turbulence angles" at the zenith show a clear dependence on z. The smaller the value of z the smaller the amplitude. For example, this is so in the case of observations obtained on August 12, 13, 14, 15, 1948,on Gakhing* Mountain (2626 m) and shows that the amplitudes in these cases are at least proportional to $(\sec z)^{0.5}$ or possibly $(\sec z)^p$, where $p < 1$. If one represents these observations by Expression (1) one obtains the following values:

night of August 14-15, 1948: $\alpha = 0''.19$; $p = 0''.85$,
night of August 12-13, 1948: $\alpha = 0''.21$; $p = 0''.50$.

A similar situation is found in a number of other cases.

In connection with the possible deviation from the $L^{0.5}$ law it is interesting to analyze separate groups of observations obtained during a single night. One must, however, remember that if observations are obtained during time intervals of a few hours,then the effect of the daily variation of turbulence on the character of image vibration may become important. For this reason one should, strictly speaking, obtain a large number of tracks at different z during a relatively short interval of time. For example, let us take those of our observations which were obtained during the night of December 19-20, 1955. For different z we found the following amplitudes:

z —	68°.7	70°.8	71°.1	72°.6	77°.4	78°.0
Δ —	0″.30	0″.53	0″.62	0″.49	0″.70	0″.75 .

If these are represented by Expression (1) then

---

*Transliteration of Russian – Publisher's note.

$\alpha = 0''.10$; $p = 1''.34$.

If other groups of observations are brought in as well, then in the majority of cases the amplitudes obey the $L^{0.5}$ law more closely then the L law for different z. Thus, among twelve groups obtained for different nights this result holds in eight cases. In the remaining cases the ratio of the amplitude is closer to the ratios of L values. This may be explained by errors of observation and possible real deviations from the law for which $p = 0''.5$. Analogous deviations from this law for separate nights in a considerably larger number of cases is noted also in the observations of the Belgian expedition to South Africa. In order to confirm this fact we chose two groups, from all the observations carried out on Gakhing Mountain, corresponding to two different values of turbulence at 0".20 and 0".16 and consisting of 45 and 55 observations, respectively. These groups correspond to the following dates of observations in August, 1948:

group I: August 9, 10, 17 and 18th,
group II: August 11, 12, 14 and 15th.

The values of turbulence in the zenith were obtained here from a reduction according to a sec z law.

The following values of α and p were obtained for the two groups:

	α	p
I	$0''.20$	$0''.98$
II	$0''.24$	$0''.46$.

Thus, in the first group the amplitudes are proportional to sec z and in the second group they are proportional to $(\sec z)^{0.5}$. It is characteristic that the observations in the second group correspond to consecutive days and, apparently, the same kind of weather. One cannot exclude the possibility that in mountain conditions such deviations are frequently observed and are a characteristic property. In this connection one notes the results of recent observations obtained in the region of the Great Alma-Ata lake reported by V.G. Fesenkov [7]. These observations have shown that the mean amplitude of vibration of star images obtained from the waviness of tracks is 0".3-0".4 and is practically independent of the zenith distance up to 80°.

The fact that amplitudes are proportional to $L^{0.5}$ appears to be a result of the presence of a very large number of irregularities along the path of a ray while the number of irregularities itself is proportional to L [4]. The fact that amplitudes are proportional to L may be connected with a small thickness of the layer [8]. It is also possible that the independence of the vibration amplitude of z is a result of a peculiar distribution of turbulence along different directions, which in its turn is a result of the particular topography. It is possible that one deals here with a kind of "cap" having a spherical form and consisting of turbulent air which lies above the particular spot and which cannot be excluded in mountain conditions.

In any case, the problem of deviations from the $L^{0.5}$ law is interesting and deserves further study.

6. Vibration Amplitude in the Zenith ("Turbulence Angle.")

The vibration amplitudes at the zenith were obtained by dividing the vibration amplitude at the given z by $L^{0.47}$, i.e., practically $L^{0.5}$. The maximum value of the turbulence angle was observed during the night of March 1-2, 1955, and was 0".95 with $T = -11°$, $p = 760$ mm, and the minimum value of this angle was observed during the night of August 15-16, 1955, and was equal to 0".11 with $T = +16°$ and $p = 752$ mm. The mean value at the observatory in Goloseevo was 0".38.

Figure 3 shows the distribution of the "turbulence angles" according to their magnitudes. The most frequent values are those between 0".31-0".40 (in about 34% of all the observations). One must remember that so far sufficient data from other observatories are not available. For this reason it is difficult to compare out data with those of other workers. In the case of Moscow, for example, according to E.Ia. Bugoslavskaia [2], $\alpha = 0''.19$, $p = 0''.51$. Similar values (0".19 and 0".21) were obtained for August 14-15th and 12-13th, 1948 in Equatorial Africa. The most frequent values obtained at all the stations in Africa are between 0".10 and 0".15 (reduction according to the sec z law). When the results from the 28 plates obtained in Kiev in 1955 were represented by the formula $\Delta = \alpha \sec z$ the value of α was found to be 0".17. In addition, the observations of Coutrez and Bossy

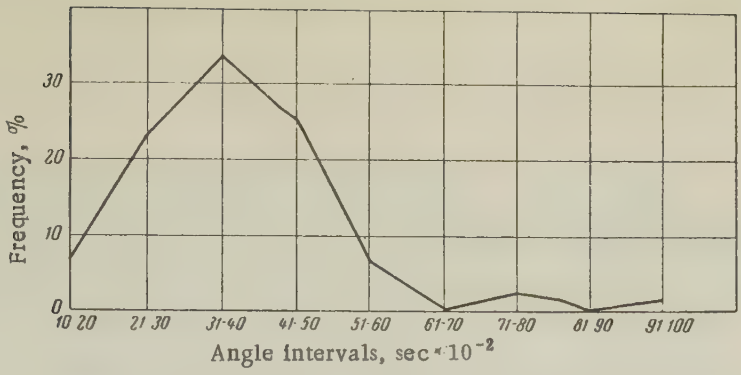

Fig. 3. Distribution of the amplitudes of vibration in the zenith ("turbulence angle") according to their magnitude.

were visual. In such observations one usually fixes the maximum deviations of the image. In our measurements, on the other hand, the amplitudes are the root-mean-square values obtained from a large number of observations and measured along the track in steps of $0^s.1$. Thus, in order to compare our results with those obtained in Africa it is expedient to multiply them by $\sqrt{2}$. When this is done we obtain for Goloseevo $\alpha = 0''.24$. This quantity is consistent with the suggestion that turbulence in the mountain should be less than in the lowlands.

7. The Dependence of the "Turbulence Angle" in the Zenith on the Temperature of Air

The results of grouping of the observations according to the temperature of the air are given in Table 2.

TABLE 2

Mean temperature	−9°.9	−1°.3	+2°.1	+8°.2	+13°.5	+17°.3	+23°.0
Amplitude of vibration in the zenith	0″.45	0″.39	0″.37	0″.36	0″.62	0″.31	0″.31
No. of observations	13	23	10	9	2	23	3

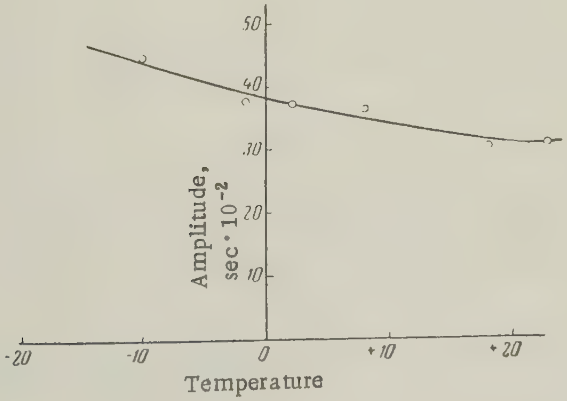

Fig. 4. Measurement of the root-mean-square amplitude of vibration as a function of air temperature.

The mean value for $t < 0°$ with $t = -4°$ ($T = 269$) is 0".41 and the mean value for $t > 0$ with $t = +13°$ ($T = 286$) is 0".35.

$$\left(\frac{T_{>0}}{T_{<0}}\right)^2 = 1.13, \qquad \frac{\text{ampl}_{<0}}{\text{ampl}_{>0}} = 1.18.$$

The tendency towards smaller amplitudes as the temperature increases can be clearly seen in Figure 4 (at the temperature of 13°.5, which includes only two observations, the corresponding point deviates from the curve apparently accidentally and is not included in the graph).

Thus, generally speaking, the amplitude increases as the temperature decreases and the actual form of this dependence is in close agreement with theory, i.e., the amplitudes are proportional to $1/T^2$ [3].

From the results of a grouping of the "turbulence angles" corresponding to different pressures no definite conclusions can be drawn as to the dependence on pressure.

8. Periods of Vibrations

Up to the present time the problem of the existence of periods of vibration has not been studied in any detail. Usually, any conclusion as to the existence of a period is based on visual estimates carried out on results of measurements represented in graphical form. When the curves are of a complex nature the periodicity cannot always be established in this way. We therefore decided to study this problem in greater detail.

We considered the curve of amplitude as a function of time as a record of some random process. In this connection it was convenient to employ methods of the usual harmonic analysis. In the case of the track No. 2 plate 141, September 15, 1950,it was decided to establish the presence of a period, if any, in the following three ways:

1. The simple method involving a count of the number of times the amplitude curve changes sign in each separate series.

2. The method involving a "periodogram" obtained on the basis of 1700 points.

3. The method involving the setting-up of an autocorrelation function.

All the calculations were carried out with the amplitudes expressed in thousandths of a turn of the micrometer screw.

1. Results of a count of the number of sign changes. The following table gives the number of such changes in each series:

TABLE 3

No. series	1	2	3	4	5	6	7	8	9	10	11	12	13	14	15	16	17
No. changes of sign	18	10	13	14	14	16	14	21	20	15	17	8	17	12	6	15	12

The mean value is 14.3.

In this table the number most frequently met with is 14. Since a "period" involves two changes of sign the mean value of a period will correspond to 14 points, i.e., 1.4 of a turn or 2.0 sec. From the mean value of the interval between zeros the period was found to be about 1,9 sec,which is practically the same as in the first case.

2. Construction of the "periodogram." We use the well-known method for finding the periods of nonharmonic periodic functions which is given in [9]. Below we give a table of the correlation η_k for a number of values of k close to the trial period.

The values of η_k have a maximum at $k = 14$, i.e., the period corresponds to 14 points or 1.4 of a turn, which was obtained before. 1700 amplitudes were used in the calculation.

TABLE 4

k	8	10	12	14	16	16	20
η_k	0.030	0.039	0.027	0.100	0.062	0.065	0.048

3. Calculation of the correlation function. The values of the correlation coefficient

$$R(u)=\frac{\overline{\xi(t)\,\xi(t+u)}}{\overline{\xi(t)^2}},$$

were calculated, where $\xi(t)$ is the initial sequence of amplitudes, $\xi(t+u)$ is the same sequence displaced through u units of time. The change corresponds to a shift through 1, 2, 3, etc. points.

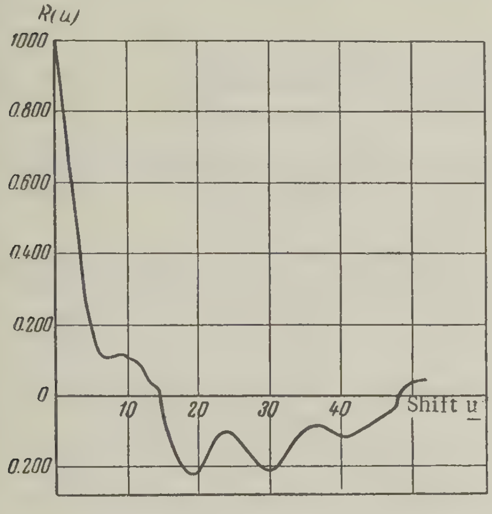

Fig. 5. Correlation function R(u) for track No. 2 plate 141.

The condition

$$\begin{matrix}\overline{\xi(t)}=0\\ \overline{\xi(t+u)}=0\end{matrix}\;\overline{\xi(t)^2}=\overline{\xi(t+u)^2}$$

holds approximately in our case.

As is known, if some random function contains hidden periodicities then they may be discovered through the correlation function [10, 11].

If each of the obtained series of amplitudes corresponding to 5-mm track sections contains one and the same hidden period, then in the sequence of amplitudes for all the series one should be able to find this period with the help of a graph of R(u), since the different phase relations which appear when all the series are combined into a single series will be unimportant.

Figure 5 shows the values of R(u) for the track No. 2 in plate 141 as functions of the shift u up to u = 51. In

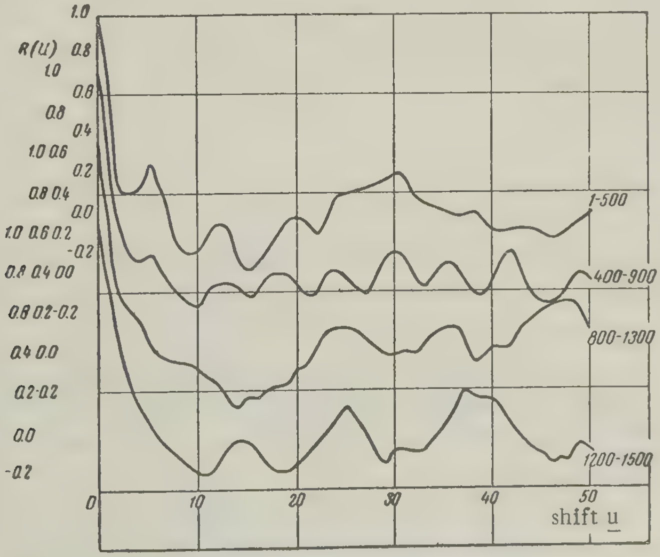

Fig. 6. Correlation functions R(u) for separate parts of track No. 2 plate 141.

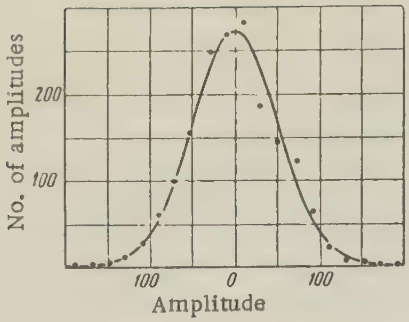

Fig. 7. Distribution of amplitudes according to their magnitude (1700 amplitudes, track No. 2, plate 141).

the calculation of R(u) 1000 amplitudes were taken each time so that amplitudes from No. 1 to No. 1051, out of a total number of 1700 measured amplitudes, took part.

It follows from this figure that the periodicity of R(u) is well defined. There are maxima at u = 23, 37, 51 which differ from each other by 14 points. The minima lie at u = 19, 30, 41 and differ from each other by 11 points.

Calculation of the correlation function for this track was also carried out for different parts of it. Figure 6 shows the R(u) curves for the following intervals: 1-500, 400-900, 800-1300, 1200-1500. In these calculations u was moved through two units. The curves are very similar, which reflects the stationariness of the random process.

Particularly well defined is the periodicity in the graph for the series 400-900. Minima are found at the following values: 20, 30, 44, 54, 66, 78, and 92. The mean value of the interval between the minima is 12. Maxima are found at the following values: 26, 38, 48, 60, 72, 84, and 98. The mean value of the distance between the maxima is also 12. Thus, in this series the period repeats through 12 points.

For the series 800-1300 and 1200-1500 the abscissas of minima and maxima are generally quite close to each other although the correlation curves were calculated for different points. Analogous calculations were carried out for other tracks also. Hidden periodicities were also found in these cases.

The preceding results show the reality of the existence of the periods and the fact that hidden periodicities can be found through the function R(u).

The "periods" obtained from a count of the number of changes of sign in each series consisting of 100 points correspond to the mean of four measured series for each plate. The periods lie in the range 1.2-3.3 sec. Only in one case, namely, plate No. 19 (March 1-2, 1955) obtained at z = 83°, the period turned out to be equal to 8.9 sec. At the same time, a very large root-mean-square amplitude of vibration was observed (2".36).

A grouping of the periods according to zenith distances shows some kind of dependence of the periods on z as can be seen from the following table:

z	<50°	50—60°	61—70°	71—80°	>80°
Mean value of period	$1^{s}.05$	$1^{s}.6$	$2^{s}.3$	$2^{s}.2$	$3^{s}.0$
No. of observations	5	9	26	16	11

Thus, the periods of pulsations increase with the zenith distance which is also the case with amplitudes. There exists also a positive correlation between the amplitudes and the periods in a number of cases, even when one deals with a single track, i.e., the same z.

It is interesting to note that as a result of studies of pulsations in the intensity of stellar light it was established that large amplitudes are largely associated with the region of low frequencies (of the order of 10-25 cps) while it was possible to detect twinkling frequencies up to 500 cps. It was also found that the frequencies decrease at large z (cf. Folke Nettelblad [12]).

The following may be a qualitative explanation of the relationships which we were able to find. Large amplitude vibrations are produced by relatively large-scale irregularities (lengths and temperatures) since these irregularities give relatively large phase differences between the rays. However, the time during which an irregularity intersects the beam of light will depend on its dimensions. In the case of large-scale irregularities the resulting random difference of phase pulsation between two rays will continue during a long interval of time which will lead to a large deviation of the image of the star from its mean position.

Results of further studies using correlation functions will be given in subsequent publications which will also include evidence for the presence of large periods (of the order of a minute).

The distribution of amplitudes according to their magnitude. For the track No. 2 plate 141, September 15-16, 1950, a distribution curve was constructed using 1700 amplitudes. As was to be expected the distribution was found to be gaussian. It is shown in Figure 7. The root-mean-square value of all the amplitudes Δ_i for this track is 50.04 and the mean value of the absolute magnitude 39.95. But, according to the well-known formula,

$$\sigma \cong 1.253 \frac{\Sigma|\Delta_i|}{n}.$$

In our case σ obtained in this way is equal to 50.05 so that the agreement is very good and shows the random character of the entire collection of amplitudes.

9. Summary

As a result of our work we have established the following facts:

1. The root-mean-square amplitude of vibration of star images in a telescope is, as a rule, proportional to $L^{0.5}$, although in a number of cases deviations from this law are possible but the reason for them remains unknown.

2. Evidently there exists a period of vibration which is of the order of a few seconds.

3. The existence of these periods may be established by the use of correlation functions.

4. Large amplitudes correspond to lower vibration frequencies.

5. The dependence of the root-mean-square amplitude of vibration on temperature is in agreement with that predicted by theory.

6. The distribution of amplitudes according to their magnitude is gaussian.

In conclusion, the author wishes to express his gratitude to the Staff of the Main Astronomical Observatory of the Ukrainian SSR and in particular to I.V. Gavrilov and A.B. Onegina, and also to Iu.K. Filippov for his help in collecting the observational material and for the calculations and V.K. Drofe of the Kiev State University Observatory who carried out the measurements on the plates.

The author is also indebted to Assistant Professor I.I. Gikhman, Kiev State University, for advice on the correlation curve and for the organization of some of the calculations by the students of the Department of Mechanical Mathematics of the Kiev State University.

LITERATURE CITED

[1] F. Schlesinger, Publ. Allegheny Observatory Univ. Pittsburgh 3, No. 1 (1912).

[2] E.Ia. Bugoslavskaia, Astron. J. (USSR) 15, 5, 6, 450-455 (1938).

[3] V.A. Krasil'nikov, Doklady Akad. Nauk SSSR 15, 3, 291 (1949).

[4] I.G. Kolchinskii, Astron. J. (USSR) 29, 3, 350 (1952).

[5] E.K. Kharadze, Biull. Abastum. Astrofiz. Observ. 1 (1937).

[6] L. Coutrez and L. Bossy, Ann. de L'Obs. Roy. de Belgique, troisieme sér. 6, No. 5 (1954).

[7] V.G. Fesenkov, Izv. AN Kaz. SSR, Astron. i Fiz. Ser. Vol. 1 (Alma-Ata, 1947).

[8] R. Boutet, Ann. Géophys. 6, 322, 1950.

[9] E. Whittaker and G. Robinson, Mathematical Treatment of Results of Observations [Russian translation] (GTTI, 1933) Chap. 13.

[10] The Theory of Tracking Systems [Russian translation] (IL, Moscow, 1951) Chap. VI.

[11] M.G. Kendall, The Advanced Theory of Statistics (New York, 1952).

[12] Folke Nettelblad, Medd. Fran. Lunds. Astron. Observ. II, 130 (1953).

Received October 28, 1956

The Main Astronomical Observatory
Academy of Sciences Ukrainian SSR
Goloseevo

ASTRONOMICAL CLOCK AChF-1 WITH ISOCHRONOUS PENDULUM

F. M. Fedchenko

The astronomical pendulum clock AChF-1, developed by the author, differs from existing astronomical clocks(manufactured by the factory "Etalon" and the firm "Synchronome Ltd") in its simplicity of construction and high accuracy. The root-mean-square variation of its daily rate is less than 0.001 sec per day, i.e., it is much more accurate than existing first-class astronomical clocks.

AChF-1 works without a secondary clock; therefore, there is no need to synchronize the pendulums.

The accuracy of its rate is achieved by the use of a special three-spring isochronous pendulum suspension and a mechanism which delivers short mechanical or other impulses to the pendulum in its equilibrium position. Such a mechanism does not disturb the isochronism of the pendulum oscillation, which is attained by means of the suspension.

The principle of action of the isochronous suspension, and also that of the impulse mechanism with mechanical impulses, is described. Curves of the clock rate for November-December, 1955, and of variations due to gravity obtained by means of the astronomical clock, are given.

The AChF-1 clock can be used as a timekeeper and also as an instrument for observing variations of gravitational acceleration.

At the present time the astronomical pendulum clock whose use is most widespread is that of Shortt, manufactured by the English firm "Synchronome Ltd." A clock of similar construction in the Soviet Union is manufactured at the Leningrad factory "Etalon." The root-mean-square variation of the daily rate of the Shortt clock reaches ± 0.002 to 0.003 sec per day. Shortt's clock is complicated in construction. It consists of a primary and a secondary clock. The secondary clock exists solely to maintain the pendulum oscillation of the primary clock. The primary synchronizes the pendulum oscillations of the secondary clock. A small disturbance of pendulum synchronism leads to a deterioration of the clock rate, and sometimes to stopping the clock.

In the time laboratory of the Kharkov State Institute of Measures and Measuring Instruments (KhGIMIP), during 1954 and 1955, the author developed and built an astronomical pendulum clock of new design, the AChF-1, which differs from existing astronomical clocks in its simplicity and high accuracy. The root-mean-square variation of its daily rate is less than 0.001 sec by comparison with the KhGIMIP quartz clock, that is, it is much more accurate than existing first-class astronomical pendulum clocks. Accuracy is due to the following:

1. A high degree of pendulum isochronism through the use of an isochronous pendulum suspension.

2. Freer oscillation of the clock pendulum, attained through minimal coupling to the mechanism, and through the use of infrequent short impulses imparted to the pendulum at its equilibrium position.

3. Impulses of high constancy both in magnitude and in the phase at which they are imparted to the pendulum.

The AChF-1 functions without an auxiliary clock; hence there is no need for synchronization of the pendulums. A general view of the clock is shown in Fig. 1.

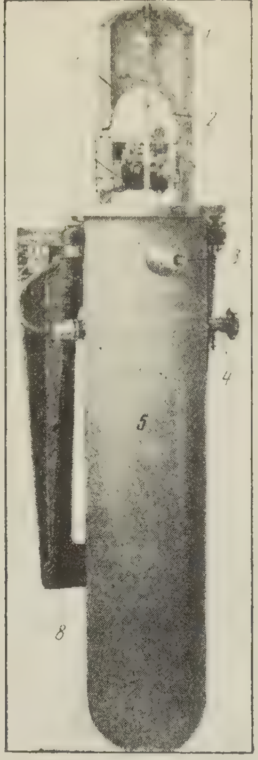

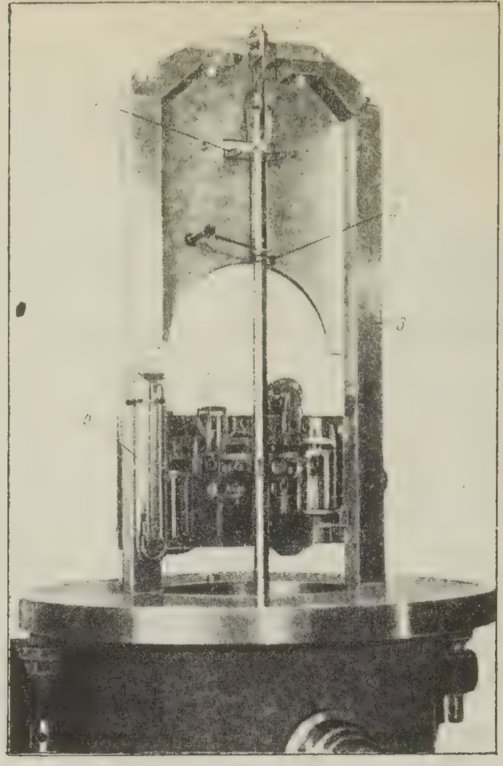

Fig. 1. Fedchenko AChF-1 astronomical clock; 1) isochronous pendulum suspension; 2) pendulum; 3) microscope for amplitude observations; 4) vacuum valve; 5) pressure chamber; 6) suspension bracket; 7) clock mechanism; 8) clock bracket.

Fig. 2. Upper part of the AChF-1 clock; 1) isochronous pendulum suspension; 2) pendulum contact; 3) suspension bracket; 4) lowering mechanism; 5) clock mechanism; 6) manometers (mercury and oil).

The clock is mounted in a steel pressure chamber 5, which is rigidly attached in the vertical position to the wall or to a clock column by means of a cast-iron bracket 8. On the cover of the pressure chamber is set the suspension bracket 6, from which the pendulum 2 is suspended by means of the isochronous spring suspension 1, and to which the clock mechanism 7 is also attached. There are located on the pressure chamber a microscope 3 for observations of the amplitude of the pendulum oscillations, a vacuum valve 4 for exhausting air from the pressure chamber, and a panel for the entry of conductors to the mechanism. Within the pressure chamber are located the spark suppressors of the mechanism contacts and a light bulb which illuminates the pendulum scale during measurements of the amplitude of oscillation.

The clock is covered by a glass dome and the pressure in the chamber is reduced to 8 to 10 mm Hg. The clock is operated from a 10 to 12 v storage battery.

An enlarged view of the upper part of the clock is shown in Fig. 2. On the left-hand column of the suspension bracket are placed the mercury and oil manometers 6 for readings of the pressure within the pressure chamber. On the bracket plate is placed the contacting stop 2 of the clock contact and a checking mechanism 4, by means of which the pendulum is lowered onto the suspension. The columns and plate of the suspension bracket are made of steel and are chrome-plated.

Isochronous Pendulum Suspension

The period of oscillation of a clock pendulum varies with the amplitude of its oscillation, i.e., the oscillations of the pendulum are not isochronous. Since the amplitude of pendulum oscillations is not constant, the clock rate will change correspondingly.

To achieve fully isochronous oscillations of the pendulum it is necessary for the restoring moment to be proportional to the angle of deflection of the pendulum. In reality, however, the pendulum is acted on by a total moment consisting of the normal restoring moment due to gravity, which is proportional to the sine of the angle of the pendulum deflection ($M = k \sin \Phi$), and the elastic moment of the spring suspension, which is proportional to the angle of deflection of the pendulum ($M = k_1 \Phi$). Expanding $\sin \Phi$ in a series limited to the first

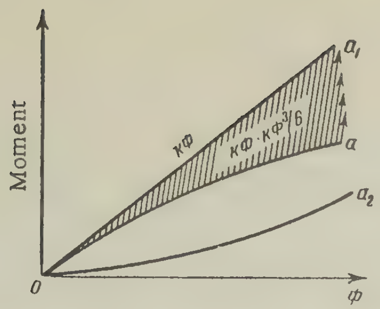

Fig. 3. Restoration moment as a function of pendulum amplitude.

two terms, we have $M = k\Phi - k\Phi^3/6$. Consequently the natural restoring moment is less than that required to produce complete isochronism by the quantity $k\Phi^3/6$, which is proportional to the cube of the amplitude. Figure 3 illustrates qualitatively the difference between the restoring moment $k\Phi - k\Phi^3/6$, represented by the curve Oa, and that necessary for complete isochronism $K\Phi$, represented by the straight line Oa_1. The area between these curves Oaa_1 gives a qualitative representation of the insufficiency of the natural restoring moment for isochronism of the pendulum oscillations.

The question of isochronism of pendulum vibrations has attracted theoreticians as well as horologists from the time when pendulums were first used in clocks, and many different mechanisms have been proposed at various times for its solution.

Huygens (1673) proposed cycloidal guides for the suspension springs during swinging of the pendulum.

Barth (1787) proposed rolling an additional weight over a cylindrical surface whose axis is situated below the axis of rotation of the pendulum.

An additional spring was proposed which the pendulum would stretch while swinging.

Many other devices were also proposed but none of them came into widespread use, since either they themselves added a larger error than the error which was to be corrected or else they were complicated and impractical.

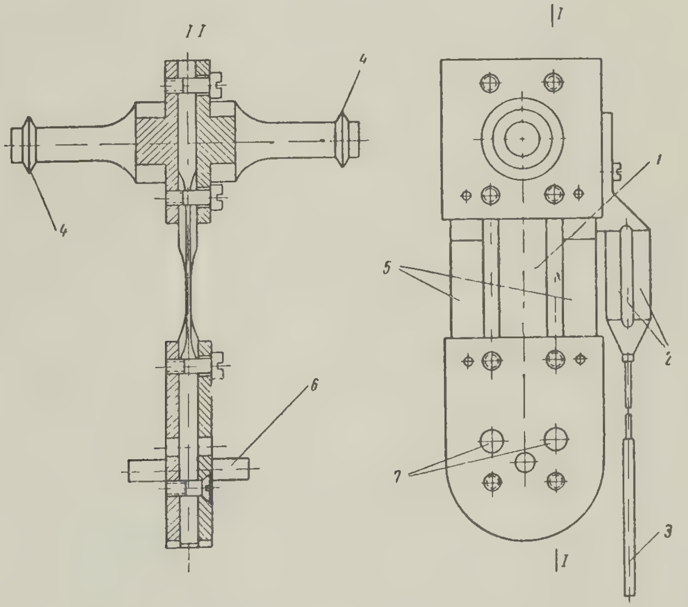

Fig. 4. Isochronous pendulum suspension. 1) Long spring; 2) contact springs; 3) contact rod; 4) bosses; 5) short springs; 6) lower suspension pin; 7) openings for screws to tighten sides of the suspension hook of the pendulum.

The assertion in the literature that a sufficient degree of isochronism of pendulum oscillations can be obtained by the selection of suitable dimensions and shapes of the suspension springs is based on a misunderstanding. In investigations carried out in support of this idea, only composite suspensions were used which permitted loose contact between the sides of the suspension and the thin springs.

This also explains the result obtained by Khain [1, 2] in experiments where a thin suspension gave overcompensation and a thick one undercompensation.

By adjusting the compression of the upper parts of the sides of a composite suspension by means of screws, different degrees of isochronism can be obtained. When there is tight upper contact with the springs, no isochronism whatever is observed. Also, one-piece suspensions provide no isochronism whatever. Isochronism obtained by using a composite suspension is an index of the poor quality of the suspension rather than of its advantage.

Numerous experiments conducted with various suspensions have confirmed that isochronism of oscillations of a free pendulum cannot be attained by altering either the dimensions or the shape of the springs of the suspension.

In order to obtain isochronous oscillations of a free pendulum, the author in 1952 developed and built an isochronous suspension, whose design is shown in Fig. 4. Unlike ordinary nonisochronous two-spring suspensions the isochronous suspension consists of three springs 1,5, situated in the plane of, and symmetrically arranged with respect to the longitudinal axis of the suspension. The middle spring is longer than the outside ones and displaced upwards. The three springs represent separate one-piece suspensions, joined in their thick portions by plates, screws, and pins. The middle spring can be moved along the longitudinal axis of the suspension, providing regulation of the degree of isochromism. Moving the middle spring upwards increases the isochronous properties of the suspension, moving it downwards decreases them. If the upper parts of all three springs are located at the same height, the usual nonisochronous suspension is obtained. The suspension pins are tied by plates. The upper pin possesses circular bosses 4, on which the suspension rests in the working position.

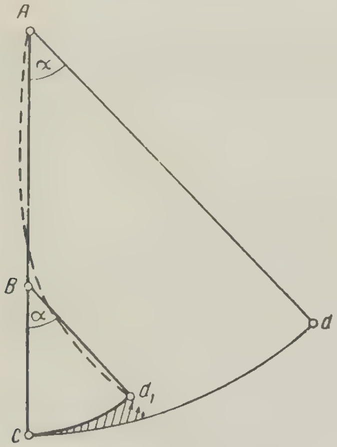

Fig. 5. Diagram of the principle of action of the isochronous suspension.

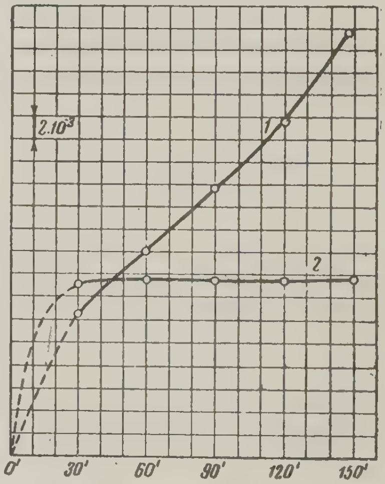

Fig. 6. Dependence of the pendulum period on amplitude: 1) for an ordinary suspension; 2) for the isochronous suspension.

For a qualitative idea of the principle of operation of the isochronous suspension let us examine the scheme shown in Fig. 5. AC is the long spring, BC is a short spring of the suspension. The springs are firmly pressed at their ends and no relative displacement is possible. Let point A be the projection of the axis of rotation of the pendulum, suspended only by the long spring in the absence of the outside springs. Point B is the projection of the axis of rotation of the pendulum suspended only by the short springs in the absence of the long one. If the pendulum is suspended by the long spring, then the lower end of the spring (point C), when the pendulum swings to the right through an angle α, would be transferred to the point d along the arc Cd. If the pendulum were suspended only by the short springs, then their lower ends (point C), with the same angle α of pendulum swing, would be moved to the point d_1 on the arc Cd_1. In actuality, however, the pendulum is suspended by the three springs, which are rigidly fastened to each other; thus the end of the long spring, when the pendulum swings, is forced to follow the path of the short springs Cd_1, and the long spring is forced to bend as shown by the dashed line Ad_1. Hence the middle spring, in addition to the common deformation caused by the pendulum swing in all three springs, undergoes a further deformation caused by the different lengths of the springs and the noncoincidence of the points at which they are fastened.

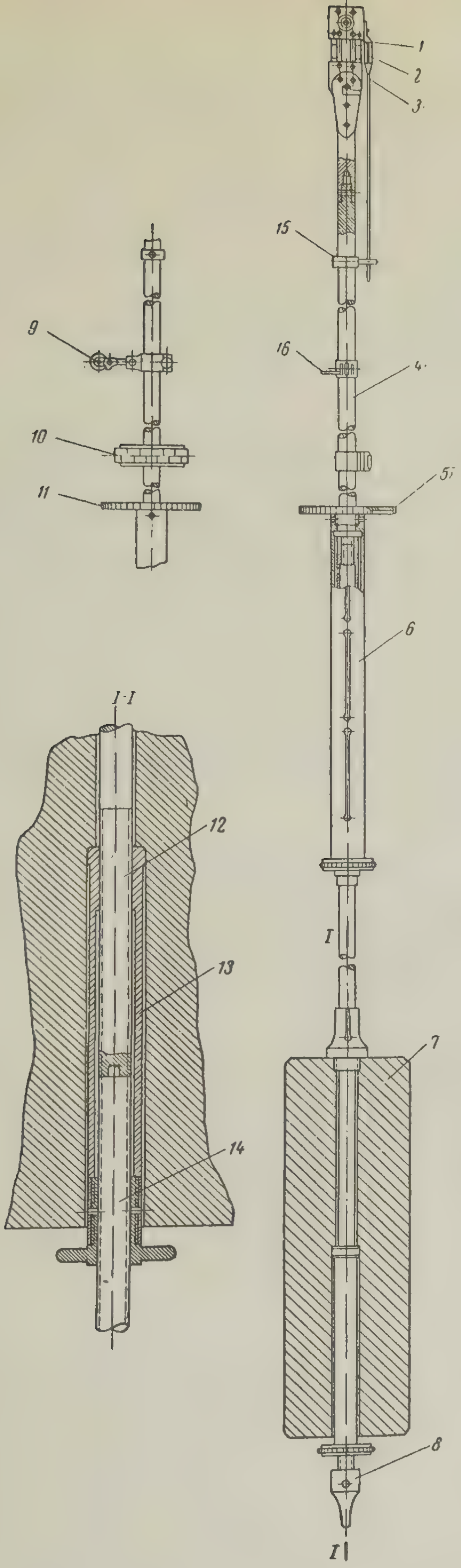

Fig. 7. Pendulum of the AChF-1 clock. 1) isochronous suspension; 2) contact springs; 3) contact rod; 4) pendulum rod; 5,11) platform for regulating weights; 6) temperature compensating tubes; 7) pendulum bob; 8,14) regulating nut; 9) impulse roller; 10) scale for observations of amplitude; 12) lower end of rod; 13) tube supporting pendulum bob; 15) pin, withdrawn; 16) release projection.

Area Cdd$_1$ in the figure gives a qualitative representation of the additional deformation of the longer middle spring. This deformation increases with an increase of amplitude more rapidly than in proportion to the displacement angle of the pendulum. This means that the common restoring moment of the isochronous suspension will increase more rapidly than in proportion to the displacement angle of the pendulum, i.e., along the curve Oa$_2$, which in a certain interval of amplitudes is symmetric with the curve $k\Phi - k\Phi^3/6$ (Fig. 3).

The combined effect of the natural restoring moment and the restoring moment of the isochronous suspension in the given interval of amplitudes is expressed by the straight line $K\Phi$, which is the condition for isochronism of the pendulum oscillations. Thus the isochronism of this suspension is caused by the presence of the longer third spring whose additional deformation supplies an additional elastic moment in a certain, sufficiently wide, range of amplitudes to compensate the insufficiency of the natural restoring moment.

The period of oscillation of the pendulum with the isochronous suspension is independent of the amplitude in the required amplitude range, as is seen from Fig. 6. Curve 1 shows the dependence of the pendulum period on amplitude with an ordinary suspension when freely damped; curve 2 shows that with the isochronous suspension.

The isochronous properties of the suspension depend entirely on the elastic properties of the springs, so that the springs must be manufactured of a suitable grade of steel and receive the necessary heat-treatment.

Isochronous characteristics obtained before installing the suspension in the clock, and after one year's and two year's running, coincided completely, which testifies to the stability of its operation. Temperature changes also have no effect on the isochronous properties of the suspension.

The Pendulum

The clock pendulum is of the usual two-second type with a ten-millimeter invar rod 4 and cylindrical copper bob 7, with a total weight of 10 kg. The construction of the pendulum is shown in Fig. 7.

The pendulum is equipped with an exposed adjustable temperature compensator made of thin tubes, the inner one being of brass and the outer one of invar. The tubes are coupled by means of a flat thread and provided with a retainer nut. The pendulum rod is cut apart and the outer invar tube is a continuation of its upper part. The lower part is

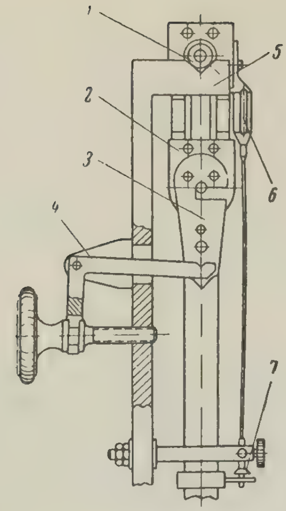

Fig. 8. Mechanism of the pendulum suspension; 1) annular bosses of the upper suspension pin; 2) isochronous suspension; 3) hook for suspending the pendulum rod; 4) lowering mechanism; 5) suspension cock with longitudinal groove, on which the annular bosses of the suspension rest at points a and b; 6) contact springs; 7) contact stop.

inserted into the end of the brass tube. The threads in the temperature compensator tubes and in tube 13, which supports the pendulum bob , are of the same pitch. This is convenient for regulation. If there should be any need to decrease the action of the temperature compensator, then one unscrews the tubes several turns relative to each other and, in order to maintain the former pendulum length, tube 13, must be given the same number of turns on the rod.

The tube carrying the pendulum bob is also of invar and is threaded at both ends. The upper thread 12 is used to screw it on the pendulum rod and the regulating nut 8 screws into the lower end. This brings about coincidence in the direction of the stresses that arise in the tube under the action of the weight of the bob and of the regulating nut.

The outer tube of the temperature compensator 6 has longitudinal slits on opposite sides to permit circulation of air around the inner tube. By this means thermal inertia is kept to a minimum in the pendulum.

The upper part of the outer tube of the temperature compensating tube ends in a platform 5, 11, on which are placed the regulating weights. The rod is coupled to the tube and also to the suspension hook by screw threads and pins.

Above the platforms are located the scale 10 for observations on the amplitude of pendulum oscillations, the impulse roller 9, and the contact-breaking pin 15.

The impulse roller is of steel with diameter of 5 mm. It turns on thin arbors in 4 jewels. In order to eliminate the effect of possible eccentricity on the clock rate, the roller is unbalanced. On the roller rod is placed the release projection 16, by means of which the pendulum periodically knocks out the rest from under the impulse arm of the clock mechanism, thus preparing the impulse. The release projection is so fastened that it is movable on the roller stem, by which means regulation of the size of the impulse is achieved. By moving the projection toward the roller the impulse is decreased, and by moving it away from the roller, it is increased.

The upper part of the pendulum rod ends in the hook of the suspension between the sides of which the isochronous pendulum suspension 1 is inserted.

A light contact is fastened by the thin springs 2 to the upper part of the suspension. When the pendulum moves to the right, the rod of contact 3 rests on the deflecting pin 15 and is inclined at the angle of inclination of the pendulum; in displacement of the pendulum to the left it rests on the contact-stop situated on the plate of the clock suspension bracket (Figs. 2 and 8). The contact is closed for half the period and open for half the period. The axes of rotation of the pendulum and of the contact coincide, thus eliminating the possibility of harmful friction arising between the contact rod and the pin which deflects it. This kind of contact takes no energy from the pendulum (apart from internal friction) since the energy expended by the pendulum in deflecting the contact returns to it in the reverse movement, exactly as occurs in the suspension itself. The place of contact is closely adjusted to the equilibrium position of the pendulum; hence the contact cannot affect the period of vibration of the pendulum at all.

The mechanism of the clock works from this contact through a high-resistance relay. It is also used for comparing clocks. Contact spread does not exceed 0.1 msec. The current broken by the contact is small (of the order of 1 to 2 ma). The pendulum contact is provided with its corresponding spark suppressor, as are all other contacts of the impulse mechanism of the clock. To avoid the possibility of chance damage to the isochronous suspension during installation, the suspension bracket has a checking mechanism 4, with the help of which the pendulum can be smoothly lowered onto the suspension.

The sides of the hook 3 are tightened by screws through openings in the lower part of the suspension, thus providing a firm connection of the pendulum to the suspension. By means of the annular bosses 1, the suspension is seated at four points on the wall of the longitudinal groove in the bracket 5 (seen at a and b). This method of suspending eliminates the possibility of longitudinal oscillations of the pendulum arising in the plane perpendicular to its basic oscillations, and also serves to damp possible vertical jolts to the suspension.

The mechanism for suspending the pendulum is shown in Fig. 8.

The Clock Mechanism

A positive impulse imparted to the pendulum after its equilibrium position lengthen its vibration period, while a positive impulse imparted before the equilibrium position shortens its. The action of a negative impulse is opposite. The effect depends also on the phase of delivery of the impulse. The further the pulse is from the equilibrium position of the pendulum, the greater its effect and, vice versa, the nearer the less. Only impulses given to the pendulum at its equilibrium position have no effect on the period of oscillation.

The pendulum oscillations of the AChF-1 clock are isochronous, and therefore the mechanism maintaining its oscillations is subject to special requirements. The impulse mechanism of the clock which maintains the pendulum oscillations must not counteract what is achieved by the use of the isochronous suspension. Existing mechansims do not satisfy this requirement. Only a mechanism giving the pendulum short impulses exactly at the equilibrium position, irrespective of the nature of the impulses, can do so.

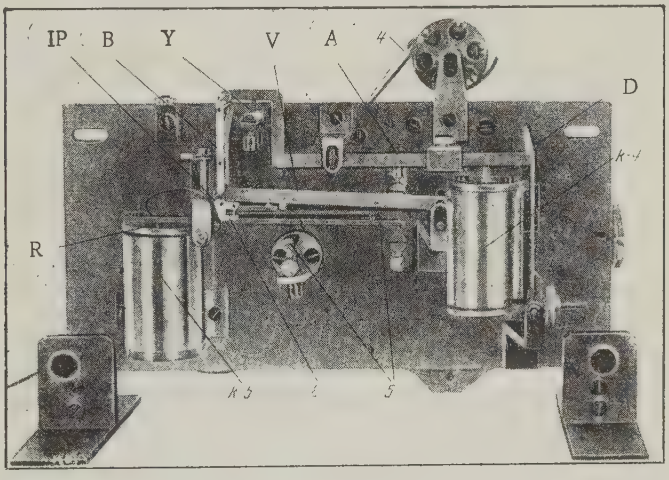

Fig. 9. Impulse mechanism of the clock; IP) impulse pin; B) hook; Y) support; V) impulse lever; A) preparing lever; 4) contact of the impulse transmitting mechanism; D) catch; K-4) electromagnet coil; 5) contacts of the restoring lever; E) movable lobe; K-5) electromagnet winding; R) restoring lever.

Any change in the magnitude of the short impulses, whether positive or negative, given to the pendulum at its equilibrium position, can only affect the amplitude. But changes of amplitude are compensated by the isochronous suspension. It was this which provided the possibility of eliminating the secondary clock, entrusting some additional functions to the pendulum of the AChF-1 clock.

Only a pendulum with period independent of the clockwork can be called free. In this sense, the pendulum of the AChF-1 clock, despite its fulfillment of certain additional functions, is freer than the free pendulum of the Shortt clock, since the oscillations of the latter are maintained by long impulses given after the equilibrium position.

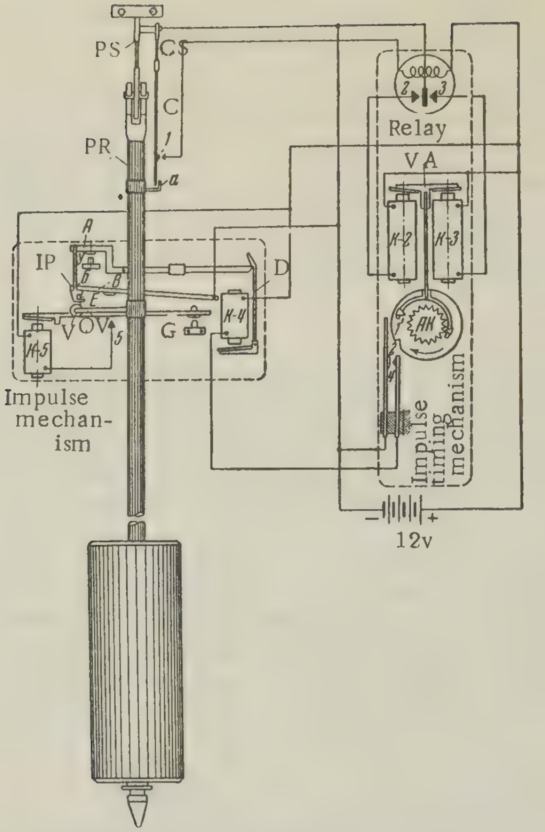

Fig. 10. Schematic diagram of the Fedchenko astronomical clock.

The AChF-1 clock contains a newly developed mechanism which gives to the pendulum in its equilibrium position short infrequent mechanical impulses of a duration which does not exceed 0.01 sec, while in the Shortt clock it reaches 0.4 to 0.5 sec. In the Shortt clock impulses are given every 30 sec and in AChF-1, every 60 sec.

The mechanism of the clock consists of an impulse mechanism (Fig. 9) and the mechanism for impulse timing. A schematic diagram of the clock mechanism is shown in Fig. 10.

In the process of oscillation the pendulum, by means of the deflecting pin a and the rod b, periodically closes and opens the contact of the pendulum 1. The polarized relay thus brought into play alternately passes current to the windings of electromagnets K-2 and K-3, as a result of which the escape yoke VA is attracted and drives the escape wheel AK. The latter has 30 teeth and makes one revolution every 60 sec. The axle of the escape wheel also bears a disk with a notch 2'. At coincidence of this notch with the 1' projection located on the contact spring of the impulse timing mechanism, the contact 4 closes. The current then enters the winding of the electromagnet K-4 with the help of which the catch D is deflected, freeing the lever A. At the left-hand end of the lever A is a light hook B, ending in the movable lobe E. On a projection of the hook (the impulse pin IP) rests the impulse lever V. Lever A, on release of the catch D, under the weight of the impulse lever V, is rotated around its axis so that its left end seats on the stop Y. E comes into engagement with the release projection of the pendulum OV, which is on a rod bearing the impulse roller IR. When the pendulum moves to the left, E is deflected and the pendulum continues to move freely. When the pendulum moves to the right, OV touches E and knocks out the hook B from under the impulse pin, thus freeing the impulse lever V. In falling, the impulse pin of the lever touches the impulse roller IR tangentially, communicating the pulse to the pendulum, after which it rests on the contacting stop and closes contact 5. Lever A at this time occupies its initial position, clamped by D. Contact 5 directs current to the winding of electromagnet K-5, which by means of lever R throws the impulse lever into its original position. The cycle described is repeated with each turn of the escapement wheel.

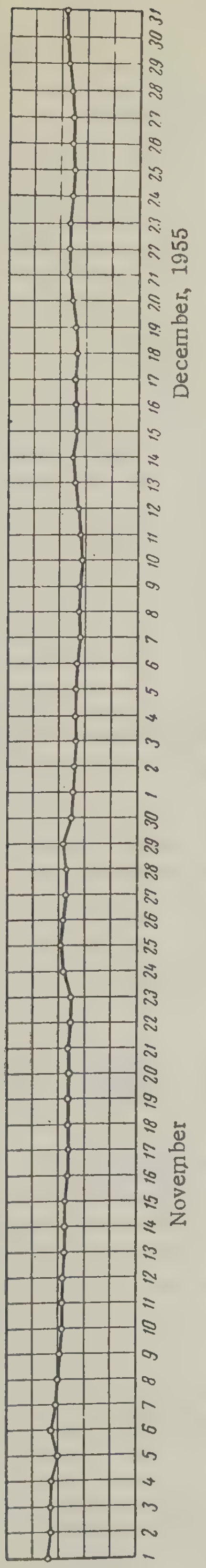

Fig. 11. Daily rate of the AChF-1 clock (Division: 0.10 sec).

The clock mechanism is mounted on an iron plate which is simultaneously a magnetic screen, protecting the pendulum from the electromagnetic field of the electromagnets in the impulse timer, which is mounted on the other side of the plate. In addition all electromagnets are encased in iron.

The levers of the mechanism are of brass. All crucial rubbing parts of the mechanism are mounted on jewels. The contacts of the mechanism are of platinum. The exact timing of the impulses relative to the equilibrium position of the pendulum is regulated by a micrometer which moves the clock mechanism as required.

Study of the Clock

In the absence of a special clock vault, the AChF-1 clock was placed on the wall of the basement room of the working building of the KhGIMIP. The clock room was not thermostatically controlled and thus the annual temperature variation reached 5 to 6°. In addition, during the winter, large daily oscillations were observed on account of nonuniform heating. Only in summer was the temperature of the room maintained more or less satisfactorily, i.e., it changed smoothly by 0.1 to 0.2° per day. A story higher, on the wall where the clock was located a motor and fan were operated periodically.

Under these conditions the clock worked for a period of almost three years while it was being studied. During this time it never stopped spontaneously. The temperature coefficient of the clock is found in the vicinity of − 0.004 sec/°C.

The clock was compared daily by means of a spark chronoscope accurate to 0.1 millisec, with a KhGIMIP quartz clock (KKh-3). The root-mean-square variation of the daily rate for a period of time when the temperature of the room changed smoothly did not exceed 0.001 sec per day. The rate of the AChF-1 is shown in Fig. 11, which gives the daily rates for November and December of 1955. Divisions on the vertical axis represent 0.01 sec. Under appropriate conditions the stability of the rate of this clock would undoubtedly be better. A perfect astronomical pendulum clock must in its rate follow accurately the variations of the acceleration due to gravity. How closely the clock AChF-1 approaches this can be seen from Fig. 12, which gives curves of the dependence of the clock rate on lunisolar variations of gravity.

The curves were obtained by comparing the AChF-1 clock with the quartz clock KKh-3 in a special program where the intervals between comparisons are equal fractions of a lunar day. The error of the comparisons is ± 0.1 millisec.

Three series of comparisons were performed in 1954:

1. November 13, 14 and 15;
2. November 25 and 26;
3. December 10, 11 and 12.

Full moon fell on November 10, new moon on November 25, and full moon again on December 10. In the figure time intervals are plotted along the horizontal axis in fractions of a lunar day. One division is equal to 3 hours 7.5 min, and 3 hour 6 min in the second series. The clock rate was taken after every two intervals and, on the graph, is plotted for every interval. One division of the vertical axis corresponds to 0.001 sec.

The variation in period of the pendulum is related to the variation of gravity by the formula $\Delta T/T = -\frac{1}{2}(\partial \Delta/\partial)$, whence the time for which a change of gravity of 0.01 milligal can be detected (which in the ratio corresponds to 1×10^{-8} when the accuracy of measurement of the period of the clock pendulum is 1×10^{-4} sec), is

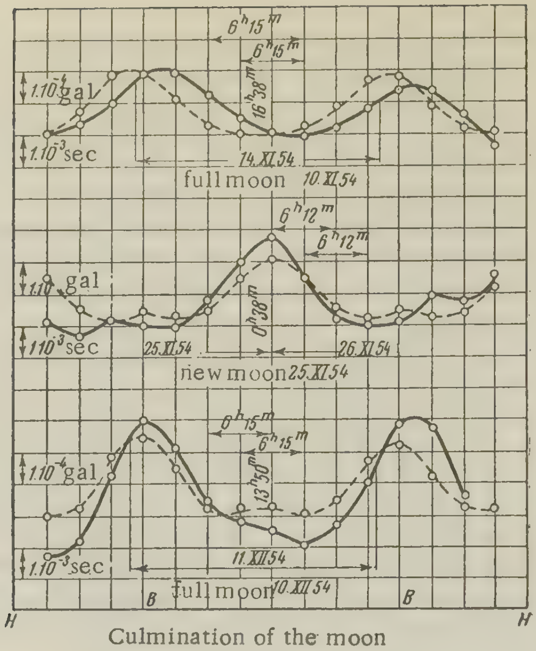

Fig. 12. Curves of observations of gravity variations by means of the AChF-1 pendulum clock; 1(continuous line) observation data; 2)(dashed line) calculated data.

$2 \times 10^{-4} \times 10^{8} = 2 \times 10^{4}$ sec or 5.5 hour. Thus a change of the clock rate during two intervals (6 hours 15 min) with small daily variation determines a variation of gravity up to 0.01 milligal. The results of the comparison of the pendulum clock with the quartz one are plotted in the graph by a continuous line.

The dashed line marks the approximate values of the corrections for gravity at Khar'kov for the lunisolar effect calculated from the tables of P. F. Shokin and according to the Astronomical Annual for 1954. The corrections are calculated to hundredths of a milligal and reckoned from the moment of time of comparison of the clocks. On the vertical axis one division corresponds to 0.1 milligal.

The calculated corrections were given by the director of the Poltava Gravimetric Observatory (Z. N. Aksent'eva).

As seen from the drawing, the curves obtained experimentally and by calculation in all three cases differ little from each other. If a group of pendulum clocks were used in these observations, the coincidence of the curves would be much better on account of the averaging of the rates.

Further investigation of the clock AChF-1 and its improvement were transferred from the KhGIMIP to the All-Union Scientific Research Institute of Physicotechnical and Ratiotechnical Measurements (VNIIFTRI). At present an astronomical pendulum clock AChF-2 already exists that differs from AChF-1 in the impulse mechanism, which permits further reduction of the impulse duration, and also in the construction of the pendulum, which is convertible from mean solar to sidereal time by a simple shifting of a special weight from the lower platform to the upper. Furthermore, work is being done on the design of an impulse mechanism with electromagnetic pulses for AChF clocks.

AChF clocks can be used widely in equipping astronomical observatories and laboratories of the time service. In addition, in conjunction with a quartz clock, they can be used for observations of the variations of gravity.

All-Union Scientific Research Institute of
Physicotechnical and Radiotechnical
Measurements

Received November 1, 1956

LITERATURE CITED

[1] L P. Shishelov, The Mechanics of Clock Mechanisms[in Russian] (KUBUCh, 1935).

[2] Z. M. Aksel'rod, Clock Mechanisms [in Russian] (MAShGIZ, 1947).

[3] Z. M. Aksel'rod, Electromechanical Clocks [in Russian] (MAShGIZ, 1952).

[4] M. P. Pavlov, TheTechnique of Measuring Speeds and Time [in Russian] (MAShGIZ, 1950).

CHARDZHOU INTERNATIONAL LATITUDE STATION

V. P. Shcheglov

A short history of the Chardzhou International Latitude Station is given in the present paper. The station was founded in 1899 and was closed in 1919. During that time about 35,000 instantaneous values of latitude were determined and were used by the International Latitude Service in studying the motion of the earth's pole.

Towards the end of the last century, due to the more accurate observations carried out at a number of observatories, the variation of geographical latitudes became an established fact and it became necessary to study systematically and exhaustively the variation of latitude in order to obtain information on the motion of the earth's poles.

It became quite obvious that the problem is of major importance not only in accurate astrometric work but also in the solution of many problems of contemporary geophysics, mechanics, geodesy, climatology and cosmogony. The idea of a permanent International Latitude Service was first put forward in 1883 at the Congress of the International Geodetic Association by the director of the Neapolitan Observatory, Fergol,* but did not receive the necessary support at the time. The idea was taken up again in 1895 when at the Second Convention of the International Geodetic Association a number of decisions were taken as to the organization of an International Latitude Service. The problem of the choice of sites for the future stations was considered at the Lausanne Conference in 1896. After considering various possibilities it was decided to organize systematic determinations of latitude at the following points on the 39°08' parallel: Misuzawa (Japan), Carloforte (Italy), Gettysburg and Ukiah (USA). These stations were soon joined by the observatory at Cincinnati (USA) which lies on the same parallel but work on variation of latitude was later abandoned by this observatory.

The large interval between the longitudes of Misuzawa and Carloforte (149.5°) meant that at least one other station had to be organized somewhere within this interval.

At the XIIth International Geodetic Conference at Stuttgart the director of the Military Topographical Department, General O.E. Shtubendorf, announced during the meeting on October 5,** 1898, that the Russian Government had agreed to set up a latitude station at Chardzhou which would take part in the program of the International Latitude Service.

In order to bring to fruition this undoubtedly useful project the director of the Tashkent Observatory D.D. Gedeonov (1854-1908), who was already an acknowledged expert on variation of latitude [1], was sent to Chardzhou in February, 1899. His mission was to choose a place for the future station on the 39°08' parallel, to acquire the necessary grounds and to submit general recommendations as to the various buildings required. The place for the station was chosen at a distance of 9.5 km from Chardzhou in Khivinskaia Road which was 3 km from the left bank of the Amu-Daria. In March of the same year Captain M.N. Osipov was appointed as the director and observer at the station.

The construction of the station was carried out under the direction of Engineer-Colonel Poslavskii. The station included a pavilion for a zenith telescope, a "mira" and a house for the caretaker which included a room in which the subsidiary apparatus was kept and which provided temporary accommodation for the observer. His permanent living quarters were at Chardzhou. The size of the station was 91 x 42 m and it was surrounded by a double bank in the form of a clay enclosure. The pavilion for the zenith telescope was square in shape, had an area of 16 m^2 and was made of pine wood set up on brick foundations. The pavilion was provided with double walls and ceiling, with free circulation of air in the space between them, which was ensured by two ventilating pipes in the ceiling and louvered shutters in the outer walls. The distance between the walls and the double ceiling was about 50 cm. This construction of the pavilion was designed to protect the instrument from excessive heating during hot days in the southern climate. The "mira" was in the form of a brick pillar to which a horizontal divided rule was attached. It was placed 73 m north of the instrument and was used as a control on the azimuth of the instrument and in the determination of some of its constants. The pillar was covered by a dome made of galvanized iron and which was designed in such a way that air could circulate freely within it. Work on the construction of the station was begun on July 16, 1899, while the pavilion and the pillar were completed on August 30th, and the observations of latitude were begun at the same time. Systematic observations of latitude were begun on the 10th of September. The construction of the house and the enclosure were completed at the same time. On October 13th work on equipping the station was completed, the clocks were set up and the electrical illumination was installed (it was supplied by a battery) [2].

---

* We were unable to check the spelling of this and several other names (marked with asterisks), and they therefore appear as transliterated from the Russian — Publisher.

** Dates are new style.

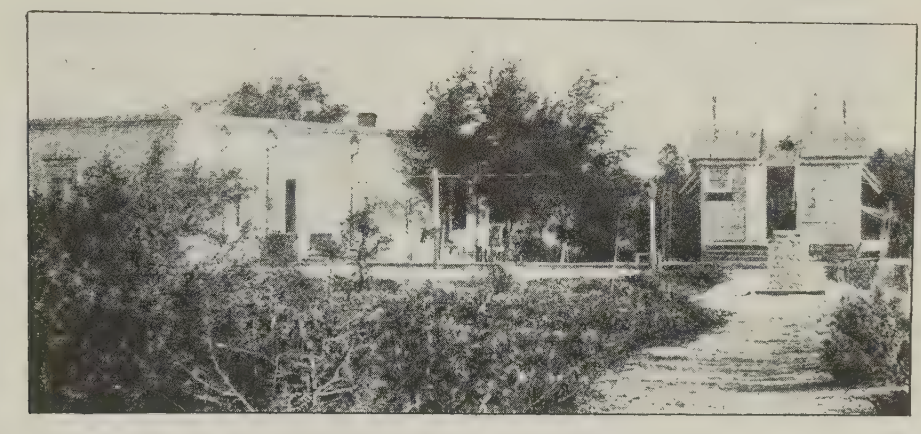

Fig. 1. A general view of the Chardzhou station at its new site.

The station had a Vanshaf*zenith telescope which was used by D.D. Gedeonov in studying changes in the latitude of Tashkent in 1895-1896 [3]. After the zenith telescope was set up its constants were investigated and the ocular micrometer was calibrated by observations on stars. From September 10th to the end of the year systematic observations were carried out during 33 complete and 5 incomplete evenings. During this period the Chardzhou International Station was one of the regular international latitude stations on the 39°08' parallel.

From the inception of the station Talcott's method was used in the determination of the latitude. The program of observations which was suggested by Professor Kimura*consisted of twelve groups, eight pairs in each. The observations were carried out using the "chain" method. The observations and the associated studies of the instrument were carried out under special instructions published by the International Latitude Service [4]. The records of observations, as soon as they were completed, were sent to Potsdam.

In 1905, in addition to the program of the station, a determination was carried out of the difference in the longitudes of the meridians of the zenith telescope and the cross on top of the orthodox church in Chardzhou. In order to determine the time at Chardzhou an old Repsol'd*circle set up on a stone pillar close to the church was used. The chronometer corrections were obtained by Tsinger's method; four pairs were obtained each evening. At the station itself the chronometer corrections were determined by means of the zenith telescope by observing the transits of stars across the meridian. Two chronometers were used in this work. In order to eliminate personal and instrumental errors during a given evening the chronometer corrections were obtained using two instruments. The difference between the longitude of the cross and the zenith telescope was found to be $+22\overset{s}{.}16 \pm 0\overset{s}{.}06$. In accordance with this, the longitude of the zenith telescope was found to be equal to

$$\lambda = 4^h 13^m 56\overset{s}{.}34 \text{ from Greenwich [5].}$$

In 1906 the program of observations was altered: 30 pairs were excluded from the previous program and were replaced by new pairs. The station continued its work normally. However, in 1908 a serious threat to its existence arose. The river Amu-Daria which passes through the Chardzhou district and has low forest banks overflowed its left bank and approached the station. In the middle of the year the distance from the bank to the station was only just over 100 meters. It may have been supposed that as the spring approached Amu-Daria would change its direction so that the station would be saved. However, this did not occur. In view of this threat to the station it was suggested in the spring of 1909 that the station might be moved to a new place. A.I. Auzan, who at the time carried out observations at the station, chose three points to which the station could be transferred. The first point was 14 km from Chardzhou on the new road to Petroaleksandrovsk (Turt-Kul), the second point was on the right bank of Amu-Daria in the neighborhood of the railway, and the third also on the right bank and 8 km southwest of the Farab station. The second point was finally chosen (see map).

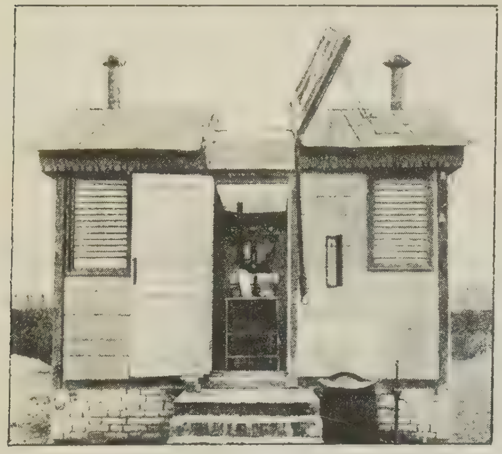

Fig. 2. The pavilion for the zenith telescope.

At the beginning of April, the director of Turkmenistan Military Topographical Department, Colonel M.N. Osipov, who was the first observer at the Chardzhou station, arrived at Chardzhou. He, and the director of the Chardzhou Railway Engineering Department, Colonel Slushko-Tsiapinskii, considered the site on the river bank opposite the latitude station for the new place for the station. The position was found to be safe and it was decided to take immediate measures to start the construction of the station on the right bank of the river. Already, in April, A.I. Auzan determined the latitude of the new place which was only 85 m from the embankment of the railway. As a result, it turned out that the new position of the zenith telescope was 0".35 north of its old position. In order to check that the passage of trains did not affect the observations, observations were carried out on the level indicator of the instruments. It was established that during the passage of both passenger and freight trains the level was constant in spite of a slight vibration of the pillar supporting the instrument and a noticeable vibration of the stellar images. However, these effects were only of importance if the observations were carried out while the train was actually passing. Such a coincidence was, however, very rare. Subsequent work showed that the passage of trains did not affect the observations as a whole.

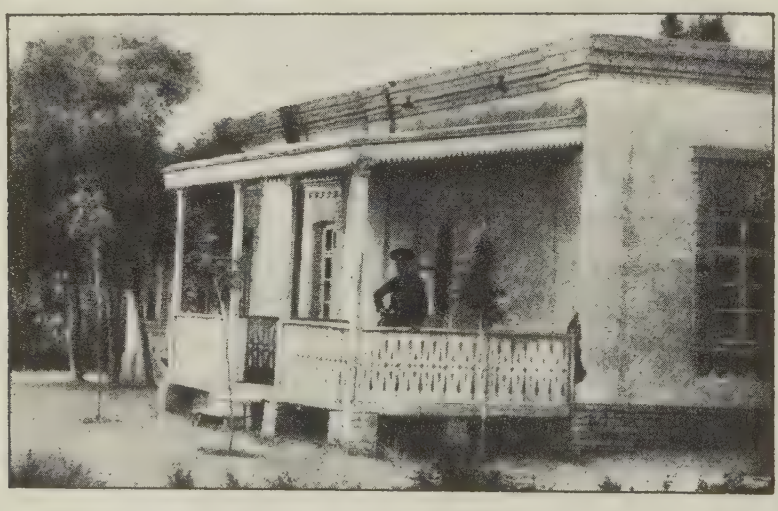

Fig. 3. The living quarters at the new station.

After the final choice of the place of the station a section of the ground was marked out, the area of the section being equal to the area occupied by the old station on the left bank. Work on the construction of the support for the instrument and the foundations for the pavilion at the new place were completed in June. On

June 16th an order was received from the director of the Military Topographical Department concerning the transfer of the station and A.I. Auzan was entrusted with carrying this out. On the following day, the buildings of the station were dismantled (apart from the pavilion for the zenith telescope) and they were transported to the new place. The transport was very difficult since it had to be carried out against the flow of the turbulent river. Observations were continued at the old place. At first it was intended to carry out simultaneous observations at the new and the old places in order to determine accurately the difference in the latitudes. However, the zenith telescope dispatched for this purpose by the Military Topographical Department of the General Staff did not arrive. In the middle of July the river approached the original position of the station so closely that it became dangerous to remain there. At the beginning of August the instrument was taken off and the pavilion dismantled. In view of the fact that the transport across the river on canoes was not completely safe the instruments were transported by a special launch supplied by the Amu-Darian flotilla. Intensive work ensured that the pavilion and the instrument were dismantled, transported, and set up in five days. The break in the observations was therefore only six days. A few days after the station was transferred to the new place, the old place was washed away by the river. The last observations at the old station are dated August 4th and the first observations at the new station are dated August 10th.

TABLE 1

Observers	Period of work
1. Lieut. Col. M.N. Osipov	from Sept. 1899 to June 1901
2. Capt. N.A. Medzvedskii	from June 1901 to April 1904
3. Lieut. Col. A.D. Davydov	from March 1904 to June 1907
4. Lieut. Col. A.I. Auzan	from June 1907 to May 1910
5. Lieut. Col. P.N. Kremliakov	from May 1910 to May 1913
6. Lieut. Col. A.N. Maksimovich	from June 1913 to June 1917
7. Astronomer L.L. Matkevich	from June 1917 to May 1919

TABLE 2

Number of Observed Pairs of Stars Per Year

Year	No. of pairs	Year	No. of pairs
1899	401	1910	2010
1900	1113	1911	1838
1901	1441	1912	2008
1902	1180	1913	1983
1903	1504	1914	1806
1904	1441	1915	1860
1905	1365	1916	1814
1906	1864	1917	2220
1907	1991	1918	1919
1908	2332	1919	515
1909	2403		
		Total	35008*

---

* According to the data of the International Latitude Service. According to the station records this number is higher. The explanation is that not all the observed pairs were included in the final calculations.

As the winter approached all the construction work at the station was completed. The new position turned out to be more convenient. The station was only 4 km from the town. It is true that the road to the town led over a railway bridge which could not be passed on horseback. On the other hand, one could use a bicycle or handcar. The new place also turned out to be more suitable for observations. The underground water was much deeper than at the old station which made the instrument more stable. The humidity was considerably lower.

The cost of the transfer was 2970 rubles [6]. The cost of maintaining the station was 700 rubles per annum.

Thus, beginning with the second half of 1909 the Chardzhou station began work at the new place which was at a distance of 7250 m from its original position.

The station continued its work at the new place until 1919. Its last observer was L.L. Matkevich of the Pulkovo Observatory. Under the war conditions he was looked upon as mobilized and remained at the disposition of the Military Topographical Department which attached him to the Pulkovo Observatory as a "clerk." When, in the summer of 1917, the observer at the latitude station was given a new assignment,he was replaced at Chardzhou by a "lower rank" L.L. Matkevich. In 1918 the station was transferred from military authorities to the People's Commissariat for Education of the Turkmenistan Republic and became a branch of the Tashkent Observatory. Its observer L.L. Matkevich was demobilized. In the following period the work of the observatory was made considerably more difficult in view of the civil war which raged in many districts of Middle Asia. In the spring of 1919 disturbing reports were received from L.L. Matkevich: the station became more and more threatened by the approach of the front line towards Chardzhou.·Furthermore, "Basmach" bands stirred up by agents of the counter-revolution began to appear in the vicinity of Chardzhou. Regular observational work which would justify the existence of the station became impossible. Both the observer and the station itself were in danger. It was therefore expedient to transfer the observer and the instrument to Tashkent. The last observations at the station were carried out on May 25, 1919. In the middle of 1919 at the intercession of the People's Commissariat for Education a special coach was sent to Chardzhou on which travelled the director of the Turkmenistan Military Topographical Department,Ivanov,and a mechanic, Stoliarov.With the help of L.L. Matkevich they dismantled the zenith telescope and the clocks, and together with other valuable equipment they transferred them to Tashkent. The buildings of the station were put in the care of the Farab railway station. Tables 1 and 2 give a list of the observers who worked at the Chardzhou station and the number of observations carried out by them.

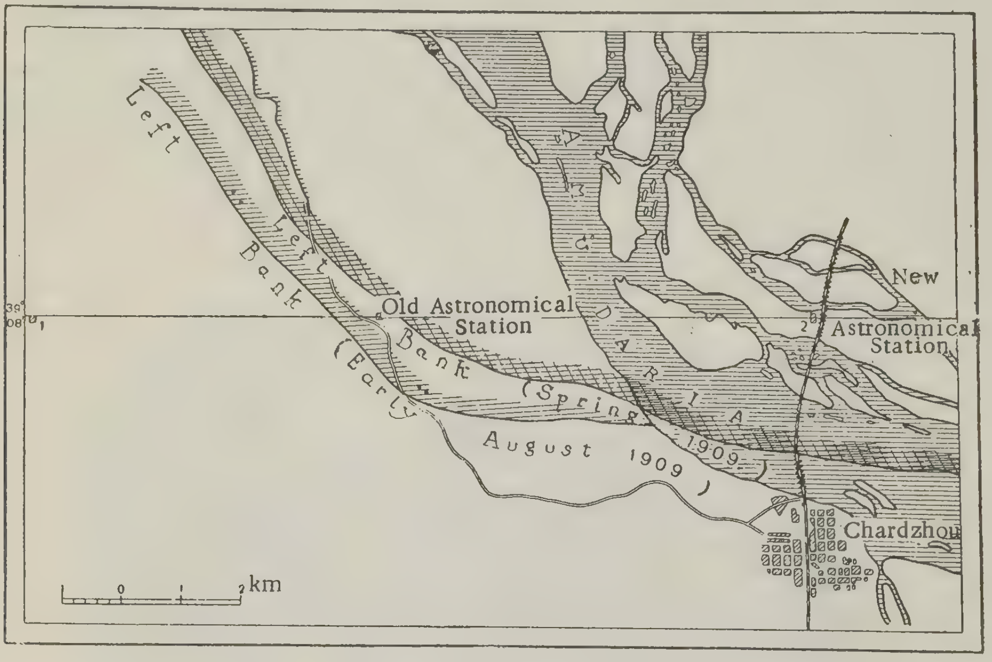

Fig. 4. A map of the neighborhood of the Chardzhou latitude station showing the old and the new position of the station.

It follows from these data that during the twelve years of its existence and in spite of very difficult conditions the Chardzhou International Latitude Station made its contribution to the study of the motion of the earth's poles having supplied about 35,000 determinations of latitude [7].

The new period of work on the study of the motion of the earth's poles under the international program was associated in our country with the activities of the latitude station near the town of Kitab in the Uzbek SSR, which was founded in 1930. This station together with four other foreign international stations is at the present time working under the International Latitude Service and is preparing for very responsible observations during the International Geophysical Year. There are grounds for believing that these stations will be joined at the beginning of the International Geophysical Year by another station, namely, the Chinese International Station which will be located near the town of Tientsin, which is being set up with the collaboration of Soviet Astronomers A.A. Mikhailov, A.N. Deich and the author of the present paper.

Apart from literary sources I have also used some data supplied to me by Z.A. Matkevich, N.F. Bulaevskii and D.I. Kravtsev. I wish to express my deep gratitude to these persons.

LITERATURE CITED

[1] V.P. Shcheglov and Dmitrii Danilovich Gedeonov, Astron. J. (USSR) 28 (1951).

[2] Zapiski VTO 58 (SPb, 1901).

[3] V.P. Shcheglov, "An investigation of the variation in the latitude of Tashkent," Astron. J. (USSR) 32 (1955).

[4] Albrecht, Anleitung zum Gebrauche der Zenittelescope auf den Internationalen Breitenstationen (Berlin, 1899).

[5] Zapiski VTO 64 (SPb, 1910).

[6] Zapiski VTO 54 (SPb, 1911).

[7] Resultate des Internationalen Breitendienstes, I-VI (Berlin, 1903-1932).

Received February 24, 1957

Tashkent Astronomical Observatory

BRIEF COMMUNICATIONS

ON THE OBSERVATION OF THE INFRARED CORONAL LINES 10747 A AND 10798 A

M.N. Gnevyshev, R.S. Gnevysheva and V.G. Kurt

A method of observation of the infrared lines 10747 and 10798 A using electron-optical converters has been developed at the high-altitude astronomical station of the Pulkovo Observatory of the Academy of Sciences of the USSR in collaboration with the P.K. Shternberg State Astronomical Institute, and systematic observations of these lines are being carried out at the present time.

In addition the helium line 10830 and the hydrogen line 10938 belonging to the hydrogen Paschen series are being obtained on the photographs.

A preliminary comparison of the distributions of intensity, in the vicinity of the sun, of the infrared lines among themselves, and with the intensities of the lines 5303 and 6374 A, shows a similarity in the behavior of the lines 10798, 10747 on the one hand, and 5303 A on the other, which can be explained by the fact that the corresponding ionization potentials are close to each other. The behavior of the line 6374 A differs considerably from the behavior of the other three lines, which may be explained by the fact that the ionization potential of line 6374 A is very different from the ionization potentials of the other lines.

This result confirms the correctness of the identification of the lines under consideration.

Latest observations confirm the presence of the helium line 10830 A at some places in the corona.

Among the emission lines of the solar corona which are the most difficult to observe there are two lines which are of particular interest. These lines are Fe XIII 10747 and 10798 A (transitions $3p_1 - 3p_0$ and $3p_2 - 3p_1$ of the configuration $3s^2 3p^2$; the ionization potential of Fe XIII is 325 ev; the excitation potentials are 1.15 and 2.30 ev, respectively).

These lines were first observed by B. Lyot on the Pic du Midi during the eclipse in 1939. By the use of hypersensitization of plates, and by increasing their sensitivity to infrared rays, Lyot succeeded in photographing both these lines using an exposure of four hours. It turned out that these lines, as well as the lines 5303 and 6374 A, are among the brightest emission lines in the corona.

However, studies of these lines were difficult because of the scarcity of observational material, which was due to the fact that an exposure of a few hours is quite inadmissible in the case of systematic observations, or even in the determination of the intensity distribution of these lines around the sun. For this reason these lines have not been observed since they have been discovered.

Quite new possibilities have been opened up through the application of electron-optical converters with caesium oxide cathodes. The sensitivity of these converters exceeds the sensitivity of photographic plates by a few orders of magnitude in the region under consideration.

The first attempt to observe the total emission of both the infrared lines using an electron-optical converter was made in 1950 by A.A. Kaliniak [1] at the high-altitude astronomical station near Kislovodsk. He used an interference filter which transmitted a wide range of wavelengths in the region of the two lines.

The next attempt to observe the infrared lines using an interference filter and an electron-optical converter was made in 1954 at Alma Ata by V.G. Kurt and M.G. Karimov, but was unsuccessful.

Fig. 1.

Further attempts to observe the infrared lines using an interference filter were abandoned since, due to the large half-width of interference filters, the scattered light summed over a wide spectral region is rather considerable, and is difficult to take into account, and also because it is more interesting to determine the intensities of the two lines separately so that their ratio may be found.

In view of the above, V.G. Kurt began, in 1955, some experiments at the high-altitude astronomical station near Kislovodsk which were concerned with the photography of infrared coronal lines using a specially constructed spectrograph attached to the coronagraph in which an electron-optical converter was employed as the radiation detector [2].

First pictures containing the brighter line 10747 A were obtained in February, 1956. However, even with an exposure of 30 minutes these pictures were underexposed. It became clear later that the reason for this was the large loss of light in the diffraction grating which concentrated light in the first order. In such a grating (1200 lines per mm) which, in the interval 4000-7000 A, concentrates most of the light in the first order, the intensity of light in the region 11,000 A is only 2% of the incident intensity. For this reason subsequent experiments were carried out with the coronal spectrograph of the high-altitude station which has a diffraction grating of 600 lines per mm and which has a "blaze" in the second order (70% of the incident intensity). Since the diffraction angle for the green region in the second order coincides with the diffraction angle for the infrared region in the first order ($n\lambda / d = \sin\alpha + \sin\beta$), photographs were taken in the first order. In this way, already in the summer of 1956 good photographs of both the infrared lines of the corona were obtained, and regular observations of the distribution of the intensity of these lines round the sun began at the end of 1956.

Figure 1 shows one of these photographs, obtained on Feburary 4, 1957, showing the coronal lines 10747 and 10798 A, as well as the helium line 10830 A. The photographs were obtained using a curved spectrograph slit which was set concentrically with the limb of the sun and at a distance of 1' of arc. The narrow dark band along the axis of dispersion in the middle of the picture is used for the determination of the position angles along the slit.

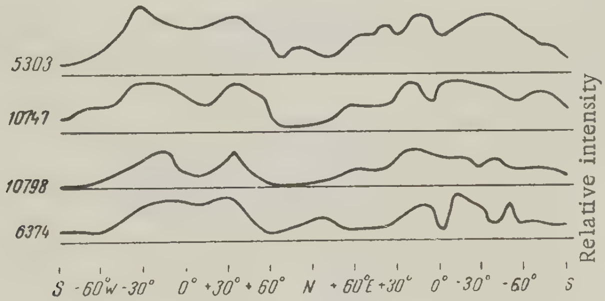

Fig. 2.

The final apparatus which is being used at the high-altitude astronomical station of the Main Astronomical Observatory of the Academy of Sciences of the USSR consists of an externally eclipsed coronagraph (the main objective has a diameter of 20 cm and a focal distance of 300 cm; the equivalent focal distance of the whole optical system of the coronagraph is 500 cm), a coronal spectrograph (the mirrors of the camera and the collimator have diameters of 50 mm and focal distances of 500 mm, the diffraction grating has 600 lines per mm, and the concentration of light is 70% in the visible region of the second order) and a recording part consisting of an electron-optical converter with a photographic camera. The recording part was designed and made at the P.K. Shternberg State Astronomical Institute.

The coronal spectrograph was described in [3].

The slit of the coronal spectrograph covers 50° (position angle). In order to obtain photographs around the entire solar disc, 11 photographs are taken, so that the edges of the photographs overlap. After a further traverse on the same photograph for photometric standardization a photograph is taken of the spectrum of the center of the solar disc through a calibrated step-wedge filter. The optimum exposure used in the case of the RF-3 plate is 2.5 minutes. The dispersion of the spectrograph in the first order is 30 A/mm but due to the fact that in the electron-optical converter the scale is reduced by a factor of 1.3, the dispersion on the plate is 40 A/mm. The small dispersion means that it is impossible to observe simultaneously both the coronal lines, and also the helium line 10830 A and the third line of the Paschen series 10938 A, in protuberances. At the same time it is impossible to study the profile of the lines, and for this reason the present paper is concerned only with an estimate of the intensity of the lines.

Fig. 3.

A comparison of the distribution around the sun of the intensity of the infrared lines 10747 and 10798 A among themselves, and with the lines 5303 and 6374 A, which was carried out using the first photographs, leads to the following results. The distribution of intensity of infrared lines is related to the distribution of intensity of the line 5303 A, and to a lesser extent to the distribution of intensity of the line 6374 A. These relations are characterized by the following values of correlation ratios calculated at 72 points:

Compared lines	Correlation ratio and its error
10747 and 10798	0.77 ± 0.05
10747 and 5303	0.75 ± 0.05
10798 and 5303	0.69 ± 0.06
10747 and 6374	0.48 ± 0.09
10798 and 6374	0.58 ± 0.08
5303 and 6374	0.55 ± 0.08

This result is quite understandable since the conditions leading to the appearance of the infrared lines are closer to the conditions leading to the appearance of the line 5303 than those for the line 6374. This is apparent from the following figures:

Line (A)	Ionization	Ionization potential (ev)
5303	Fe XIV	355
10798	Fe XIII	325
10747	Fe XIII	325
6374	Fe X	233

Figure 2 shows a comparison of the distribution of intensity of the above four coronal lines for January 4, 1957. It is clear from this figure that the infrared lines also have maximum intensities in the near-equatorial regions.

It was shown in [2] that in some places in the corona the helium line 10830 A may be observed. This was confirmed by subsequent observations and is shown in Figure 3 in which one can see the line 10830 A on either side of the protuberance. An analogous luminescence of helium in the corona in the D_3 line was described by M.N. Gnevyshev and R.S. Gnevysheva in [4].

LITERATURE CITED

[1] A.A. Kaliniak, Doklady Akad. Nauk SSSR 72, 661 (1950).

[2] V.G. Kurt and O.L. Vaisberg, Astron. Tsirk. 174, 11 (1956).

[3] M.N. Gnevyshev and R.S. Gnevysheva, Biull. KISO 10 (24), 60 (1954).

[4] M.N. Gnevyshev and R.S. Gnevysheva, Izv. Krymsk. Astrofiz. Obs. 16, 212 (1956).

Received April 10, 1957

High-Altitude Astronomical Station
of the Main Astronomical Observatory
Academy of Sciences, USSR
P.K. Shternberg State Astronomical
Institute

THE SPECTRUM OF THE CRAB NEBULA

P. V. Shcheglov

The emission spectrum of the Crab Nebula for the region 3300-9000 A is obtained from various data, including photographs taken with an image converter. The distribution of energy in this spectral region is represented by the expression $I_\nu \sim \nu^{-2}$, which indicates a steeper differential energy spectrum of the relativistic electrons, $N(E) \sim k/E^5$ instead of the one adopted previously $N(E) \sim$ $\sim k/E^{3.3}$. It is shown that there is a necessity for measuring the radiation flux on the millimeter wavelengths and also in the infrared region with the help of photoresistors.

The current ideas on the nature of the emission from the Crab Nebula have altered radically; the emission in the radio-frequency and optical regions has been explained by one and the same mechanism — the radiation emitted by relativistic electrons in weak magnetic fields [1].

Because of this, the problem of determining the emission spectrum of the Crab Nebula in the radio-frequency as well as in the optical region has become very important.

The energy distribution in the spectrum radiated by the relativistic electrons is related to their differential energy spectrum. If the latter is given by the expression

$$N(E) = \frac{k}{E^{\gamma}},$$

then the spectrum of the radiation emitted is described by the expression $I_\nu \sim \nu^{(1-\gamma)/2}$ [2]. Therefore, from the emission spectrum of the Crab Nebula information can be obtained on the energy spectrum of the radiating relativistic electrons.

In the radio-frequency region there is a fairly large number of measurements of the radiation flux from the Crab Nebula at wavelengths between 3.2 cm and 11.2 m. The radio-frequency data are not affected by interstellar absorption and the measurements give directly the values of the radiation-flux density without the need of corrections. In addition, the radio-frequency data have been obtained for a fairly wide interval of frequencies; this decreases the influence of the random and systematic errors of measurement on the determination of the spectrum.

The situation is considerably worse for the optical region. At the present time there are only a few determinations of the brightness of the Crab Nebula in the region of the spectrum accessible to observation (0.3-1.0 μ). The optical results are usually given in the form of the integral stellar magnitude of the Crab Nebula or in the form of spectrophotometric data. These results must be reduced to the radiation-flux density and also corrected for interstellar absorption. The magnitude of the latter, however, is known rather inaccurately [3, 4]. It must be pointed out that, at present, the region of the spectrum accessible to optical observation is only a little wider than one octave (0.3-1.0 μ) and this increases the influence of the observational errors on the gradient obtained.

Up to the present, the behavior of the spectrum has been obtained by combining one of the points in the optical region with the points in the radio-frequency region; doing this, the value of the quantity $(1 - \gamma)/2$ is found equal to -1.15, which gives $\gamma = 3.3$.

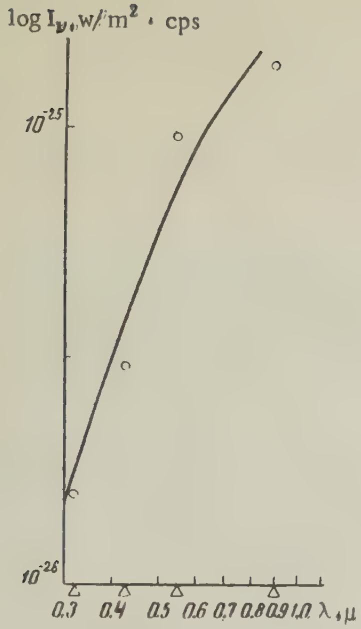

Fig. 1. The distribution of energy in the spectrum of the Crab Nebula for the region of the spectrum 3300-9000 A.

We have attempted to reduce into one system all of the existing results on the measurement of the intensity of emission from the Crab Nebula in the optical region. In addition, we have measured the magnitude of the Crab Nebula in the region 8000-10000 A.

Photographs of the Crab Nebula were taken in 1955 and 1956 with a camera of the AN SSSR Crimean Astrophysical Observatory having d = = 64 cm, d : f = 1 : 1.4. An image converter, with an oxygen-cesium cathode, was used in combination with an Agfa filter No. 587. The exposures did not exceed 1 minute because of the high background from the hydroxyl emission from the night sky. The cathode of the image converter was cooled with solid carbon dioxide. The image of the Pleiades was used for calibration, while the stellar magnitude of the standard was checked against the magnitudes of the stars in the cluster M39 as there is practically no absorption of the light from it. The standard star in the Pleiades was also situated in a region of the cluster for which the absorption is comparatively small.

The effective wavelength of the equipment is nearly 9000 A. The infrared magnitude of the Crab Nebula was found to be equal to $6^m.5$ (from two photographs). This value is explained, not so much by the high brightness of the Crab Nebula as by the low brightness of the comparison star (B9 spectrum) in the infrared region. To evaluate the radiation-flux density, the theoretical and observational results on the distribution of energy in the spectrum of this star were used [5, 6].

The photographic magnitude of the Crab Nebula was determined in the same way. It was found to be equal to $9^m.3$ (from two photographs) which is in satisfactory agreement with the data of other authors [3, 7]. The spectrophotometric data for the region 4700-3300 A were also used [8] to obtain the spectrum. The absorption for the Nebula was taken to be $1^m.2$ for photographic light [3, 4]; the absorption was assumed to be inversely proportional to the wavelength.

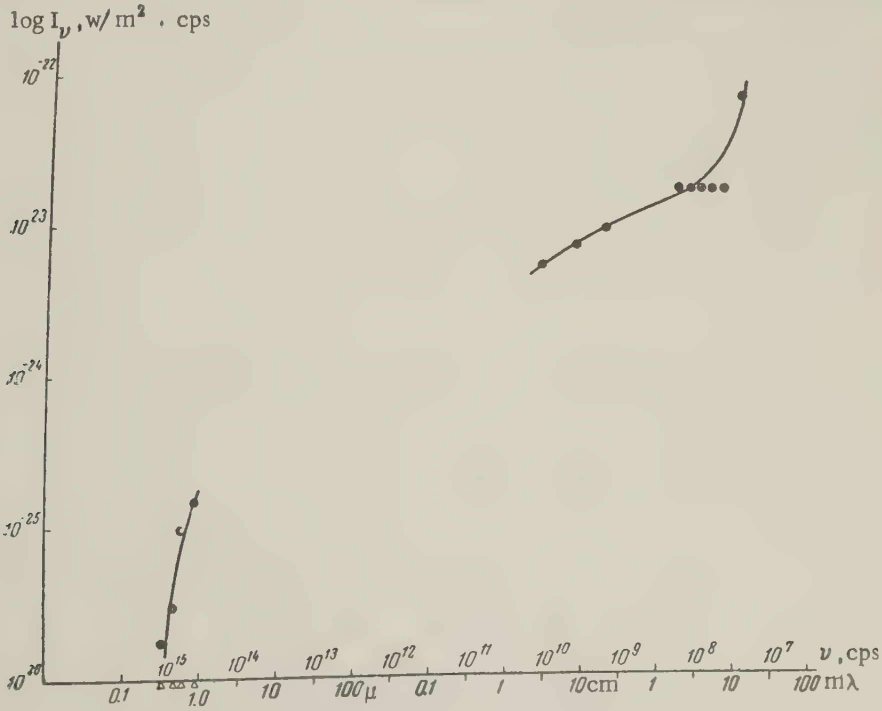

Fig. 2. The spectrum of the Crab Nebula according to the data available in May, 1957.

The spectrum of the Crab Nebula for the region of wavelengths 3300-9000 A was constructed from these data (Fig. 1). The spectrum in this region can be represented by $I_\nu \sim \nu^{-2}$ or, perhaps, even by $I_\nu \sim \nu^{-2.5}$, which gives a more rapid fall of the intensity with frequency than the interpolation between the optical and radio-frequency spectra. The differential energy spectrum of the electrons responsible for the optical emission can therefore be represented by $N(E) = K/E^\gamma$, where γ is likely to be greater than 5.

The data available at the present time (May, 1957) on the radiation flux of the Crab Nebula are given in Figure 2. The optical data are taken from [3, 4, 7, 8] and our observations, the radio-frequency data from [2] and [9].

The measurement of the radiation flux from the Crab Nebula in the millimeter region, as well as in the more distant infrared region, is of considerable interest. In the region of transparency of the earth's atmosphere at 19-2.3 μ, the expected radiation flux from the Crab Nebula is of the order of 10^{-12} w (telescope diameter 70 cm); this flux can apparently be observed at the limit of sensitivity with the help of modern photoresistors. A somewhat higher flux can be expected in the next region of transparency of the earth's atmosphere (from 3 to 4 μ).

I am deeply grateful to I. S. Shklovskii, who supervised the present work, and also to the directors and staff of the Department of Nebular Physics of the AN SSSR Crimean Astrophysical Laboratory for their attention and support.

P. K. Shternberg
State Astronomical Institute

Received May 15, 1957

LITERATURE CITED

[1] I. S. Shklovskii, Doklady Akad. Nauk SSSR 90, 983 (1953).

[2] I. S. Shklovskii, Cosmic Radio Emission [in Russian] (GTTI, Moscow).

[3] W. Baade, Astrophys. J. 96, 188 (1942).

[4] R. Minkowski, Astrophys. J. 96, 199 (1942).

[5] E. R. Mustel', Uspekhi Astron. Nauk 3, 173 (1947).

[6] J. Stebbins and A. Whitford, Astrophys. J. 102, 318 (1945).

[7] J. Oort and Th. Walraven, Astronomische Nachrichten 102, 318 (1945).

[8] D. Barbier, Ann. Astrophys. 1945, No. 1-2, 35.

[9] H. Wells, J. Geophys. Research 61, 541 (1956).

THE VIRIAL THEOREM AS APPLIED TO THE DYNAMICS OF STELLAR SYSTEMS

A. M. Mikisha and F. A. Tsitsin

It is shown that the virial theorem can be applied to the study of a much larger range of stellar systems than had previously been thought, including systems which are highly nonstationary.

1. The virial theorem gives the relation between the kinetic and potential energy of a set of point masses. Unlike the law of energy conservation, this theorem does not refer to all conservative systems, but only to those whose moment of inertia satisfies a certain condition.

The moment of inertia of a set of point masses is given by

$$I = \sum m_i r_i^2, \tag{1}$$

where m_i is the mass of the ith point, and r_i is the distance of the ith point from the point O relative to which the moment of inertia is taken. In a stationary Cartesian coordinate system, whose origin is at O, the moment of inertia can be written in the form

$$I = \sum m_i (x_i^2 + y_i^2 + z_i^2). \tag{2}$$

Differentiating Equation (2) twice with respect to time, we obtain

$$\frac{1}{2}\frac{d^2 I}{dt^2} = \sum m_i (\dot{x}_i^2 + \dot{y}_i^2 + \dot{z}_i^2) + \sum m_i (x_i \ddot{x}_i + y_i \ddot{y}_i + z_i \ddot{z}_i). \tag{3}$$

The quantity $\Sigma m_i (x_i \ddot{x}_i + y_i \ddot{y}_i + z_i \ddot{z}_i)$ is called the virial of Clausius.

The equations of motion can be written for each point mass of the system in the form

$$m_i \ddot{x}_i = -\frac{\partial \Omega}{\partial x_i}, \quad m_i \ddot{y}_i = -\frac{\partial \Omega}{\partial y_i}, \quad m_i \ddot{z}_i = -\frac{\partial \Omega}{\partial z_i}, \tag{4}$$

where Ω is the potential energy of the system, that is where

$$\Omega = -G \sum_{i \neq j}\sum \frac{m_i m_j}{r_{ij}}, \tag{5}$$

in which G is the gravitational constant.

Inserting (4) into the expression for the virial, Euler's theorem for homogeneous functions gives

$$\sum m_i(x_i\ddot{x}_i + y_i\ddot{y}_i + z_i\ddot{z}_1) = -\sum\left(x_i\frac{\partial\Omega}{\partial x_i} + y_i\frac{\partial\Omega}{\partial y_i} + z_i\frac{\partial\Omega}{\partial z_i}\right) = \Omega.$$

Thus Equation (3) can be written in the form

$$\frac{1}{2}\,\frac{d^2I}{dt^2} = 2T + \Omega. \tag{6}$$

It is clear that if the moment of inertia I is a linear function of time or a constant, then

$$2T + \Omega = 0. \tag{7}$$

We arrive finally at the following theorem:

The Virial Theorem. If a set of point masses interacts according to Newton's law of gravitation, and its moment of inertia is a linear function of time (or, in particular, is time-independent), then its potential energy is equal in absolute value to twice its kinetic energy.

2. The virial theorem has applications in stellar dynamics, where it has long been used in the study of stationary systems. We recall that a stationary stellar system is one whose stellar coordinate and velocity distribution function is time-independent. Obviously the mass distribution and, therefore, the moment of inertia of a stationary system are time-independent.

It was known also that the virial theorem is valid also for nonstationary systems whose moment of inertia depends linearly on the time. Such a point of view was reflected in the formulation of the virial theorem given by P. P. Parenago in his "Course in Stellar Astronomy". This formulation ("Course in Stellar Astronomy", 3rd edition, p. 397) is the following: "in a stationary (or linearly nonstationary) stellar system the potential energy is equal in absolute magnitude to twice the kinetic energy". Parenago calls a linearly nonstationary system one whose moment of inertia depends linearly on the time.

It is easily shown, however, that even this formulation of the virial theorem is not equivalent to the one we have given above, but is much weaker.

Let us consider that case I = const. It is clear that all stationary systems satisfy the condition I = const. But it is easy to conceive of a system which is clearly nonstationary, yet for which I = const. Indeed, let us consider a system of N point masses. The moment of inertia of this system relative to some stationary point is

$$I = \sum_{i=1}^{N} m_i r^2.$$

We are assuming that I = const. Then we can write

$$I = m_1 r_1^2 + m_2 r_2^2 + \sum_{i=3}^{N} m_i r_i^2 = \text{const},$$

where m_1 and m_2 are any points of the system.

Let $r_i = r_{i_0}$ = const for $i \geq 3$. It is clear that then $a = \sum_{i=3}^{N} m_i r_1^2$ is time-independent. Writing $b = m_1 r_1^2 + m_2 r_2^2$, we note that in order for b to be constant it is not necessary that $r_2 = r_{2_0}$ = const and $r_1 = r_{1_0}$ = const. Since $r_1 = \sqrt{(b - m_2 r_2^2)/m_1}$, where $b = m_1 r_{1_0}^2 + m_2 r_{2_0}^2 \neq 0$ we can give arbitrary values to $r_2(t)$ in the interval $0 \leqslant r_2 \leqslant \sqrt{b/m_2}$, obtaining a continuous set of real values for $r_1(t)$ in the interval $0 \leqslant r_1 \leqslant \sqrt{b/m_1}$.

Thus, we have constructed a clearly nonstationary system whose moment of inertia is constant. This example shows that the traditional formulation of the virial theorem in stellar dynamics is not complete. A similar statement can be made about a system whose moment of inertia is a linear function of time.

Note. The term "linearly nonstationary" is not very fortunate, since it reflects only the linear time dependence of the moment of inertia of the system, without in any way stating the degree to which it is nonstationary.

3. We have pointed out above that a nonstationary system some of whose stars converge towards the center of gravity, while other diverge from it, may have a constant moment of inertia. Since movement of point masses perpendicular to the radius vector does not change the moment of inertia of a system, we arrive at the following conclusion: the virial theorem can be applied to study a much larger class of stellar systems than had previously been supposed, including several classes of systems which are highly nonstationary.

P. K. Shternberg State Astronomical Institute

Received January 30, 1957